UNIVERSITY OF NOTTINGHAM
DEPARTMENT OF MECHANICAL ENGINEERING

Tow Placement Studies for Liquid Composite Moulding

by

Matthew Turner
B.Eng

Thesis submitted to the University of Nottingham
for the degree of Doctor of Philosophy
October 1998

Contents

Abstract

Tow Placement Studies for Liquid Composite Moulding

by

Matthew Turner

B.Eng

This thesis describes the work undertaken developing techniques for the design and manufacture of continuous fibre preforms for liquid composite moulding. A prototype tow placement facility based on the roller placement of up to 5 tows onto a flat bed was developed. This was used to prepare preforms for 4 industrially based demonstrator components which were subsequently successfully moulded. In tests vibrational performance of parts so manufactured showed slight improvements in mechanical performance compared with those manufactured from conventional reinforcement.

The facility was also used to lay down preforms, the fibre structure of which had been generated by undraping a 3 dimensional model of the finished component. In this manner the performance of the composite, of both mechanical strength and permeability during injection could be optimised. The lay down machine was also used to generate preforms with a well defined built in waviness to the fibre structure. This material was used to generate information regarding the degradation in performance when waviness is introduced and also the effect on permeability during the injection phase.

Acknowledgements

The author would like to thank his supervisors Professor C.D. Rudd and Dr A.C. Long for their guidance and support throughout this research. The assistance of Professor V. Middleton is also gratefully acknowledged.

The representatives of the organisations that funded this project are thanked, in particular Paul Greaves and Robin Bradley (Rolls Royce plc), Roy M^{c}Carthy (Dowty Aerospace), Gordon Creighton (Hexcel Composites), Roger Goodwill (PPG), Graham Pledger (Ciba Polymers), David Tanner (Island Plastics Industries), John Klintworth (MSC Ltd) and Richard Pawley (Newall Aerospace).

The Head of Department, Professor B.R. Clayton, is thanked for the use of the departmental facilities and the Faculty Workshop. Many thanks must be given to Geoff Tomlinson who with his personal touch encouraged things to work. The help and natural good humour of other technical staff within the department is also appreciated, especially Brian Foster, Roger Smith, Andrew Kingham, Dave Smith and Paul Johns.

Thanks are given to my fellow researchers who made the journey a lot more fun: Dr Al-Hamdan for keeping me on my toes, Mohammed Tufail for being in the office as well, Paul Smith, Chris Duffy, Tim Cain and Tom Vincent for the much needed recreation time, and all of the other guys who helped make my time at the Uni so enjoyable.

Finally I would like to thank my family for their support in enabling me to have written this.

Glossary

Anisotropic	Having properties which vary with direction within the material
ATP	Automated Tape Placement
Binder	A substance which provides cohesion between fibres within a reinforcement
BMC	Bulk Moulding Compound
CAD	Computer Aided Design
CAE	Computer Aided Engineering
CAM	Computer Aided Manufacturing
CAIO	Computer Aided Internal Optimisation
CFRM	Continuous Filament Random Mat
CLT	Classical Laminate Theory
CNC	Computer Numerically Controlled (referring to machine tools)
Crimp	Undulation of a yarn, usually from a weave structure
CSM	Chopped Strand Mat
Cure	Polymerisation of a resin - changing from liquid to solid
DMC	Dough Moulding Compound
E-glass	Electrical glass, the type of glass most commonly used for fibre reinforcement
Efficiency	The structural competence of a reinforcement
FRP	Fibre Reinforced Plastics
Fibre Laydown	Two dimensional reinforcement that has been manufactured on the tow placement facility
Filament	A single glass fibre
Filament Winding	An FRP manufacturing technique, involving the wrapping of dry or impregnated roving or tow around a mandrel
GRP	Glass Reinforced Plastics
Homogeniser	A pressure pot used for resin delivery
Impregnation	The displacement of air and penetration of a fibre preform by liquid resin

Injection gate	A device to allow resin into a mould
Isotropic	Having properties which do not vary with direction within the material
Lamina	A ply within a composite structure (laminate)
LCM	Liquid composite moulding
NC	Numerically Controlled (referring to machine tools)
Newtonian Fluid	A fluid whose viscosity is independent of the shear rate
OGV	Outlet Guide Vane
PC	Personal Computer
Permeability	The property of a porous material which characterises the ease of fluid penetration
Porosity	The volumetric fraction of voids in a porous material
Preform	An arrangement of dry fibres in the shape of a mould cavity
Prepreg	Reinforcement in sheet form that has been pre-impregnated with resin
Pressure Pot	A device used to supply resin under pressure to a mould
PLMP	Preforms for Liquid Moulding Processes
RTM	Resin Transfer Moulding
Reinforcement	Fibres used to provide strength in a composite
ROM	Rule of Mixtures
Roving or Tow	An assembly of strands and filaments
SMC	Sheet Moulding Compound
SRIM	Structural Reaction Injection Moulding
Size	The surface treatment applied to glass fibres during manufacture which protects the surface during processing and provides a chemical link with the resin (using a coupling agent)
Spray-up	The application of chopped fibres onto a surface by means of a spray gun
Tex	The mass per unit length (g/km) of a fibre strand or roving
Thermoplastic	A polymeric material which is softened by the application of heat and hardened by cooling in a reversible process

Thermoset	A material which is hardened by an irreversible chemical reaction
Tow	An assembly of strands and filaments
Tow Placement	Automated system for producing novel net-shape reinforcement for LCM
Warp	The direction along the roll of a commercial reinforcement material
Washing	The disturbance of fibre within the preform by the oncoming flow front (or by the passage of air in tow placement)
Waviness	Fibre undulation (usually caused by the crimp in woven fabrics)
Weft	The direction across the roll of a commercial reinforcement material
Wet-out	Contact between fibre surface and matrix after polymerisation.

Nomenclature

			Units
a	=	Amplitude of sine wave (representing tow misalignment/waviness)	m
a_n	=	Proportion of fibres oriented at angle θ_n to applied force	
A	=	Cross-sectional area	m^2
c	=	Kozeny constant	
d	=	Shape factor used in Gebart's [73] model for permeability prediction	
E	=	Tensile modulus	Pa
G	=	Shear modulus	Pa
h	=	Cavity thickness	m
K	=	Reinforcment permeability	m^2
K_{avg}	=	Average permeability through a unit cell of a sine wave	m^2
L	=	Flow path length	m
P	=	Pressure	Pa
$P_{m,n}$	=	Draped point	
Q	=	Volumetric Flow Rate	m^3/s
R	=	radius	m
R_{eff}	=	Effective fibre radius	m
S	=	Length of a sine wave (representing tow misalignment/waviness)	m
S_m, S_n	=	Directional reinforcement inter-fibre spacings	m
[S]	=	On-axis compliance of a composite lamina under plane stress	
t	=	Time	s
[T]	=	Matrix used in the off-axis transformation of [S]	
$U_{m,n}$	=	Undraped point	
V_a	=	Available volume fraction	
V_f	=	Fibre volume fraction	
x,y,z	=	global coordinates	
α	=	Degree of reinforcement anisotropy for flow properties	
β	=	Aspect ratio of ellipse formed by impregnated region	
Δp	=	Change in Pressure	Pa
δ^2	=	Mean square angular deviation	
θ	=	Angle of inclination	radians
θ_n	=	Angle subtended by fibre path with X-axis	radians
ε	=	Axial strain	
γ	=	Shear strain	
σ	=	Axial stress	Pa
τ	=	Shear stress	Pa
η	=	Reinforcement efficiency	
λ	=	Sine wavelength	m
ν	=	Poisson's ratio	
ϕ	=	Porosity	
λ	=	Wavelength	m
μ	=	Viscosity	cP

v	=	Macroscopic resin velocity	m/s
v_0	=	Superficial resin velocity	m/s

subscripts

1,2,6	=	Material Principal Directions
x,y,z	=	Parallel to coordinate axes
c	=	Composite properties
eff	=	Effective
f	=	Fibre properties
ff	=	Flow front
i	=	Node number, principal value or summation index
m	=	Matrix properties
m,n	=	Nodal indices

Chapter 1
Introduction

1.1 Structural Fibre Reinforced Plastics in Industry

Structural fibre reinforced plastics (FRP) are commonly used within the aerospace industry and are also becoming increasingly popular for automotive and industrial applications. The use of FRP within such diverse manufacturing sectors demonstrates the flexibility of composites for use in products ranging from purely aesthetic, non-load bearing applications such as automotive seat backs [1] to fully structural components such as wing stub boxes [2] that need to withstand large forces and undergo strict certification criteria.

The aerospace industry has been the traditional user of composites since the early 1940's as the high cost of raw materials and the slow processing times made composites uneconomical for many other applications. Radomes were first manufactured from glass reinforced plastics (GRP) for US aircraft in 1942 [3]. The development of materials, processes and technology has allowed continued growth in aerospace applications. Current aerospace components manufactured from polymer composites, all of which are structural, include wing flap seals, vertical tail ribs, horizontal tail skins and fuselage skins used on the US Navy F/A-18E/F fighter aeroplane [4] and main rotor blades, rotor blade spars, aft fuselage and wing skins of the V-22 Osprey tilt-rotor aircraft manufactured by Bell Helicopters and Boeing [5,6].

In the late 1990's, the largest non-aerospace user of composites, and probably the largest user overall, is the automotive sector. Increasing environmental pressures require more economic (fuel efficient) vehicles and composites are being used within the structure of vehicles to satisfy such requirements due to the design flexibility, high specific stiffness and weight reductions possible by replacing steel components with composite ones. Current composite components used in the automotive industry are numerous and are present in models made by most of the large manufacturers of commercial and private vehicles. Examples include vehicle sideguard systems [7], an extra high composite van

roof [8], foam cored spoilers, front bumper beams, vehicle front ends and seat backs [9].

1.2 Automated Composites Manufacture

It is widely regarded in the aerospace industry that developments in automation of the composites manufacturing processes are required to produce better quality, repeatable parts with improved performance, whilst increasing materials utilisation and reducing production costs [10-12]. In recent years, many research programmes have investigated the possibility of implementing process automation for composites manufacturing. A number of major developments in process automation for the manufacture of structural composites have been observed in the following processes:

- Automated Ply Cutting
- Filament Winding
- Automated Tape Placement (ATP)
- Tow-Preg Placement

Automated Ply Cutting

Automated ply cutting describes a process whereby computer controlled lasers, water-jets or ultrasonic knives are used to cut dry reinforcement or pre-preg fabric from roll stock [13]. Although this form of automation enables accurate, net-shaped plies to be cut, the process still requires manual laying of each individual ply into the mould which can induce positional errors. Additional automation to reduce such errors can be seen in the form of CAD/CAM cells where the automated ply cutting station forms part of the cell which also includes automated ply lay-up and tacking [14]. To reduce ply positional errors Sikorsky have used a laser ply alignment system that eliminates the need for the "hard tool" ply alignment masks usually used and this has helped reduce part completion times by 27% [15].

Filament Winding

Filament winding involves the winding of individual tows or tape onto a rotating mandrel from a fibre delivery head that traverses the mandrel at controlled rates which govern the

fibre angle. Lay-up compaction can be altered by the degree of tension maintained on the fibres during application. The majority of structures manufactured by filament winding use tow-pregs (tows pre-impregnated with a thermoset resin) which are impregnated on-line [16] or in a prior operation. Structures are cured directly on the mandrel with application of heat or, for more demanding structures, in an autoclave. In an effort to reduce production times, thermoplastic *in-situ* consolidation of filament wound components has been investigated [17,18]. The process is similar to conventional filament winding but replacing the thermoset tow-preg with a thermoplastic one. Consolidation occurs during winding by the application of heat and pressure to the region of fibre laydown. Reports [18] indicate advantages such as higher fracture toughness, recyclability, unlimited shelf life and reductions of volatile solvents although currently the process is slow and material costs are inhibitive. Whether thermoset or thermoplastics are used, filament winding is generally only useful for parts with circular or near-circular cross sections and convex surfaces [11] and is limited to fibre orientations of between 15 and 85 degrees.

Automated Tape Placement

Automated tape placement (ATP) is a reliable, cost effective process for fabricating large parts with relatively simple contours [11]. It involves dispensing pre-impregnated thermoset or thermoplastic tape, typically between 25mm and 300mm wide, directly onto a tool or mandrel. An application roller stays in contact with the tape over the mould surface and (with the addition of a heat source for thermoplastic tape) provides enough pressure to consolidate the material. As for filament winding, thermoplastic tapes are consolidated *in-situ* whilst thermoset tapes must be cured in a separate operation, usually by autoclave. Many of the large US aerospace corporations use ATP in the manufacture of structural components including Bell Helicopter Textron [6] who manufacture wing skins for the V-22 Osprey tilt-rotor aircraft from thermoset pre-impregnated carbon fibre. Thermoplastic automated tape placement systems are also being investigated by NASA [19] and the University of Delaware [20] for their potential to reduce manufacturing costs. The major drawback of ATP is the inability to form to large changes in fibre orientation and tool curvature. It is also limited to fibre paths that have equal lengths on

each edge of the tape because the tape is cut perpendicular to its length.

Tow-Preg Placement

Tow-preg placement is an innovative new technology that blends some features of filament winding with ATP into a single process [11]. A number of pre-impregnated (thermoset or thermoplastic) yarns are collimated into a wide band near the tool tip and applied onto a rotating mandrel under low tension by a compaction roller. The roller remains in contact with the tool to provide compaction and also allows processing into concave surfaces. The pre-preg tows are individually controlled so enabling the manufacture of 3D components using the minimum quantity of material.

A variety of tow-preg placement facilities have been set up at both research establishments [21,22] and by industrial corporations [23-25]. Several systems are available "off-the-peg" from the major manufacturers [26,27]. US aerospace organisations are researching the tow-preg placement process as a means of producing highly structural components such as Boeing 747/767 engine inlet cowlings and the aft fuselage from the V-22 [11]. Cincinnati Milacron produce the Raytheon Premier I business jet fuselage [28], generic helicopter rotor blade spars and RAH-66 Comanche upper tailcone spars [11]. Hercules have manufactured CH47 long range fuel pods [11]. A submarine dry dock shelter is being constructed by McDonnel Douglas Aerospace [23] and a variety of components are being produced for the F/A-18E/F fighter aeroplane by the Great Lakes Composites Consortium [24].

Automating the lay-up reduces the size restrictions associated with manual tailoring and enables parts integration. Materials utilisation is also high since tow is only laid on the mandrel where necessary. An example of the advantages of tow-preg placement can be seen in the production of the V-22 Osprey tilt-rotor grip assembly [29]. Bell Helicopter Textron and Automated Dynamics Corporation have produced a 38kg carbon fibre rotor grip assembly using tow-preg placement from just 5 parts (a 97% reduction in parts count compared to the traditional composite manufacture route of hand layup and filament winding). Manufacturing time was reduced from 728hrs to 163hrs and material waste

reduced by 92% to 3.2kg. Bell Helicopter predict that total savings for the grip manufacture over the full V-22 production run will be $100 million [25,29]. The main disadvantage of the process is its capital equipment cost which starts at around $2 million [27] and limits the technology to the large manufacturers and to high production runs of complex components. The process also uses pre-preg materials which are more expensive than purchasing the separate reinforcement and matrix systems and must be stored under cold conditions.

1.3 Liquid Composite Moulding

Liquid composite moulding (LCM) describes a family of processes where a liquid thermoset resin is forced through a dry fibre preform in a closed mould. The resin may be forced through the preform by applying a positive pressure to the resin via a pressure pot or positive displacement pump, by applying a vacuum or by a combination of the two. Two processes of interest are resin transfer moulding (RTM) and structural reaction injection moulding (SRIM) [30]. Both rely on the same basic principles: A dry fibre preform, formed and cut to shape, is placed in a mould tool. The tool is closed and a thermosetting resin is forced through the dry preform. The mould is usually heated to speed the resin cure. After the resin has cured, the mould is opened and the composite part is ejected and deflashed as necessary.

RTM is a low pressure (typically less than 6 bar) process involving the use of thermosetting resins. Mould filling usually takes between one and ten minutes depending on component size and complexity [7]. Because of the low flow rates and pressures involved, the forces needed to clamp the moulds are small, allowing low cost composite moulds to be used for small production runs. SRIM differs from RTM in that the process uses a two-component resin system that is mixed just prior to injection into a mould cavity containing the reinforcement. In the mould cavity, the resin rapidly reacts and cures to form the composite part. To achieve adequate mixing of the reactant monomers, they must be injected at high speed. This makes SRIM a higher pressure process (in the region of 20bar) requiring high clamp forces (200 tonne) and metal tooling.

Many industrial manufacturers are interested in LCM because, apart from the traditional advantages of composites, LCM offers potential energy reductions and low mould clamping forces. Lee [30] states that the energy required to produce an LCM component is one quarter of that required to manufacture a comparable steel unit. Mould clamping forces are also low compared with compression moulding [30]. The automotive sector has recently produced a range of LCM components. Ford have launched several RTM parts including the Escort Cosworth rear spoilers, Escort/Sierra Cosworth undershield [31] and Transit van roof [8] as well as running a pilot production run of 5000 structural crossmembers manufactured by SRIM [32]. Automotive applications produced by LCM range from small components such as bumper beams and instrument panel supports [30] to complete car body panels including the Lotus Elan and Dodge Viper [31].

The aerospace industry is another source of increased LCM activity where the versatility of the process allows for the production of high performance structural components. Conventional composites manufacturing processes for the aerospace sector use autoclaves for the consolidation and curing of the component which require heavy investment in capital equipment. RTM is believed to be a good example of a process that could lower the manufacturing costs of advanced composites [30]. Several high performance components are being manufactured by LCM, including the wing flap seals and vertical tail ribs used on the US Navy F/A-18E/F fighter plane [4], tail rotor driveshafts and quill shafts used on the RAH-66 Comanche helicopter [33], blocker doors for Boeing 747 and 777 aircraft [34], aeroplane and hovercraft propeller blades manufactured by Dowty Aerospace [35] and wing rib skin tensioner and propeller spinners for kitplanes [36].

Although LCM is a semi-automated process, research is aimed at reducing the cycle times. Rudd et al [37] showed that injecting cold resin into a hot mould caused mould quench which accounted for 60% of the cure cycle time. Microwave pre-heating of the resin prior to injection [38] reduced mould quench and cycle times by 36%. Further study by Blanchard [39] showed that by using two stage initiator systems, RTM cycle times can be reduced by 48%.

1.4 Preforms for Liquid Composite Moulding

Apart from being a low cost process, one of the benefits of LCM is that it allows the user to design and manufacture preforms using a wide variety of reinforcement. The separation of the preform and moulding processes allow large, complex, net-shape, structural, preforms to be manufactured at precise fibre volume fractions and at low cost. The flexibility of the process enables reinforcement to be oriented with the load path as well as allowing the use of a variety of reinforcements. Although much research has been performed on reducing cycle times, it is widely agreed **[40,41]** that, for LCM, the overall part completion time is dependent on preform manufacture. The conventional approach to the manufacture of structural preforms involves manual tailoring, i.e cutting each ply from roll stock material and stacking in a forming tool. The reinforcement is heated to soften any thermoplastic binder present and then consolidated in the tool. Subsequent cooling of the reinforcement stack solidifies the binder, forming the reinforcement to the required shape. This method, although allowing flexibility through the use of various roll-stock materials, is only suitable for low volume applications due to its reliance on manual intervention at all stages. Automation of the preforming process is seen as essential to increasing the throughput and repeatability of components manufactured by LCM **[4,10,42]**. The following section reviews some of the automated processes used to manufacture structural preforms for LCM.

Thermoforming

Continuous filament random mat (CFRM) consists of multiple layers of random glass fibre oriented in a swirl pattern and usually include a thermoplastic binder. Plies of CFRM are cut to shape and stacked usually in a pinch frame to hold the reinforcement. Heat is then applied to the stack so that the thermoplastic binder melts. The reinforcement is then placed in a matched die and stamped to the required shape. The reinforcement is allowed to cool sufficiently to solidify the binder and the preform is ejected from the tool. Trimming of the preform is usually necessary to remove excess reinforcement and to produce a net shaped preform ready for moulding. This process has advantages over the conventional tailoring approach in that it is easily automated, although because of the random nature of the reinforcement, it is not suited to critical applications such as highly

loaded components. The process also generates high levels of waste [43] and can suffer from localised tearing and wrinkling when forming to complex shapes [44].

Like CFRM, textile reinforcements such as woven cloth can be preformed by hot stamping. By using aligned textile fabrics, preforms with improved structural properties can be manufactured. The process offers potential for cost reduction [30] through low equipment and setup costs and the ability to work with a variety of material forms. However the process suffers from large levels of waste and the act of forming a 2D fabric over a 3D pattern will induce fibre reorientation. In the simplest form this will alter the structural properties and resin flow characteristics through the preform, but can also cause material tearing and wrinkling.

Although thermoforming of reinforcement is usually wasteful of material and suffers long cycle times due to manual intervention in the cutting and assembly stages, automation is possible. Canon BV [9] have produced a range of thermoforming preformers which are said to be capable of producing preforms in cycle times of 60-90 secs (excluding the final trimming stage which is still completed manually). In a similar process, American GFM Inc.[45] are able to produce preforms using a low cure UV binder. The process coats near net-shape, ultrasonically cut broadgoods with a UV sensitive binder that is cured under vacuum with the application of UV light. Although Buckley [45] states that the forming system is capable of curing an 8 layer preform (constructed from 460g/m^2 continuous strand glass mat) in 15 secs, the process is limited to UV transparent materials (which excludes carbon fibre) and in the depth of penetration of the UV light.

Automated Ply Cutting and Robotic Placement

Automated ply cutting machines [13] use laser, water or ultrasonics to cut reinforcement from roll stock. Although this reduces manual interaction, the reinforcement must still be stacked in the preforming tool, usually by an operator. Efforts have been made to reduce manual intervention further by integrating automated ply cutting stations within robotic CAD/CAM cells. Zhang and Sarhadi [14] describe a laser ply cutting device linked to a robotic tacking device by an electrostatic pick-and-place device. Robotic tacking

produces a handleable preform with automatically positioned plies, reducing manual error. Although the system is capable of switching between the manufacture of a range of components, automated ply cutting and robotic placement units suffer from high equipment costs and can be restricted to using either glass or carbon fibre reinforcement.

Two-Dimensional Braiding

Braiding involves interlacing three or more tows helically around a mandrel or core. It is a low-cost, repeatable process for the manufacture of net-shape preforms with torsional stability, shear resistance and good impact damage tolerance [30]. Braiding also allows inserts or holes to be built into the preform with a greater degree of stability than holes which have to be machined into the composite after moulding [46]. Examples of braided structures for LCM include hybrid composite propeller blades [35], and tail rotor driveshafts and quill shafts used on the RAH-66 Comanche helicopter [33]. Although preforms can be manufactured at rates consistent with high volume applications [47] the process is limited to the production of convex preforms. The process also suffers from preform size limitations and the control of fibre orientations and tow spacing over non uniform cross section components.

Three-Dimensional Braiding

This is an extension of the well established two dimensional braiding technology wherein the fabric is constructed by the intertwining or orthogonal interlacing of two or more yarn systems to form an integral structure [48]. The braid carriers do not move in a circular "maypole" manner as for two dimensional braiding but in a pre-programmed, discreet series of motions depending on the cross section of the preform being manufactured. One of the advantages of the three dimensional braiding process is reported to be that the integral structure of the preform results in a damage resistant structure [49] although the process is essentially limited to producing components of constant cross section such as I-sections [49] and T-sections [50] which have limited appeal in composites manufacture.

Three-Dimensional Weaving

Three-dimensional woven fabrics are produced by many different processes but possibly

the most important method currently is the multiple-warp weaving method [48]. This differs from the normal weaving process in that some of the warp yarns are moved through the thickness of the fabric to build up a three-dimensional structure. By incorporating these through thickness fibres, three-dimensionally woven structures exhibit damage tolerance [51] but suffer from reduced in-plane properties. Three-dimensional woven fabrics possess good dimensional stability in two mutually perpendicular directions permitting easy handling of fabrics into moulds [52]. The flexibility of the process also allows fabrics to be manufactured with improved drape properties or reduced crimp [52]. However, fabric architectures are constrained to 0° and 90° orientations and the preforms are limited to near constant cross section or tapered sections such as solid orthogonal panels, box-beams or I-sections [48]. The process is also slow and capital equipment can be expensive.

Knitting

Both warp and weft knitting offer potential for automated preform manufacture. Warp knitted fabrics are multi-axial structures developed for multidirectional reinforcement of composites. Multiple layers of linear yarns are assembled in warp (0°), weft (90°) and bias ($\pm\theta$°) directions to provide in-plane reinforcement in specific directions, and are stitched together by knitted yarns to provide structural integrity and through thickness reinforcement [53]. The main drawback to warp knitted structures are that they are limited to flat fabrics. Weft knitted preforms can be produced in complex net-shape 3-D shell forms. The knitted structure results in a reinforcement that is highly compliant which can undergo high levels of deformation. This is partly due to the looped structure of the reinforcing fibres. This looped structure, however, causes local stress concentrations that can induce fibre breakage reducing the mechanical properties of the reinforcement. Because of the addition of through thickness fibres, through thickness strength and impact damage resistance are very good compared to traditional composites [46] but in-plane mechanical properties suffer.

Embroidery

Embroidery offers the potential for producing net-shaped preforms by fastening high

modulus fibres onto a carrier cloth in the desired orientation. Its main advantage, compared to other textile preforming processes, is the ability to arrange the fibres in any direction within the plane and also along curved paths [54]. When holes or cut-outs are introduced to a component, the lines of maximum stress flow around the holes in curved paths. Using conventional reinforcement with straight fibres would not provide maximum structural integrity for the component. Crothers et al used FEA to help orient reinforcing tows to minimise shear stresses between adjacent fibres [55] and showed that load to failure can be increased by 45% for open hole tension specimens. The process has been used to manufacture composite cycle brake boosters, mountain bike suspension link plates and a bicycle frame [56]. It is reported that embroidery is best suited to components requiring local reinforcement around areas such as fasteners or cut-outs [57] because of the time required to stitch large areas of reinforcement.

Tow Placement

It is believed that the automated direct placement of fibres is one of the most promising fabrication methods for rapid, cost effective, net-shape composites manufacture [47,58-60]. Similar to the tow-preg placement process described in 1.2, tow placement describes the automated placement of dry tows onto a flat 2-D surface or into a curved 3-D tool. The difference between tow-preg placement and tow placement is that tow-preg placement uses pre-impregnated tow to build up reinforcement onto a rotating mandrel whereas tow placement uses dry fibres to build up a preform for LCM. The process combines the advantages of tow-preg placement with those of LCM to provide a low-cost, net-shape automated composite manufacturing system. Very little work has been performed on direct tow placement. Jander [61] has described equipment to produce oriented fibre preforms by spraying continuous tows onto a preform screen in a similar manner to chopped fibre spray-up. A further process was developed by McGeehin [59] and Long [58] who produced an effective design and manufacture system using an airjet to deposit random or directional fibres onto a flat bed. The system allowed for flexibility with the ability to place reinforcement along any straight or random path and has been used for the successful prototyping of a Ford Cosworth undershield. The process has also been shown to reduce preforming times by 10% and material waste by 15% for the

manufacture of a Dowty Aerospace General Aviation propeller blade compared to manual tailoring methods. Although the systems developed by Jander and by Long and McGeehin attempted to automate the production of structural preforms, both methods still required manual intervention and suffered from poor reinforcement positional accuracy.

Although the preforming processes described above are suitable alternatives to manual tailoring, they only offer limited appeal such as the manufacture of near constant cross-sectional components, convex parts, or the processes are expensive, inaccurate, time consuming or wasteful of material. There remains a requirement in industry for a low-cost, near net-shape preforming process that offers design flexibility with low waste and no restrictions on component geometry, size or material. It is this need for a preforming process for structural components which has resulted in the project from which this thesis was drawn.

1.5 Project Objectives

This work was performed within the DTI/EPSRC LINK Structural Composites project "Application of Advanced Preforming Methods for Liquid Composite Moulding". The project follows a previous LINK project, "Preforms for Liquid Moulding Processes" **[58,59]**

Current industrial practice involves the use of tailored mats and fabric reinforcement which is very laborious and wasteful of material. Problems with current automated manufacturing processes include high levels of materials waste, long cycle times or restrictions to certain shapes and sizes of components. The objectives of the LINK project were to design, develop, manufacture and prove the elements of a CAE system for the design and manufacture of fibre preforms. A CAE system enabled a three dimensional preform to be designed to meet the structural requirements of the part. This 3D geometry was then "undraped" to yield a flat blank shape that was manufactured using a high speed placement device and post-formed. Particular objectives of this thesis were:

- To identify techniques for fibre deposition, retention and consolidation.

- To perform processing and performance studies on preforms produced using the laydown facility.
- To reduce preform cycle time, waste and manual intervention.
- To show the applicability of the design and manufacturing system for industrial components.

Four research papers have been published or accepted for publication as a result of the work performed within this project (see Appendix 1.1)

1.6 Theme of this Work

This thesis is concerned with the design and manufacture of preforms for liquid moulding. A drape algorithm developed under a previous research programme [58] was used to anticipate possible preforming problems and to help manufacture preforms that are more flexible from a design viewpoint than commercial reinforcements. The preforms were manufactured using a 4-axis fibre placement machine that allowed accurate placement of up to five tows of fibre in any desired 2D path.

One of the main focuses of the project was the development of the fibre placement cell. The effects of process parameters on the performance of reinforcement produced using the tow placement facility are reported and optimum conditions are described. Developments to allow multiple fibre laydown (glass or carbon) with accurate control are presented which allowed novel preforms to be manufactured and enabled the validation of processing and performance models.

The drape algorithm was used to anticipate fibre movements within preforms during forming. Re-arrangement of the fibres within a 3D model enabled the preform to be designed with an optimised user-defined fibre architecture. Using an algorithm to undrape (mapping the fibres from the 3D model back to a flat sheet) the 3D model created a net-shape 2D map of the desired fibre paths. Production of the 2D fibre laydown using the laydown facility and subsequent forming into its 3D shape created a preform with fibres

positioned in their designed architecture.

Models to predict the processing and performance of preforms produced on the fibre laydown facility are presented. The models which predict permeability and tensile modulus allowed for fibre waviness, which occurs in tow placed and woven reinforcement and were validated using the facility to produce preforms with controlled sinusoidal tow paths.

Finally three case studies are used to show the application of this work. A Dowty Aerospace propeller blade shows the application of the tow placement facility to produce preforms with reduced waste and cycle times compared to manual tailoring. A power bulge is used to highlight fibre deformation problems and the subsequent adjustment of fibre paths to reduce these problems. The application of the design and manufacturing unit to produce high performance parts is demonstrated for a Rolls Royce aero engine outlet guide vane (OGV).

List of Figures

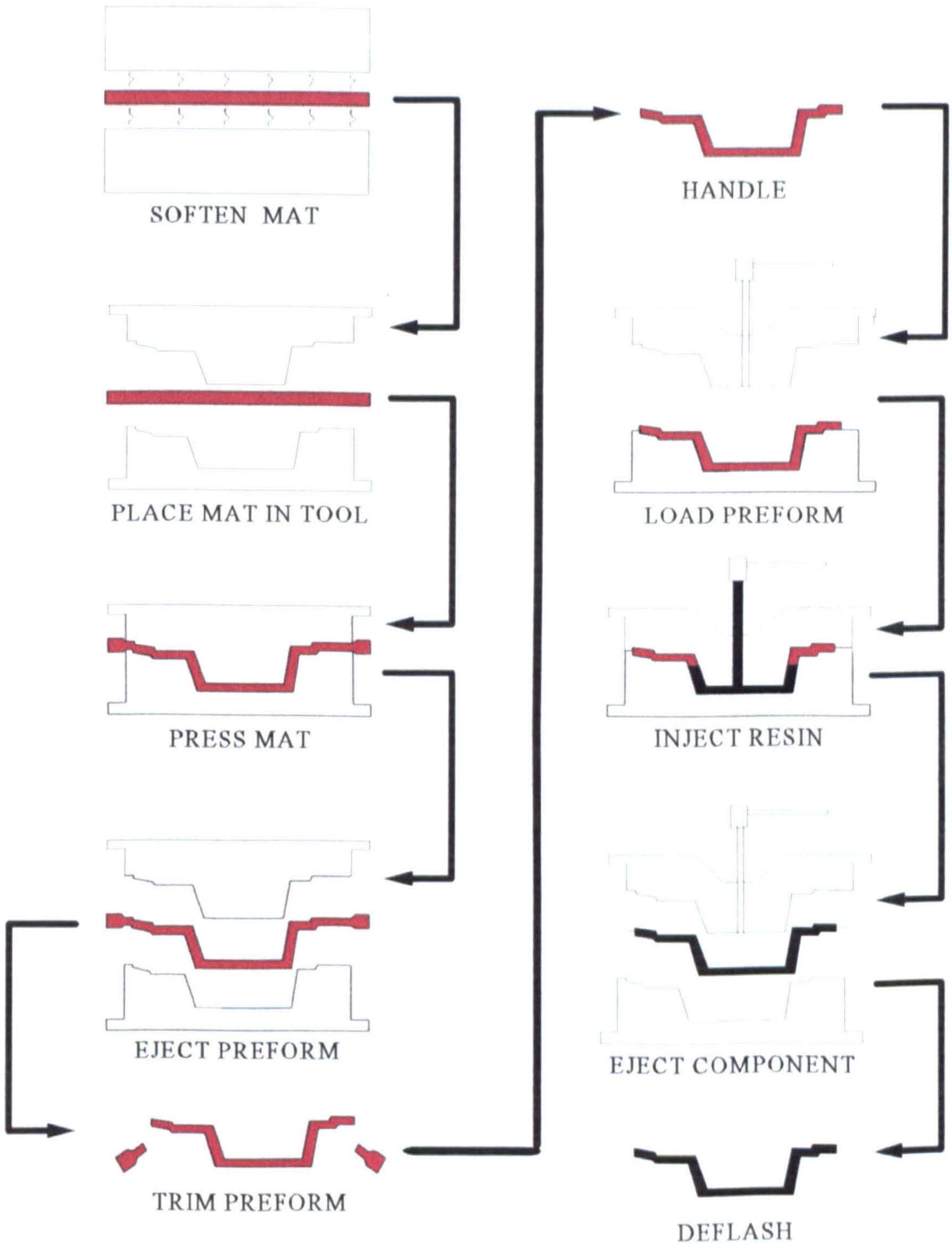

Figure 1.1 [38] Schematic of Liquid Moulding Process

Chapter 2
Literature Review

2.1 Introduction

This chapter discusses the current literature relating to the manufacture of composites by LCM. Processing considerations such as methods for determining preform permeability are reviewed. Preform design considerations such as performance properties are then considered. Both processing and performance properties are seen to be highly dependent on fibre architecture that is affected in turn by fibre waviness and by fibre deformation during post forming. Models to predict the processing and performance characteristics of preforms are described along with a review of existing deformation modelling techniques with consideration given to the optimisation of the deformed fibre structure.

2.2 Prediction of In-Plane Permeability

Several issues must be addressed to ensure that a preform is suitable for the desired application. The primary concern with preforms for LCM is resin impregnation. Prediction of the resin flow front during the mould filling stage is useful in addressing critical issues such as anticipation of dry spots and voids which can occur at merging flow fronts [62]. The accurate prediction of preform permeability will allow the designer to optimise the mould design, preform layup and processing conditions prior to the mould being built, thus avoiding potential problems. Flow of resin through a preform is widely modelled by Darcy's law [63] which describes the flow of a Newtonian fluid through a porous medium and relates the fluid flow to the pressure gradient using the fluid viscosity and preform permeability:

$$Q = -K \frac{A}{\mu} \frac{\Delta P}{L} \qquad (2.1)$$

The constant, K, is termed the permeability (units m^2) and is a measure of the ease with which fluid will permeate the reinforcement. The permeability of a preform is usually calculated from measured values of flat reinforcement. Measurements are conducted

either in rectilinear or radial flow rigs. The rectilinear approach measures the flow of a liquid through a reinforcement placed in a rectangular mould. The approach is simple but allows only the permeability in one direction to be calculated for each experiment and can incur potential errors from mould edge effects [64]. Hirt et al [65] and Adams et al [64] developed a radial flow technique that enabled measurement of both principal permeabilities without errors induced from mould edge effects. The method involved injecting oil under constant pressure through a reinforcement retained in a circular cavity. Reinforcement permeability was determined by measuring the rate of change of the fluid flow front position which was measured by employing a clear glass or acrylic sheet as the top mould plate. The low stiffness of such clear plates allowed for mould deflections at high pressures and this led to the development of a technique by Chick et al [66] which used constant flow rate injection. Permeability was determined from the pressure changes at points along orthogonal axes within the mould, enabling a stiff metal mould to be employed thus reducing cavity distortion.

Although accurate measurements of reinforcement permeability can be obtained from experimental analysis, such investigations are very labour intensive as experiments must be performed for each reinforcement. In an attempt to reduce the number of tests to determine permeability and to reduce manual errors, several models have been developed for predicting the in-plane permeability of a reinforcement. The Kozeny-Carmen equation is the most common [67]. This was originally developed for granular beds consisting of ellipsoids and models the variation of permeability with fibre volume fraction:

$$K = \frac{R_f^2}{4c} \frac{(1 - V_f)^3}{V_f^2} \qquad (2.2)$$

where c is termed the Kozeny constant and is determined experimentally. Cai [68] reports that problems exist in choosing an accurate value of Kozeny constant with values between 0.38 and 0.7 reported for flow through homogeneous graphite fibre beds. A further problem with this model is that the predicted permeability is isotropic which is clearly untrue for a unidirectional reinforcement. The model does not account for flow

restrictions in the transverse direction although Kardos [69] has suggested using the same formula as in equation (2.2) but using a modified Kozeny constant of 11.0 thus producing a permeability ratio in the longitudinal to transverse fibre directions of around 19 to 1.

Gutowski et al [70] proposed an adaptation to the Kozeny-Carmen model for transverse permeability by taking account of the maximum fibre packing density:

$$K_2 = \frac{R_f^2}{4c_2} \frac{\left(\sqrt{\frac{V_a}{V_f}-1}\right)^3}{\left(\frac{V_a}{V_f}+1\right)} \qquad (2.3)$$

where V_a is the so-called available fibre volume fraction at which transverse flow stops and c_2 is the Kozeny constant in the transverse direction. Gutowski et al measured c_2 to be about 0.2 for a unidirectional carbon fibre bed [70] whilst V_a was determined to be around 0.8 to 0.85.

The problem with equation (2.3) for predicting transverse permeability is that the model parameters still have to be determined experimentally. Gebart modified the Kozeny-Carmen equation and the Gutowski model by taking into account the detailed geometry of the fibrous reinforcements used in composites processing [71]. Gebart suggested that the fibres of a unidirectional reinforcement would be packed in a quadratic or hexagonal structure. He also proposed that the flow of fluid through the reinforcement can be split into the macroscopic flow around the fibre bundles and microscopic flow through the tows. As a result he suggested using an effective fibre radius, R_{eff}, which is an averaged value falling between the filament and tow radii that is found by curve fitting to experimental data. The permeability for both cases of quadratic and hexagonal arrangement of fibres can be written as:

$$K_1 = \frac{8\ R_{eff}^2}{d_1} \frac{(1 - V_f)^3}{V_f^2} \qquad (2.4)$$

where equation (2.4) describes the permeability to flow along the fibre axis and equation (2.5) predicts the permeability across the fibres. The parameters d_2 and $V_{f\max}$ in equation (2.5) depend only on the fibre arrangement (hexagonal or quadratic) whereas the shape

$$K_2 = d_2 \left(\sqrt{\frac{V_{f\max}}{V_f}} - 1 \right)^{\frac{5}{2}} R_{eff}^2 \qquad (2.5)$$

factor d_1 is related to the Kozeny constant, c, as $d_1 = 32c$. Excellent agreement was reported [71] between experimental and theoretical results, but this relied on the shape factors d_1 and d_2 and the effective fibre radius R_{eff} being chosen to fit the experimental data.

2.3 Prediction of Mechanical Properties

In the aerospace industry and other sectors that use high performance materials, the attraction of polymer composites lies in their high specific structural properties such as strength and stiffness. The ability to tailor mechanical properties by placing reinforcing fibres along lines of maximum stress allows the manufacturer to gain the greatest structural potential from the composite. Two methods are commonly used to predict the stiffness of a composite with a specific fibre architecture.

Reinforcement Efficiency

A simple method of predicting the laminate modulus can be made using the modified rule of mixtures:

$$E_1 = \eta E_f V_f + E_m(1-V_f) \qquad (2.6)$$

This uses the load bearing efficiency, η, of the reinforcement defined by Krenchel [72] to predict the effect of fibre orientation. on laminate stiffness:

$$\eta = \sum a_n \, Cos^4\theta_n \qquad (2.7)$$

This efficiency factor is based on the orientation, θ_n, of the fibres with respect to the direction of loading. For a unidirectional laminate with fibre and load axes parallel the efficiency factor is equal to one. When load is applied perpendicular to the fibre axis, the efficiency of the reinforcement becomes zero. Although research [67] has shown that the model can give a reasonable estimate for composite stiffness, the approach is simplistic and neglects the effects of transverse deformation (Poisson effects) which becomes increasingly important as the fibres become transverse to the load.

Classical Laminate Model

The classical laminate approach to predicting laminate stiffness is well documented for the design of composite structures [73-75]. The model is less restrictive than the modified rule of mixtures approach given above in that it includes the effects of shear modulus and Poisson's ratio in the calculation of laminate stiffness. In its basic form, for a single ply, classical laminate analysis uses matrix notation to show the relation between on-axis stress and strain:

$$\begin{bmatrix} \varepsilon_1 \\ \varepsilon_2 \\ \gamma_{12} \end{bmatrix} = \begin{bmatrix} S_{11} & S_{12} & 0 \\ S_{12} & S_{22} & 0 \\ 0 & 0 & S_{66} \end{bmatrix} \begin{bmatrix} \sigma_1 \\ \sigma_2 \\ \tau_{12} \end{bmatrix} \qquad (2.8)$$

where:

$$S_{11} = \frac{1}{E_1} \;,\; S_{22} = \frac{1}{E_2} \;,\; S_{12} = -\frac{\nu_{12}}{E_1} \;,\; S_{66} = \frac{1}{G_{12}} \qquad (2.9)$$

Equation (2.8) is termed the on-axis compliance matrix and is useful for predicting the material elastic properties when a unidirectional laminate is subjected to loading along the principal material directions. However, as the majority of composites are manufactured from laminates with different fibre orientations and loading is not always applied along the principal material directions, it becomes necessary to translate the on-axis compliance

matrix to an off-axis compliance matrix. Morley [74] describes the application of a transformation to equation (2.8) that enables the stiffness of a laminate to be predicted where the laminate principal fibre direction is at an angle, θ, to the loading axis:

$$\begin{bmatrix} \varepsilon_x \\ \varepsilon_y \\ \gamma_{xy} \end{bmatrix} = \begin{bmatrix} \overline{S_{11}} & \overline{S_{12}} & \overline{S_{16}} \\ \overline{S_{12}} & \overline{S_{22}} & \overline{S_{26}} \\ \overline{S_{16}} & \overline{S_{26}} & \overline{S_{66}} \end{bmatrix} \begin{bmatrix} \sigma_x \\ \sigma_y \\ \tau_{xy} \end{bmatrix} \tag{2.10}$$

where:

$$\begin{aligned}
\overline{S_{11}} &= S_{11}\cos^4\theta + S_{22}\sin^4\theta + (2S_{12} + S_{66})\sin^2\theta\cos^2\theta \\
\overline{S_{12}} &= S_{12}(\cos^4\theta + \sin^4\theta) + (S_{11} + S_{22} - S_{66})\cos^2\theta\sin^2\theta \\
\overline{S_{16}} &= (2S_{11} - 2S_{12} - S_{66})\sin\theta\cos^3\theta - (2S_{22} - 2S_{12} - S_{66})\sin^3\theta\cos\theta \\
\overline{S_{22}} &= S_{11}\sin^4\theta + S_{22}\cos^4\theta + (2S_{12} + S_{66})\sin^2\theta\cos^2\theta \\
\overline{S_{26}} &= (2S_{11} - 2S_{12} - S_{66})\sin^3\theta\cos\theta - (2S_{22} - 2S_{12} - S_{66})\sin\theta\cos^3\theta \\
\overline{S_{66}} &= 2(2S_{11} + 2S_{22} - 4S_{12} - S_{66})\sin^2\theta\cos^2\theta + S_{66}(\sin^4\theta + \cos^4\theta)
\end{aligned} \tag{2.11}$$

The properties of a multi-axial laminate are found by averaging the individual ply properties with respect to the laminate thickness.

Measurements from pre-sheared aligned reinforcements [67] have shown that the classical laminate model of predicting off-axis laminate stiffness gives a better approximation to experimental results than the modified rule of mixtures approach. This is especially so for ply angles above ±45° where transverse deformation and Poisson's effect play an important role in the material stiffness.

2.4 Fibre Movement During Forming

A very important issue in preform manufacture is to ensure that the reinforcement can actually be formed to the required shape and to understand the consequences of forming. Ideally it would be desirable to determine whether a geometry can be preformed to allow

for redesign in the early stages of part development. The main problem occurs when fabric, usually a bi-directional woven or stitch bonded non-crimp fabric, is stamped or formed, causing the reinforcing fibres to re-orientate. In simple cases, these fibre movements will result in deviations in fibre volume fraction and orientation resulting in discrepancies from the expected processing and performance properties of the preform. In extreme situations, the fabric will deform to such an extent that wrinkling or buckling will occur thus making the preform unusable. An understanding of the reinforcement structure after the preforming process is required to enable efficient materials utilisation and controllability of the performance and properties of the three-dimensional preform [76].

Several researchers have developed fabric deformation or "drape" models to account for fibre movements during the forming stage [77-82]. The majority of these models are based on the relatively simple principle developed by Mack and Taylor [83] who considered a bi-directional material to be analogous to a pin-jointed net with inextensible yarns. This kinematic approach assumed that the only fabric deformation mode was by simple shear. Mack and Taylor developed differential equations to identify the yarn orientations when a fabric was draped over a sphere. Development of these ideas by Van West [80] led to the modelling of a woven fabric draped over an arbitrary surface. The modelling involved the iterative solution of three non-linear simultaneous equations, representing the possible end points of the warp and weft fibres and the surface of the draped component. Long [81] developed a PC based kinematic drape model which differed from previous models by solving the solutions to the fibre crossover points explicitly by describing the drape surface as a series of flat patches (see Appendix 6.1).

As well as there being several research codes for drape analysis there also exist commercial models for predicting fabric deformation. Both Composite Design Technologies and MSC use fabric deformation codes in their commercial software. Composite Design Technologies use a drape code in their FiberSIM composite manufacturing simulator [15] and MSC use one in their Patran Laminate Modeller [84].

Although experimental analyses support the use of a purely kinematic (pin-jointed) approach for small levels of fabric deformation [77], at more severe levels of deformation, as the fibre locking angle is approached, relative fibre slip becomes increasingly important [85]. Although the current models cannot predict locking angle or relative fibre slip, they are still an effective tool to warn of possible areas of wrinkling brought on by high levels of shear.

As well as causing potential formability problems, fibre movement during the preforming operation can also have significant impact on reinforcement permeability and composite mechanical performance.

Although computer flow analyses of LCM processes exist, most users assume the preform to have constant permeability throughout the mould cavity. This is not true for real preforms, which are stretched and sheared during forming [86]. Several experimental studies have been performed to integrate the effects of fabric deformation during the preforming stage with flow analyses of the deformed reinforcement [86-88]. Although predictions show that reinforcement deformation during preform manufacture could have a significant effect on the filling phase during LCM [86,87], there exist many problems in predicting such effects. Bickerton et al [88] described difficulties in predicting flow front shapes that were attributed to several mechanisms: reduced permeability arising from an increased volume fraction, subsequent reduction in the volume of fluid required due to the increased volume fraction, and fibre re-orientation causing the principal permeability components to change direction. Smith et al [67] also found the interaction between fabric shear and permeability to be a complex one where permeability changes with varying ply angles due to the combined effect of fibre orientation and increased volume fraction.

Local fibre re-orientation and volume fraction changes within the preform due to reinforcement deformation also affect the mechanical performance of the composite part. Smith et al [67] performed tensile tests on sheared woven and engineered fabrics and showed that reductions in ply angles from ±45° to ±25° typically increased tensile modulus

by 100%. Cucinella et al [89] also performed studies on the effect of fabric deformation on mechanical properties and showed that significant fibre re-orientation occurred during the forming of a prototype wheel hub manufactured from stitch bonded 0°/90° fabric, resulting in large variations in fibre volume fraction. The effects of these changes in fibre orientation and volume fraction were highlighted by the variation in compressive stiffness of up to 31% around the edge of the component.

Although drape models are being developed to predict limitations such as the potential problems with resin flow through the deformed fibre architecture and mechanical properties of the finished component, researchers have suggested that it would be better to use drape models in reverse [58,80,90]. It would be preferable to design the 3-D fibre architecture of the finished component rather than predict the architecture resulting from deformation of a flat reinforcement. This would provide the designer with a more suitable and stable platform from which to design and assess the processing and performance characteristics of the preform by knowing exactly where the fibres will be positioned. Long [58] suggested a computer integrated design and manufacturing system, in which deformation modelling is used to assess the quality of any particular fibre laydown design. Long considered the possibility of using drape analysis in reverse to "undrape" an optimised fibre architecture 3-D component to a flat two-dimensional sheet that could be produced using a direct fibre placement system. Modelling studies on optimising an automotive component revealed that optimisation of the fibre paths could reduce volume fraction variations and avoid problems with wrinkling although no experimental validation was performed.

Although orienting fibres in composites for purposes such as coincidence with major stress paths has been considered for automated manufacturing routes such as filament winding [91], tape placement [6] and fibre placement [25], the only production technique for oriented fibre placement for LCM is by embroidery [54]. It is with this requirement for an improved design and manufacture system that this thesis is based.

2.5 Effects of Fibre Misalignment/Waviness

Although the processing and performance of preforms is affected by fibre movement during the preforming process, fibre misalignment especially in the form of fibre waviness can also cause problems. Fibre waviness can occur in many types of reinforcement but is mostly found in woven fabrics due to the crimp between the warp and weft yarns.

Permeability

As has been described in 2.2, preform permeability is usually determined either from measured values of flat reinforcement or by predicting the properties of the preform using one of the permeability models (Kozeny-Carmen, Gebart etc.). The permeability models described earlier rely upon unidirectional reinforcement and do not take account of the waviness found in many reinforcements. Advani et al [63] cited fibre preform waviness to be the most uncontrollable and unpredictable effect responsible for inconsistent permeability results. To account for fibre waviness, a tortuosity factor can be applied to the Kozeny-Carmen capillary model (eqn 2.2):

$$K = \frac{R_f^2}{4\,(L_e/L)^2\,c_t}\,\frac{(1 - V_f)^3}{V_f^2} \qquad (2.12)$$

where L_e is the length of the actual flow path, L is the length of the porous medium and c_t is a dimensionless shape factor for the tortuous flow. However, because c_t is still an experimental parameter, it can be shown that $(L_e/L)^2 c_t$ is equal to the Kozeny constant c in equation (2.2). Equation (2.12) still suffers from the same limitations as the Kozeny-Carmen model: it only models non-Newtonian fluids, gives poor transverse predictions, assumes isotropic flow and is a semi-empirical equation. However it can be useful as a qualitative method.

Mechanical Properties

Fibre misalignments and fibre and ply waviness are believed to be one of the most significant factors affecting the tensile and compressive behaviour of composites [92-94]. As well as fibre waviness in the form of the crimp of a woven fabric, fibre and ply

misalignments can also be induced in a variety of manufacturing processes. Wrinkles may occur due to part-tool interaction (i.e. thermal expansion mismatch) or instabilities during the forming operations [94]. Ply waviness is also found in processes such as filament winding where post-consolidation processes can induce waviness in the hoop layers.

The effects of fibre waviness on the mechanical properties of otherwise unidirectional composites have been investigated by several researchers. Bolotin [95] first developed expressions for the modulus of composites containing random initial irregularities which were reduced to sine waves and predicted a linear relationship between compliance and the square of the angular deviation:

$$E_x = \frac{E_1 G_{12}}{G_{12} + \delta^2 E_1} \tag{2.13}$$

where δ^2 is the mean square angular deviation of the fibre from the principal direction and can be calculated from:

$$\delta^2 = 2\pi^2 \frac{a^2}{\lambda^2} \tag{2.14}$$

Chou and Ishikawa [96] developed three analytical models for the stiffness of woven fabric composites. Their work in creating a "fibre undulation model" uses the classical laminate approach to predict stiffness. Bogetti et al [94] also used classical laminate theory to predict the behaviour of thermoplastic composites with layer waviness. Their analysis predicted individual ply stress and strain distributions and found that stiffness reduction due to ply waviness was most significant in the direction of ply undulation but other in-plane mechanical properties were relatively insensitive to ply waviness. The classical laminate method has been used as the basis for work by many other researchers [97-99] where the effective modulus at an out-of-plane angle, θ, is given by:

$$E_x(\theta) = \frac{1}{\overline{S}_{11}} \tag{2.15}$$

Many of the models assume waviness to be modelled by a sine wave. Chan and Chou [97] and Rai et al [98] modelled fibre waviness by assuming the effective modulus of a composite constructed of sinusoidal fibres to be obtained using the average strain approach:

$$E_x = \frac{\overline{\sigma_x}}{\overline{\varepsilon_x}} = \frac{\lambda}{\int_0^{\lambda} \overline{S_{11}}\, dx} \qquad (2.16)$$

where $\overline{S_{11}}$ is the reduced compliance for a ply oriented at an angle, θ. As θ varies along the axis of the sine wave, the effective stiffness is calculated by numerical integration.

Although several models exist for the prediction of composite mechanical properties with fibre or ply waviness, few validations have been presented due to difficulties in producing samples with controlled fibre waviness. Mrse and Piggot [100] tested a series of unidirectional carbon pre-preg samples which had been crimped to various degrees to vary the fibre waviness. They reported a reduction in compressive strength and modulus due to fibre waviness that correlated with Bolotin's model. Hsaio and Daniels [99] also report significant reductions in compressive modulus for carbon composites containing uniform fibre waviness. A reduction in compressive modulus of 42% was noticed for samples containing only 4.3% waviness (determined as the ratio fibre amplitude to wavelength) which compared well to the classical laminate approach shown in equation (2.16). Although Mrse and Piggot and Hsaio and Daniels have reported some work on the effects of fibre waviness on composite performance only compressive properties were analysed. The method of imposing sinusoidal waviness also allowed for inaccuracies with Mrse and Piggot using a crimping tool utilising cylindrical rods and Hsaio and Daniels relying on local buckling of hoop wound tows in thick filament wound composites. Other limitations in the two studies include the range of materials and degree of fibre waviness used [99,100].

2.6 Summary

One of the most important concerns with designing preforms for LCM is modelling of the resin impregnation stage. Flow of resin through a preform is widely modelled on Darcy's law. The measurement of preform permeability is obtained by experiment. Several models exist for the prediction of permeability but most assume flow through unidirectional reinforcement and rely upon empirical terms to describe the fibre architecture which are specific to particular reinforcements. Also important in preform design is the ability to predict structural performance. Predictions for laminate elastic properties are commonly based on either the modified rule of mixtures or classical laminate analysis. Of these two models, classical laminate analysis has been found to offer better estimates of laminate behaviour but involves more complicated analysis.

The deformation of flat reinforcement to the final mould geometry causes fibre re-orientation within the reinforcement. This causes deviations in fibre volume fraction and orientation that result in discrepancies from the expected processing and performance properties, as well as potentially making the preform unusable due to reinforcement wrinkling and buckling. Several predictive studies have been performed on the deformation of aligned fabrics. The majority of these are based on a kinematic model that assumes the material to be analogous to a pin-jointed net structure. Although these models are reasonably effective at predicting the deformation behaviour of 2-D reinforcements, it has been suggested that it would be preferable to optimise the structure of the flat reinforcement to produce the desired properties in the formed component. However very little work has been reported on this process. As well as changes in fibre architecture during reinforcement post-forming, preform processing and performance characteristics are affected by fibre misalignments especially in the form of fibre waviness. Models have been proposed for the prediction of laminate elastic and preform permeability properties containing fibre waviness but very little work has been performed for model validation.

Based on the above observations an automated tow placement facility for the net-shape manufacture of preforms for LCM will be developed in Chapter 4. Process optimisation

of the tow placement facility will be reported in Chapter 4 including typical reinforcement processing and performance properties. The tow placement facility will be used to produce laminates with varying quantities of fibre waviness that will be used to validate processing and performance models in Chapter 5. Optimisation techniques for the manufacture by tow placement of net-shaped 2-D reinforcements which are post-formed to produce components with the desired properties are described in Chapter 6. Descriptions of the experimental procedures and equipment used in this project are provided in the following chapter.

Chapter 3
Experimental Techniques

3.1 Introduction

Experiments were performed to characterise the processing and performance of preforms manufactured using the tow placement facility. Particular attention was given to fibre movement during preforming, permeability of laydowns and composite mechanical properties. Work was also performed to validate processing and performance models described later in this thesis and to produce demonstrator components. The following chapter describes the materials and equipment used and the techniques applied to measure the properties. Particular attention is given to the RTM facilities used to produce test specimens and to the various test methods to measure material properties.

3.2 Materials

3.2.1 Reinforcement

Several different types of tow and fabric were used during the study as discussed later in this thesis. Table 3.1 summarises properties of the reinforcement materials used.

PPG 1062/2400 : This 2400 tex E-glass roving was produced from eight tows of 300 tex strands coated with a silane based size treatment. The material was used in the manufacture of tow placed preforms for the validation of processing and performance models as described in Chapters 4,5 and 6.

Tenax HTA 5131 : This standard modulus 6k, 400 tex carbon filament yarn was treated with an epoxy size. The yarn was used in the manufacture of tow placed preforms for the production of demonstrator components (Chapter 7) and to validate performance models as described in 5.2.3.

Tech Textiles E-LPb 567 : This quasi-unidirectional stitch bonded fabric was manufactured using 2400 tex E-glass rovings in the longitudinal direction with 10%

transverse fibres. The superficial density was 567g/m² with approximately 2% by mass PET thermoplastic binder. The fabric was used as a comparison for unidirectional preforms manufactured using tow placement.

Table 3.1. Reinforcement Material Properties (from manufacturers' data)

Manufacturer	Name	Style	Fibre Modulus (GPa)	Filament Diameter (μm)	Linear Mass / Superficial Density	Binder Content (%)
PPG	1062/ 2400	2400tex E-glass roving	84	13	2400g/km	0
Tenax	HTA 5131	12k carbon filament roving	260	7	400g/km	0
Tech Textiles	E-LPb 567	quasi-UD stitch bonded E-glass	70	15	2400g/km 567g/m²	2
Hexcel Composites	CGG 108-T300	five end satin weave ±45° 6k carbon fabric	230	7	400g/km 210g/m²	0
Flemings Fabrics	W/R 600	plain weave 0°/90° E-glass	72	15	1200g/km 600g/m²	4

Hexcel Composites CGG108-T300 : This was a five-end satin weave ±45° 6k carbon fibre fabric with a nominal superficial density of 210g/m². This material was used to quantify the effects of fibre waviness on tensile modulus as described in 5.2.5.

Flemings Fabrics W/R 600 : This 600g/m² plain weave bi-axial 0°/90° E-glass fabric was manufactured by Flemings Industrial Fabrics. The fabric was used to quantify the effects of fibre waviness on tensile modulus as described in 5.2.5.

3.2.2 Fluids

Several fluids were used to manufacture test specimens and prototype components and to measure permeability. Table 3.2 lists the properties of the fluids used.

Table 3.2. Properties of Fluids used in this Project (from manufacturers' data unless specified)

Manufacturer	Product	Type	Modulus (GPa)	Viscosity @ 25°C (mPa.s)
Cray Valley	Synolac 6345.001	unsaturated polyester resin in styrene	3.5	4600
Hexcel Composites	RTM6	mono-component pre-mixed epoxy resin	2.89	>5000
Ciba Polymers	LY/HY 5052	cold curing epoxy resin	3.15	700
Trent Oils	HDX30	mineral oil		180 *(m)*

(m) = measured value

Cray Valley Synolac 6345.001 : This was an unsaturated polyester resin in styrene mixed with 2% by mass Akzo Perkadox 16 Bis-(4-tert.butyl cyclohexyl) peroxydicarbonate initiator processed at 70-80°C. It was used in the manufacture of cold pressed, power bulge mouldings for the validation of fibre architecture optimisation described in 6.4.2.

Hexcel Composites RTM6 : This was a mono-component, pre-mixed, aerospace epoxy resin that was used in the manufacture of a prototype demonstrator component for Rolls Royce as described in 7.4.

Ciba Polymers LY/HY 5052 : This was a cold curing, low viscosity epoxy resin that was used to produce tensile test specimens as well as the hemispheres described in 6.4.1.

Trent Oils HDX 30 : This was a mineral oil that was used in the measurement of

preform permeability as described in 5.3. Viscosity vs. temperature data were measured for use in the measurement of permeability and a graph is shown in Figure 3.1.

3.2.3 Binders

Two different types of binder were used to manufacture test specimens and prototype components:

Fothergills Engineered Fabrics M0924/532 Admesh : This was a plain weave polyester fibre scrim with latex binder and polyester resin finish. The superficial density was 15.5g/m^2 and the scrim was used as an aid to fibre retention in the tow placement process.

DSM Neoxil 940 : This was a thermoplastic bisphenolic polyester resin powder and was also used to help bind tows in the manufacture of preforms by tow placement.

3.3 Preform Manufacture

Preforms were manufactured from roll-stock fabrics as described above and using tow placement by airjet and roller placement techniques as described in 4.4 and 4.5. The procedures for manufacturing preforms by these three methods are reported below.

3.3.1 Roll-Stock Preforms

The manual method of producing preforms was to cut individual plies from roll-stock. The plies were cut oversized and stacked in the required orientation. If no binder was present, DSM Neoxil 940 polyester binder was added using a salt shaker between the layers at approximately 5% by mass. The reinforcement stack was then consolidated between the aluminium platens in the Fox and Offord press (described in 3.4.1) under a pressure of 2 bar at 80°C for 20 minutes. After allowing to cool, the preform stack was removed from the press and cut to size.

3.3.2 Airjet Placed Laydowns

Single tow, airjet placed laydowns were manufactured using the tow placement facility,

described in 4.4, in order to compare fibre straightness with roller placed laydowns and to evaluate mechanical properties. Laydowns were manufactured from PPG 1062/2400 tex E-glass and were retained using either polyester powder or polyester scrim. Directional fibre tows were deposited on the laydown bed using an air supply pressure of 0.75 bar whilst random tows were propelled on to the laydown bed at 2 bar which caused the tow to split into its constituent strands and form loops on the laydown bed. Fibre retention was aided by the use of a porous bed constructed from a 2m x 1m mild steel perforated sheet. A 0.36kW electric axial fan located in an expansion chamber under the porous bed was employed to create a pressure differential of 48Pa over the bed, thus helping retain the fibres in their as-laid position.

Laydowns were produced by traversing the tip of the nozzle at a height of 5mm above the bed. Unidirectional laydowns were manufactured by depositing tows along both the positive and negative machine axis directions in a "square wave" pattern as shown in Figure 3.2. Each individual layer was retained using a fresh layer of polyester scrim or polyester powder. Bi-axial laydowns were produced in a similar manner with the second layer being laid at 90° to the first. Random laydowns were manufactured in the same manner as bi-axial laydowns but at higher air supply pressures. A hand held domestic iron was used to consolidate the laydowns to help retain the fibres.

3.3.3 Roller Placed Laydowns

A roller placement technique (described in 4.5) was developed by the author and used to manufacture preforms for demonstrator components and to validate the fibre architecture optimisation and fibre waviness models described in Chapters 5 and 6. Both 1062/2400 tex E-glass and HTA 5131 carbon were used to produce reinforcements. Fibre retention was provided by either Neoxil 940 polyester powder or by polyester scrim. Both type of binders were heated by a platen heater set into the facility bed. Tows were laid on the bed in either a single direction by laying a series of tows, then returning to the start point to lay the next series (Figure 3.3a) or by employing the rotary A-axis to enable bi-directional laydown in a fashion similar to the airjet laydown (Figure 3.3b). Consolidation was performed during laydown by the action of the platen heater and the compaction roller.

3.4 Resin Transfer Moulding

The majority of the laydowns manufactured using the tow placement facility and from roll-stock reinforcement were moulded by RTM. The following section describes the moulds and processes used to produce test specimens and demonstrator components.

3.4.1 Fox and Offord Press

A 50 tonne hydraulic upstroke press manufactured by Fox and Offord Ltd (Figure 3.4), was used to consolidate all flat plaque reinforcements. The press was also used in conjunction with a pressure pot to make flat plaque unidirectional E-glass specimens for tensile testing using matched aluminium plaque moulds. The press was equipped with a pair of 3.5kW electrically heated aluminium platens that heated the mould to around 70°C. Additional 1kW strip heaters were located in the injection and venting gate areas which were the areas last to cure. The 3.6mm x 518mm x 538mm cavity was sealed with a 4mm O-ring around the mould periphery. Resin was injected from a single line gate through a thermal break valve, venting from a gate at the opposite tool edge. A 1.5mm gallery in the injection end of the tool was used to heat the resin and reduce mould quench during injection and to promote rectilinear flow through the preform. Pressure and temperature histories were recorded from pressure transducers and thermocouples set into the tool and logged using a Burr Brown PCI-20000 data acquisition system linked to a PC to help determine resin cure inside the tool. Typical injection times ranged from 1 to 6 minutes depending upon tool temperature, injection pressure, fibre volume fraction and fabric orientation. Cured plaques were ejected from the tool 15mins after injection and post cured in a hot air oven for 90 minutes at 80°C.

3.4.2 Pressure Pot

Because of the cost of carbon fibre and to reduce material waste, a small mould containing three cavities each measuring 250mm x 40mm x 2mm was designed for the manufacture of carbon fibre reinforced tensile test specimens. This mould was also used to manufacture composites with induced fibre waviness to validate fibre waviness models described in Chapter 5. The tool (Figure 3.5b) was edge gated as before to help reduce mould quench and promote rectilinear flow. A pressure pot (Figure 3.5a) was connected

to the aluminium tool by flexible PVC tubing and was used to inject resin using laboratory supplied air at up to 6 bar. The two mould halves were clamped using G-clamps and the mould was preheated in a hot air oven at 80°C before injection to aid resin flow through the preform. Ciba Polymers 5052 epoxy resin was used and typical injection times ranged from 2 to 6 minutes depending upon fibre volume fraction and orientation and injection pressure. Injection terminated when resin exited the vent gate. The specimens were cured following the end of injection in a hot air oven at 80°C. Post curing was done between sheets of glass to prevent warping, in a hot air oven at 80°C for 90 mins.

3.4.3 Hemisphere Mould

Hemispherical mouldings were produced to determine fibre movement during forming of 2D reinforcements as part of the validation of the kinematic drape model described in 6.2.1. Mouldings were produced from both E-glass and hybrid E-glass / carbon tow-placed reinforcements using either polyester scrim or polyester powder to bind the preforms. The laydowns were formed and hot-press moulded in a single stage within a 70°C matched aluminium hemispherical mould (Figure 3.6). The reinforcement was placed across the top of the female tool. Fibre tension was maintained by placing a peripheral 0.5kg steel ring on the material. The male tool was attached to the crosshead of an Instron 1195 testing machine. With the reinforcement in place and 70g of epoxy resin in the female tool, the tool was closed at 50mm/min. The mould was opened after 20 minutes and the moulding ejected.

3.4.4 Rolls-Royce Outlet Guide Vane

Twenty one laydowns, each consisting of three plies, were created on the tow placement facility to produce an outlet guide vane (OGV). The laydowns were manufactured from 12k carbon fibre tow which were retained using polyester scrim. The laydowns were assembled, preformed and moulded by Rolls Royce plc at their composites manufacturing facility in Derby. The plies were assembled and formed in a flexible tool by applying full vacuum. The preform was transferred to a matched oil heated steel mould tool (Figure 3.7) which was heated to 150°C. Hexcel Composites RTM6 resin was injected into the tool at a pressure of 4 bar that was maintained until the resin had gelled. After curing, the

tool was allowed to cool to 100°C and the vane was removed.

3.4.5 Power Bulge

This geometry was developed as a challenging geometry to test the fibre architecture optimisation, described in 6.4.2. Net-shape preforms were manufactured from both E-glass and hybrid E-glass / carbon by tow placement using polyester scrim to retain the fibres and were cold pressed using Cray Valley Synolac 6345.001 polyester resin within a plaster/epoxy mould (Figure 3.8). The reinforcement was placed across the top of the female tool. Fibre tension was again maintained by placing a 0.5kg steel frame on the material. The male tool was attached to the crosshead of an Instron 1195 testing machine. Cold curing polyester resin was placed in the female tool, and the tool was closed. The mould was opened after 15 minutes and the moulding ejected.

3.5 Material Characteristics

The tow placement techniques were evaluated by comparing the in-plane permeabilities and physical properties of test laminates with those made using conventional reinforcements.

3.5.1 In-Plane Permeability

In-plane permeability measurements were made using a radial flow, constant flow-rate test using Trent HDX30 mineral oil as the permeant. The principal permeabilities were determined using the method described by Chick et al [66]. The rig (Figure 3.9) consisted of a 25mm aluminium base with a 2mm deep, 400mm diameter cavity fitted with a central, 10mm diameter inlet port. A 5mm deep gallery at the periphery was vented via two 10mm bore outlet hoses into a waste container. An upper (aluminium) platen, 25mm thick, was stiffened with an array of aluminium webs to minimise mould deflections. Eight 8mm diameter (diaphragm type) miniature pressure transducers and a K-type thermocouple were located along a pair of orthogonal axes of the base. Pressure and temperature histories were recorded using a PC fitted with Burr Brown analogue input modules. Oil was injected under constant flow rate into the centre of the cavity

using a hydraulic cylinder operated by an Instron 1195 testing machine which was capable of maintaining a constant crosshead speed. The pressure and temperature histories were downloaded into a Microsoft Excel spreadsheet. The pressure and temperature data were used in the spreadsheet along with data for oil viscosity, reinforcement porosity, cavity thickness and fluid flow rate to determine the wetting permeability of the fabric. Permeability was obtained by manipulating Darcy's law as described in 2.5. A detailed account of the equations for determining permeability are provided in Appendix 3.1.

3.5.2 Tensile Properties

Tests were made using an Instron 1195 universal testing machine to methods adapted from BS 2782. Tensile modulus measurements were performed on unidirectional E-glass laminates measuring 250mm x 25mm and on E-glass and carbon laminates with induced fibre waviness measuring 250mm x 40mm. Parallel samples were used throughout. The specimens were clamped between the jaws of an Instron 1195 test machine and strain was monitored using an Instron 2630-100 four arm Wheatstone bridge clip-on extensometer attached to the specimen. The cross-head speed for testing was 5mm/min and the gauge length was 50mm. Samples were tested to failure and modulus was calculated automatically from a least squares straight line fit made through the steepest linear region of the stress-strain curve.

3.5.3 Fabric Drape

To verify the kinematic drape model, described in 6.2.1, for fibre laydowns produced using the tow placement system, a series of hybrid E-glass/carbon 0°/90° fibre laydowns were manufactured. One set was bound with thermoplastic polyester net and another with polyester powder. Alternate tows of carbon and E-glass were laid to facilitate measurement of the included angle between intersecting fibres before and after post-forming. The laydowns were post-formed at 70°C in the hemispherical mould described in 3.4.3. The angles at the tow intersections were determined along the geodesic 45° axis from pole to equator (Figure 3.10a) by measuring the major and minor axes of the cells formed by four intersecting tows. The major and minor axis lengths were measured using a flexible rule and the corresponding angles were determined using trigonometry.

3.5.4 Preform Superficial Density

To validate the fibre architecture optimisation technique described in 6.4, a method was developed for determining changes in preform superficial density. Optimised and conventional 0°/90° E-glass reinforcements bound with polyester scrim were manufactured using the tow placement facility. The reinforcements were formed and impregnated in the hemispherical and power bulge tools described in 3.4. The post cured mouldings were cut into quadrants along the axes of symmetry and 20mm strips were cut from the edges of these quadrants. For the hemisphere, the 20mm strip was subsequently cut into five more specimens as shown in a cutting template in Figure 3.10b. The power bulge quadrants were cut into three 20mm high strips with several smaller samples taken from each strip as shown in the cutting plan in Figure 3.11. Each specimen was measured (without accounting for specimen curvature) and the superficial fibre density was determined by weighing glass fibre in each sample after combustion of all other materials in an ashing furnace for 60 mins at 600°C.

3.5.5 Fibre Deviation

Positional accuracy of tows laid using the tow placement facility were determined and are described in 4.6.1. Single tows of glass fibre were laid onto the laydown bed and then photographed. The photographs were scanned and processed using image analysis software Visilog® to obtain a skeletal image of the tow. Deviation was determined from the average of the absolute deviations of the coordinates of the skeletal image from the desired path was calculated using a Microsoft Excel® spreadsheet.

3.5.6 Fibre Misalignment

To assess the level of fibre misalignment present in the laminates manufactured from the airjet and roller laid preforms, measurements of fibre orientation were taken at discreet sections as described in 4.6.2. Specimens measuring 10mm x 10mm in-plane were cut from arbitrary positions from the mouldings and set in casting resin. Each specimen was ground and polished along the plane of the fibre axis using sequentially finer abrasive paper and finally 1μm alumina powder on a Struers DAP-7 rotary polishing machine. Images of the polished sections were taken at 40x magnification using a closed circuit

digital camera mounted on a Zeiss-Axiolab reflected light optical microscope. Fibre misalignment was measured directly from the polished micro-section images using image analysis software Picture Publisher 4®. Fibre coordinates were measured from 40 fibres chosen randomly within each image which were then converted to off-axis misalignment angles using trigonometry. Average fibre misalignment angles for each specimen were calculated from the mean of the 40 values.

3.5.7 Uniformity of Tow Coverage

Uniformity of tow coverage was measured for various processing conditions as described in 4.6.3. The experiments involved laying a 300mm x 200mm rectangle of 12k carbon tow at 3mm pitch (the average tow width was 2.9mm) onto a white sheet of paper using polyester scrim as a binding agent. Photographs were taken of each laydown and scanned into tiff format images using an Epson GT9000 flatbed scanner. The scanned images were processed using image analysis software Visilog® to calculate the proportion of black and white on each image. This related to the proportion of black carbon fibre and white paper seen through gaps in the carbon fibre laydown which gave an indication of the percentage fibre coverage.

3.6 Summary

This chapter has described the materials and equipment developed for the production of preforms and laminates and the techniques used to assess their properties. A tow placement facility has been developed by the author and the manufacture of tow-placed preforms has been described as well as methods for producing preforms from roll-stock reinforcement. The author has also designed equipment for the production of flat plaque laminates containing fibre waviness used in the validation of models developed in Chapter 5 and moulding tools for the manufacture of power bulge components used in the validation of fibre architecture optimisation techniques described in Chapter 6. This chapter has also described the equipment and methods used in the production of tensile test specimens, and demonstrator components and the methods for characterising reinforcement properties. The processes for determining preform permeability, laminate tensile modulus and preform superficial density are reported as well as a method for

measuring the included angle between intersecting fibres after post forming used in the validation of the drape model described in Chapter 6.

List of Figures

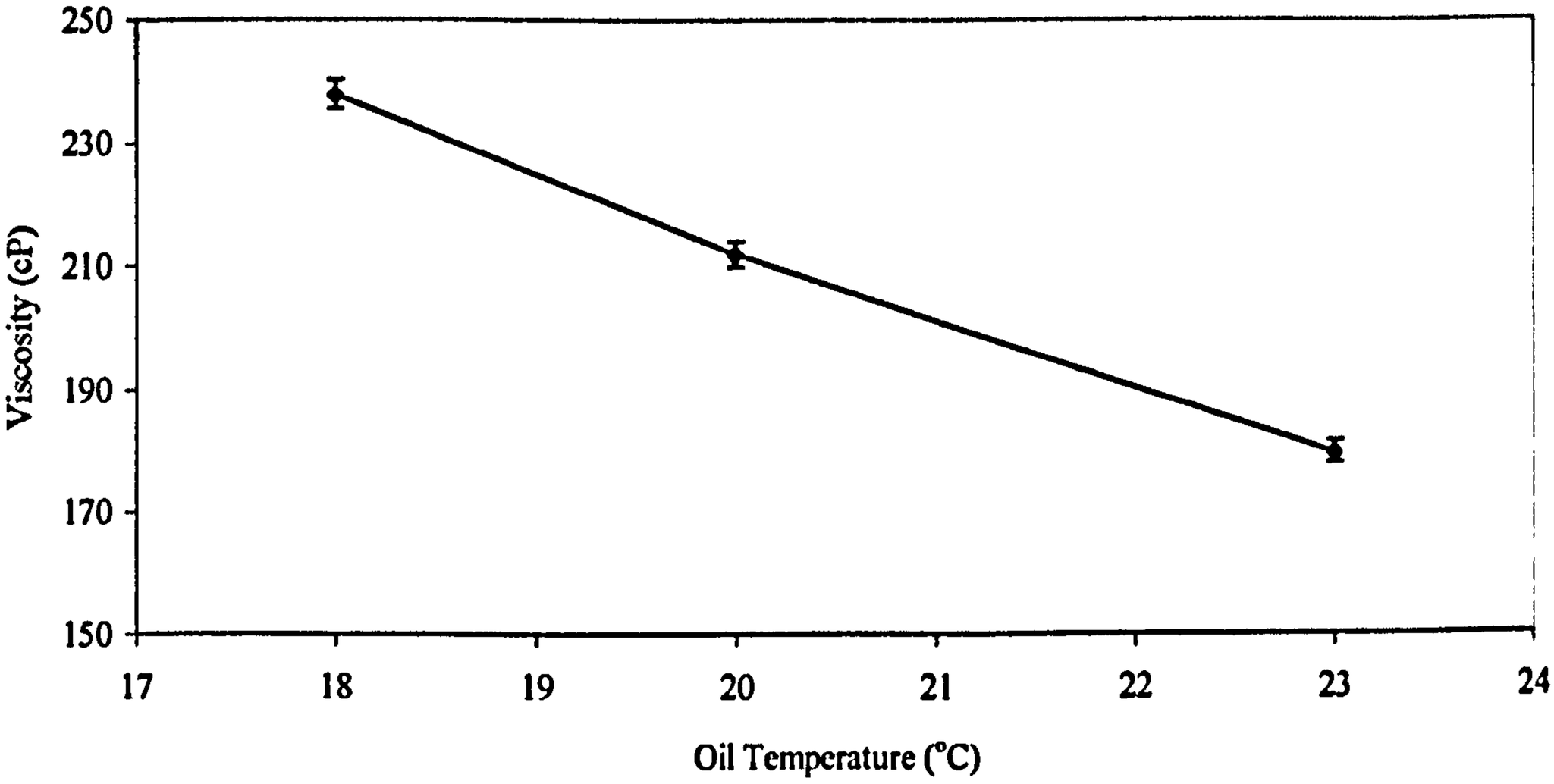

Figure 3.1 Viscosity vs. temperature for Trent Oils HDX30 mineral oil used for the measurement of permeability.

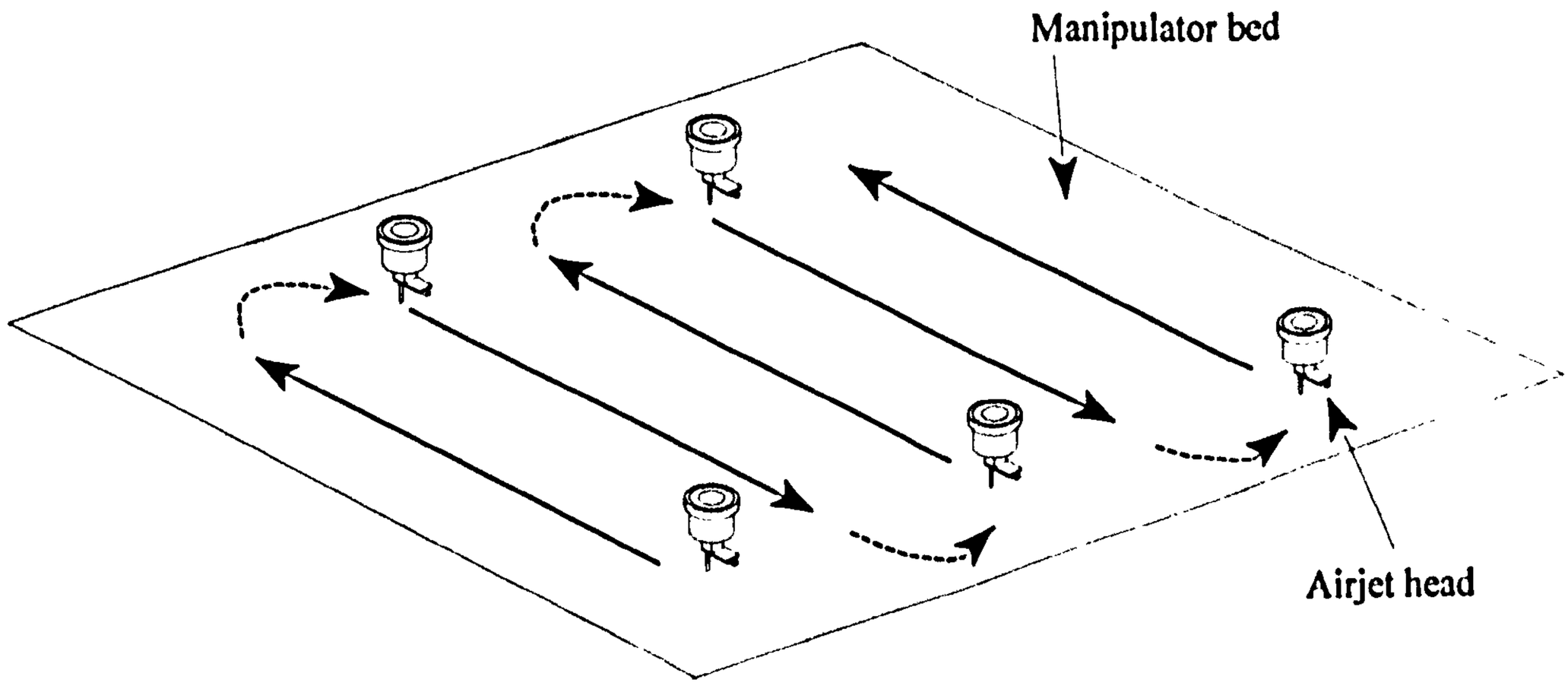

Arrows depict head movement

Figure 3.2 Schematic showing "square wave" pattern of directional laydown manufacture using airjet placement

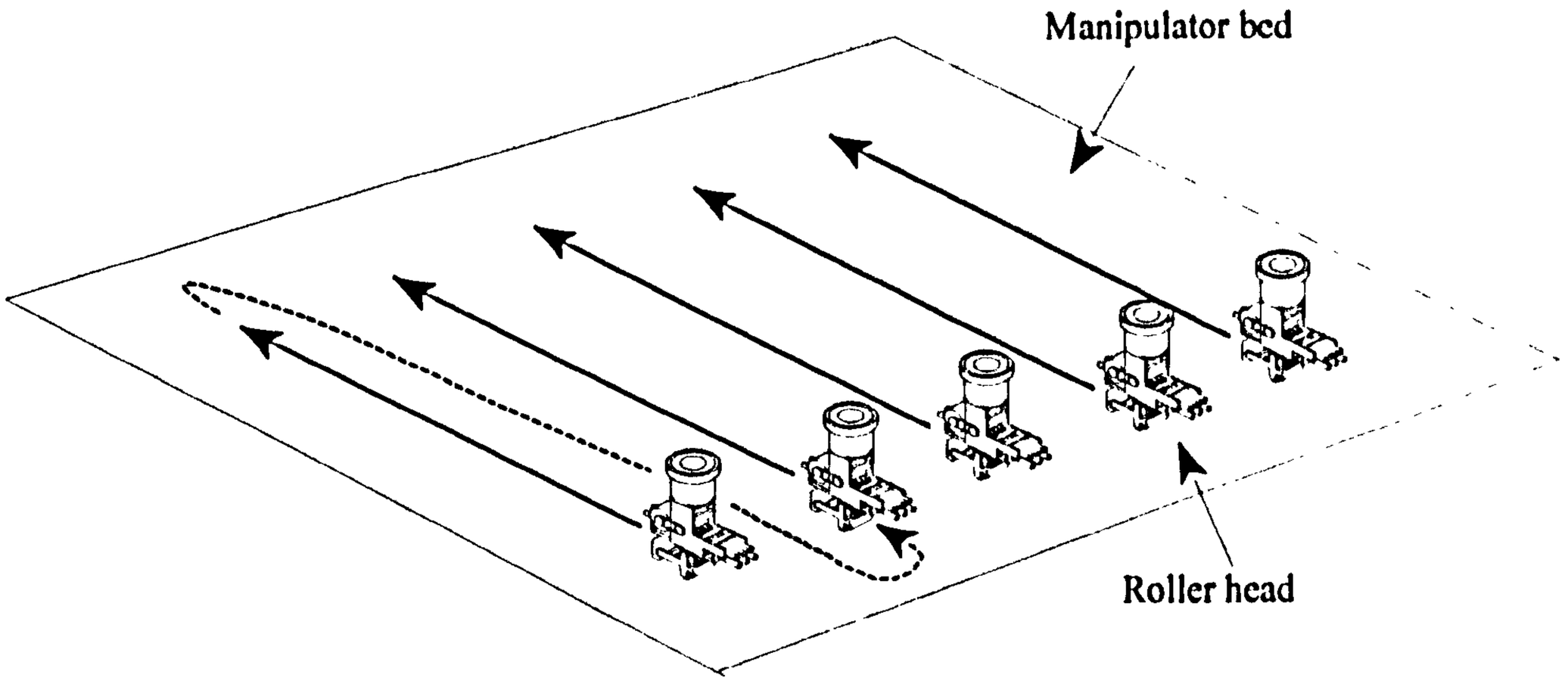

Arrows depict head movement

(a) Single direction

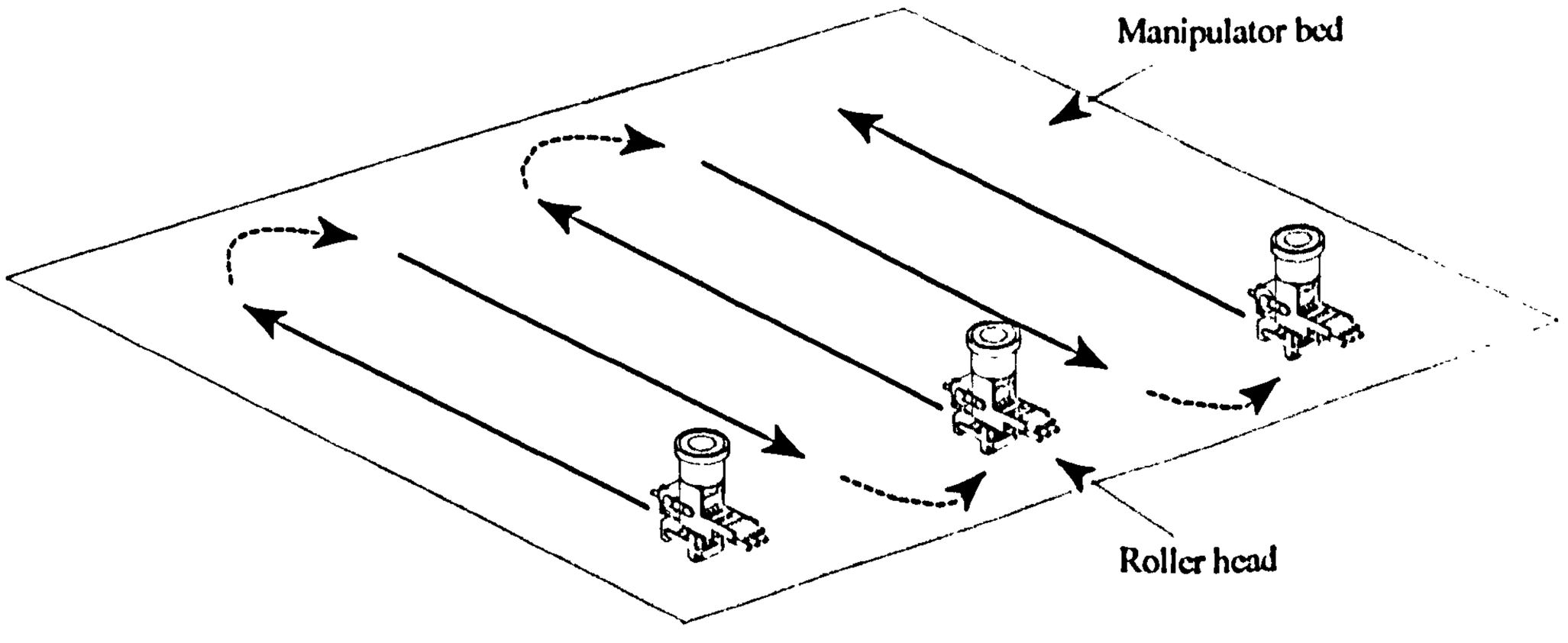

Arrows depict head movement

(b) Bi-directional

Figure 3.3 Schematic showing laydown pattern using roller placement

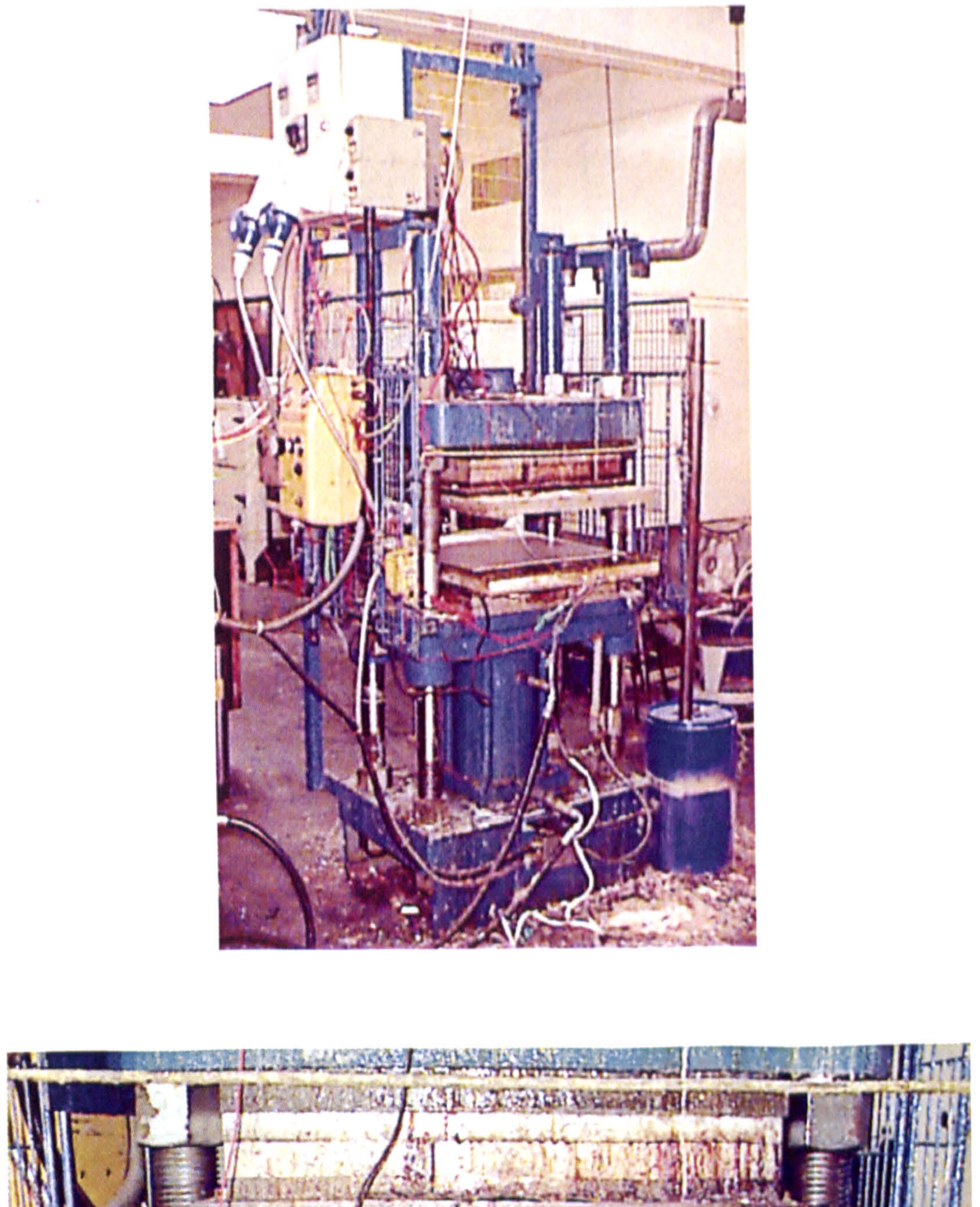

Figure 3.4 Fox & Offord 20 tonne upstroke press [58]

(a) Pressure pot

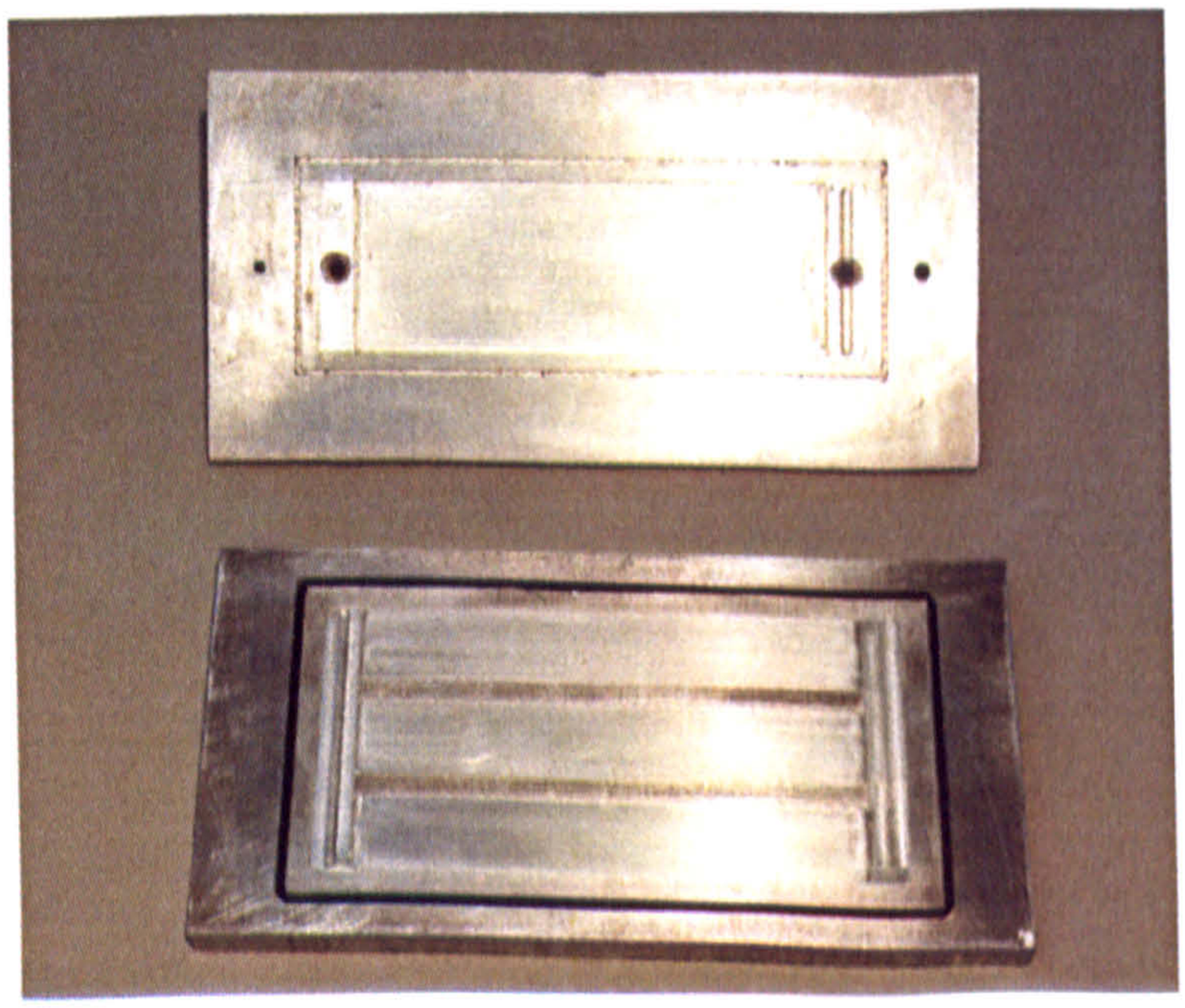

(b) Aluminium tool

Figure 3.5 Pressure pot RTM system

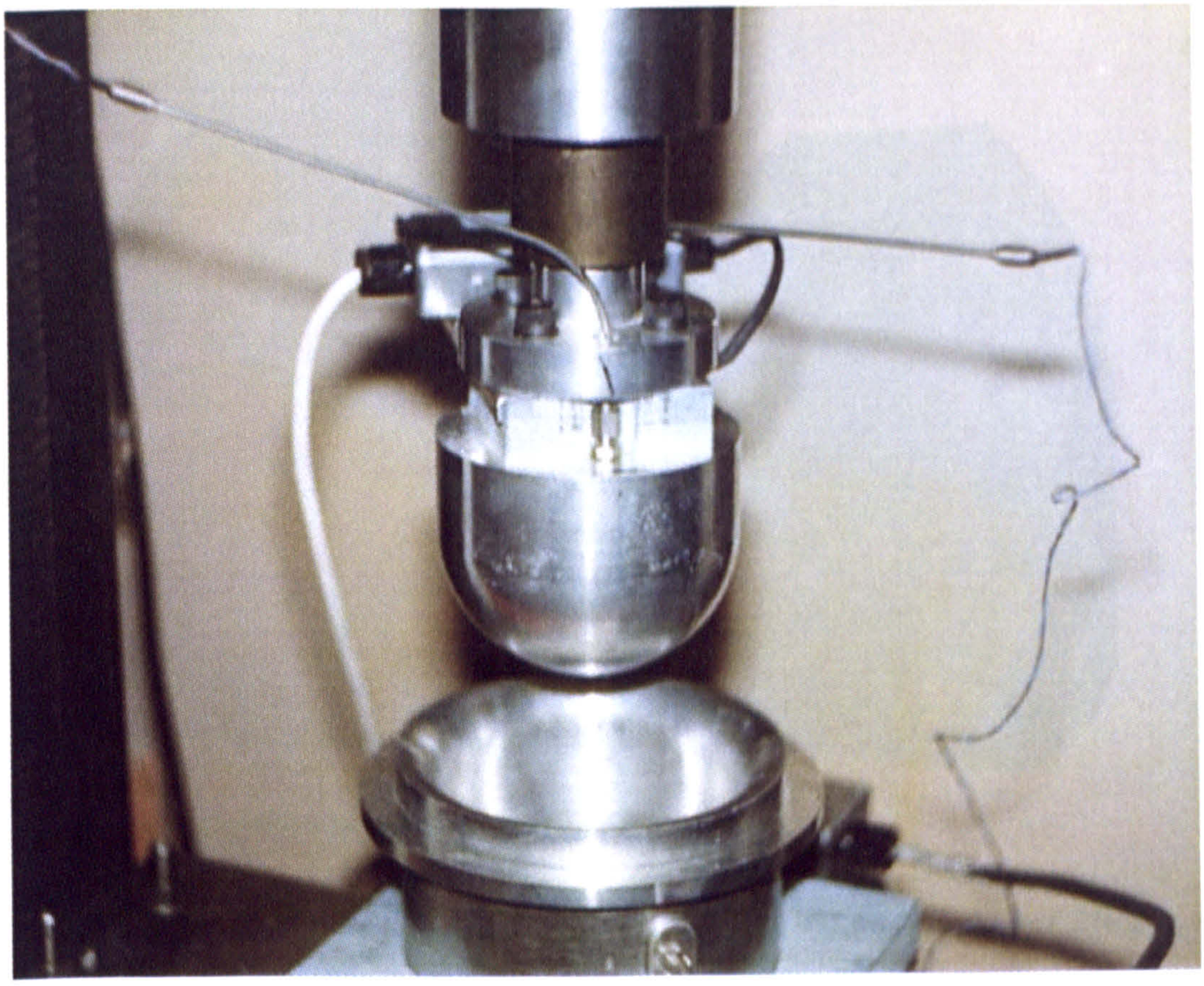

Figure 3.6 Heated matched hemispherical mould

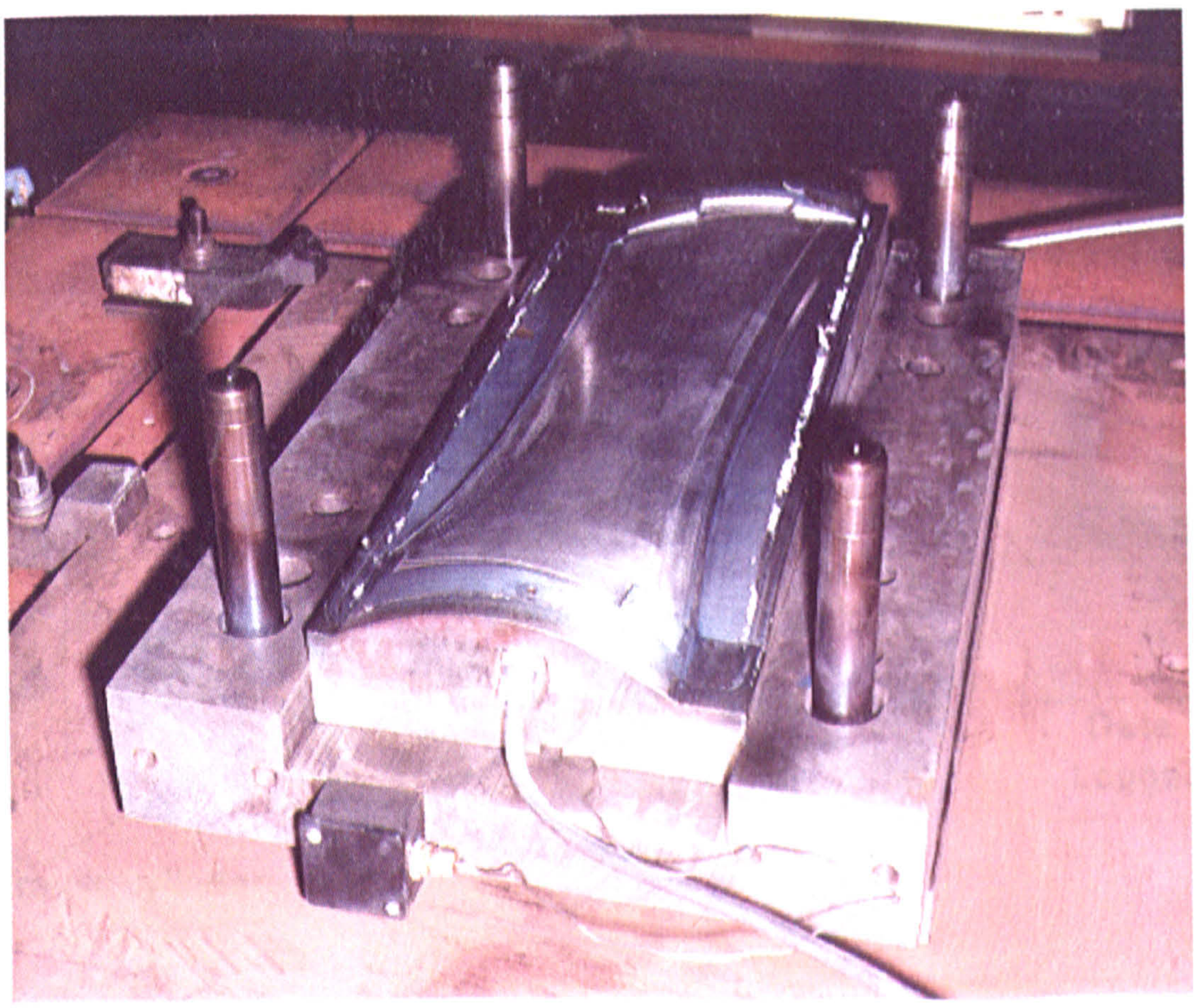

Figure 3.7 OGV moulding tool (courtesy of Rolls Royce plc.)

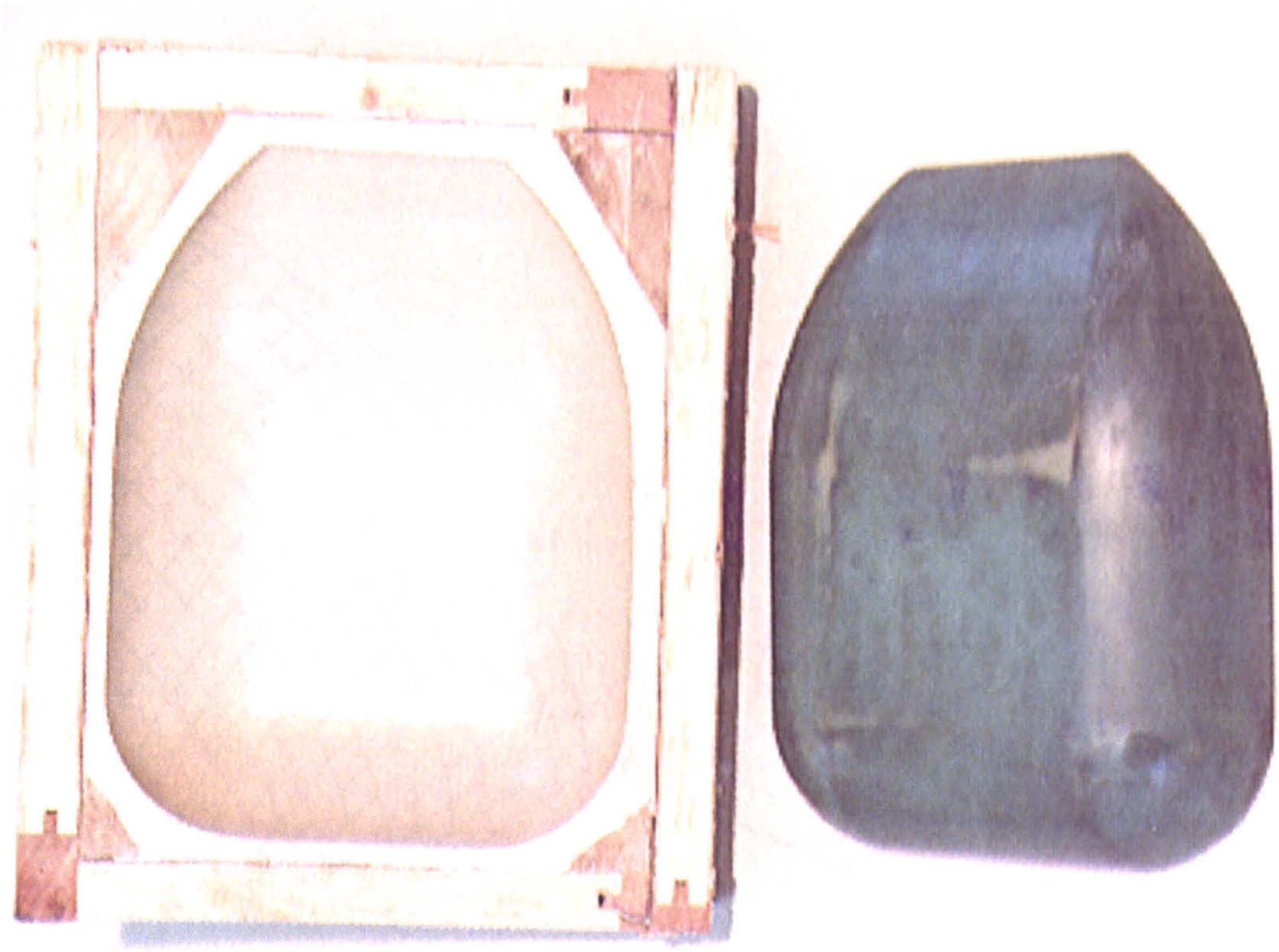

Figure 3.8 Matched tool used to preform and mould generic power bulge

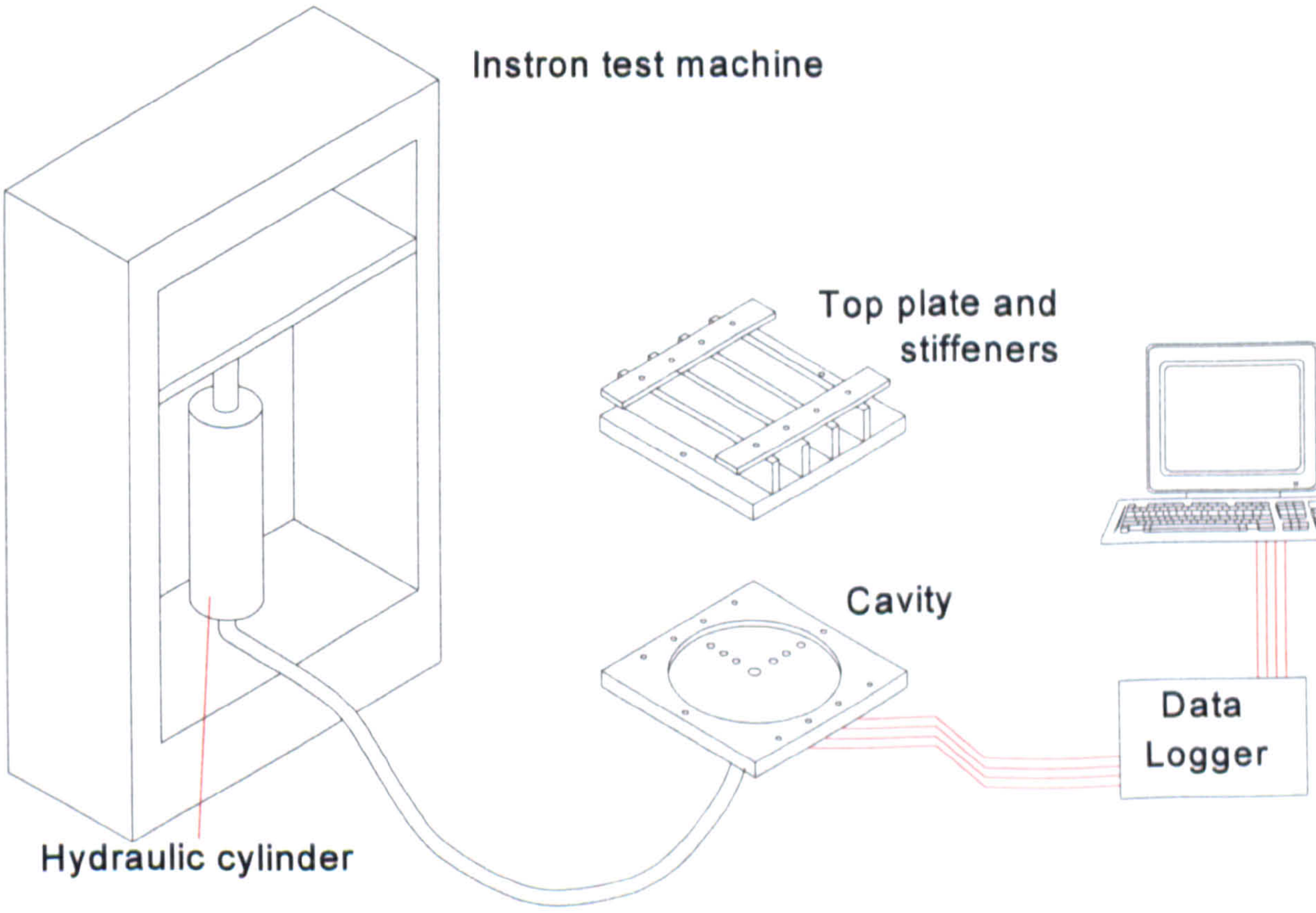

Figure 3.9 Schematic of permeability measurement facility

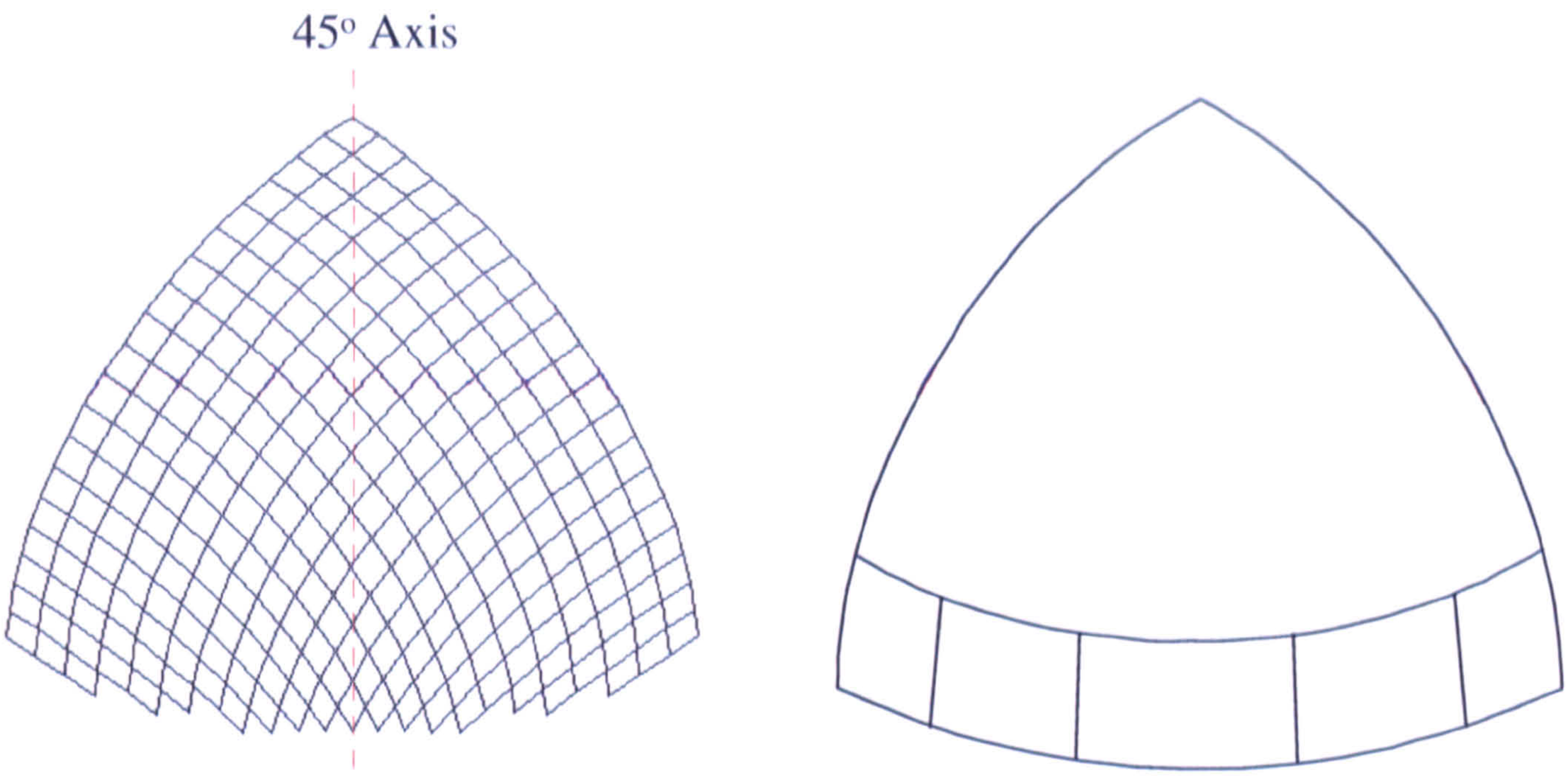

(a) 45° axis along which reinforcement shear was measured

(b) Cutting template used for the production of burn-off samples

Figure 3.10 Hemispherical preform

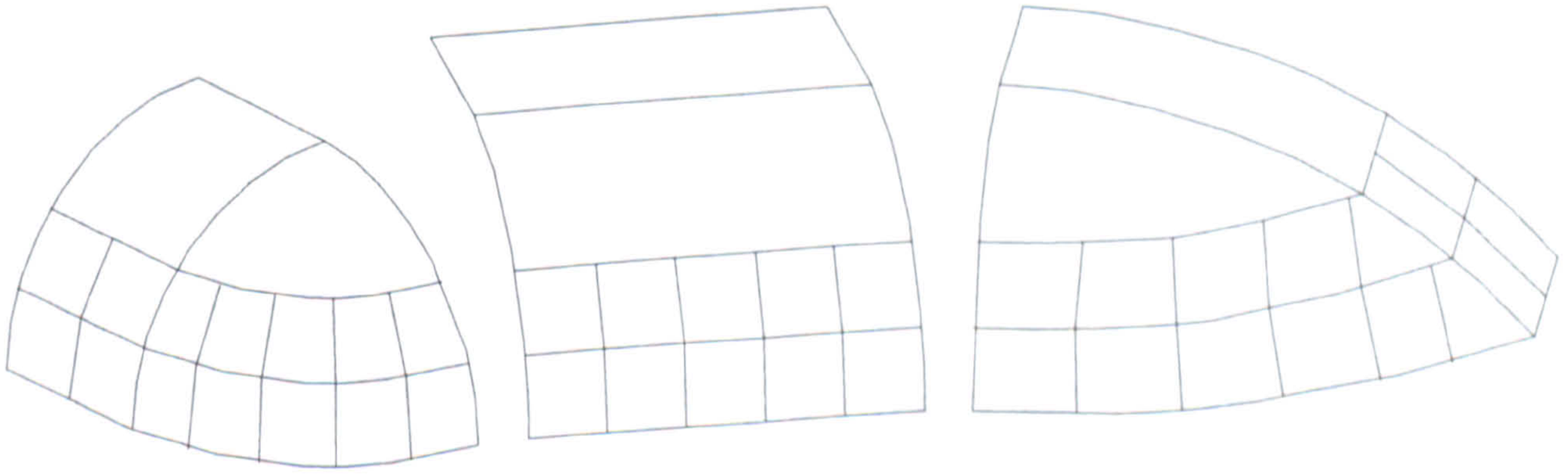

Figure 3.11 Cutting template used for the production of burn-off samples for power bulge

Chapter 4
Tow Placement Facility

4.1 Introduction

This chapter describes the hardware used to place reinforcement for test plaques and the technology demonstrators described in Chapter 7. Two types of laydown are reported: airjet laydown and roller placement. Experiments determined the quality of preforms manufactured using airjet and roller placement techniques with particular emphasis on fibre alignment, laminate modulus and preform permeability. The mechanical performance of tow placed laminates are also compared with laminates constructed from commercial reinforcement. Optimisation of the roller placement system is reported for increasing uniformity of fibre coverage with the aid of external heaters and by altering the method of fibre deployment.

4.2 High Speed Manipulator

Two methods for creating dry fibre laydowns were developed: airjet placement and roller placement, both of which were based around the same high speed (x and y axes 100m/min) CNC manipulator. A Crispen 2015/4-axis CNC manipulator (Figure 4.1) was designed and constructed by SOS Newall. X and Y movements were achieved with friction drive units. Two units were used for X movements, one each side of the gantry to reduce moments on the bridge or guides. The X and Y axes drove the bridge at speeds up to 1.67m/s with positional accuracy of ±1μm. The Z-axis was operated by a lead screw with positional accuracy of ±10μm and the A-axis by a belt drive. The rotational accuracy of the A-axis was ±0.1°.

4.3 CNC Control

The high speed manipulator was controlled by a separate hard wired unit. In order to lay fibres to a predetermined scheme, a CNC part program was required. Three approaches were used for generating part programs:

- Two dimensional CAD drawings were post processed along with a preform specification (ply orientations, tow spacings) to generate an NC part program for tow placement. The laydown geometry (in IGES format) was loaded into a post processor and the existing outline was edited as necessary (to add a trimming allowance for example) before defining the preform specification. The part program was output as an ASCII file and transferred directly to the memory of the manipulator control unit via a standard RS232 connection. This process is shown schematically in Figure 4.2. The post processor used to produce part programs was developed from an existing procedure used by McGeehin [59].

- Kinematic draping software [58] was used to generate a template file which provided the basis for the net-shape part programs. The drape software described the deformed geometry of the nominal fabric or laydown in three-dimensional space. A mapping algorithm was then applied to flatten the elements or "patches" in a surface model to produce the flat template. This geometry was then post processed as before to generate the NC part program which enabled the net-shape laydown to be produced. This procedure is shown schematically in Figure 4.3.

- Surface models were created and a user specified fibre pattern was applied using CAD. Kinematic draping was then used to map the fibres onto a horizontal surface, thus producing an "optimised" laydown that when formed would contain the desired fibre paths in three dimensional space. Section 6.4 describes the procedure in more detail and Appendix 6.2 summarises the algorithm used to produce the "optimised" laydown.

4.4 Airjet Placement

A single tow airjet, as used by McGeehin [59], was attached to the gantry of the manipulator. Air wash from the airjet tended to displace fibres from their designed paths and as a result, a multi-tow roller placement device was designed and developed as described in 4.5. However, because of the modularity of both designs, it was feasible to

change from airjet placement to roller placement in a relatively short time. Although it will be shown later that roller placement was more accurate and created a more uniform laydown, airjet placement was advantageous in creating random fibre laydowns at high speed which was well suited to composite structures in non-critical applications such as automotive body panels. The following section describes the operation and relevant parts of the airjet placement head.

Airjet

The airjet head (Figure 4.4) was attached to the gantry of the manipulator on the Z-axis and acted as a propellant to deliver the tow onto the bed of the manipulator. The design of the airjet was based on those used in the textile industry for replacing shuttles on weaving looms [59]. The airjet was designed by McGeehin [59] and was composed of two concentric nozzles (Figure 4.5), the inner feeding the roving, the outer supplying air at elevated pressure to propel the tow through the nozzle.

Payout Control

During initial development it was found that air pressure affected tow exit speed at the nozzle and that fluctuations in the tow tension occurred as a result of this. Thus a separate device was designed by McGeehin [59] to provide accurate tow payout control. The system (Figure 4.6) was based on drive belt theory and used a series of rollers driven by a MacLennan M372TE 7.4Ncm dc servomotor to deliver reliable quantities of tow to the airjet. The tension applied to the tow by the airjet created sufficient friction to allow accurate control. The drive motor was connected to a Norwen Electronics NE-P-061 amplifier board and the system was calibrated over a range of input voltages by measuring tow length deposited over a 60 second period.

Cutting

Cutting of the tows was achieved using a guillotine attached near the bottom of the airjet. The device consisted a truncated scalpel blade attached to a dual action 20mm bore Compair Maxam pneumatic cylinder operating at 6 bar pressure. The blade passed through the airjet exit tube, shearing the tow as it did so. Because the airjet remained

active during the cutting phase of laydown, exhaust vents were located above the cutting device to prevent a pressure build up in the system whilst the blade was cutting.

Retention

During tow placement, it was found that the airjet needed to be positioned between 5mm and 8mm from the deck of the manipulator for minimal fibre disturbance. The airjet was pressurised at anything up to 0.75 bar to propel the tow. The air exhausted from the same exit tube as the tow and as a result caused fibre displacement on the bed. To reduce this effect, suction assistance was employed using a 0.36kW axial flow fan under a porous bed (although it was ultimately abandoned in favour of a solid, fibreboard bed when operating with the roller placement technique as described in 4.5).

Tows were retained on the bed using polymer binders so that the laydowns could be handled and impregnated without any serious fibre re-orientation. Directional fibres were held in position using Fothergills Engineered Fabrics M0924/532 Admesh (as described in 3.2.3) which was tacky at room temperature.

4.5 Roller Placement

Because of problems of fibre displacement by exhaust air, a multi-tow roller placement device was designed and developed by the author and Newall Aerospace (Figure 4.7) that was more effective in producing uniform preforms with superior mechanical properties, as described in 4.6. The following section summarizes the design of the roller placement head and its method of operation.

Compaction Roller

The roller placement head was modular in design and attached onto the same station as the airjet head. The head was based around a sprung compaction roller (Figure 4.8) which acted to pinch the tow between itself and the manipulator bed during laydown. The compaction roller was constructed from mild steel and was free running with bearing end caps. Twelve 0.1mm slots were machined along the length of the roller and an air bleed

(1bar) was supplied to the roller cavity to help prevent fibres sticking to the roller. A small, curved guide in front of the roller prevented the tows from buckling as they hit the manipulator bed.

Tow Payout

Delivery of tow to the compaction roller was controlled by a separate payout system (Figure 4.7). A 0.2Nm Maclennan M286 dc servomotor with tachogenerator and encoder drove a pinch roller which delivered tow down a set of stainless steel tubes to the compaction roller. The pinch roller was manufactured from Nylatron®, a material based on Nylon 66, modified by the addition of molybdenum disulphide which results in a tough, self lubricating material with very low friction. The roller placement head was able to lay up to five tows independently. Tow delivery was governed by a set of five clutches which pinched the tows against a driven pinch roller. The clutches were constructed from free running roller bearings attached to single acting, 6mm bore, spring loaded SMC CJ286-15R pneumatic cylinders operating at 6 bar. Tow payout was regulated by the vector sum of the velocities of the X and Y axes of the manipulator and had the capability to operate at speeds of up to 50m/min. Feedback using a tachogenerator and encoder on the pinch roller motor allowed for accurate control of tow payout.

Because of the nature of multi-tow placement, sometimes it was necessary to arrest one or more tows whilst others continued to be laid. During this time it was easy for the inactive tow to become un-threaded from the head. To prevent this, a system of brakes were developed (Figure 4.9) which acted on the simple action of an eccentric cam. As the tow was pulled from the payout unit the cam lifted to allow the tow easy passage. If the tow was pulled from the other side, the cam locked and prevented the tow from moving.

Cutting

Cutting of the tows was achieved using five guillotines similar to those used on the airjet placement head. The cutting device was located between the tow payout system and the compaction roller (Figure 4.8) 110mm above the laydown bed resulting in a minimum laydown length of 110mm. Again the cutting device used truncated scalpel blades

attached to dual acting, 10mm bore, SMC CJ2810-15 pneumatic cylinders that operated at 6bar to shear the tows. Because of the small space in which the cutters must operate, three of the cutters were located on one side of the head, with the other two cutters functioning from the opposite side. To prevent the blades moving out of plane during operation and to increase the efficiency of the cutters, bronze bearings were attached to the rear of the blades which operate in grooves. Because of the way in which the CNC codes are processed, no manipulator movements were allowed during a cutting operation.

Retention

Without the airjet, the problem of fibre displacement due to wash was eliminated and the porous manipulator bed was replaced with a solid table constructed from 18mm thick medium density fibreboard (MDF). Tows were retained on the bed using polyester scrim. Although the polyester scrim was tacky at room temperature, its effectiveness increased with temperature, as described in 4.6.3, and therefore two heaters were incorporated. The first, a Watlow 2500 Watt 400mm x 600mm metal sheathed mica platen heater (Figure 4.10) was set into the MDF bed with a 6mm aluminium plate flush with the bed to prevent damage. The second, (Figure 4.7) a Watlow 550 Watt infra red emitter strip, was attached to the roller placement head in front of the compaction roller. Both heaters were controlled independently to heat the polyester scrim to approximately 50°C using Watlow controllers. Consolidation of these preforms was achieved continuously by the action of the compaction roller, with compliance increased by the local heating.

4.6 Effects of Processing Conditions on Preform Properties

This section studies the effects of processing parameters on the properties of tows and preforms laid using the tow placement facility.

4.6.1 Fibre Deviation

Because of the novelty of the laydowns produced using the tow placement facility it was thought useful to determine their processing and performance characteristics. This also allowed for direct comparisons between airjet and roller produced laydowns and

commercial reinforcement. Initially, positional accuracy was measured directly from laydowns. Single tows of glass fibre were laid at different speeds (50m/min and 100m/min) and to different lengths (between 250mm and 1000mm) and deviation was determined using the technique described in 3.5.5. Figure 4.11a shows a typical photograph of a single E-glass tow and Figure 4.11b shows its skeletal image. Table 4.1 shows the average deviation of the 0° fibres. Trials were performed using the multi-tow roller placement head and the single tow airjet head. Laydown speed and length had little effect on the results. It can be seen that the airjet placed fibres had over five times the average deviation of the multi-tow roller placed tows.

Table 4.1. Deviation from Straightness (mm/m) using Airjet and Roller

Fibre Deposition System	Average Deviation from Desired Path (mm)
Airjet	2.53
Multi-Tow Roller	0.48

4.6.2 Processing and Performance Characteristics

To quantify the processing and performance characteristics of laydowns produced using the tow placement facility, a series of unidirectional glass fibre preforms were produced using the airjet and multi-tow roller placement devices. Tests were performed to determine fibre alignment, laminate tensile modulus and preform permeability. Tensile specimens were also produced using quasi-unidirectional commercial reinforcement (Tech Textiles ELPb-567).

Fibre alignment and tensile modulus were measured from the same moulded specimens which were produced in the Fox and Offord press as described in 3.4.1. The fibre volume fraction was approximately 30%. Although the commercial fabric included 10% transverse tows this was accounted for by producing the specimens at a higher volume fraction. It can be seen in Table 4.2 that the commercial fabric specimens were produced at approximately 37% fibre volume fraction in total which equated to a normalised fibre

volume fraction in the principal fibre direction of approximately 34%, not accounting for the stitching material.

To assess the level of fibre misalignment present in the laminates manufactured from the airjet and roller laid preforms, measurements of fibre orientation were taken at sections as described in 3.5.6. A typical image of a polished section can be seen in Figure 4.12.

After the laminates were post cured (as described in 3.4.1), tensile modulus was determined from 6 specimens from each moulding as described in 3.5.2. Table 4.2 shows the results from the fibre alignment analysis and tensile testing of the plaques produced from airjet and roller placed tows compared with the commercial fabric at a slightly higher fibre volume fraction. It can be seen that the misalignment angles occurring in roller placed laydowns were about 80% lower than those found in airjet placed laydowns. These results are supported by the superior modulus of the composites produced using roller placement which outperform composites made using airjet placed laydowns. The tensile modulus of the mouldings manufactured from roller placed laydowns were also slightly superior to those made using the stitch bonded fabric probably due to filament damage caused by the stitching process.

To determine the processing properties of typical tow placed preforms, a series of permeability experiments were performed using the equipment described in 3.5.1. Twelve unidirectional glass fibre preforms were produced using the airjet and multi-tow roller placement devices. Three preforms were manufactured using each process at fibre volume fractions of approximately 30, 40, 50 and 60%. The measured permeabilities are shown in Figure 4.13. The degree of anisotropy of each reinforcement was measured directly via the ellipticity of oil impregnation after test completion. It can be seen that the permeabilities of both airjet and roller produced preforms are very similar. Although the degree of scatter of the results is relatively high, (between ±19% and ±29%) the permeability of the reinforcements manufactured using roller placement are 11% higher on average along the fibre direction and 28% lower transverse to the fibre direction than those manufactured from the airjet head. This result suggests that the roller placed

reinforcements are more anisotropic which could be explained by the reinforcement having greater unidirectionality and containing fewer fibre misalignments.

Table 4.2. Comparison of Tensile Properties - Quasi-Unidirectional Fabric, Airjet and Roller-placed Tow

Material	Fibre Volume Fraction (%) [normalised]	Misalignment (°)	Tensile Modulus (GPa) [Std Deviation (GPa)]
Tech Textiles	37.5 [33.7]	n/a	24.69 [0.63]
ELP-b 567	37.6 [33.9]		25.25 [1.97]
Airjet	30.6	2.11	25.09 [3.05]
	30.9	2.84	25.97 [1.60]
Roller	28.8	0.74	27.55 [1.44]
	28.9	0.25	26.45 [1.38]

4.6.3 Uniformity

Having established that aligned reinforcements produced using roller placement were straighter and produced composites with better mechanical properties to those manufactured using the airjet, experiments were performed to optimise the uniformity of the multi-tow roller placement head. Uniformity of tow coverage was determined using the method described in 3.5.7. Several process conditions were altered to determine their effects on the uniformity of the resulting laydown:

- ❑ method of fibre pull-off (tangential or circumferential)
- ❑ applied heat (none, emitter strip heater, platen heater or both heaters)

The method of fibre pull-off is related to the manner in which the fibre is unwound from the creel. Tangential pull-off (Figure 4.14a) allowed the tow to be used in its original untwisted state whereas circumferential unwinding of the carbon tows (Figure 4.14b) imparted a twist into the tow. The applied heat refers to the two heaters described in 4.5 which for the purposes of these tests were set at a temperature of 60°C. Eight tests were

performed in total (each method of fibre pull-off tested for each combination of heaters). Photographs were taken of each laydown and scanned (Figure 4.15). The scanned images were processed using the procedure described in 3.5.7 to give an indication of the percentage fibre coverage. A figure of 96.6% represents perfectly aligned laydowns due to the average tow width (2.9mm) being smaller than the pitch (3mm). This allowed for an effective comparison between the different processing conditions without the concern of any tow overlap occurring. The percentage fibre coverage for each test is shown in Figure 4.16. It can be seen that, except for the case of no heat, there is an increase in coverage for tangentially unwound tows. The application of heat (especially from the platen heater) also helped create a more uniform laydown with an increase in coverage of 18% by using both heaters with tangential pull-off.

4.7 Summary and Conclusions

This chapter has described the operation of the various systems and the mechanisms involved in the production of dry fibre preforms using a novel tow placement facility. An airjet or roller placement head was attached to the gantry of a high speed manipulator for tow placement. The airjet placement technique was developed from that used in a previous LINK project [59], and was used to lay single tows in directional or random fibre architectures. The roller placement technique allowed for multiple tows to be laid simultaneously and produced more accurate laydowns with better uniformity and mechanical properties. In order to lay tows to a predetermined scheme, a CNC part program to control the movement of the manipulator was produced. Along with manual preparation on the control unit, three methods of creating NC code for the production of laydowns were available: two dimensional CAD drawings (in IGES format) of the component were post processed; kinematic draping software [58] was used to generate a template file which provided the basis for the net-shape part programs; kinematic drape modelling was used to map tows developed in a three dimensional model onto a horizontal surface, thus producing an "optimised" laydown that when formed will contain the desired tow paths in three dimensional space.

Mechanical tests performed on composites manufactured using airjet and roller placement techniques showed tensile modulus to be comparable with manually stacked commercial reinforcement. This demonstrates that tow placed laydowns can be used effectively as reinforcement for LCM and suggests that the process does not induce significant weakness into the reinforcement.

Comparative tests have shown that the roller placement technique outperforms the airjet in terms of tow positional accuracy and the resulting mechanical and processing properties of the preform. Probable reasons for the enhanced performance of the roller technique are that the tow is in intimate contact with the bed during laydown and that the airjet generates its own wake which causes tow movement. For applications where precise fibre positioning is required (e.g highly structural components or for the optimised fibre architecture routine described in Chapter 6), it would be favourable to use the roller placement technique. For non-critical parts, especially where the preform would benefit from random reinforcement, airjet placement would be more suitable.

List of Figures

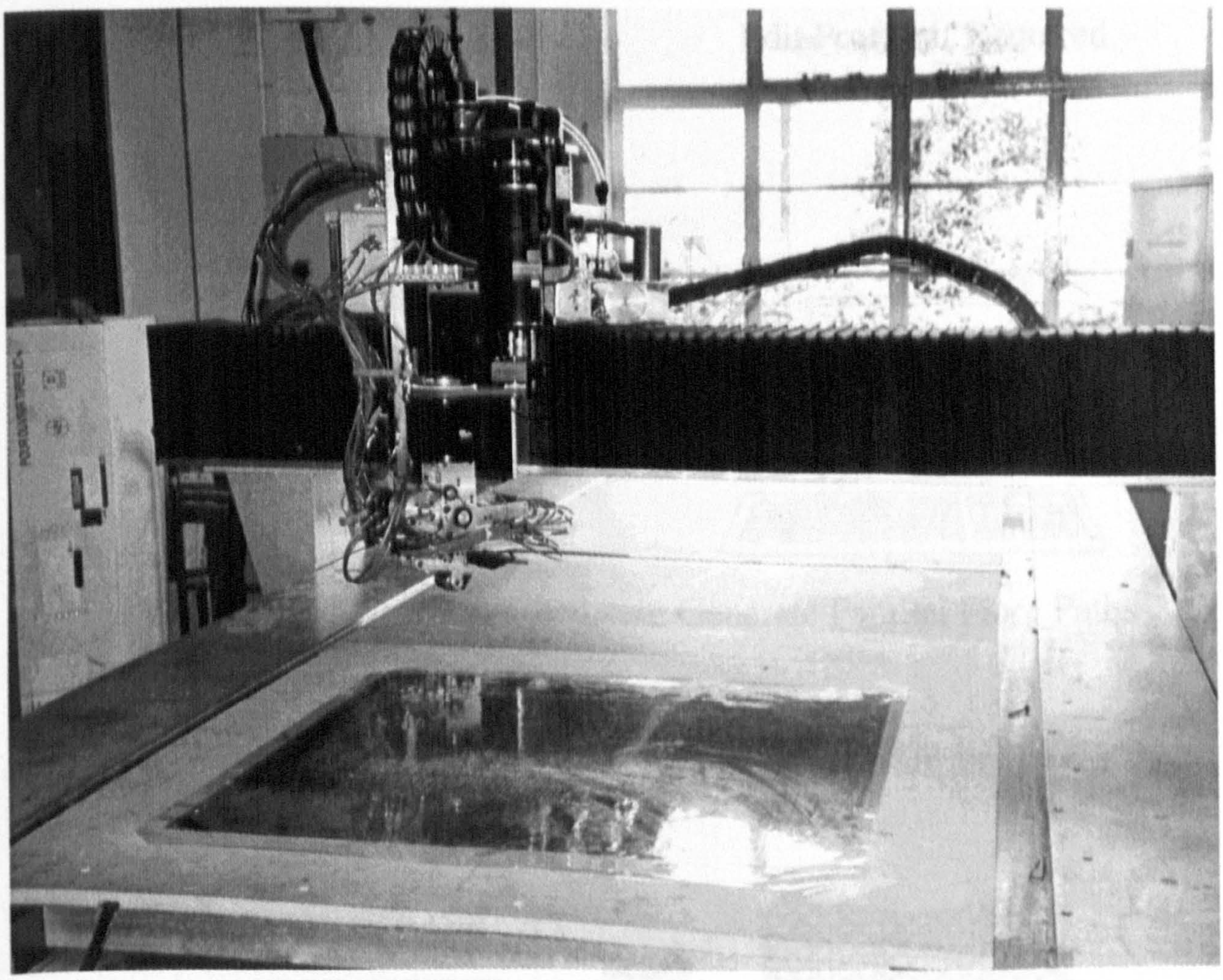

Figure 4.1 Photograph of high speed CNC manipulator

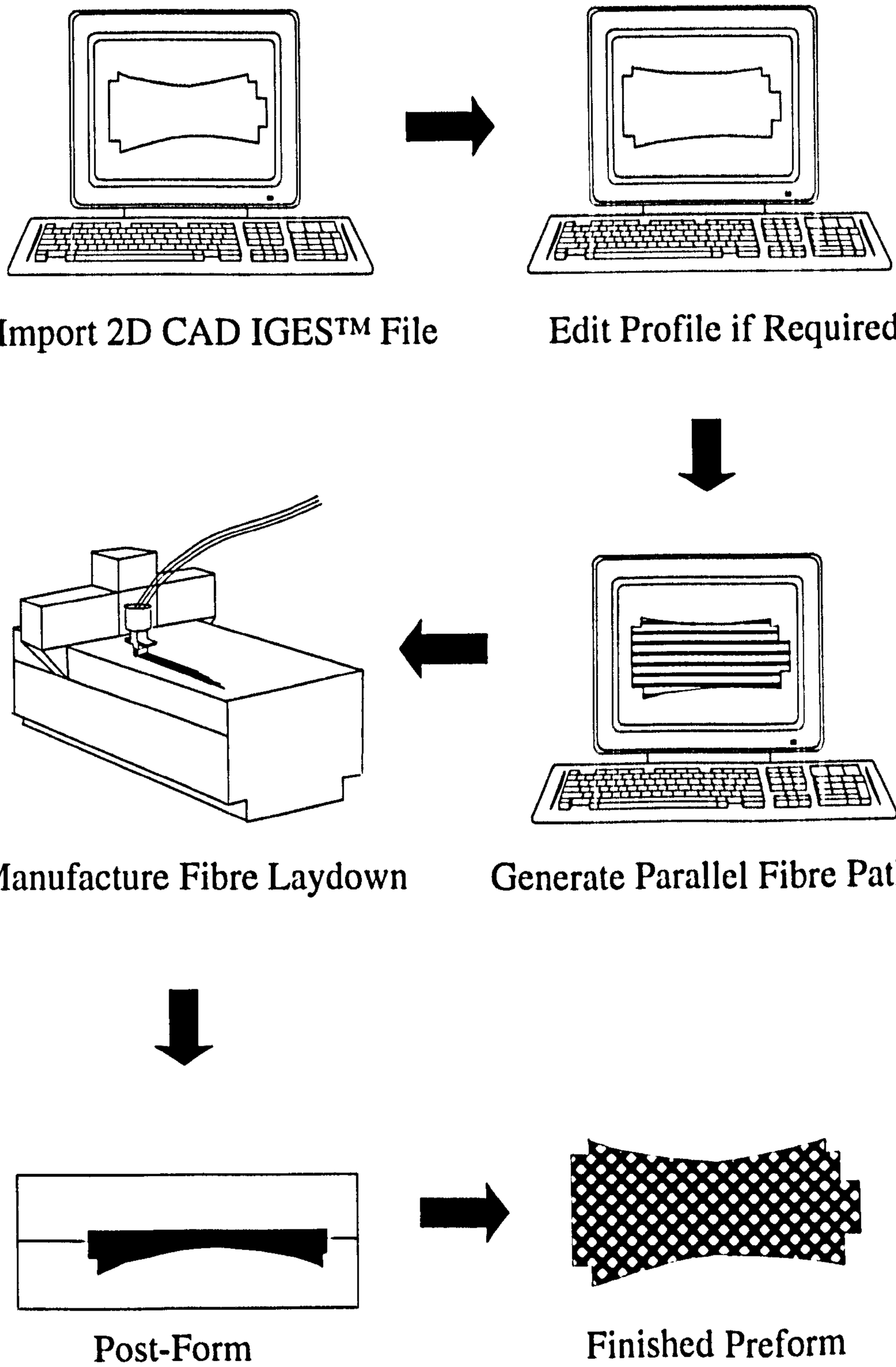

Figure 4.2 Schematic illustrating NC part program production using 2D CAD description of component

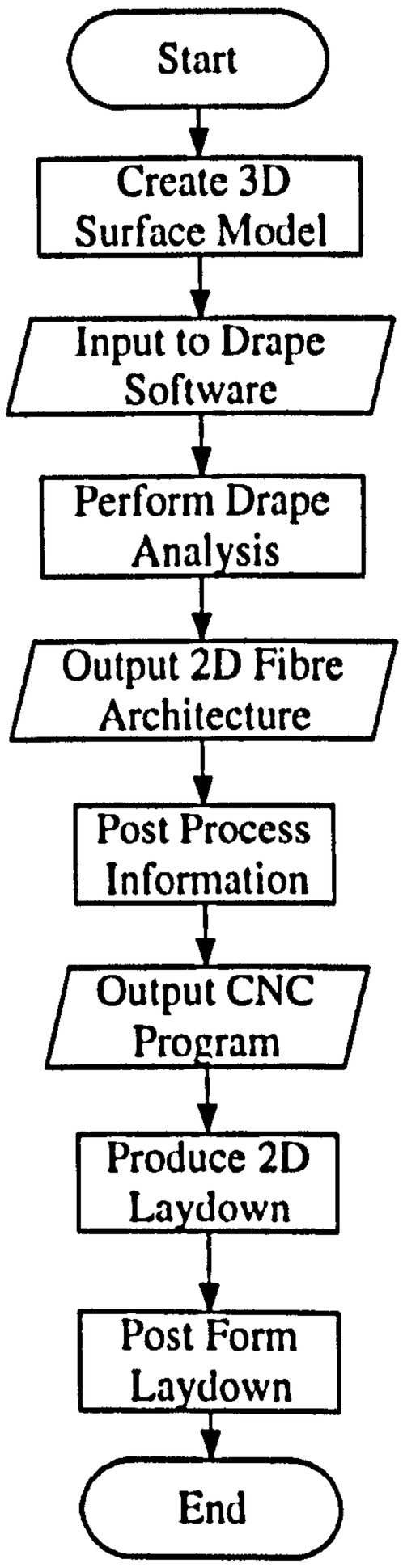

Figure 4.3 Flow diagram illustrating NC part program production using drape analysis.

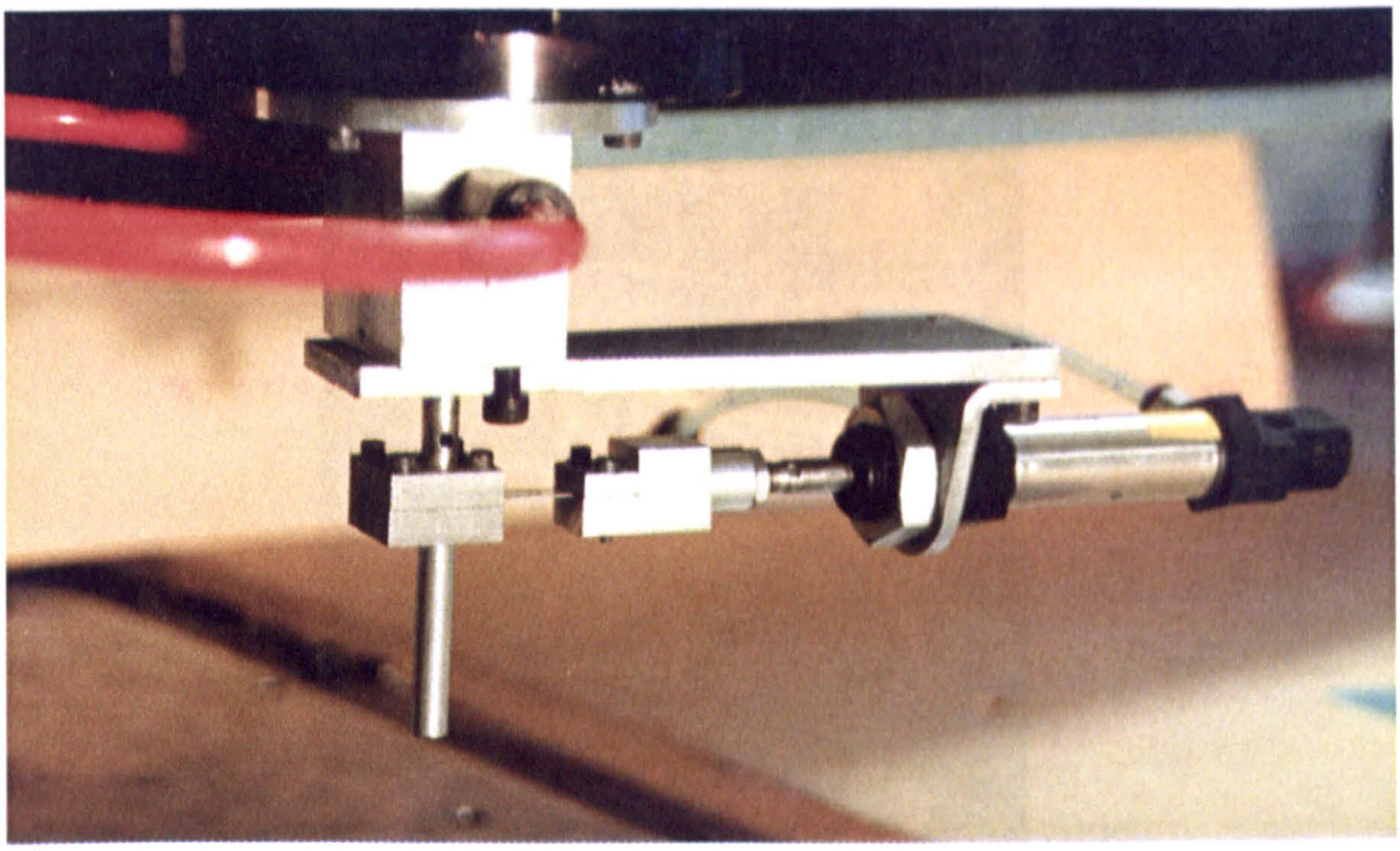

Figure 4.4 Photograph of single tow airjet tow placement head

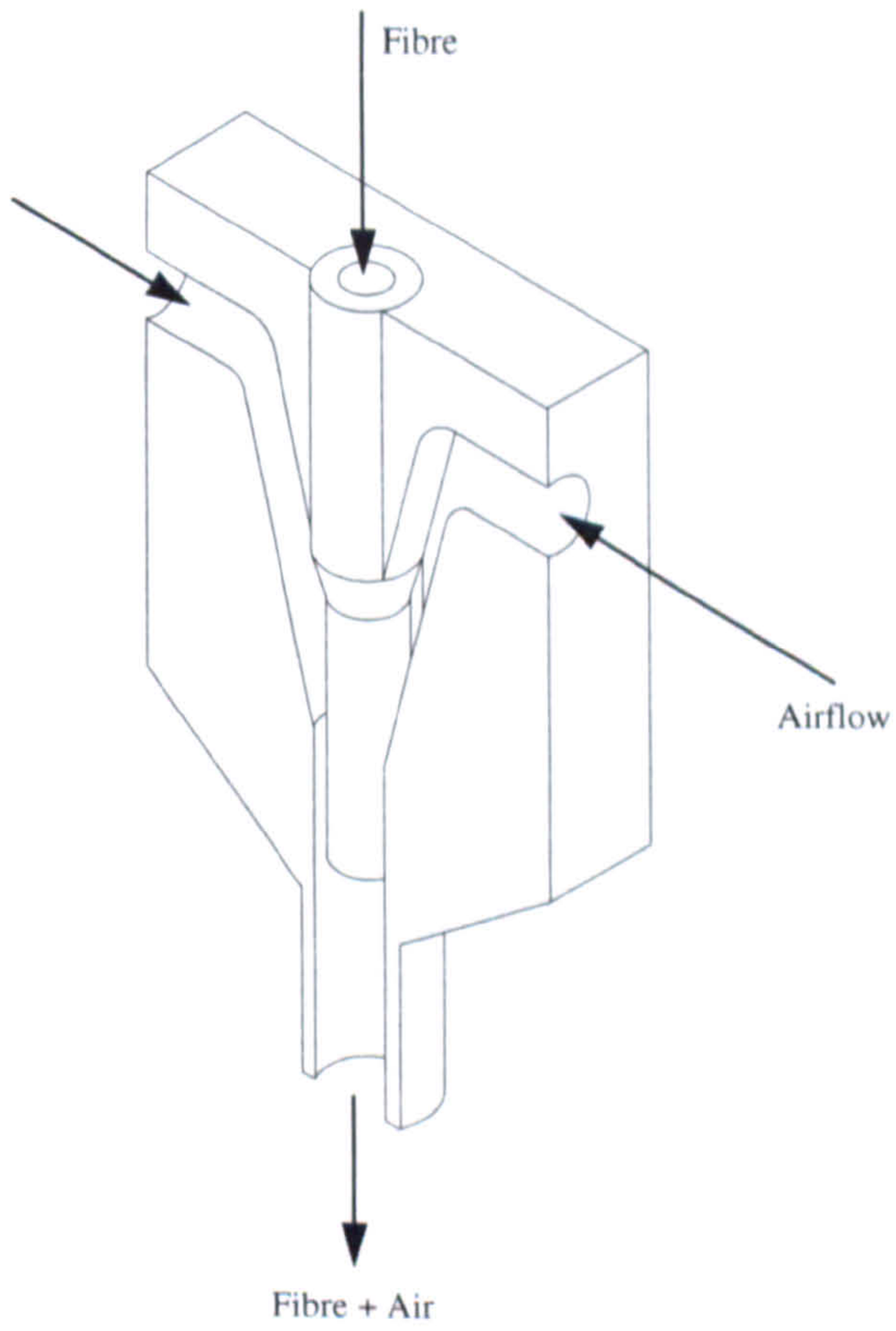

Figure 4.5 Schematic of concentric nozzles used to propel tow from airjet head

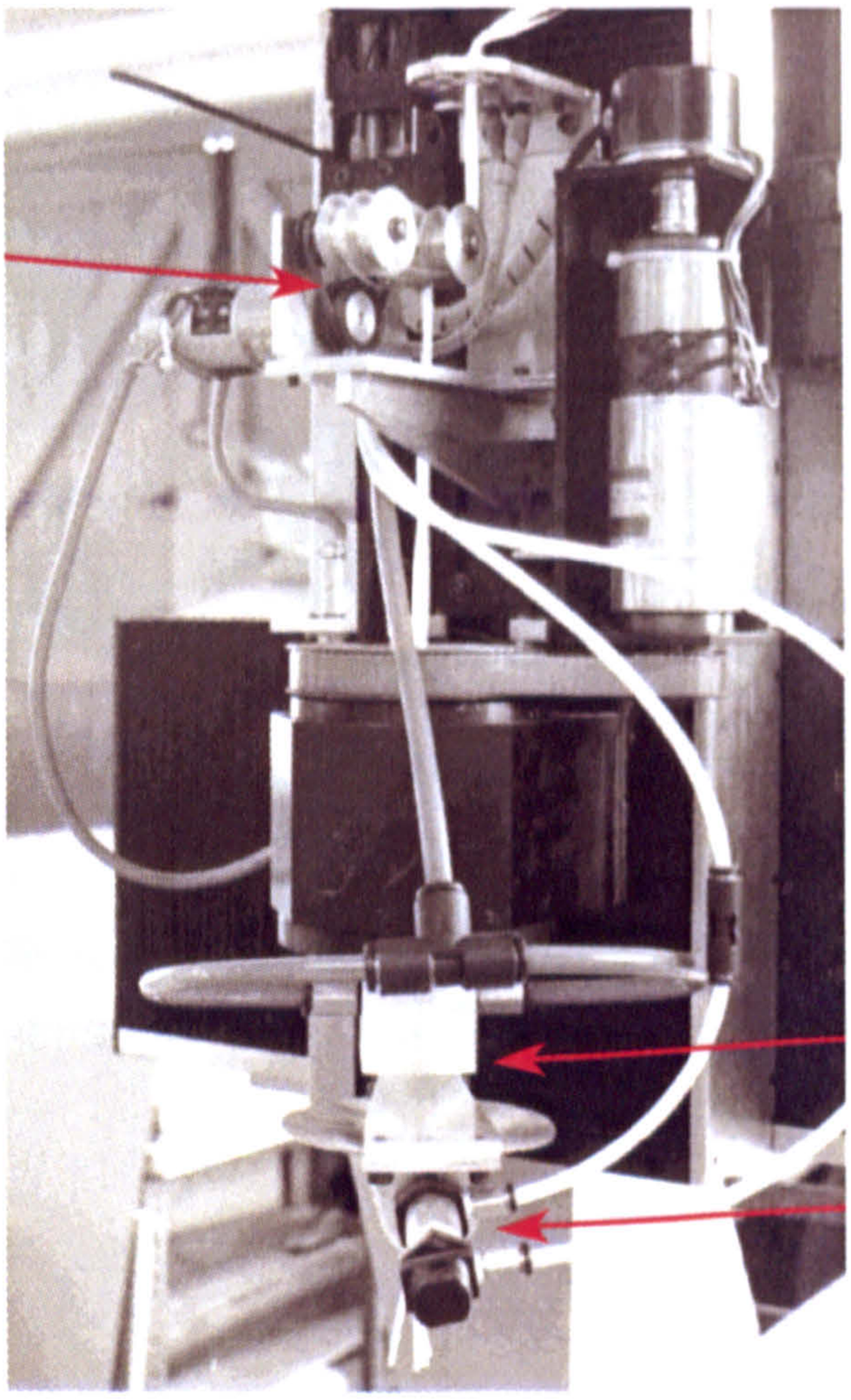

Figure 4.6 Airjet tow payout unit

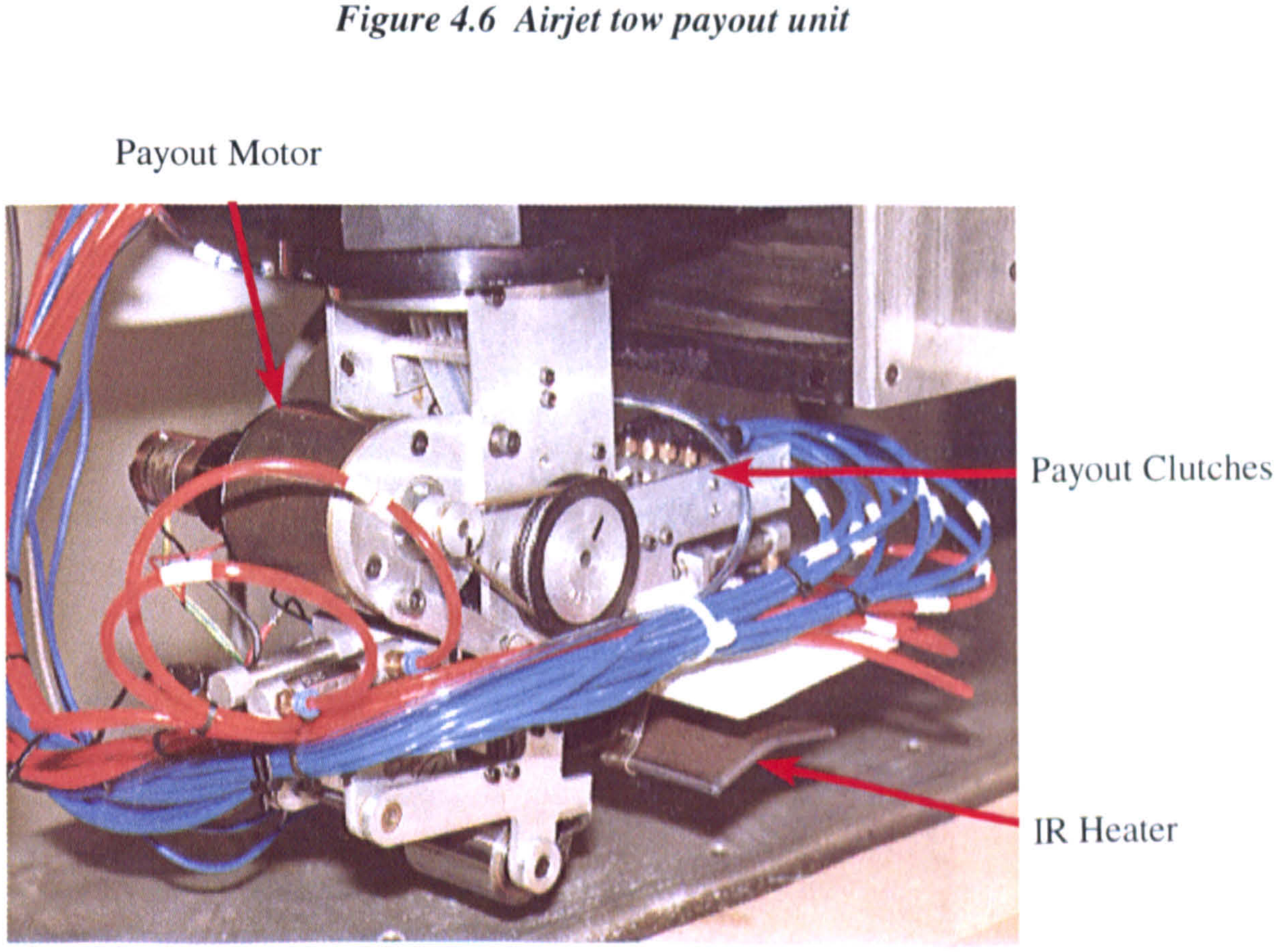

Figure 4.7 Multi-tow roller placement head showing payout motor and clutches and infra red emitter strip

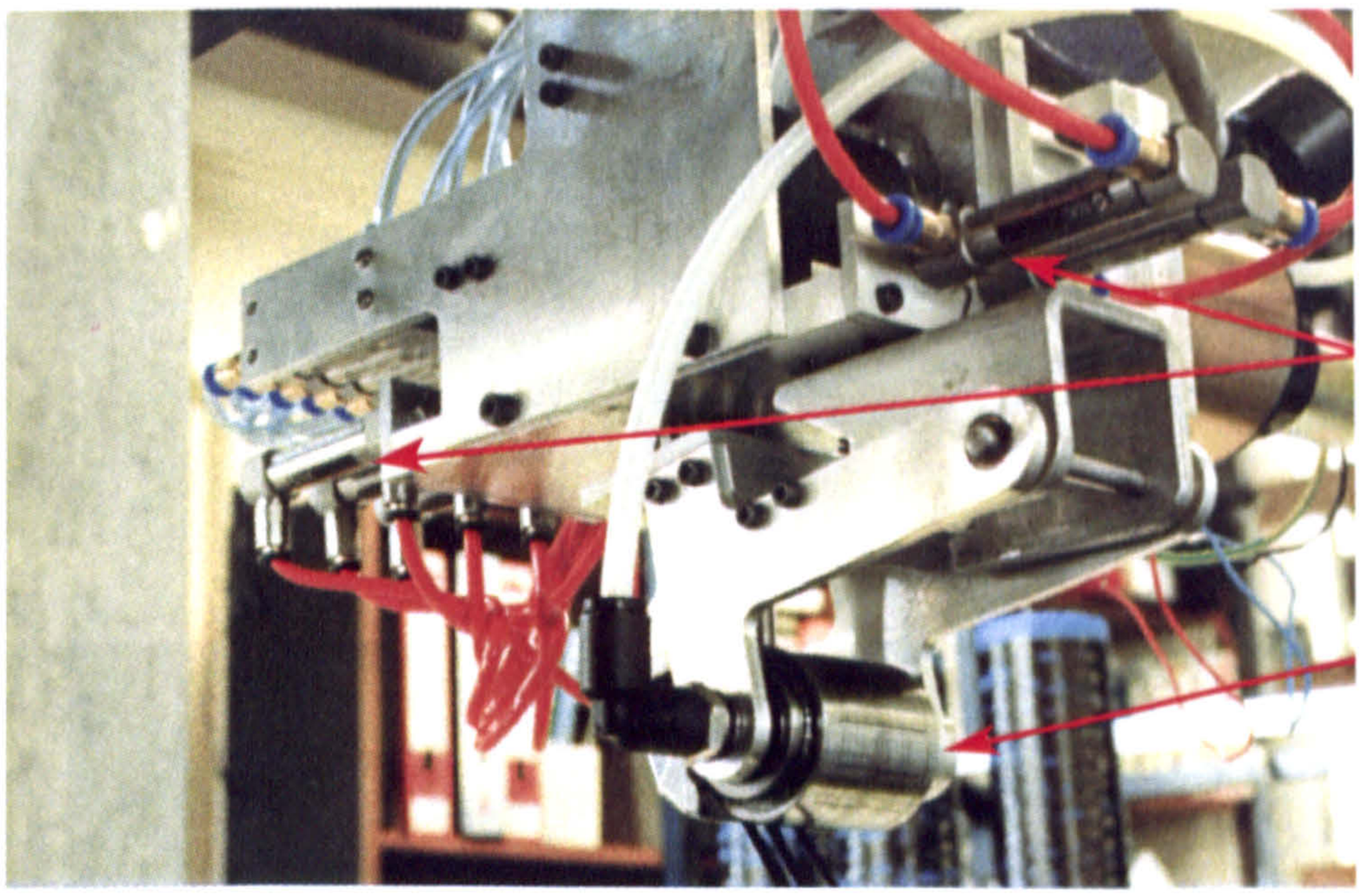

Figure 4.8 Underside of multi-tow roller head showing compaction roller and tow cutting system

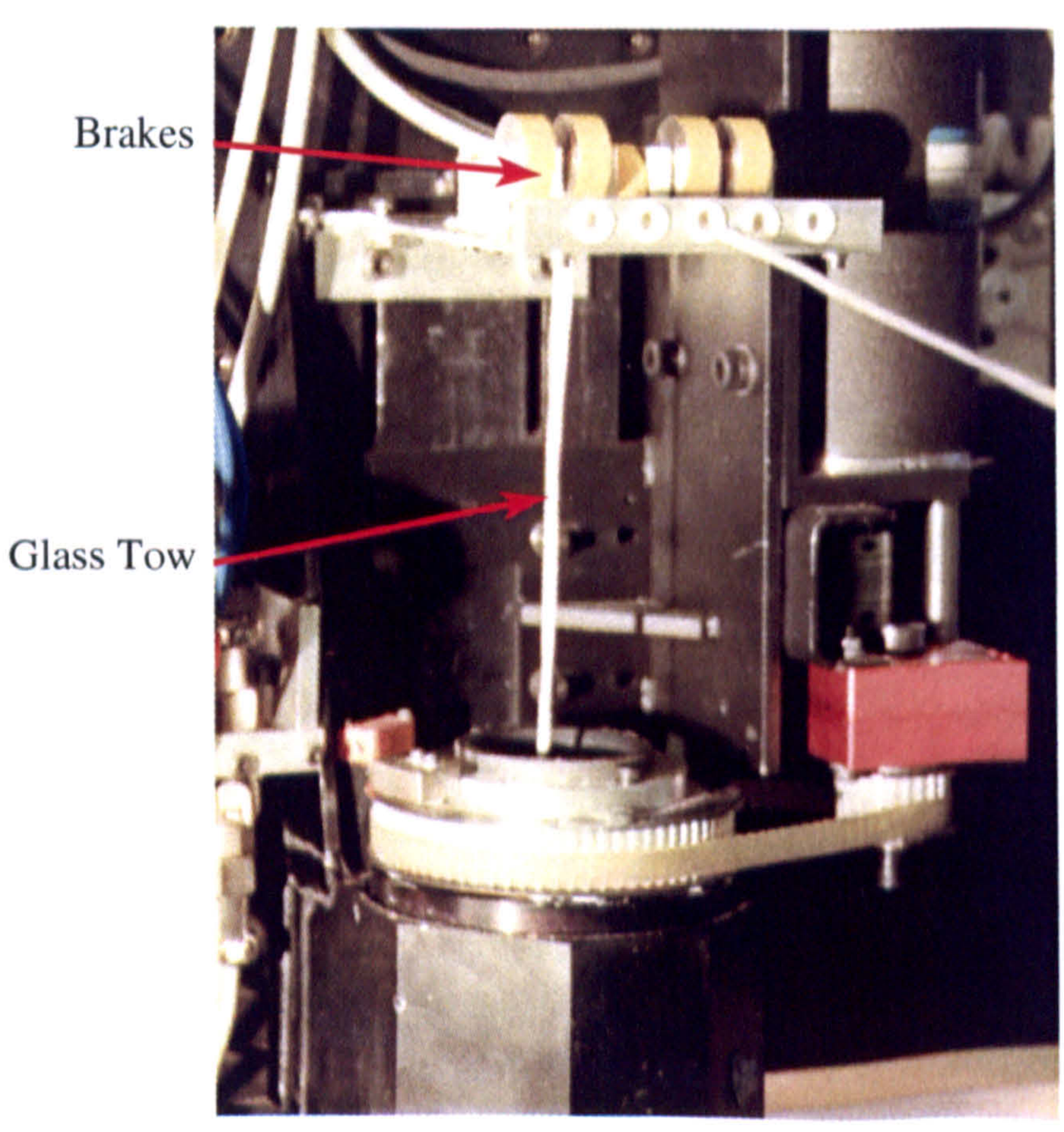

Figure 4.9 Multi-tow roller tow brakes

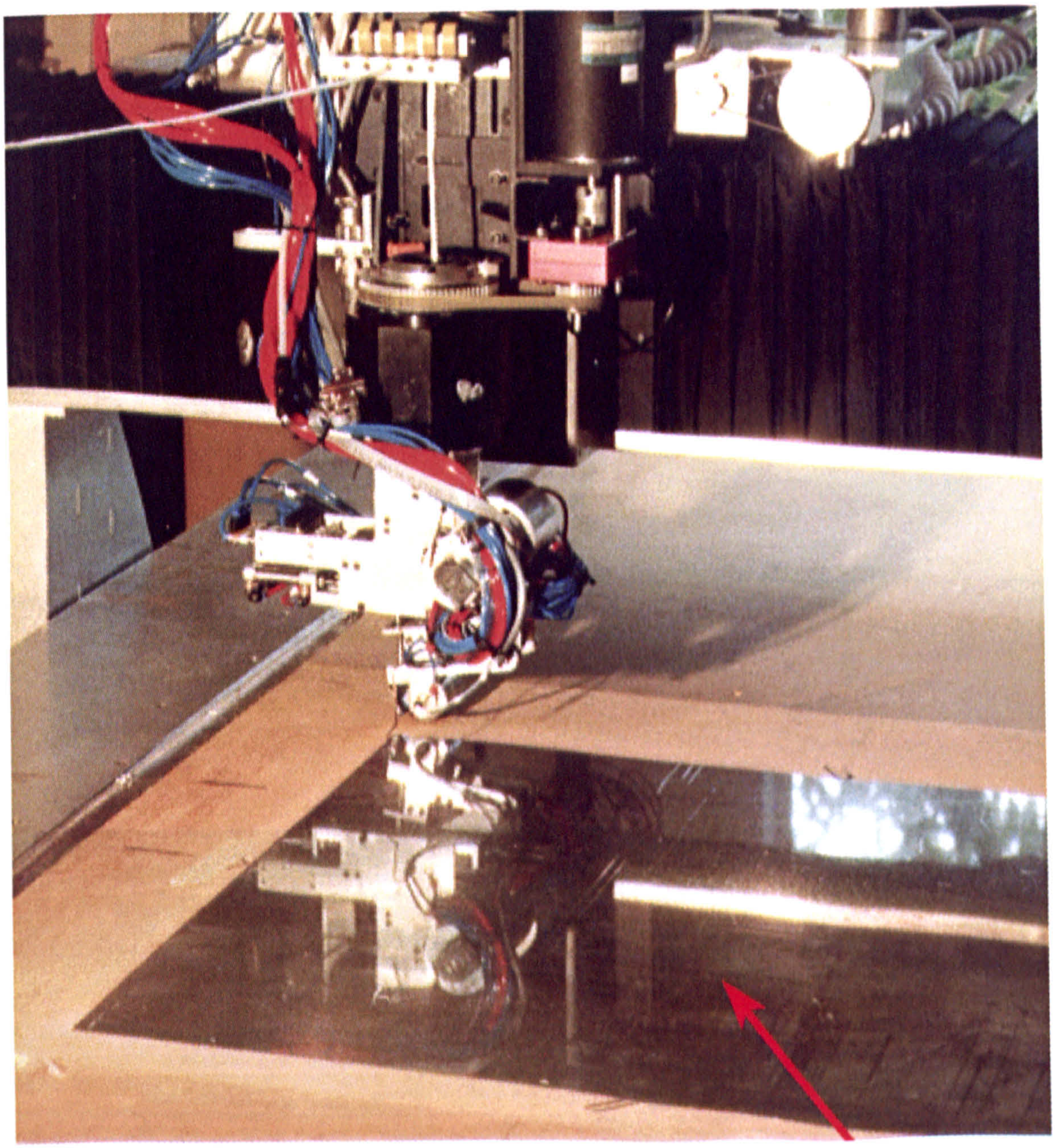

Figure 4.10 Watlow metal sheathed mica platen heater

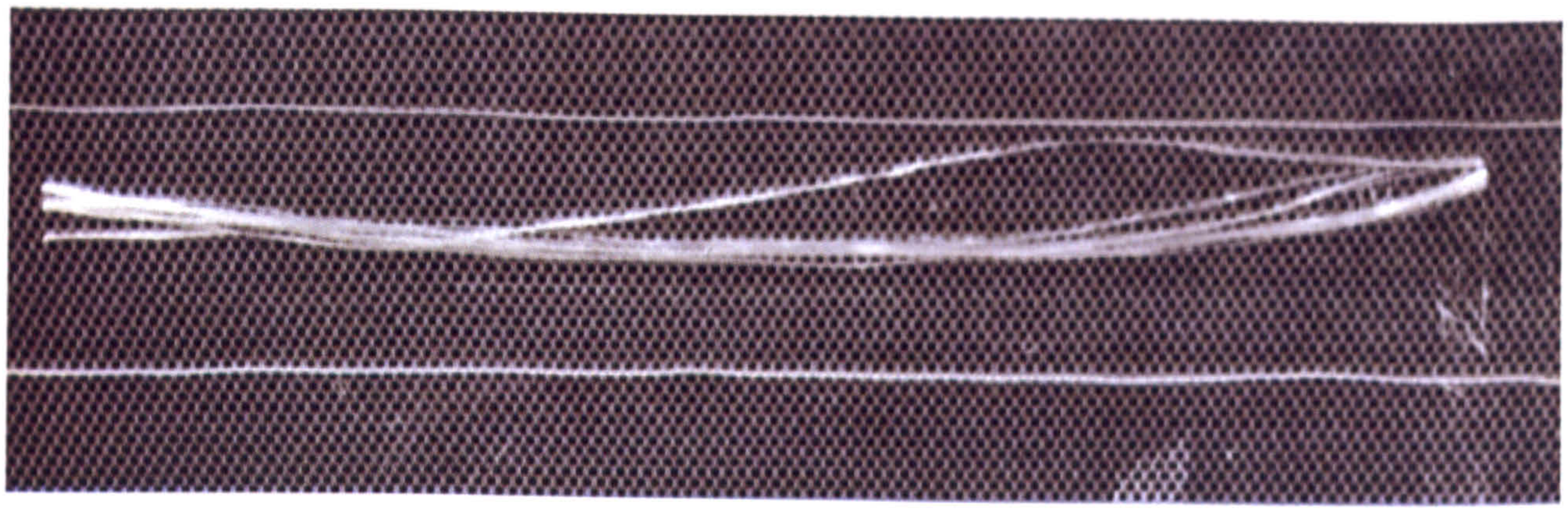

a) Scanned photograph

b) Skeletal image

Figure 4.11 Single E-glass tow used to determine straightness

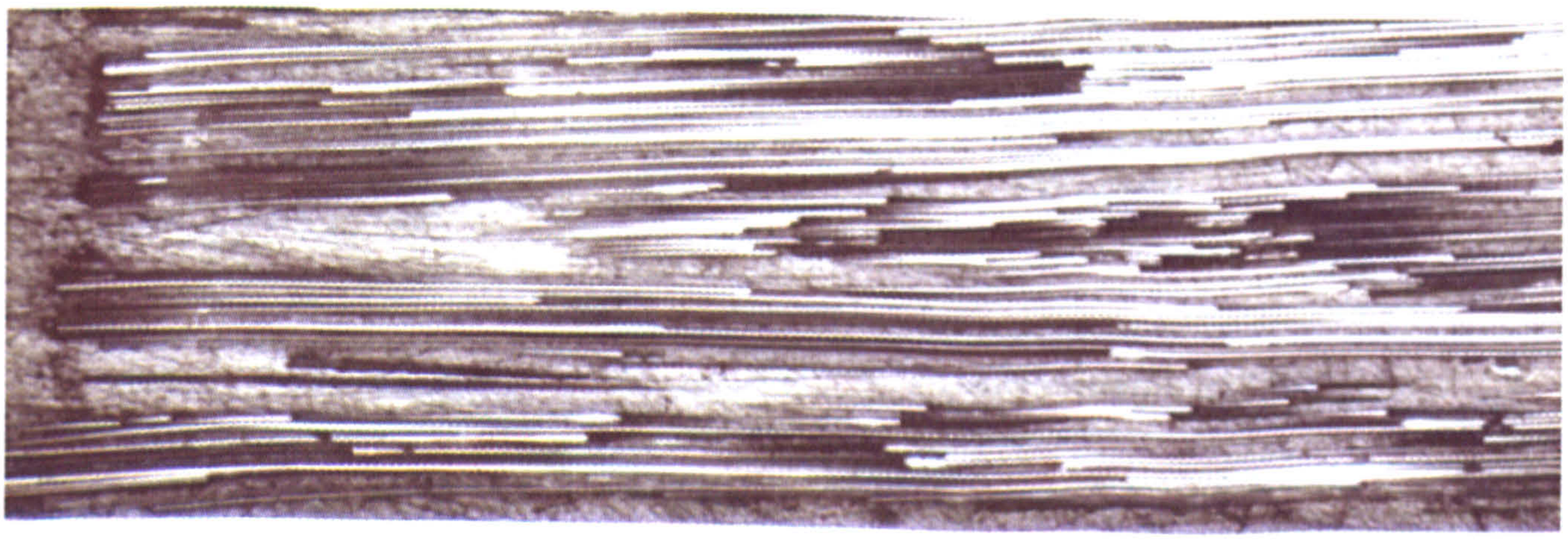

Figure 4.12 Image of E-glass/epoxy polished section taken at 40x magnification to determine fibre misalignment

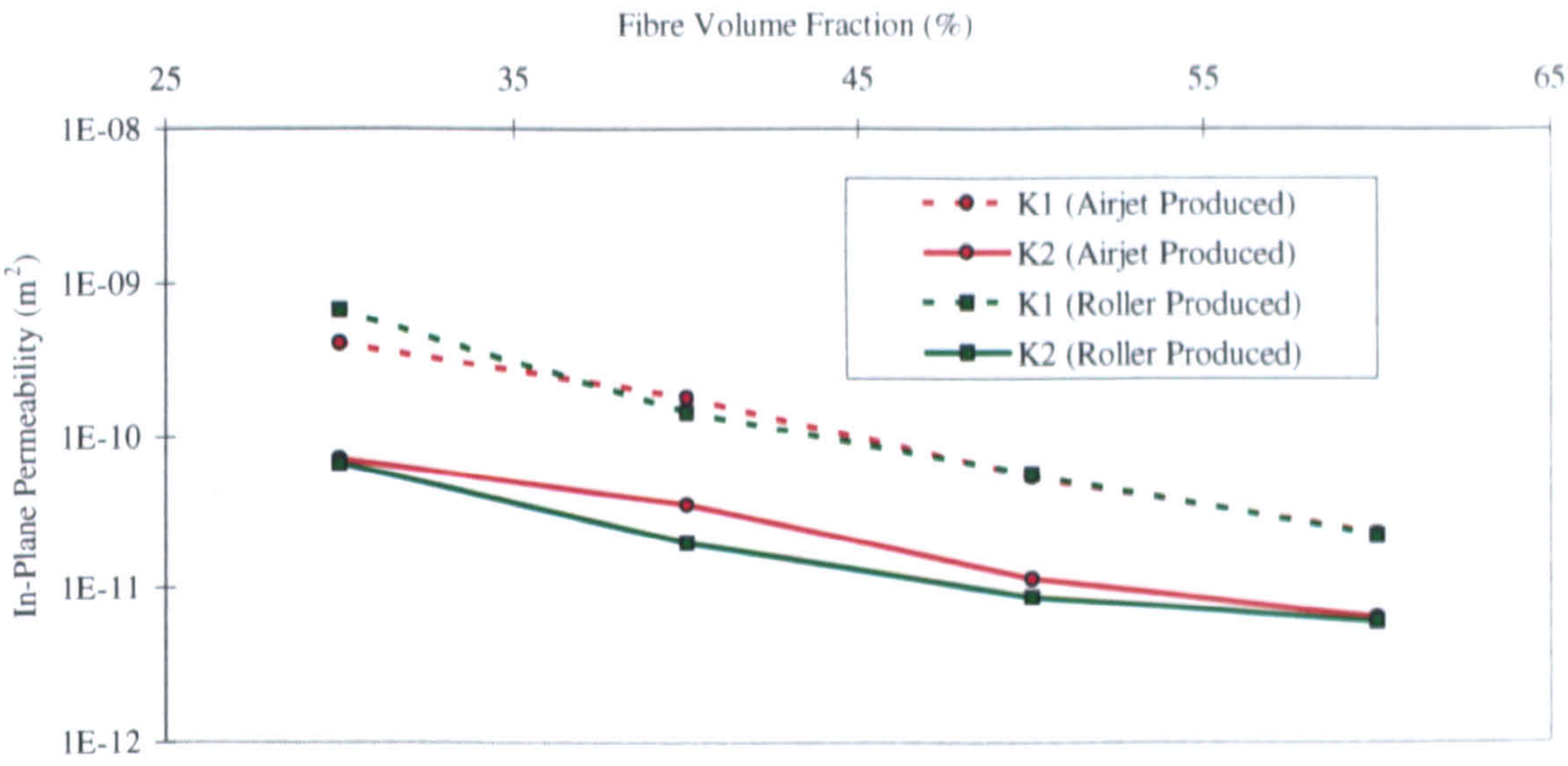

Figure 4.13 Permeability of tow placed unidirectional E-glass reinforcement

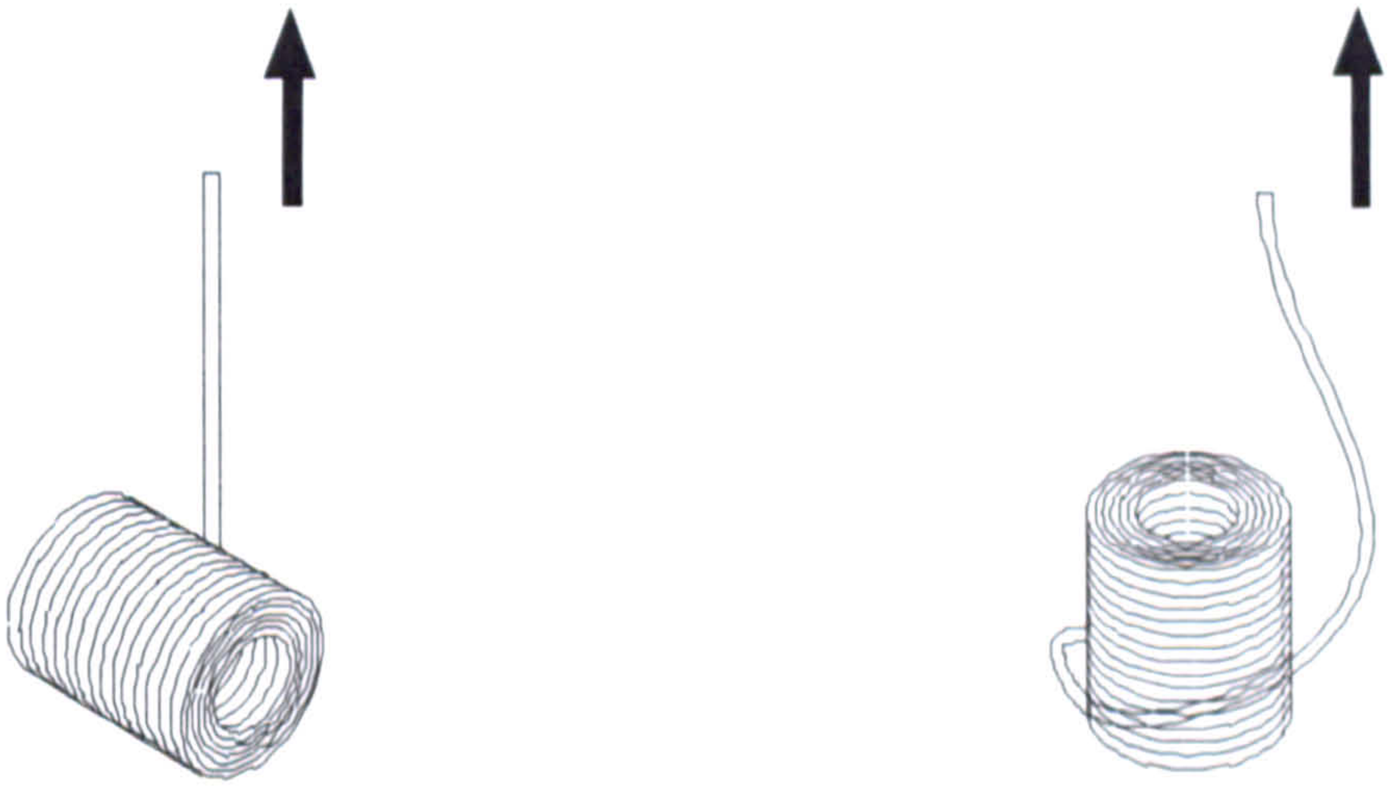

a) Tangential ***b) Circumferential***

Figure 4.14 Methods of unwinding tow from creels

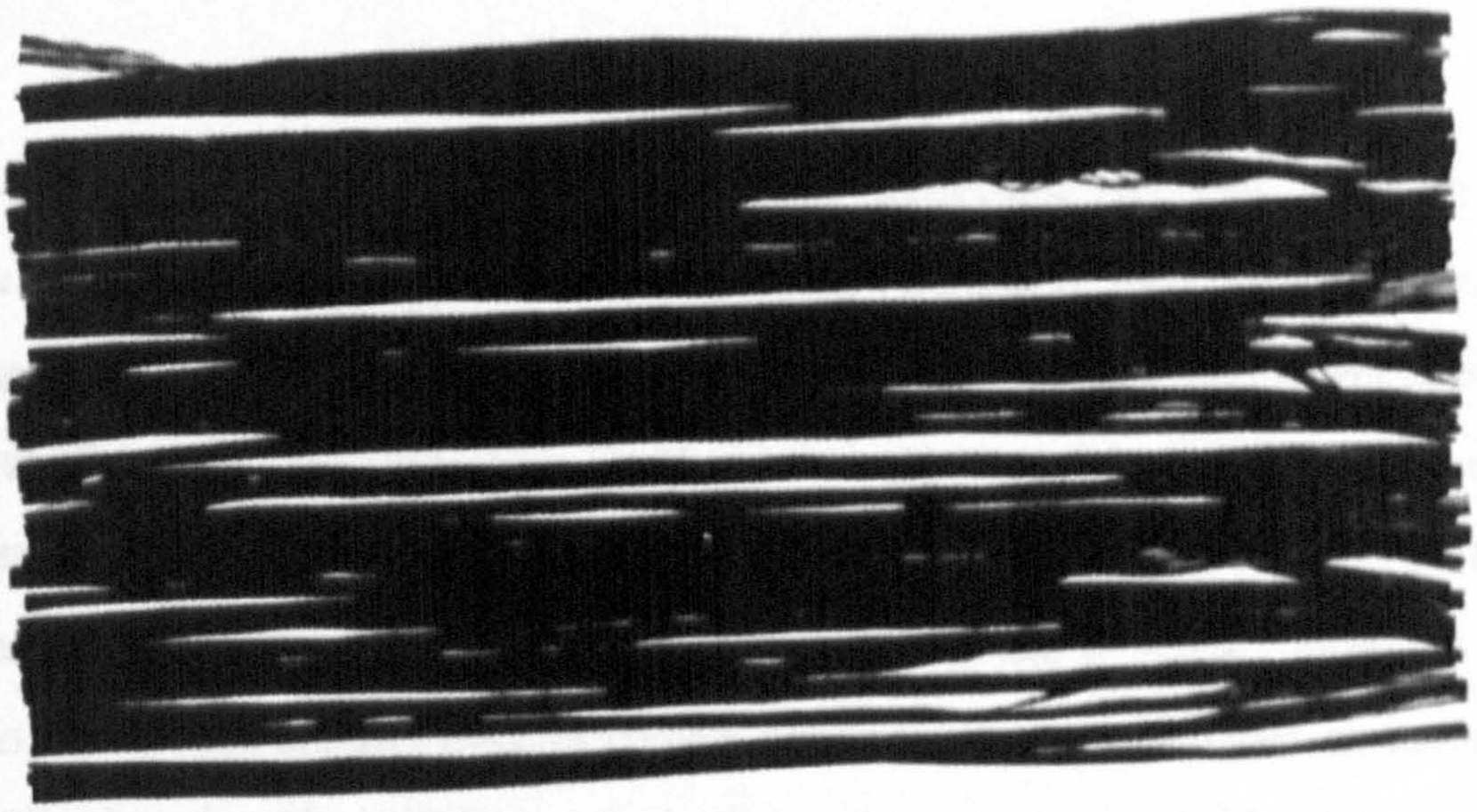

Figure 4.15 Photograph of carbon laydown used to determine uniformity of fibre coverage

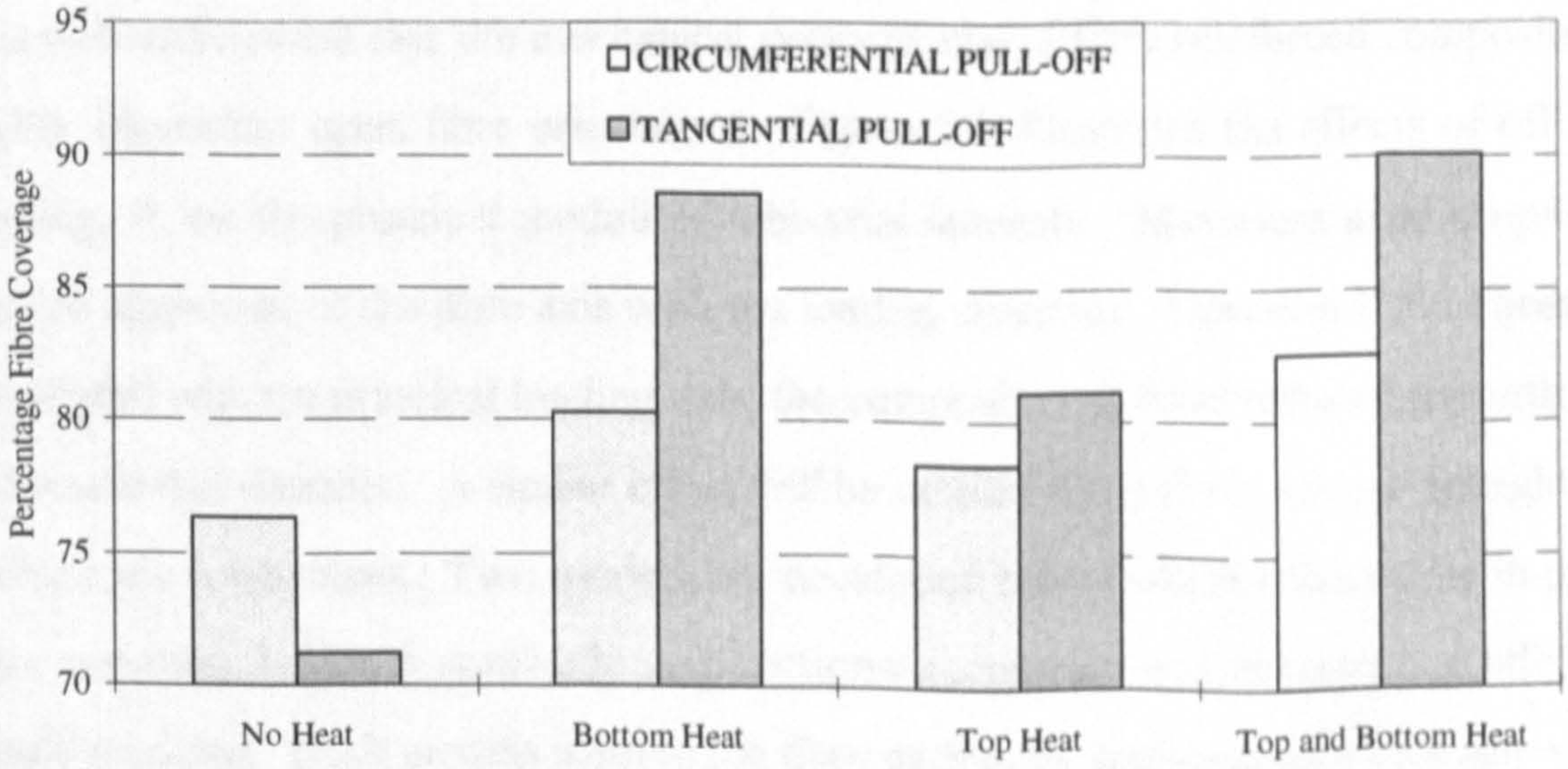

Figure 4.16 Percentage fibre coverage at various processing conditions

Chapter 5
Effects of Fibre Waviness on Composite Performance

5.1 Introduction

Out-of-plane waviness is inherent in all woven fabrics due to crimp. In-plane waviness tends to be associated more with the effects of handling or forming operations but was also evident to a small extent in preforms produced using the tow placement system when several plies were laid in one pass. Waviness changes the axial properties of an otherwise unidirectional preform. Chapter 2 described existing models for prediction of the effects of waviness on composites manufactured from woven fabric [95-98], although waviness is also problematic in other kinds of composites such as in thick filament wound structures [94,99] where buckling of fibres results from the pressure exerted by the over-wrapped layers. Existing work in this field [92-100] applies to a relatively small degree of waviness and usually considers only out-of-plane waviness. Four models were investigated here to estimate the effects of waviness on the in-plane permeabilities and the resulting laminate tensile moduli. The following chapter describes the four models and reports on their validation for a larger range of waviness in both E-glass and carbon reinforcements manufactured using tow placement.

5.2 Mechanical Properties

It is well understood that the mechanical performance of fibre reinforced composites is highly dependent upon fibre orientation. Figure 5.1. illustrates the effects of off-axis loading, θ, on the principal moduli of a bi-axial laminate. Maximum axial properties require alignment of the fibre axis with the loading direction. However if the fibres are not aligned with the principal loading axis, the composite will have reduced strength and stiffness in that direction. A similar effect will be noticed if the fibres are not straight but include some waviness. Two models are developed below which account for in-plane fibre waviness within a nominally unidirectional composite and estimate the effective tensile modulus. Both models assume the fibre path to be approximated by a sine wave where waviness factor (a/λ) is measured as the ratio of amplitude(a) of the sine wave to the wavelength(λ).

5.2.1 Modified Rule of Mixtures Model

The simplest model uses the load bearing efficiency of the reinforcement based on Krenchel's [72] efficiency factor within the modified rule of mixtures:

$$E_1 = \eta E_f V_f + E_m (1 - V_f) \tag{5.1}$$

The efficiency factor is based on the orientation of the fibres with respect to the direction of loading as shown in Figure 5.2. The efficiency of a fibre path following a sine wave is described by:

$$\eta = \frac{1}{S} \int_0^{\lambda} \cos^3 \theta \quad dx \tag{5.2}$$

where the length of the fibre over one cycle is:

$$S = \int_0^{\lambda} \frac{1}{\cos \theta} \, dx \tag{5.3}$$

and the angle subtended by the fibre with the longitudinal axis is:

$$\theta = \tan^{-1} \left[\left(\frac{2\pi}{\lambda} \right) a \, .\cos \left(\frac{2\pi x}{\lambda} \right) \right] \tag{5.4}$$

The full derivation for the efficiency factor is provided in Appendix 5.1. The laminate efficiency factor for a sinusoidal fibre distribution was calculated by numerical integration of Eqns (5.2) and (5.3) using the trapezium rule in a MS Qbasic™ program.

5.2.2 Classical Laminate Model for In-Plane Waviness

A second model was applied to predict the modulus of a laminate containing in-plane sinusoidal fibre distribution based on classical laminate theory [74]. This includes the effects of shear modulus and Poisson's ratio in the calculation that were neglected in the

modified rule of mixtures approach. Here the laminate modulus for a 0° composite with off-axis loading at an angle, θ, to the fibres is given by:

$$\frac{1}{E_x} = \overline{S_{11}} - \frac{\overline{S_{16}^2}}{\overline{S_{66}}} \qquad (5.5)$$

Where $\overline{S_{11}}$, $\overline{S_{16}}$, $\overline{S_{66}}$ are the modified compliance terms for off-axis loading described in more detail in Appendix 5.2.

For a sinusoidal fibre, θ varies along the wavelength of the fibre as described in Figure 5.2. At any point along the wavelength, θ is derived from eqn (5.4). The modulus is derived by integrating eqn (5.5) over one wavelength:

$$\frac{1}{E_x} = \int_0^{\lambda} \frac{\left(\overline{S_{11}}\,\overline{S_{66}} - \overline{S_{16}^2}\right)}{\overline{S_{66}}}\,dx \qquad (5.6)$$

The modulus is again determined by applying numerical integration to eqn (5.6) within a MS Qbasic™ program similar to that described in 5.2.1.

Modulus estimates using both the modified rule of mixtures and classical laminate theory were produced for waviness factors from 0 to 1. The model laminates in each case consisted of E-glass/epoxy and carbon/epoxy with in-plane sinusoidal fibre distribution and at a fibre volume fraction of 30%. The constituent properties used in the calculations are given in Table 5.1.

Table 5.1. Constituent Material Properties used in the Prediction of Composite Modulus with Sinusoidal Fibre Distribution (from manufacturers' data unless otherwise stated)

	E_1 (GPa)	E_2 (GPa)	G_{12} (GPa)	ν_{12}
Epoxy (Ciba 5052)	3.15	3.15	0.98	0.38
E-Glass (PPG 1062)	84	84	32.8 [102]	0.22
Carbon (Tenax 5131)	260	20	104 [102]	0.2
Glass/Epoxy	27.4 [R]	6.62 [102]	1.74 [102]	0.33
Carbon/Epoxy	80.2 [R]	7.0 [102]	5.3 [101]	0.33

[R] = *Estimation using the rule of mixtures*

5.2.3 Specimen Manufacture

To validate the in-plane waviness models, glass and carbon laydowns were produced using the tow placement facility at nominal volume fractions of 30%, although these values actually varied between 25-34% (glass) and 25-30% (carbon) to accommodate accurate waviness factors. Figure 5.3 shows photographs of fibre paths used to produce the tensile specimens. One tow was laid with a predetermined waviness factor under CNC control. The next tow was laid over the top of the first but offset along the nominal fibre axis between 5mm and 20mm depending on the wavelength of the specimens. This procedure was repeated until an even coverage and the required fibre volume fraction were achieved. The 40mm x 250mm specimens were moulded by RTM in the heated (80°C) aluminium tool using Ciba Geigy 5052 epoxy resin as described in 3.4.2 and post cured for one hour at 100°C in a hot air oven prior to testing

5.2.4 Results

Following post cure, the wavy specimens were tested in tension using the Instron 1195 screw driven testing machine according to the procedure discussed in 3.5.2. Figure 5.4a shows the results for the glass/epoxy laminates along with the predicted results from the classical laminate theory and modified rule of mixtures models. Six samples were produced for each of eight distinct values of fibre waviness from 0 to 0.4. The experimental points on the graph are the average of these six samples. The standard

deviation of the samples was 5.6% on average and can be accounted for by the variation in fibre volume fraction in each sample set. The y-axis shows the modulus normalised to the experimental unidirectional (0°) value (30.1GPa). Generally the predicted values follow the experimental data very well. The classical laminate model gives an excellent agreement to the results for the first four points (waviness = 0 to 0.05) with deviations from the experimental results of less than 3%. From a/λ=0.1 the classical laminate model over-predicts the reduction due to waviness although it still follows the results closely. The modified rule of mixtures approach follows the correct trend of the results, but under-estimates the effects of waviness by up to 20%.

Figure 5.4b shows the results for the carbon/epoxy laminates along with the predicted results from the two models. Again, six samples were produced for each fibre waviness factor (from 0 to 0.3). The plotted data are the average of these six samples. The standard deviations were reduced compared to the glass/epoxy samples at 3.3%. The plotted values are normalised to the experimental unidirectional (0°) modulus (80.2GPa). The modified rule-of-mixtures approach provides a surprisingly good approximation of the experimental data over the range of waviness factors evaluated. However, the classical laminate model underestimates the results over the entire range. Possible reasons for this difference could be that the facility, although programmed to lay the specimens in a sine wave pattern, may induce tension during laydown, resulting in the fibre deviating from its sine wave path. A further explanation can be attributed to the laminate properties (such as transverse and shear modulus) used in the predictions which were taken from literature [101] due to a lack of unidirectional laminate data for the material tested. As the classical laminate model is highly dependent on the shear modulus of the unidirectional laminate, more accurate values may result in a significant improvement in the predicted properties.

Figures 5.4a and 5.4b also show the predicted reduction in laminate modulus with increasing fibre waviness for another fibre waviness model used by researchers such as Bolotin [95] and Mrse and Piggot [100]. The Bolotin prediction assumes a linear relationship between compliance and the square of the angular deviation and predicts modulus as:

$$E_x = \frac{E_1 G_{12}}{G_{12} + \delta^2 E_1} \tag{5.7}$$

where δ^2 is the mean square angular deviation of the fibre from the principal direction and can be calculated from:

$$\delta^2 = 2 \pi^2 \frac{a^2}{\lambda^2} \tag{5.8}$$

It can be seen in Figures 5.4a and 5.4b that the Bolotin model over-predicted the modulus reduction due to waviness compared with the modified rule of mixtures and in-plane classical laminate models.

5.2.5 Application to Woven Samples

Although the two models described above predicted the effects of fibre waviness on the mechanical performance of composites produced using tow placed laydowns with good agreement, the majority of composites that suffer currently from fibre waviness are those manufactured from woven fabrics. The difference between fibre waviness associated with tow placed laydowns and woven fabric is the plane in which the waviness occurs. Tow placed fabrics contain waviness in the plane of the fabric whereas the waviness due to crimp in a woven material occurs out-of-plane. Similar models can be applied to out-of-plane waviness as those described above. The modified rule of mixtures model (Eqn 5.1) is as relevant to out-of-plane waviness as it is to in-plane waviness and so remains the same. The classical laminate model, however is modified slightly to account for the change in architecture. This results in changes to the boundary conditions due to the shear coupling effect of in-plane waviness. The full derivation of the model is provided in Appendix 5.3 where it is shown that for out-of-plane waviness, the effective modulus can be determined from:

$$E_x = \int_0^{\lambda} \frac{1}{\overline{\overline{S_{11}}}} dx \tag{5.9}$$

which was used by many researchers [97-99] to predict the effects of yarn undulation on the mechanical performance of woven composites.

To test whether in-plane or out-of-plane waviness had a greater effect on the tensile modulus of composites, test specimens were produced from woven E-glass and carbon fibre fabrics. The E-glass samples were produced from Flemings W/R 600 plain weave fabric and Ciba Geigy 5052 epoxy resin at a fibre volume fraction of 56.6% (±2.8%). Six carbon/epoxy samples were manufactured from Hexcel CGG108 five end harness satin weave fabric and 5052 resin at a fibre volume fraction of 46.1% (±2.5%). Fibre volume fractions for both types of specimen were determined by ashing as described in 3.5.4. Both materials were moulded in 40mm wide x 250mm long plaques using RTM in the heated (80°C) aluminium tool and post cured for one hour at 100° C prior to testing as described in 3.4.2.

Waviness was determined by preparing a 20mm x 20mm sample of the specimen taken normal to the fabric plane and parallel to the fibre axis. The samples were polished and photographed as described in 3.5.6. Fibre waviness was determined by importing the scanned images into the Visilog® image analysis package and measuring the fibre amplitude and wavelengths directly. Waviness was measured for ten tows chosen randomly within the samples. A typical digital image of a polished section is shown in Figure 5.5. Average waviness values and standard deviations for the glass/epoxy and carbon/epoxy laminates were calculated to be 0.033 ±15% and 0.03 ±56% respectively.

Predictions of the effects of the measured waviness on the tensile modulus of the samples were developed from the modified rule of mixtures and the out-of-plane classical laminate models described above. Constituent properties are listed in Table 5.2

The models for the woven materials were validated by testing the samples described above using an Instron 1195 screw driven test machine. Tensile tests were performed on all samples and the results are shown in Table 5.3 The results shown are the average of the six specimens with standard deviation also provided.

Table 5.2. Constituent Material Properties used in the Modulus Prediction of Composites Manufactured from Woven Cloth (from manufacturers' data unless otherwise stated)

	E_1 (GPa)	E_2 (GPa)	G_{12} (GPa)	ν_{12}
Epoxy (Ciba 5052)	3.15	3.15	0.98	0.38
E-Glass (Flemings W/R 600)	75	75	29.3 [**102**]	0.22
Carbon (Hexcel CGG108)	230	20	100 [**102**]	0.2
Glass/Epoxy	29.8 [**R**]	29.8 [**R**]	3.2 [**102**]	0.33
Carbon/Epoxy	62.4 [**R**]	62.4 [**R**]	5.3 [**101**]	0.34

[**R**] = *Estimation using the rule of mixtures*

Table 5.3. Experimental and Estimated Woven Composite Moduli

	Glass/Epoxy	Carbon/Epoxy
E_1 (Rule of Mixtures) (GPa) (%)	29.8 (100%)	62.4 (100%)
E_x (Modified Rule of Mixtures) (GPa) (%)	26.9 (90%)	57.2 (92%)
E_x (Classical Laminate) (GPa) (%)	26.3 (88%)	54.1 (87%)
E_x (Experimental) (GPa) (%) [S.D.]	27.5 (92%) [1.08]	53.4 (86%) [3.86]

Glass/epoxy results

Using the experimentally derived properties, manufacturers data and Halpin-Tsai [**102**] predictions for ply properties as shown in Table 5.2, the predicted modulus for a 0°/90° E-glass/epoxy composite at 56.6% fibre volume fraction using the rule of mixtures was 29.8GPa. Using a modified rule of mixtures approach with an included fibre waviness ratio of 0.033, the predicted modulus was reduced by 10% to 26.9GPa. With the classical laminate model, the predicted modulus was reduced by 12% to 26.3GPa. The average experimental modulus for the six specimens was 27.5GPa (a reduction of 8% on the rule of mixtures value). Standard deviation of the results was 1.08GPa. Both models over-

estimated the severity of the effects of fibre waviness on the modulus, although only by 2% (modified rule of mixtures) and 4% (classical laminate). Although the deviation of the results shows a range of values as high as 28.7GPa (a 4% decrease over the predicted rule of mixtures value) and as low as 26.5GPa (11% decrease), this can be attributed mainly to the variation in fibre volume fraction (55% - 59.4%) and it can be seen that both models show good agreement with the experimental values.

Carbon/epoxy results

Using the values in Table 5.2, the estimated modulus for a 0°/90° carbon/epoxy composite at 46.1% fibre volume fraction was 62.4GPa using the rule of mixtures. The classical laminate model with a fibre waviness of 0.03, predicted a reduction in modulus of 13% to 54.1GPa. A reduction in modulus of 8% to 57.2GPa is predicted by the modified rule of mixtures. The experimental modulus was 53.4GPa (a reduction of 14% on the rule of mixtures predicted value). The classical laminate theory and modified rule of mixtures models both under-estimated the severity of the effects of fibre waviness by 1% and 6% respectively. The modified rule of mixtures model is less accurate because it is a very simple geometry based model and does not take account of laminate properties such as shear modulus and Poisson's ratio.

To determine whether similar results were obtained from literature, the modified rule of mixtures and the out-of-plane classical laminate models were applied to the results obtained by Alif and Carlsson [103] and Falzon and Herszberg [104] for woven composites. The material property data, model and experimental results for the two investigations can be seen in Table 5.4.

The experimental results obtained by Falzon and Herszberg [104] for E-glass/vinylester composites manufactured using plain weave fabric suggest that there is an effect of fibre waviness on modulus reduction but because of the low modulus of the reinforcing fibres the reduction is small. Both the modified rule of mixtures and the out-of-plane classical laminate models predict the effective modulus to lie within the bounds of the experimental results in this case. Alif and Carlsson [103] provided experimental results for the tensile

modulus of carbon/epoxy and E-glass/epoxy laminates manufactured using satin weave fabrics. The results for the E-glass/epoxy composites again show that there is a small reduction due to waviness but both models over predicted the modulus. The results for the carbon/epoxy composite however show that for a waviness factor of 0.036 the tensile modulus dropped from a rule of mixtures predicted 96.4GPa to 59.5GPa. The modified rule of mixtures under-predicted the effect of the waviness on modulus significantly (92.5GPa) but the out-of-plane classical laminate model provided a satisfactory prediction of 57.6GPa which supports the experimental results reported in Table 5.3.

Table 5.4. Constituent Material Properties, Experimental and Predicted Moduli of Woven Composites (from literature unless otherwise stated)

	ALIF [103]		FALZON [104]			
	carbon /epoxy	E-glass /epoxy	E-glass / vinylester warp	E-glass / vinylester weft	E-glass / vinylester warp	E-glass / vinylester weft
V_f (%)	71	56	70	70	56	56
E_f (GPa)	234	72	74	74	74	74
E_m (GPa)	4.2	4.2	3.2	3.2	3.2	3.2
ν_f	0.27	0.3	0.2	0.2	0.2	0.2
ν_m	0.35	0.35	0.38	0.38	0.38	.038
G_{12} (GPa)	3.2 [102]	2.6 [102]	6.9 [102]	6.9 [102]	4.7 [102]	4.7 [102]
ν_{12}	0.32	0.34	0.32	0.32	0.32	0.32
E_1 (GPa)[107]	96.4	31.3	35.3	35.3	29.2	29.2
a/λ	0.036	0.013	0.056	0.027	0.033	0.021
E_{EXP} (GPa)	59.5	26.6	31.5 - 34.7	31.5 - 34.7	27.5 - 30.5	27.5 - 30.5
E_{MROM} (GPa)	92.5	31.2	32.5	34.5	28.4	28.9
E_{CLT} (GPa)	57.6	30.3	31.3	34.2	27.3	28.4

Subscripts: *EXP = experimental data*
MROM = prediction using the modified rule of mixtures
CLT = prediction using the out-of-plane classical laminate model

It can be seen from the above that out-of-plane waviness is more detrimental to laminate stiffness than in-plane waviness. A summary of some of the results for both in-plane and out-of-plane carbon and glass reinforced laminates is shown in Table 5.5.

Table 5.5. Comparison of Experimental Results for Tensile Moduli of Laminates Containing In-Plane and Out-of-Plane Fibre Waviness.

Specimen	Volume Fraction (%)	Waviness	E_x/E_1
In-Plane Glass/Epoxy	30	0.03	0.94
In-Plane Carbon/Epoxy	30	0.05	0.94
Out-of-Plane Glass/Epoxy	56	0.033	0.92
Out-of-Plane Carbon/Epoxy	46	0.03	0.86
Out-of-Plane Glass/Epoxy [103]	56	0.013	0.84
Out-of-Plane Carbon/Epoxy [103]	71	0.036	0.62

5.3 Permeability

5.3.1 Theory

Permeability characterises the ability of a fluid to flow through a reinforcement and is defined by Darcy's law as described in 2.2. A model to predict the permeability of a preform with a sinusoidal fibre distribution has been developed. For a unidirectional reinforcement, the principal permeabilities are described by K_1 and K_2. A transformation of the matrix of principal permeabilities gives the permeability [63] at an angle, 0, to the fibre axis:

$$K_x = K_1\cos^2\theta + K_2\sin^2\theta - \frac{(K_2 - K_1)^2 \sin^2\theta\cos^2\theta}{K_1\sin^2\theta + K_2\cos^2\theta} \qquad (5.10)$$

Considering a unit cell of reinforcement with sinusoidal shape as shown in Figure 5.2, it is possible to determine the average principal permeabilites at any point within the preform. The permeability at any point within the cell can be obtained from:

$$\frac{\pi}{K_{avg}} = \int_0^{\lambda} \frac{dx}{K_x} \tag{5.11}$$

which by substituting Eqn (5.10) into Eqn (5.11) can be solved using numerical integration techniques (trapezium rule) within a simple MS Qbasic™ program. A detailed derivation of these equations can be found in Appendix 5.4.

This model was used to predict the longitudinal and transverse permeabilities of a set of nominally unidirectional E-glass preforms at a fibre volume fraction of 43% with a range of induced waviness factors. Principal permeabilities of the unidirectional reinforcement were $7.8 \times 10^{-11} m^2$ and $1.9 \times 10^{-11} m^2$ for flow longitudinal and transverse to the fibre axis. The predicted effect of fibre waviness on the principal permeabilities can be seen in Figure 5.6 where it is shown that the model predicts reductions in longitudinal permeability and increases in transverse permeability with rising waviness factors.

5.3.2 Specimen Manufacture

To validate the above predictions, a set of nominally unidirectional 2400 tex E-glass preforms with induced fibre waviness factors from 0.0 to 0.1 were manufactured using the tow placement facility (Figure 5.7). This represents a reduced range compared to the mechanical property tests but was imposed by the need to produce wider specimens to suit the permeability test facility. The laydowns were produced by offsetting successive tows along the Y-axis (mechanical property specimens were offset along the X-axis) and the arising fibre tensions resulted in some disturbance of the as-laid architecture at smaller radii of curvature thus limiting the waviness factors to 0.1. All preforms were produced to a fibre volume fraction of 42.8% (±1%) by altering the spacing between consecutive tows.

5.3.3 Results

The preforms were tested for permeability using the bench-top permeability rig as described in 3.5.1. Between three and six fibre laydowns were tested for each value of

waviness ($a/\lambda = 0$, 0.02, 0.05 and 0.1). The results are shown in Figure 5.6 and include the estimated values based on the principal permeabilites of a 0° fibre bed at 43% fibre volume fraction. Both the averaged longitudinal and transverse permeabilities follow the trend of the estimated values although the experimental results generally show greater isotropy which could be attributable in part to inaccurate loading of the preforms along the principal axes.. Also, standard deviation of the experimental values is quite large ranging from 1.3% to 53%. This is probably an effect of the variation in preform superficial density within each sample or a slight change in the clamping pressure of the permeability rig.

5.4 Conclusions

This chapter described the effects of fibre waviness on the axial properties of an otherwise unidirectional reinforcement. Four models were developed to predict the effects of both in-plane and out-of-plane fibre waviness on laminate tensile modulus and preform permeability. Validation of the models was performed by testing woven reinforcement and reinforcement manufactured using the tow placement facility.

It was found that for in-plane waviness, the modified rule of mixtures and the classical laminate theory models both predicted reasonable reductions in tensile modulus for a wide range of waviness factors. For laminates containing out-of-plane waviness (e.g. containing woven fabrics) the classical laminate theory model outperformed the modified rule of mixtures model probably because it takes account of the material shear modulus and Poissons effects. Because of its simplicity, the modified rule of mixtures model seems acceptable for predicting the effects of waviness on laminates with in-plane waviness. For out-of-plane waviness, the classical laminate model would give better predictions.

The final model was used to predict the effects of fibre waviness on in-plane permeability. Nominally unidirectional E-glass reinforcement was manufactured on the tow placement facility at 43% fibre volume fraction and with a range of waviness factors (0 to 0.1). Although the model was unable to predict exact values, the predicted trend was found to

be similar to that of the experimental results for both longitudinal and transverse permeability. The model still requires the experimental permeability values of the unidirectional preform but gives a good indication of the likely effects of waviness.

List of Figures

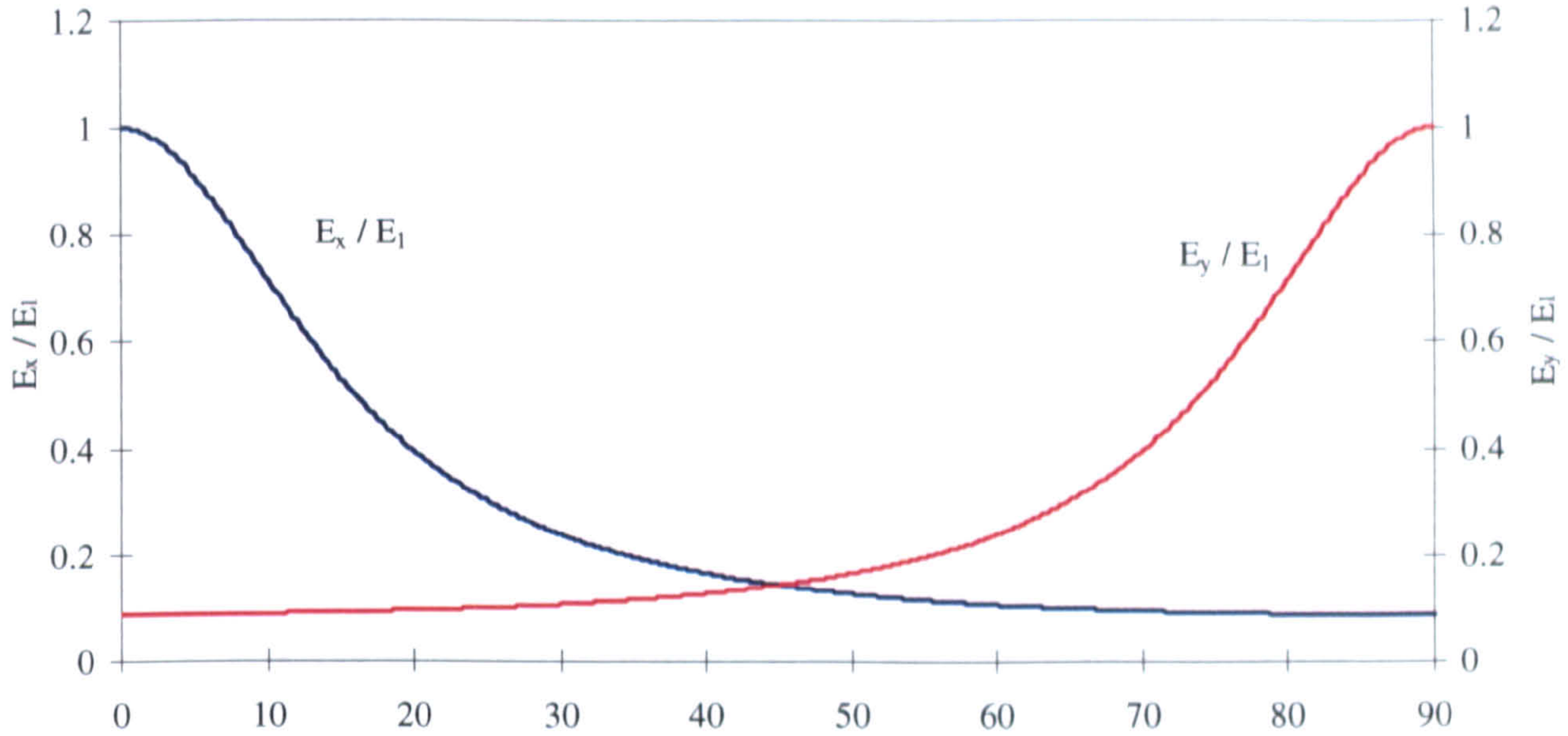

Figure 5.1 Dependancy of mechanical properties of fibre reinforced composites upon fibre orientation *(For the purpose of this work, however, fibre misalignments should be within 10 degrees)*

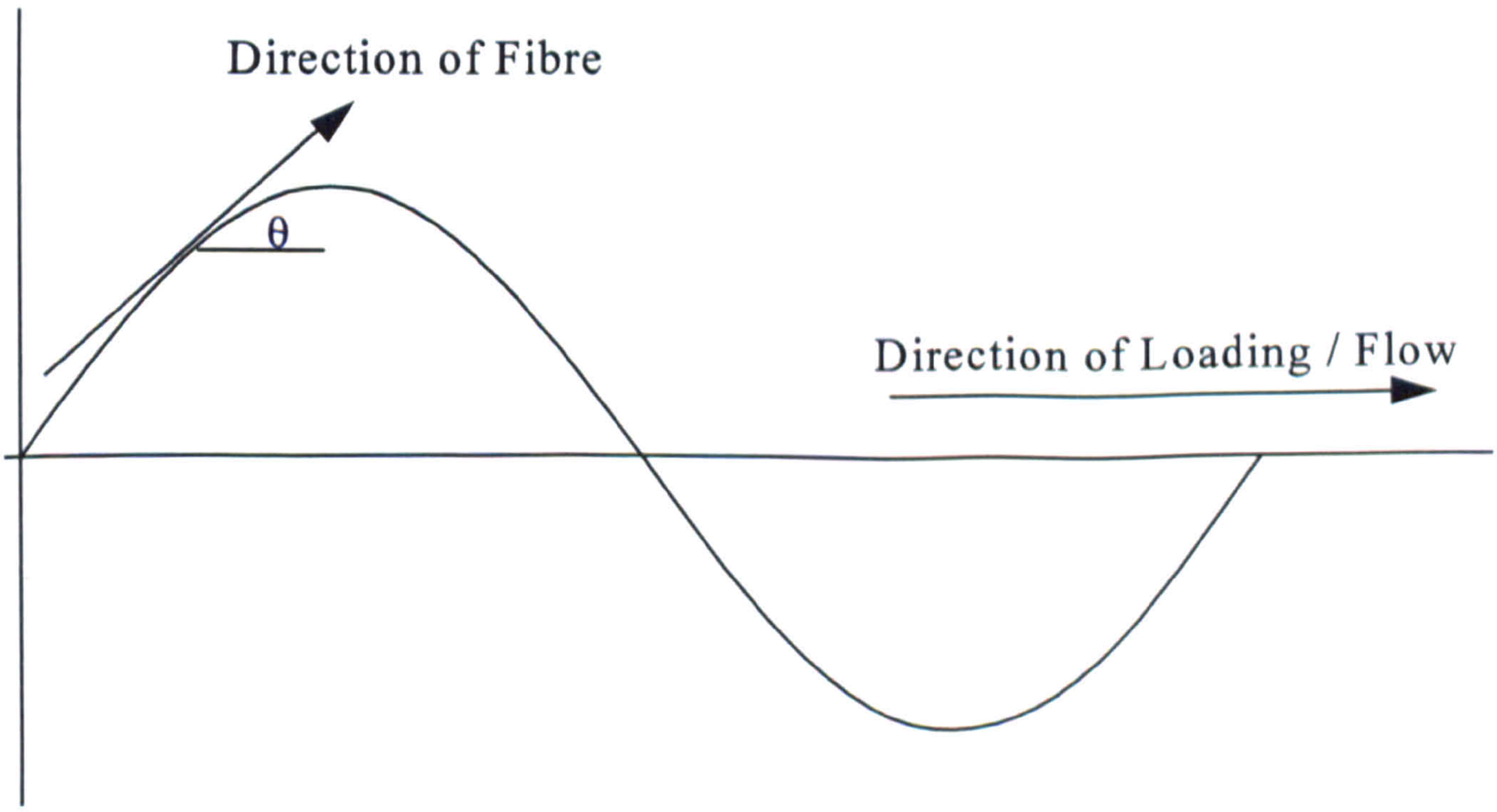

Figure 5.2 Variation of off-axis angle, θ, with distance along the axis of a sine wave

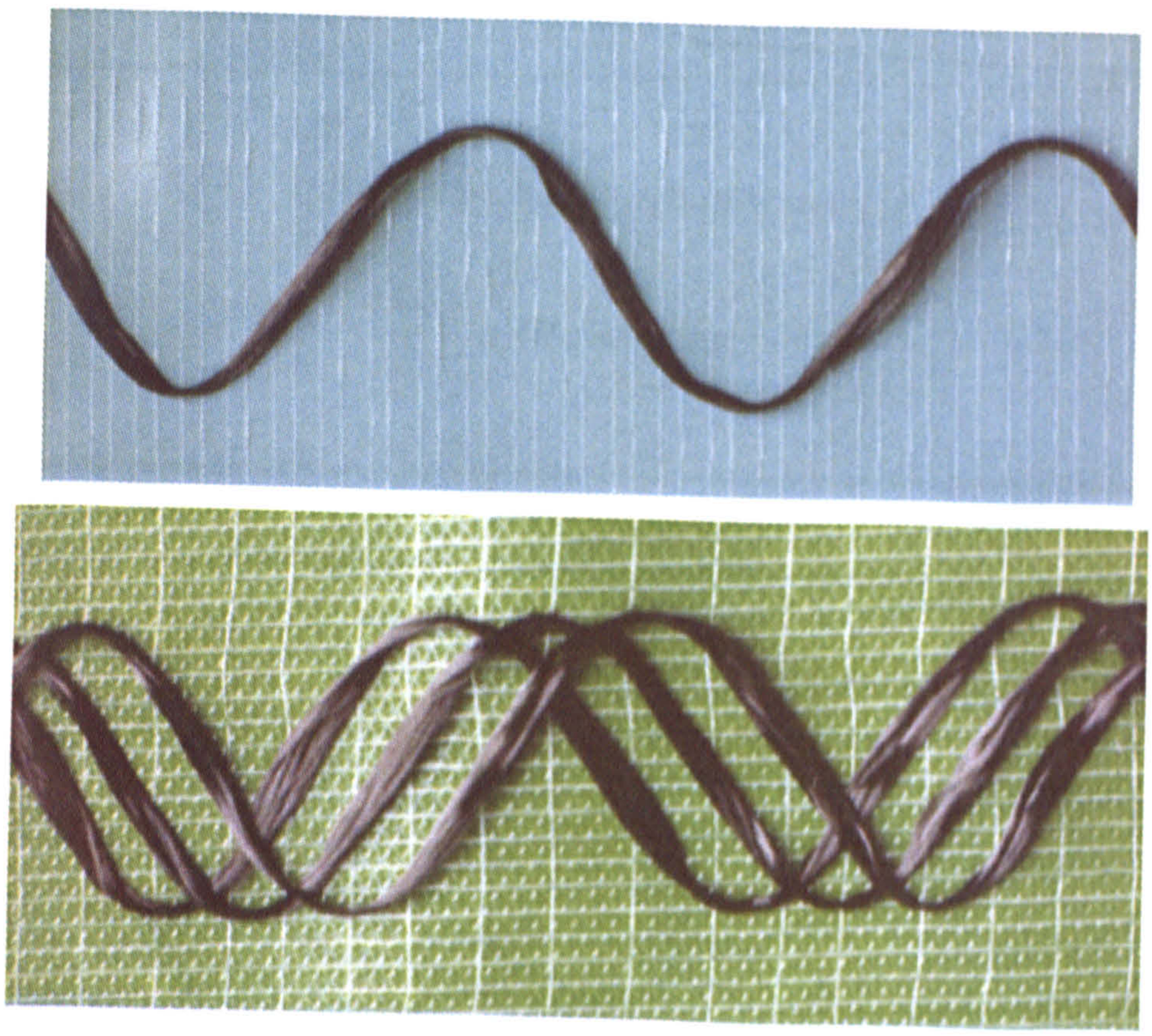

Figure 5.3 Photographs showing the method of construction to produce carbon fibre reinforced tensile specimens with sinusoidal fibre distribution

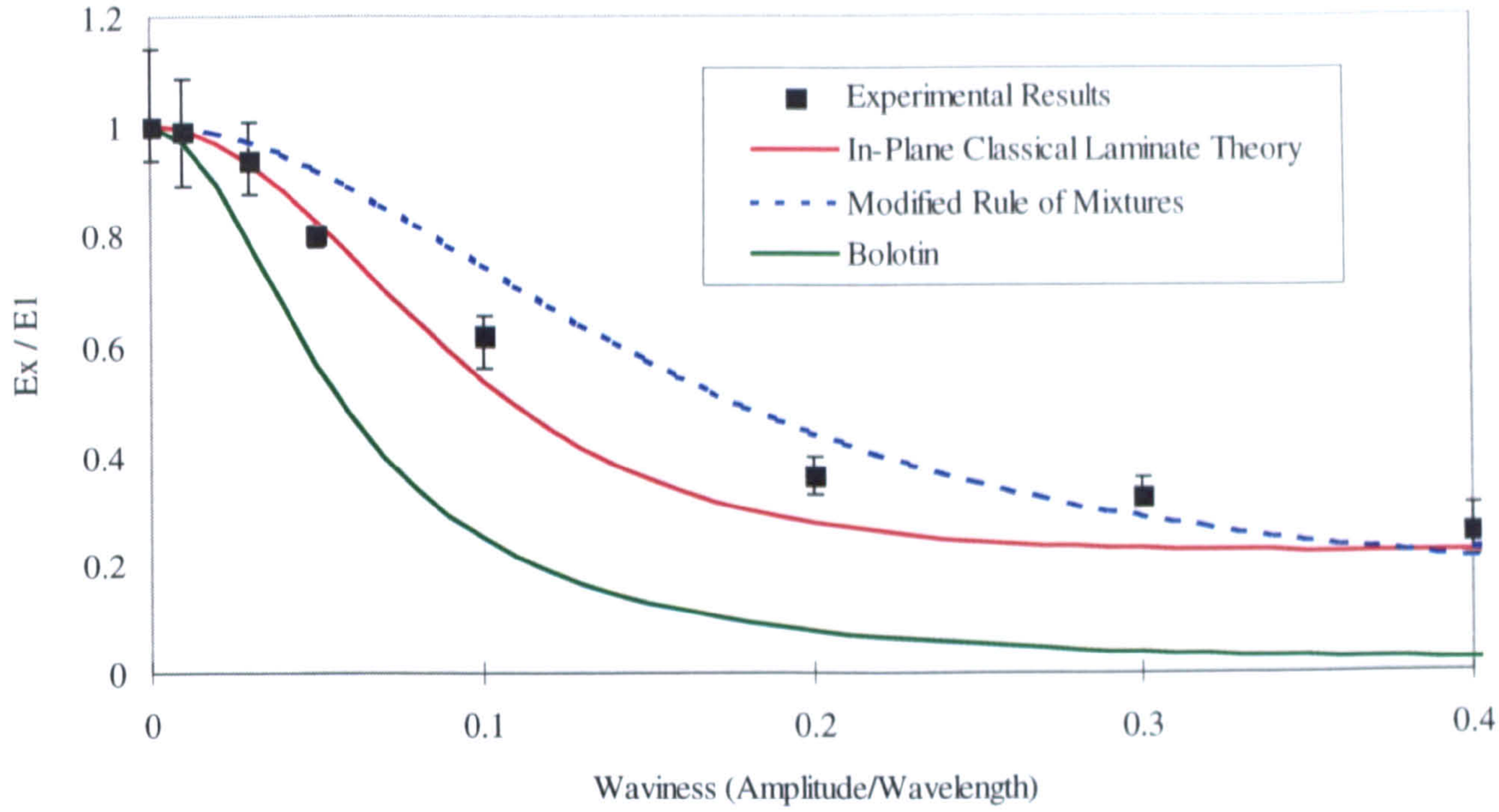

a)Glass/epoxy

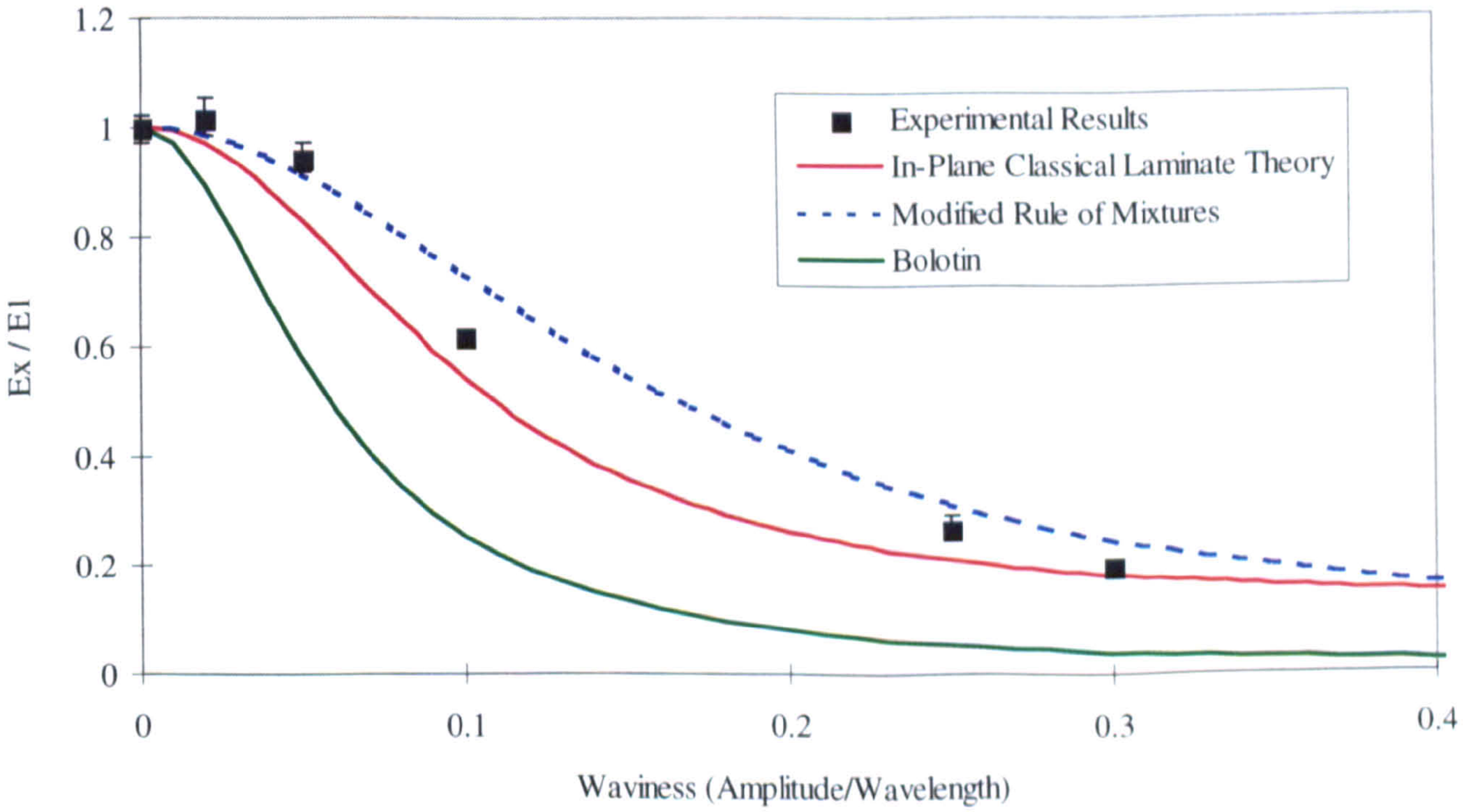

b) Carbon/epoxy

Figure 5.4 Predicted and experimental results for laminate modulus of samples containing sinusoidal fibre distribution

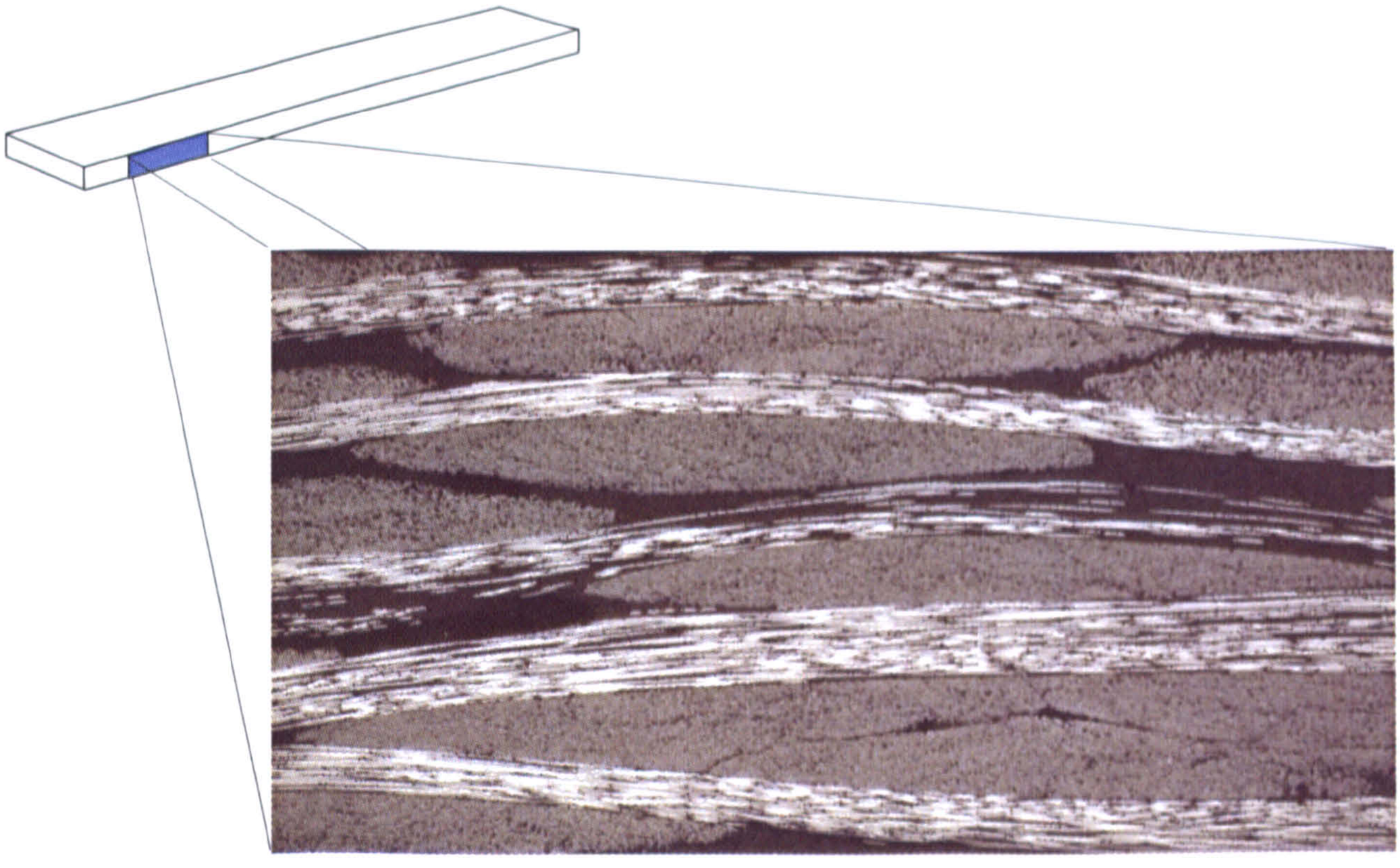

Figure 5.5 Photomicrograph of a 20mm x 20mm sample of a glass/epoxy laminate produced using a woven fabric (Flemings W/R 600) taken normal to the fabric plane

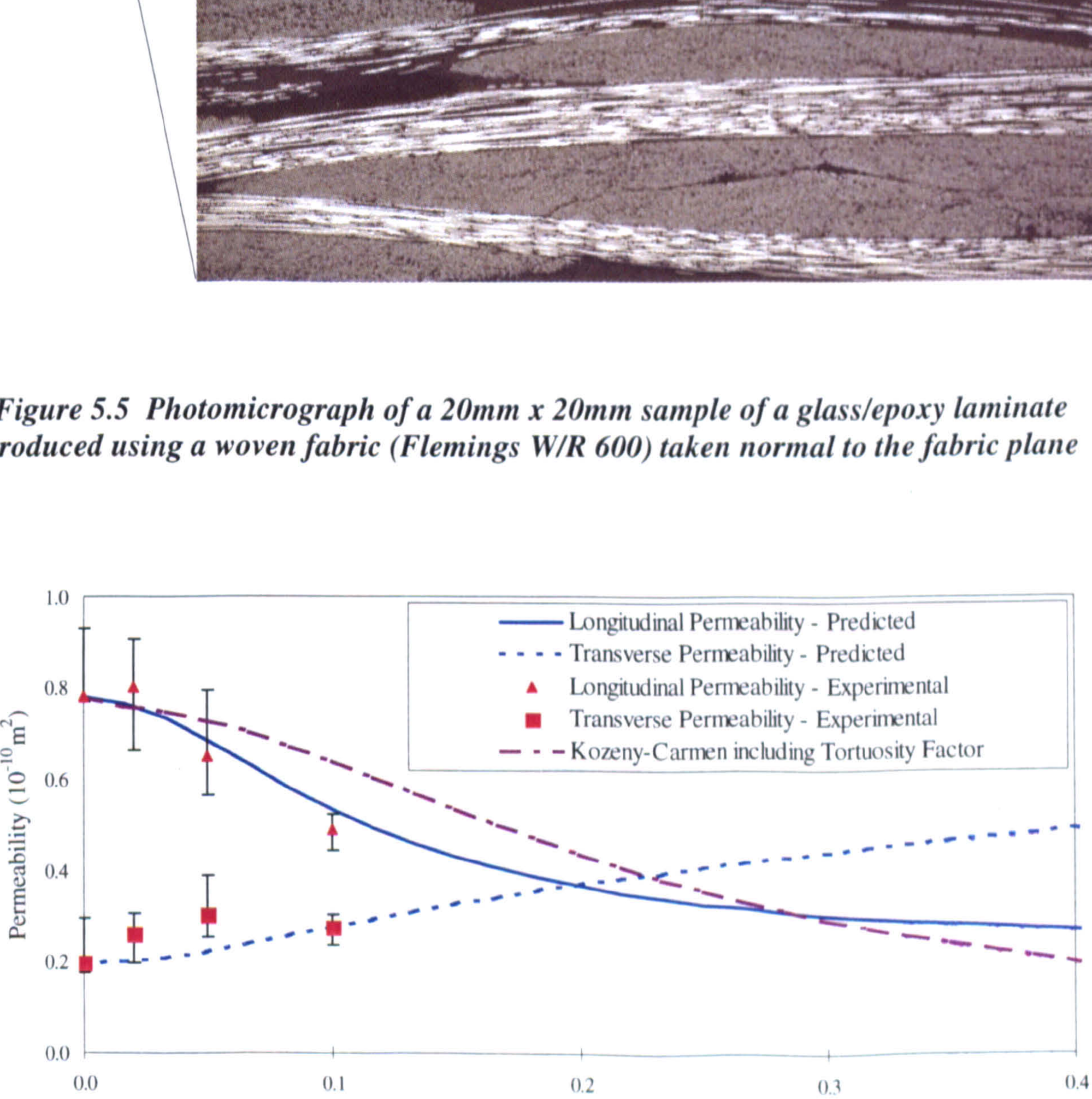

Figure 5.6 Predicted and experimental permeability of glass fibre preforms (43% fibre volume fraction) containing sinusoidal fibre distribution

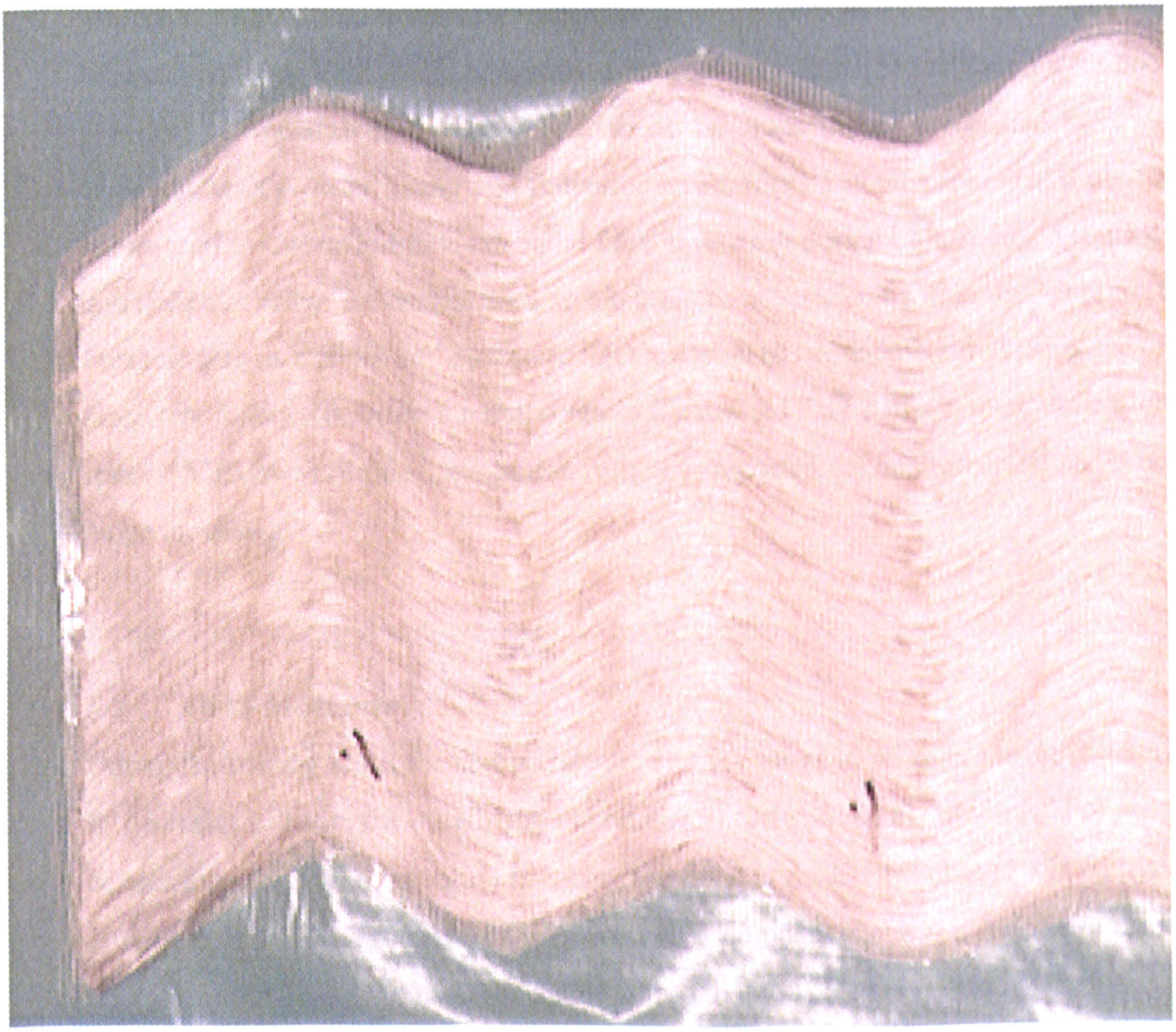

Figure 5.7 Photograph of E-glass preform with sinusoidal fibre distribution manufactured for permeability testing with a waviness factor of 0.1.

Chapter 6
Fibre Architecture Optimisation

6.1 Introduction

This chapter addresses some of the problems of fibre movement during preforming. The validity of a kinematic drape model for determining the deformation of a bi-directional reinforcement produced by the tow placement facility is demonstrated. The drape model is based upon simple shear and is described in detail elsewhere [58] although a resume is provided in Appendix 6.1. The validation of the drape model is reported for 0°/90° laydowns with powder binder and polyester scrim, formed in hemispherical tools. To reduce some of the undesirable effects of fibre movement during preforming, a routine is described that allows the desired fibre architecture to be specified within the 3D preform. Further analysis enables an "optimised" 2D laydown to be manufactured using the tow placement facility that, when formed, contains the desired fibre paths in three dimensional space. Validation of this optimisation routine is reported for hemispherical and power bulge mouldings.

6.2 Fibre Movement

During the forming stage, the fibre architecture must change to account for the difference in geometry between the usually flat 2D reinforcement and the 3D preform. For simple components, (i.e. single curvature or where the draw is small), this change will be trivial. However if a 2D reinforcement is formed to a complex shape (i.e. one with double curvature) the fibre re-orientation can be substantial [78].

The dominant form of fibre movement in directional reinforcements is generally assumed to be by inter-fibre shear (Figure 6.1) although some fibre slip (a change in tow spacing) may also occur [58]. During shear, the inter fibre angle (the included angle between the fibres of the two principal directions of a bi-axial reinforcement) will change. In severe cases this inter-fibre angle can reduce until the reinforcement locks and will no longer deform by simple shear. If further deformation occurs, the fibres can buckle leading to

reinforcement wrinkling, producing a defective preform. The change in fibre orientation from that of the 2D reinforcement to the 3D preform will also affect subsequent properties as described below:

Resin Flow

The flow of resin though a preform is usually modelled by performing experimental studies on individual plies to determine their (flat plaque) permeabilities. Knowing the permeabilities of each ply within a preform, one can estimate the effective permeability of the whole preform by applying simple plug flow analysis. However, if during preforming the reinforcement undergoes a change in architecture, the permeability data may need to be modified to take account of this. Smith et al illustrated this by measuring the permeability of a reinforcement for various levels of shear [70] (Figure 6.2). In extreme cases, reinforcements can deform to produce areas of densely packed fibre which have relatively low permeabilities and can cause dry spots in the finished moulding as illustrated by Bakharev and Tucker [86] in the mould filling analysis of a shallow hat shape.

Structural Properties

Laminate analysis is generally used to predict the mechanical performance of a composite constructed from multiple layers of reinforcement. However this approach does not account for any change in fibre orientation produced by the forming stage of preforming. Fibres may be re-oriented during forming to produce a composite with varying stiffness throughout the component. Fabrics can also shear to form areas of high and low fibre volume fraction which can cause problems of poor fibre wet-out and resin rich areas respectively which can lead to poor mechanical performance. An example of the effects of fibre re-orientation on structural properties is described by Cucinella *et al* [90] who discovered that the radial modulus of a composite wheel hub varied by up to 31% around the circumference.

6.2.1 Kinematic Drape Model

In order to predict the effects of forming a 2D aligned reinforcement over a 3D structure, Long [58] applied a kinematic drape model based on simple shear. The model assumed

the reinforcement to be a pin-jointed structure (Figure 6.1). The fibres were represented by the inextensible connections between the pins which were assumed to be fibre cross-over points. The pin-jointed model was incorporated into a computer program developed in Borland Pascal on a PC. The application of drape modelling in this work is detailed in Appendix 6.1 and summarised as follows:

- A surface model of the required component is developed and imported into the drape algorithm.
- Two intersecting fibre paths are defined on the surface model which represent the initial orientation of the reinforcement.
- The algorithm maps the 2D reinforcement onto the surface model and creates a data file for the pin-jointed nodal points in three dimensional space.

If required, the program will produce a visual output showing the deformed fibres on the surface of the component.

The inter-fibre angles (angle at a fibre crossover point) for each element (the area bound by single tows) are calculated and a surface plot is produced showing the deformed fibre architecture and the included angles between adjacent tows. Using these inter-fibre angle data, the model may be used to estimate fibre volume fraction variations within the component. This may be extended to estimate the change in preform permeability and laminate modulus as well as predicting the blank shape required to drape to the final geometry without trimming.

6.3 Validity of the Kinematic Drape Model for Laydowns

Although the deformation model has been demonstrated to give a reasonable level of agreement with experimental observations for commercial fabrics [58], the novel nature of the tow placed reinforcements suggested that their dominant deformation mechanisms should be validated. Validation of the kinematic drape model was also required for the development of a fibre architecture optimisation routine described in 6.4.

To validate the kinematic drape model for tow-placed reinforcements, the hemisphere

described in 3.4.3. was used. The continuously changing surface and high degree of draw produced significant fibre movements and an interesting technical challenge. A surface model of the hemisphere quadrant was produced using 400 triangular patches (Figure 6.3a). Symmetry enabled one quadrant of the hemisphere to be modelled. Constrained fibre paths were positioned along the quadrant axes which modelled a conventional 0°/90° fabric with an imposed fibre spacing of 5mm. The predicted deformed fibre geometry is shown in Figure 6.3b. Inter-yarn angles appear on the output in the form of coloured regions which represent bands of deformation. Maximum predicted fibre re-orientation occurred at the extremity of the quadrant along the fabric 45° axis where inter-fibre angles are reduced from 90° to 42°.

To verify this result, a series of hybrid carbon/E-glass 0°/90° flat preforms were manufactured on the tow placement facility. One set were bound with thermoplastic polyester net and another with polyester powder binder as described in 3.2.3. Alternate tows of 12k carbon and 2400 tex E-glass were laid to allow for accurate measurement of the included angle between intersecting fibres before and after post-forming. The laydowns were post-formed and moulded in a single operation in the heated, (70°C) matched aluminum hemispherical mould as described in 3.4.3. Figures 6.4a and 6.4b show mouldings produced from 0°/90° bidirectional reinforcement bound with polyester powder binder and polyester net respectively. The angles at the tow intersections were determined along the 45° axis (axis of maximum deformation) by measuring the major and minor axes of the cells formed by four intersecting tows and are referred to a geodesic from the pole to the equator. Figure 6.5 shows the inter-tow angles generated by the kinematic drape model together with the experimental data from polyester netting bound and powder bound preforms. The results show that the fibre distribution arising from both types of preform is very similar to that predicted by the drape model. Of the two preform types, the samples using the polyester net followed the estimates more closely and were subject to less scatter. This was attributed to the restraint offered by the continuous polyester filaments which inhibited inter-tow slippage that is thought to occur at the normal limits of preform compliance.

6.4 Preform Optimisation

Tow placement permits, potentially, some of the detrimental effects of forming such as fibre buckling and large variations in superficial density to be reduced. The kinematic drape model described in 6.2 was modified to investigate this possibility in the following way:

(a) Surface models of the component were created and the desired fibre pattern applied using CAD.

(b) A modified kinematic draping (undraping in this case) algorithm developed by Long [58], based on the same assumptions as the drape model described in 6.2.1, was then used to map the fibres onto a horizontal surface, thus producing an "optimised" geometry.

© The geometry file from b) was then processed by an interface module developed by the author that enabled the production of laydowns to the desired geometry using the tow placement facility.

First, a three dimensional surface model of the component (including the desired fibre paths) was produced. The algorithm was then applied to "undrape" or map the fibre paths back to a flat sheet. The resulting, "optimised" laydown geometry was then processed to produce a CNC part program which was used to manufacture the flat preform that could be post-formed to create the "optimised" three dimensional preform. A detailed description of this process is presented in Appendix 6.2.

6.4.1 Hemisphere

The feasibility of this procedure was investigated for the hemisphere described above using a hybrid E-glass/carbon arrangement. It was shown in 6.3 and can be seen in Figure 6.3b that for a conventional 0°/90° reinforcement with 5mm fibre spacing, the inter-fibre angles ranged from 90° at the hemisphere pole down to 42° at the equator. This fibre deformation will produce a preform with variable superficial density and non-uniform properties.

In an effort to reduce the effects of the fibre re-orientation and in particular to lessen the variation in preform superficial density, a surface model of one quarter of the geometry including tow paths at a uniform perpendicular spacing was developed (Figure 6.6). This was intended to ensure constant superficial density (thus uniform fibre volume fraction). The fibre pattern was used as input data into the kinematic undraping algorithm described above which mapped the fibres onto a horizontal surface, producing an "optimised" 2D geometry. This geometry file contained the coordinates of the fibres that when formed would contain the desired fibre paths in the final component to produce constant superficial density.

Figure 6.7a shows the "undraped" pattern for a hemisphere. This "optimised" laydown geometry was processed using a program developed by the author in Microsoft Qbasic™ (described in more detail in Appendix 6.2) to produce a CNC part program which was used to produce a flat preform on the laydown facility. Figure 6.7b shows the "optimised" laydown as produced using the tow placement facility. Superficial comparison between the desired pattern (Figure 6.7a) and the experimental laydown (Figure 6.7b) suggests that the tow placement was reasonably successful. While the process is, in principle, aimed at net-shape manufacture the final laydown was produced oversize to assist in retaining the tows in their as-laid positions since short fibres were subject to spring-back when laid on a steeply curved path. To test the optimisation routine, a series of experiments were undertaken to determine the change in preform superficial densities for conventional 0°/90° reinforcements and for optimised, constant fibre spacing (in 3D), reinforcements. Several flat preforms were produced to test the uniform fibre volume fraction hypothesis in carbon/E-glass and were formed to the hemispherical geometry and moulded as described above. Figure 6.8 shows finished mouldings produced using a tow-placed 0°/90° reinforcement and the arrangement "optimised" for uniform superficial density. It can be seen that the 0°/90° reinforcement has undergone shear along the °45 axis, suggesting a higher superficial density in that region. The optimised structure (Figure 6.8b) exhibits smaller inter-fibre angles along the 45° axis but because of its design, the reinforcement contains a more uniform fibre spacing.

In order to test the uniformity of the fibre spacing, four E-glass preforms were produced at 0°/90° orientations and four using the "optimised" geometry. Each laydown was preformed and hot pressed (with Ciba Geigy LY/HY 5052 epoxy resin) in the matched aluminium tool described in 3.4.3. The mouldings were sectioned along the axes of symmetry to produce quadrants for ashing specimens. The cutting plan for the burn-off samples is included in Figure 6.9. Due to symmetry, the two outer samples (0° and 90°) and the two intermediate samples (22.5° and 67.5°) in each quadrant were grouped together thus leaving three samples (0/90°, 22.5°/67.5° and 45°) for each quadrant. Again due to symmetry, each quadrant should be similar and so for each hemisphere, only three values are required (the 0°/90°, 22.5°/67.5° and 45° axes). The fibre contents were measured by ashing as described in 3.5.4.

Tests were performed on eight mouldings and the results are shown in Figure 6.9. The results are depicted as the normalised (normalised to unity for the average of each complete moulding) superficial density of the samples plotted against sample position. The results confirm that the "optimised" fibre architecture produces a more uniform superficial density content around the equator which is the region where such variations would be most extreme using conventional reinforcements. The normalised superficial densities range from 0.98 at the 45° axis to 1.01 at the 0°/90° axes. The corresponding variation for the conventional 0°/90° reinforcement ranges from 1.09 to 0.92. The standard deviations for the optimised samples (3.9%-4.2%) are also lower than the conventional architecture (4.9%-6.9%). This uniformity has potential for improving mould filling characteristics due to a more even permeability and porosity and should reduce variabilities in mechanical performance.

6.4.2 Power Bulge

As a further investigation into the effects of fibre re-orientation on superficial density, the generic "power bulge" described in 3.4.5 was studied. A drape analysis performed on the surface model (showing initial fibre orientations (Figure 6.10)) showed high levels of fibre shear (inter-fibre angles reduced from 90° to 42°) at each corner of the bulge (Figure 6.11a). This fibre shear represented an increase in fibre volume fraction of up to 15%

(Figure 6.11b) which could cause substantial local property changes.

As before, a surface model was produced with uniform fibre spacing (Figure 6.12). This model was used as an input to the "undrape" software to produce an "optimised" laydown which when formed would produce a preform with uniform superficial density throughout. Several "optimised" laydowns were produced using the tow placement facility. The laydowns were preformed and moulded in the matched tool using Cray Valley polyester resin as described in 3.4.5. For comparison, several conventionally oriented (0°/90°) laydowns were also produced and moulded. Figures 6.13a and 6.13b show the mouldings manufactured from the conventional style material and the "optimised" laydown. Carbon tows were added to these preforms to increase contrast. Superficial inspection of the mouldings (Figures 6.14a, 6.14b, 6.15a and 6.15b) reveal that the 0°/90° mouldings deformed in a similar manner to the drape analysis prediction (Figures 6.14c and 6.14d) and that the "optimised" laydowns have also deformed to produce mouldings with a fibre architecture similar to the original design (Figures 6.15c and 6.15d).

In order to test the uniformity of the preforms, an E-glass laydown was produced for each fibre architecture. Each laydown was preformed and moulded as above. Burn-off specimens were cut from the perimeter of the mouldings to the cutting plan in Figure 6.16 The results, Figures 6.16a and 6.16b, show the normalised superficial density (again normalised to unity for the average of each complete moulding) for each burn-off specimen. The normalised values for the "optimised" structures (Figure 6.16a) range from 0.90 to 1.08. The corresponding range for the conventional 0°/90° reinforcement (Figure 6.16b) is from 0.86 to 1.18. Although the "optimised" laydown did not produce a preform with uniform superficial density, it reduced the variation in superficial density around the edge of the component, which is the region where such variations would be most extreme using conventional reinforcements. Possible reasons for the reduction in accuracy between the power bulge preform and the hemisphere preform could be the non-symmetrical shape of the bulge which could have allowed the preform to be drawn into the mould faster from one side resulting in the reinforcement being offset in the moulded component. A second possible reason is the non-uniform clamping pressure observed

from the tension ring which had to be manufactured to the same shape as the mould (rectangular) and which lifted from the reinforcement corners during the latter stages of moulding as the reinforcement was drawn into the mould.

6.5 Conclusions

This chapter has addressed the problem of fibre movement during the preforming stage for composites manufactured by LCM. Fibre movement can change composite processing and performance properties. A model to predict the deformation of aligned reinforcements during the forming stage has been developed by Long [58]. The model was validated for tow placed reinforcements which were found to deform in a similar way to commercial reinforcements such as woven or stitch bonded fabrics. This enabled the drape model to be developed as a tool for optimisation of fibre architecture.

Although the drape model could predict the fibre architecture of a preform with reasonable accuracy, it is more desirable to be able to design and manufacture the preform with an optimised fibre architecture. A kinematic undrape algorithm was developed by Long [58] which was successfully validated with the reduction of superficial density in a hemispherical component from ±9% to ±2% for an optimised preform compared to a standard 0°/90° fabric. The optimisation routine was also validated for a generic power bulge, again designed with a constant superficial density, which has shown that the technique can also be used for more complex geometries. The optimised power bulge reduced variations in preform superficial density from 0.85-1.2 to 0.9-1.1 which, although not as successful as the hemisphere, showed that the optimisation technique produces preforms with enhanced qualities compared to conventional reinforcements.

Although the design of the fibre architecture for both components illustrated optimisation with regard to uniform superficial density, the process should be applicable for various design scenarios: to optimise architecture for enhanced flow properties (to reduce mould filling times and avoid dry spots); localised tow placement (for extra reinforcement in highly loaded areas); alignment of reinforcement with major load paths (for increased

mechanical performance).

Although the optimisation process has only been shown applicable by manufacturing preforms using the prototype tow placement facility, it could be possible to incorporate the optimisation routine into other preform manufacturing systems such as knitting and embroidery.

List of Figures

6.10 Surface model of power bulge including two intersecting fibre paths representing the initial orientation of the reinforcement.

6.11 Drape model output for power bulge

a) Predicted deformed fibre architecture and the inter-fibre angles between adjacent tows.

b) Predicted fibre volume fraction variation.

6.12 Surface model of power bulge with uniform tow spacing

6.13 Power bulge mouldings

a) Conventional 0°/90° tow placed reinforcement

b) Optimised laydown

6.14 Power bulge moulding produced from conventional 0°/90° reinforcement

a) Photograph of front of component

b) Photograph of rear of component

c) Predicted fibre architecture of front of component

d) Predicted fibre architecture of rear of component

6.15 Power bulge moulding produced from optimised fibre architecture reinforcement for uniform fibre volume fraction

a) Photograph of front of component

b) Photograph of rear of component

c) As-designed fibre architecture of front of component

d) As-designed fibre architecture of rear of component

6.16 Normalised superficial density from burn-off specimens in power bulges

a) Optimised laydowns.

b) Conventional 0°/90° tow placed reinforcement.

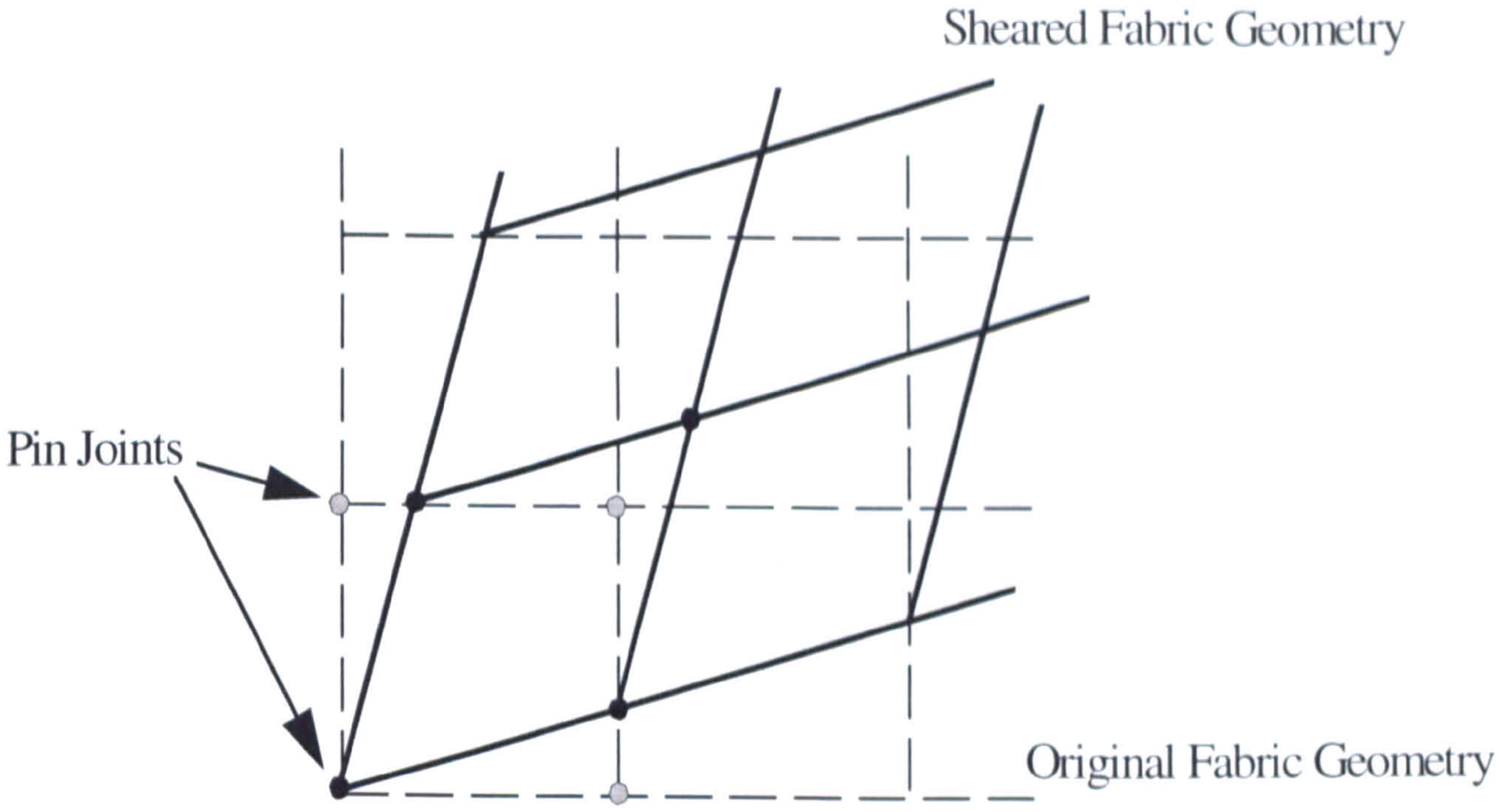

Figure 6.1 Pin-jointed model of bi-directional fabric deformation used in drape algorithm.

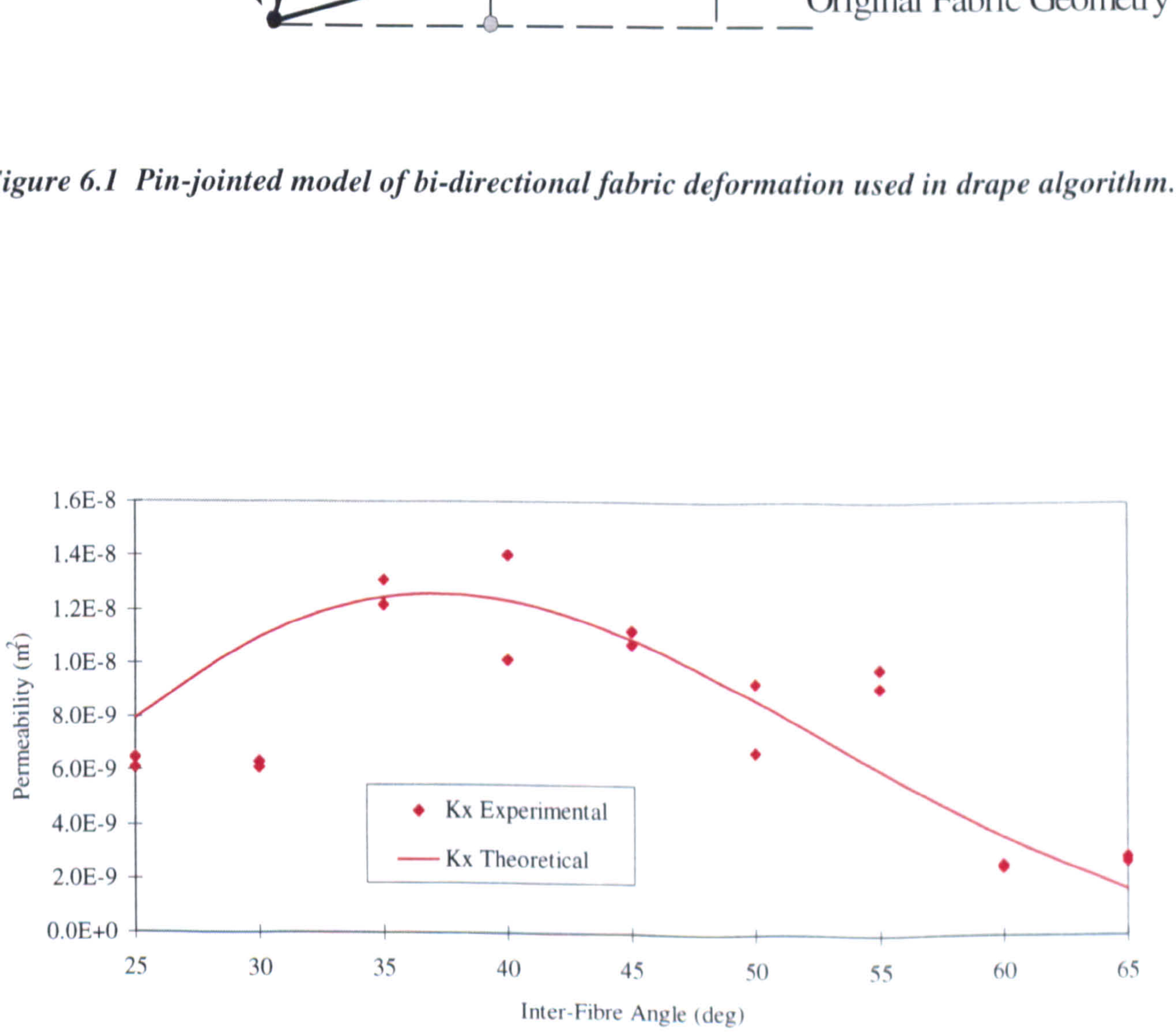

Figure 6.2 Change in preform permeability as a function of fabric shear (Smith [67]).

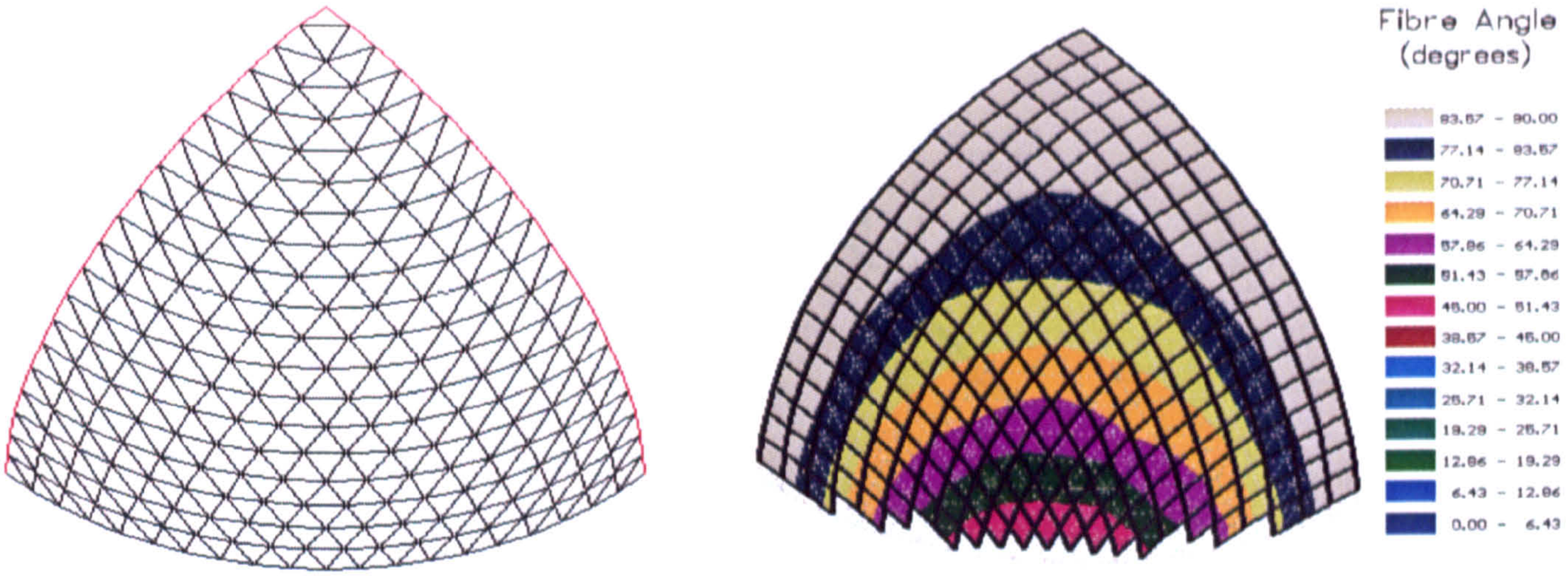

a) Surface model used in drape analysis

b) Predicted deformed fibre architecture with a nominal fibre spacing of 5mm

Figure 6.3 Hemisphere quadrant

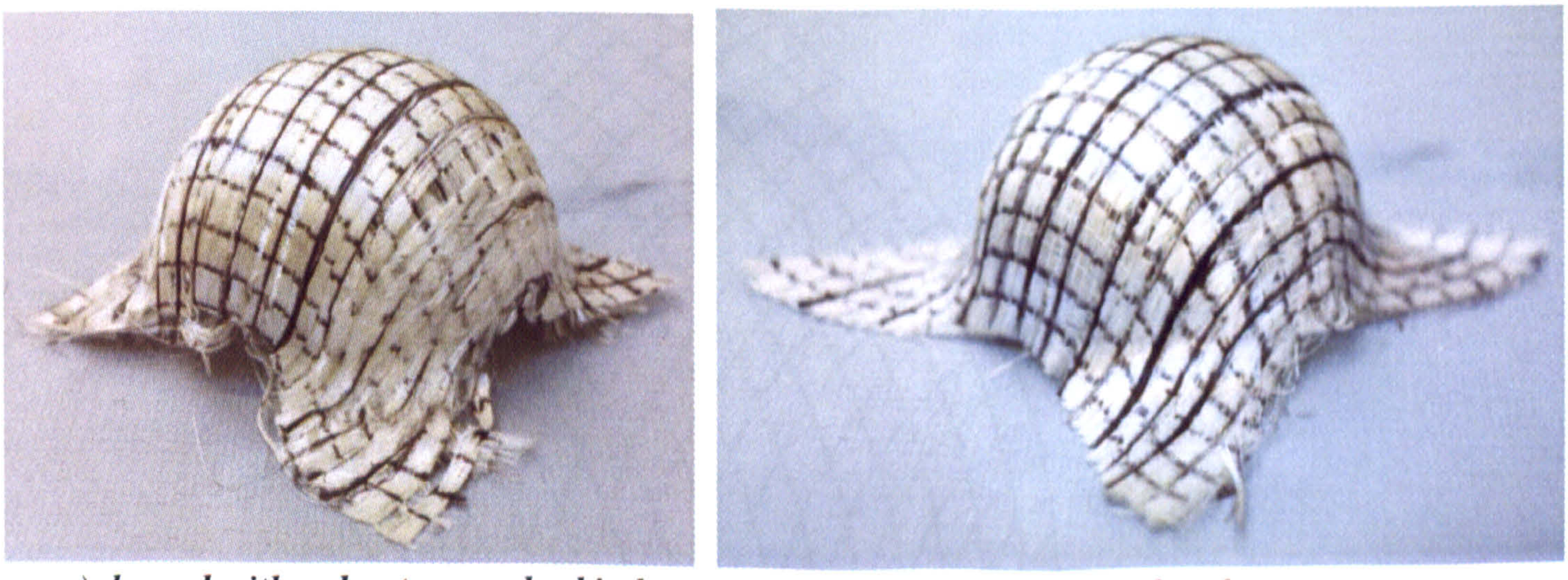

a) bound with polyester powder binder.

b) bound with polyester net.

Figure 6.4 Preforms produced from $0^o/90^o$ bidirectional tow placed reinforcement

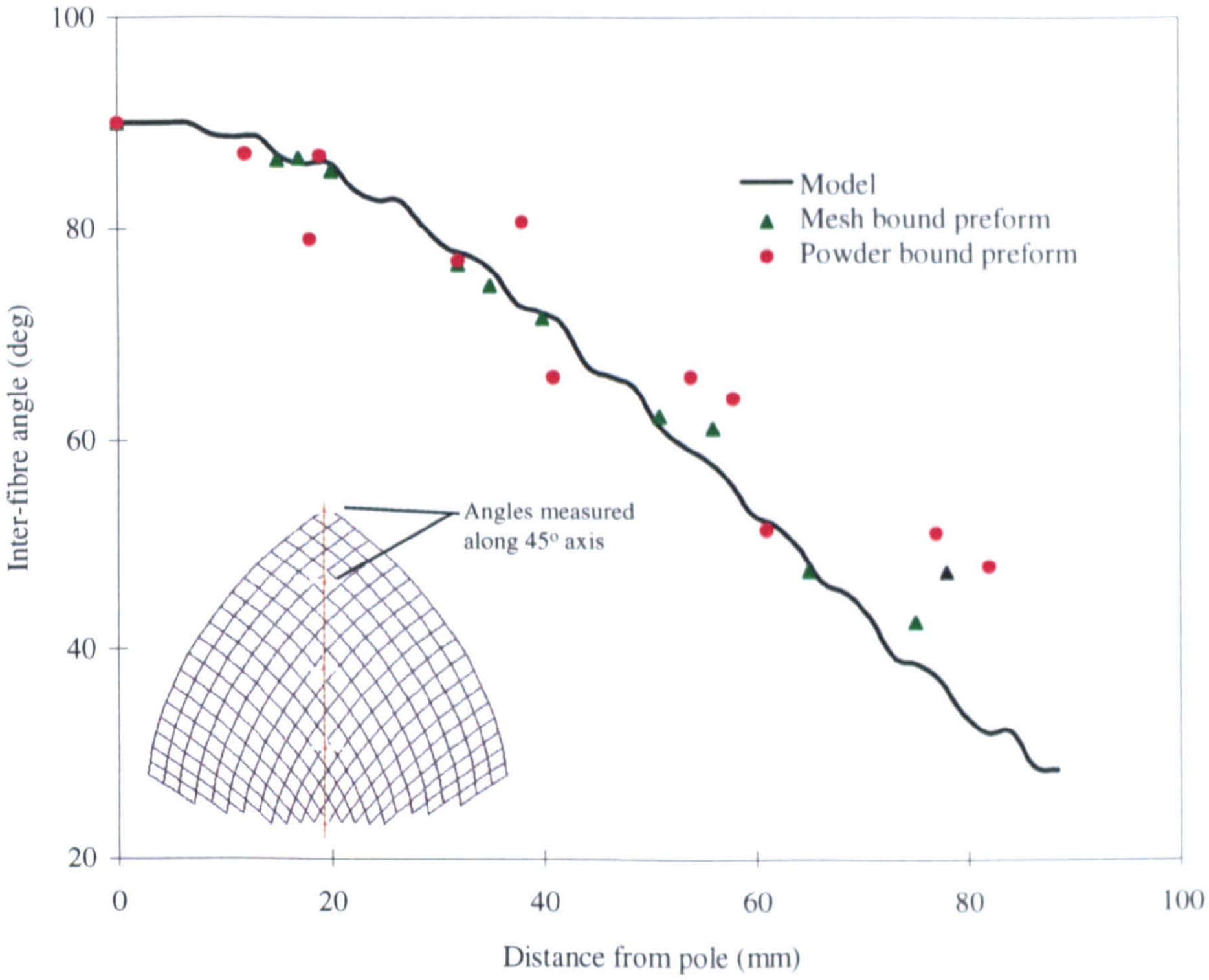

Figure 6.5 Inter-tow angles generated by the kinematic drape model together with experimental data from polyester netting bound and powder bound preforms.

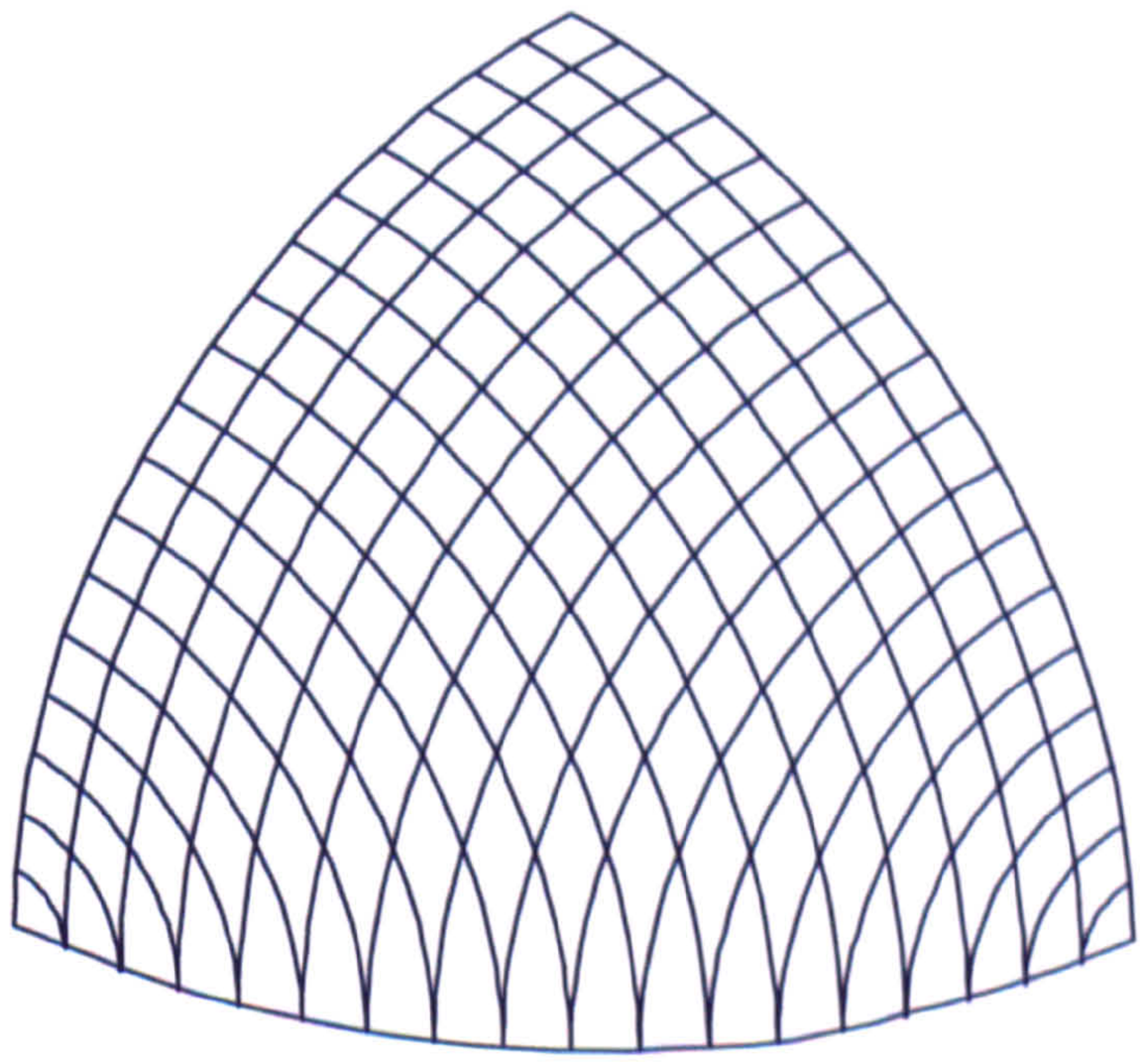

Figure 6.6 3D surface model of one quarter hemisphere including tow paths at a uniform perpendicular spacing.

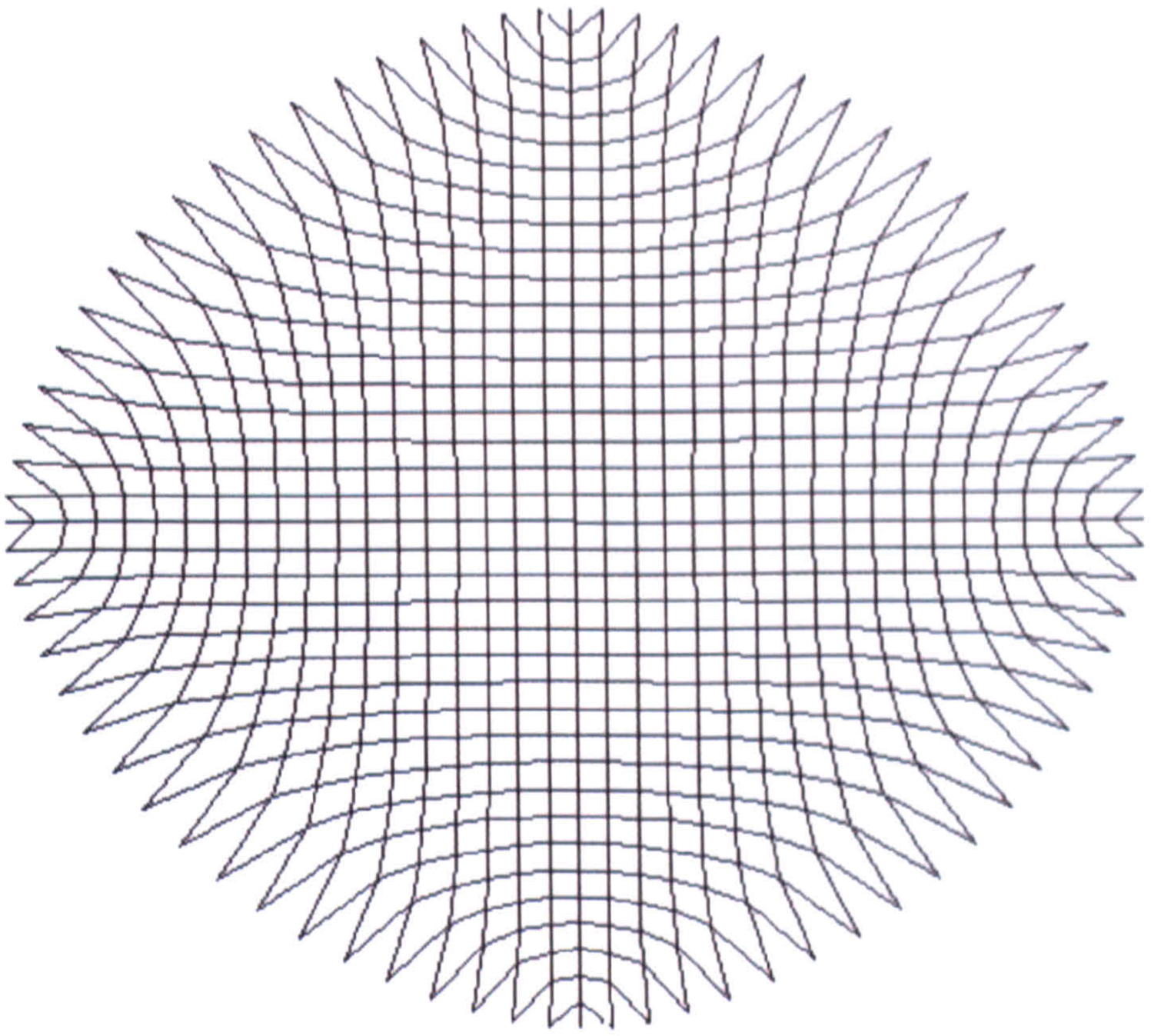

a) Undraped laydown pattern

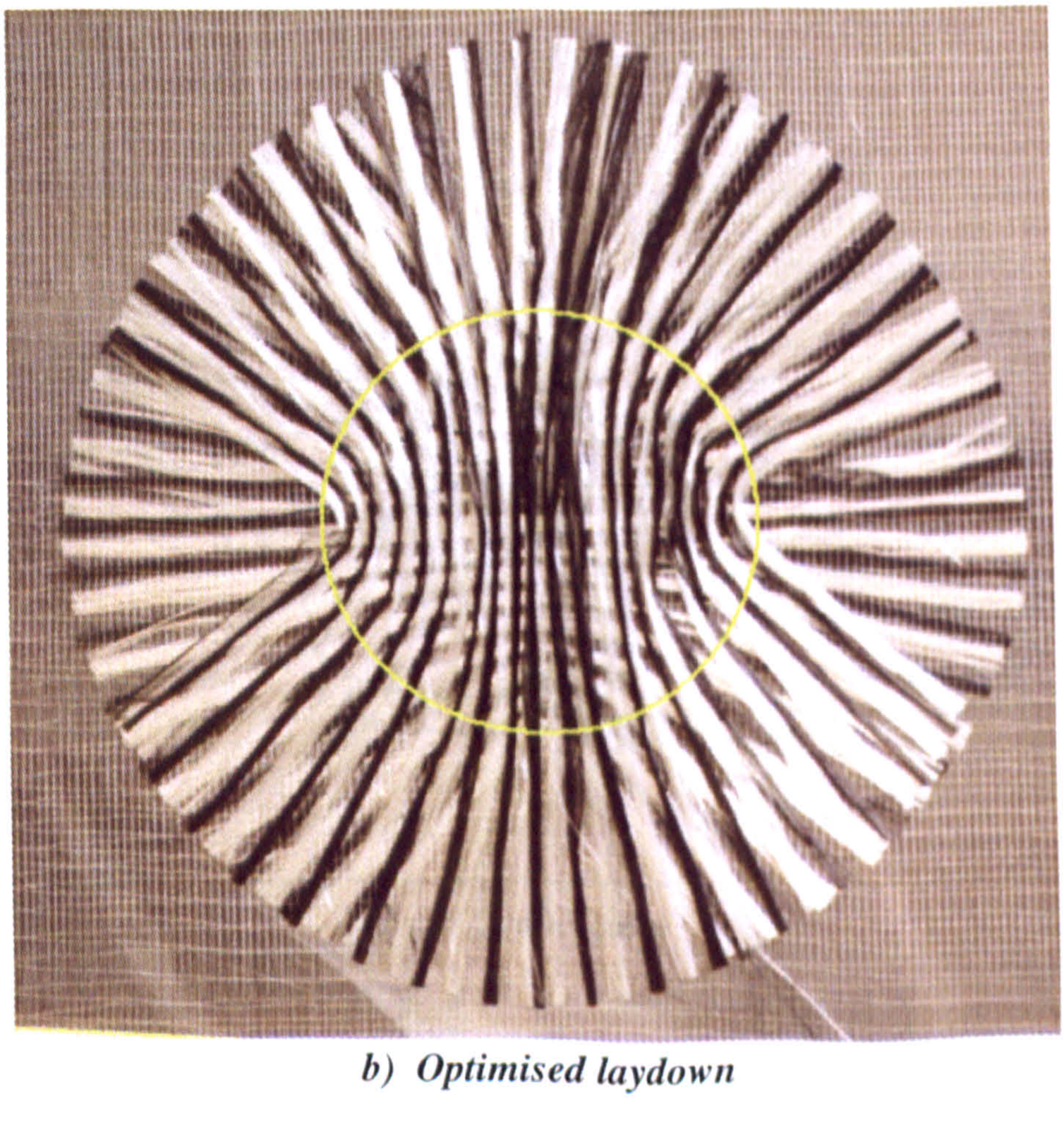

b) Optimised laydown

Figure 6.7 Optimised hemisphere with constant superficial density

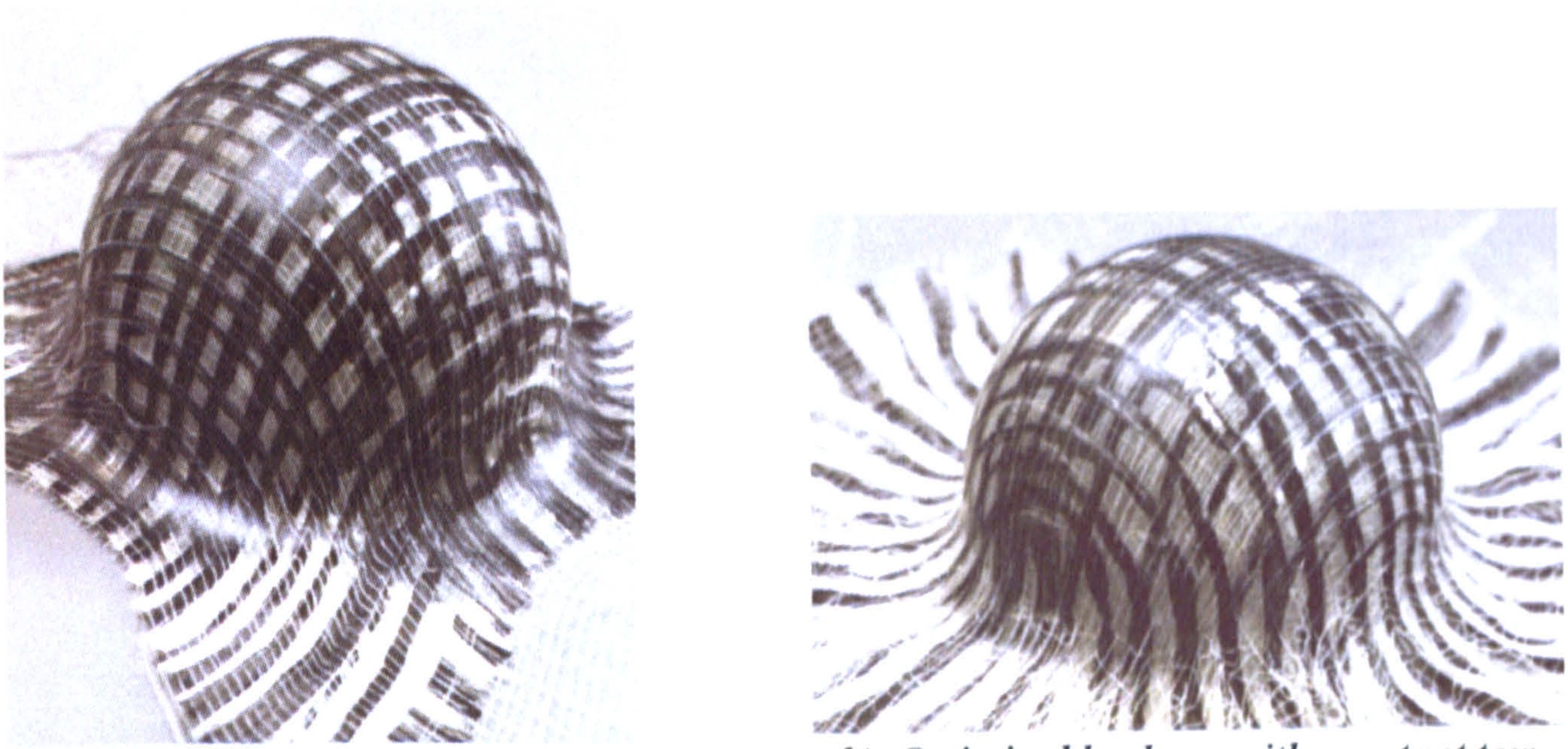

a) Conventional 0/90° tow placed reinforcement

b) Optimised laydown with constant tow pitch

Figure 6.8 Hemispherical mouldings

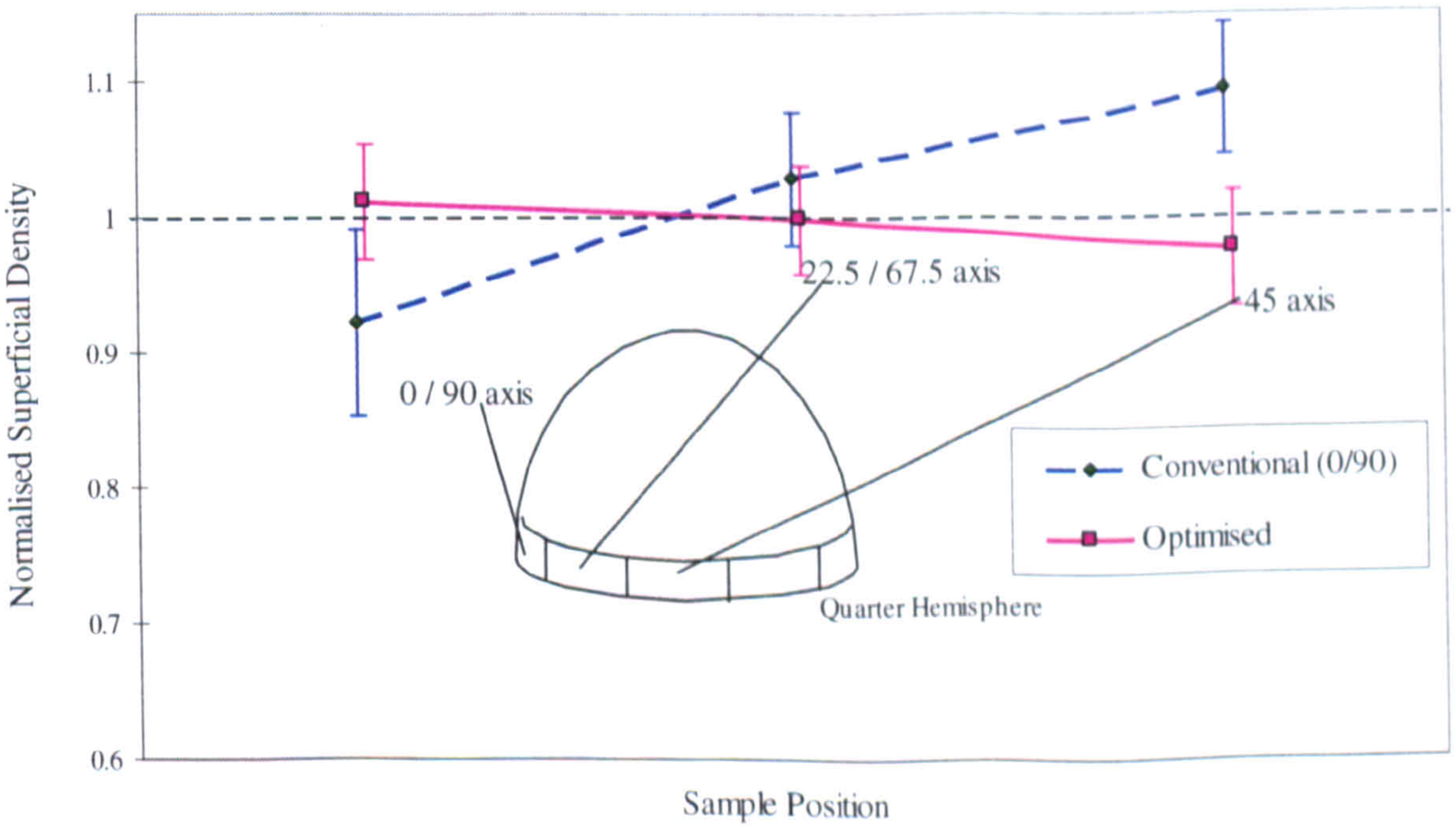

Figure 6.9 Normalised superficial density from burn-off specimens in hemispheres produced using conventional 0°/90° reinforcement and optimised laydowns

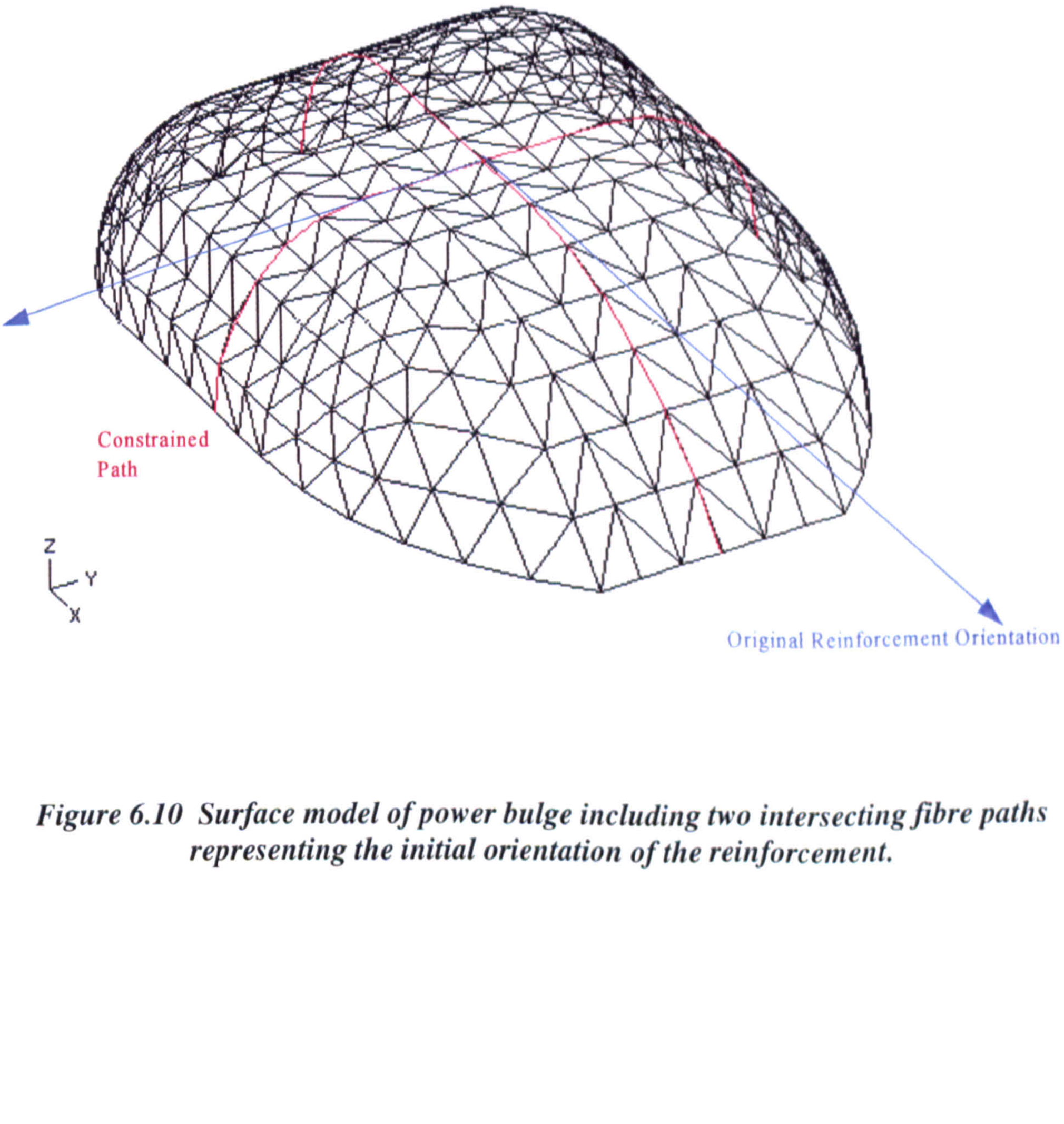

Figure 6.10 Surface model of power bulge including two intersecting fibre paths representing the initial orientation of the reinforcement.

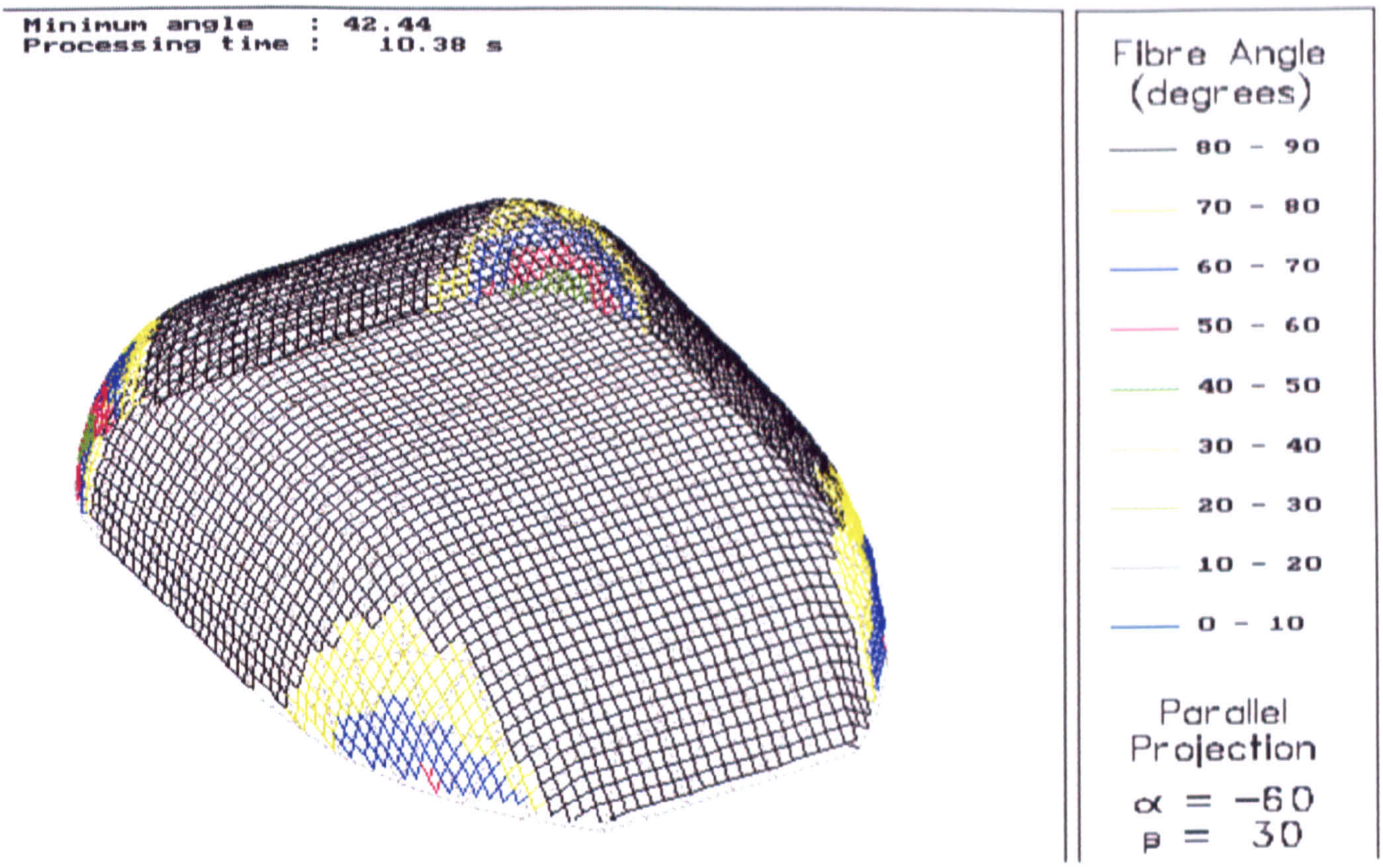

a) Predicted deformed fibre architecture and the inter-fibre angles between adjacent tows.

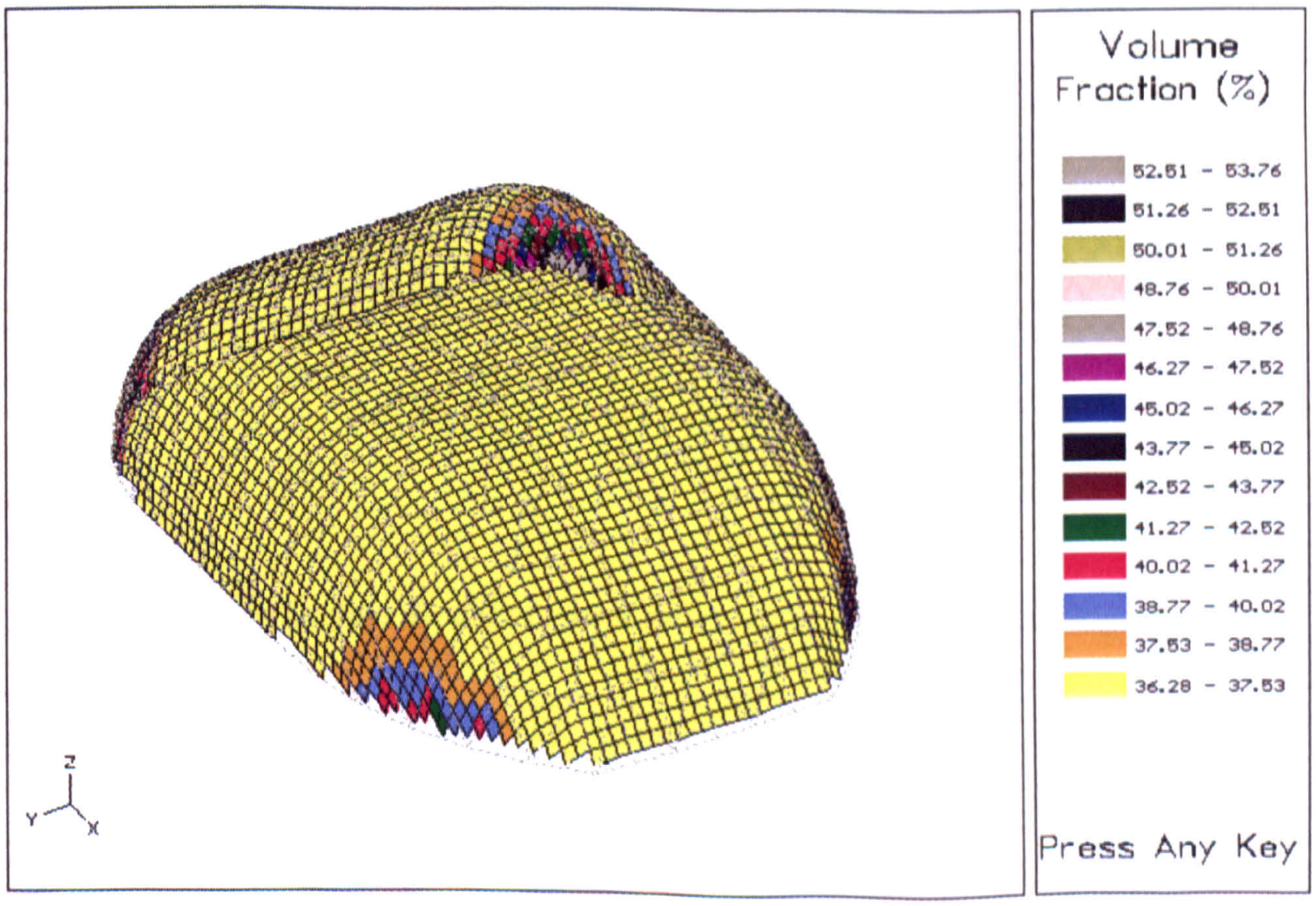

b) Predicted fibre volume fraction variation.

Figure 6.11 Drape model output for power bulge

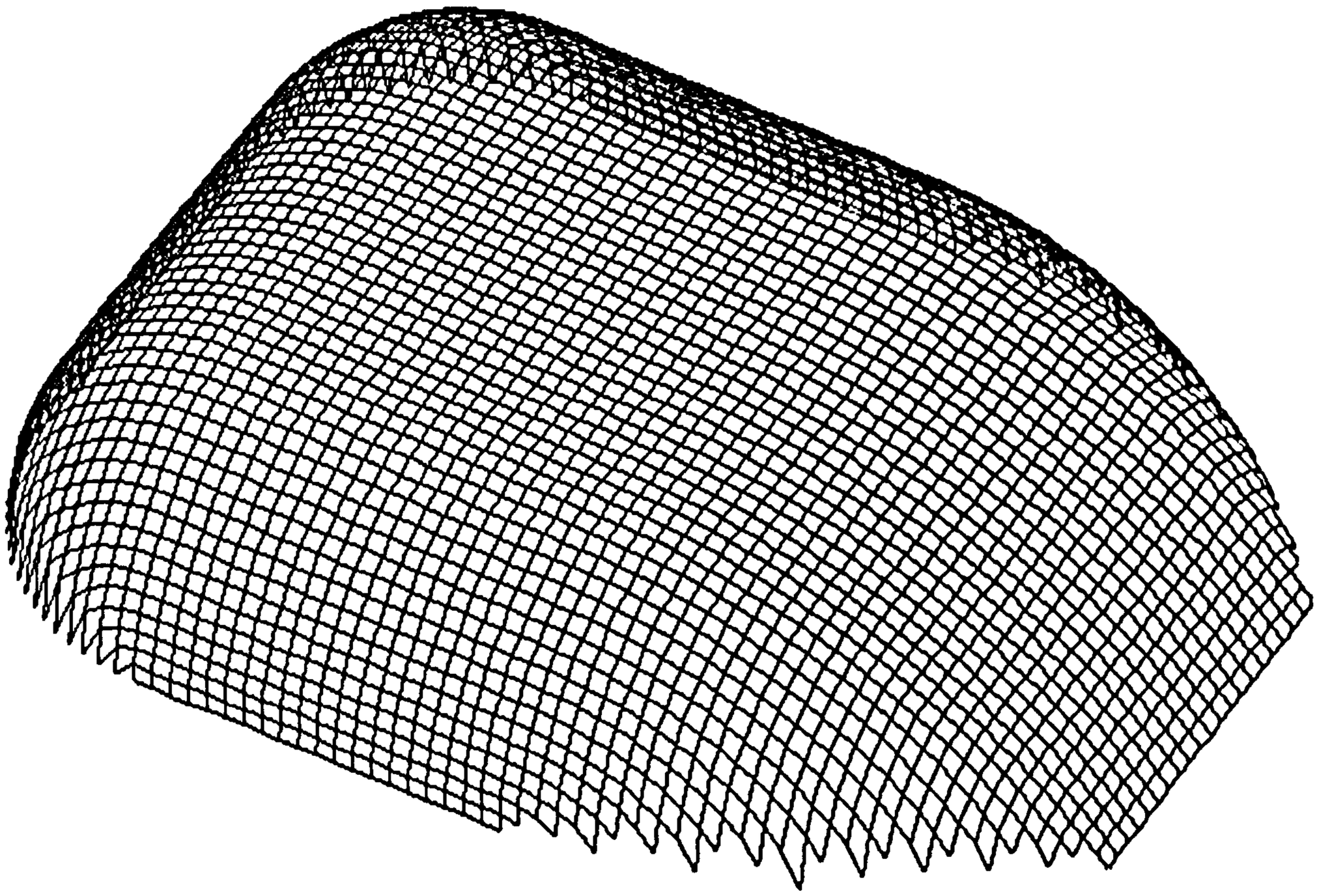

Figure 6.12 Surface model of power bulge with uniform tow spacing

a) Conventional 0°/90° tow placed reinforcement

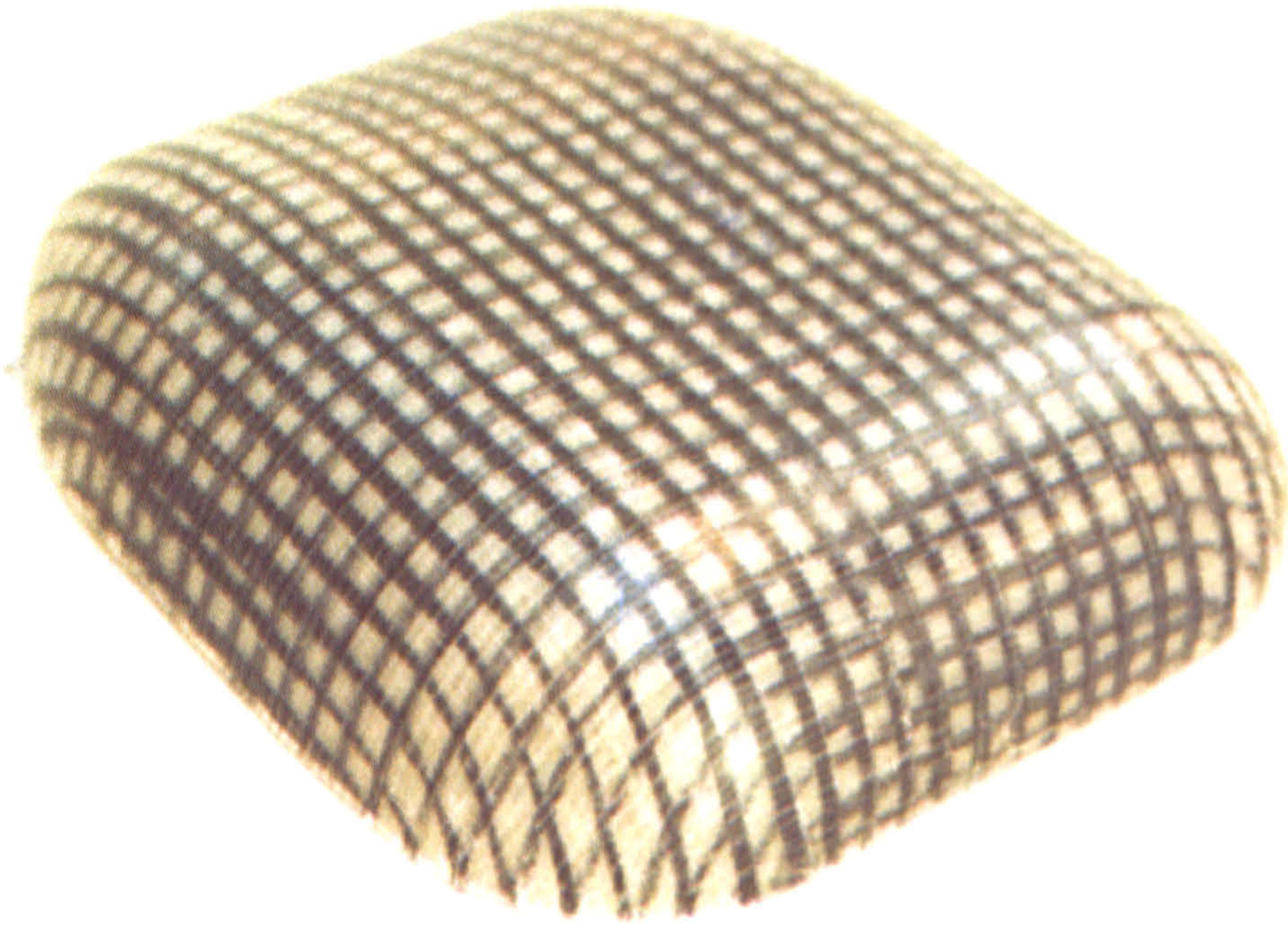

b) Optimised laydown

Figure 6.13 Power bulge mouldings

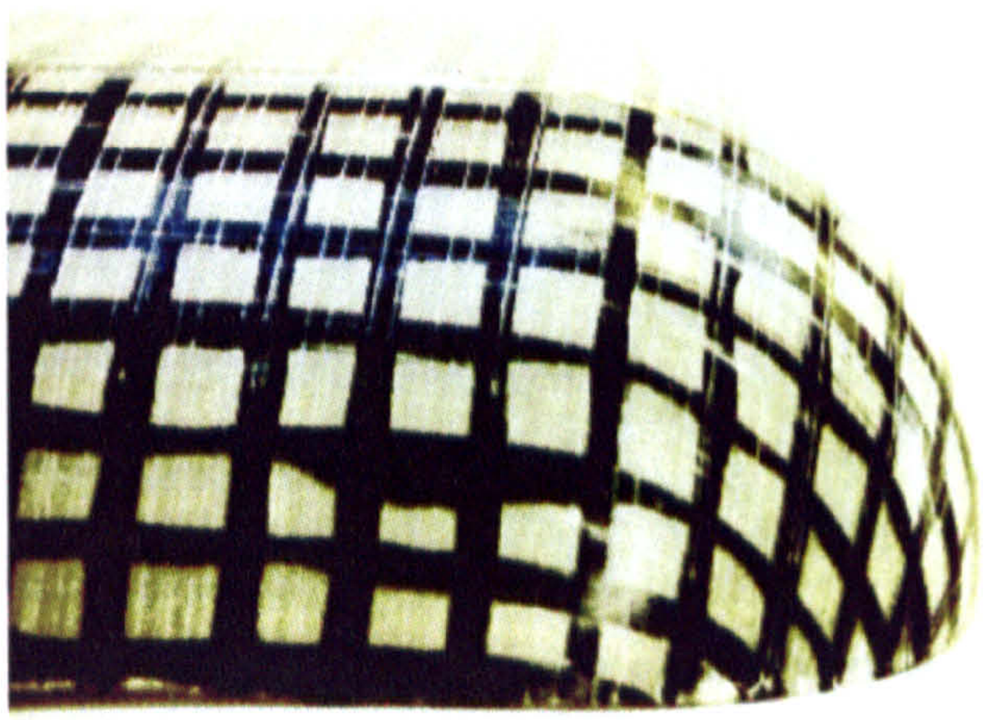

a) Photograph of front of component

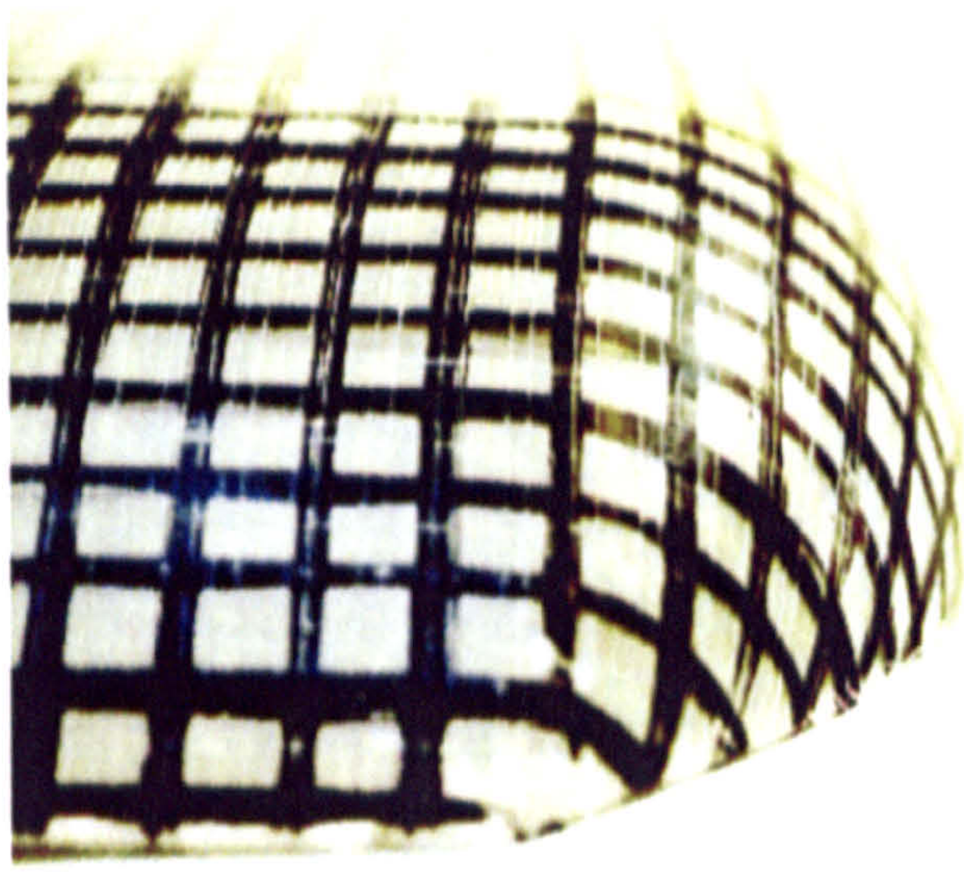

b) Photograph of rear of component

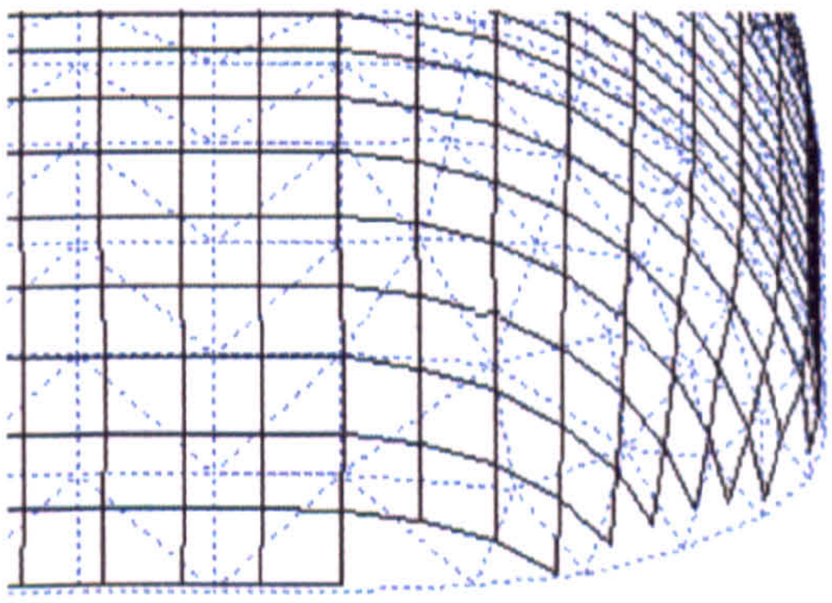

c) Predicted fibre architecture of front of component

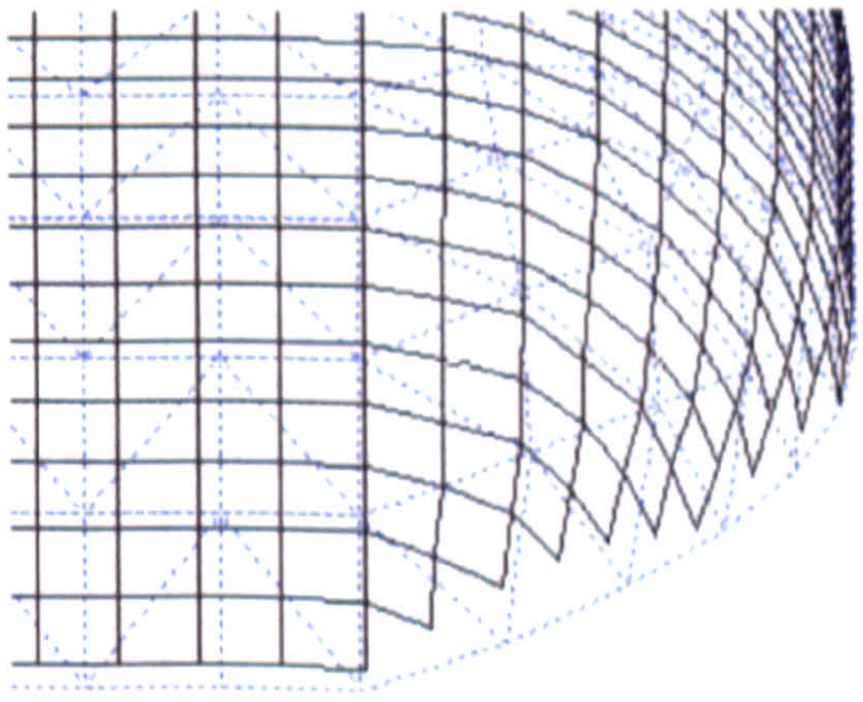

d) Predicted fibre architecture of rear of component

Figure 6.14 Power bulge moulding produced from conventional $0^o/90^o$ reinforcement

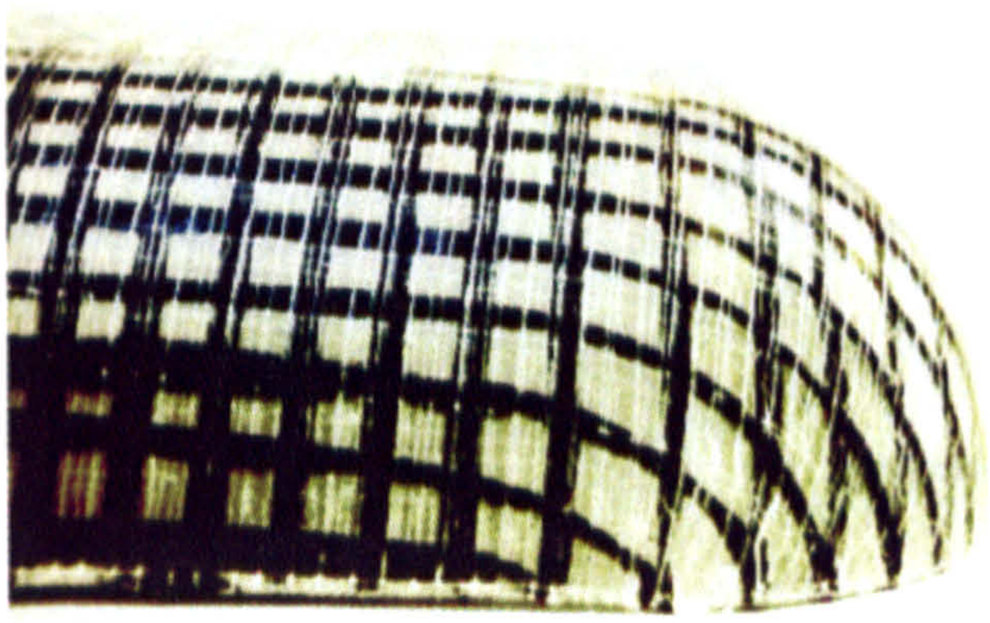

a) Photograph of front of component

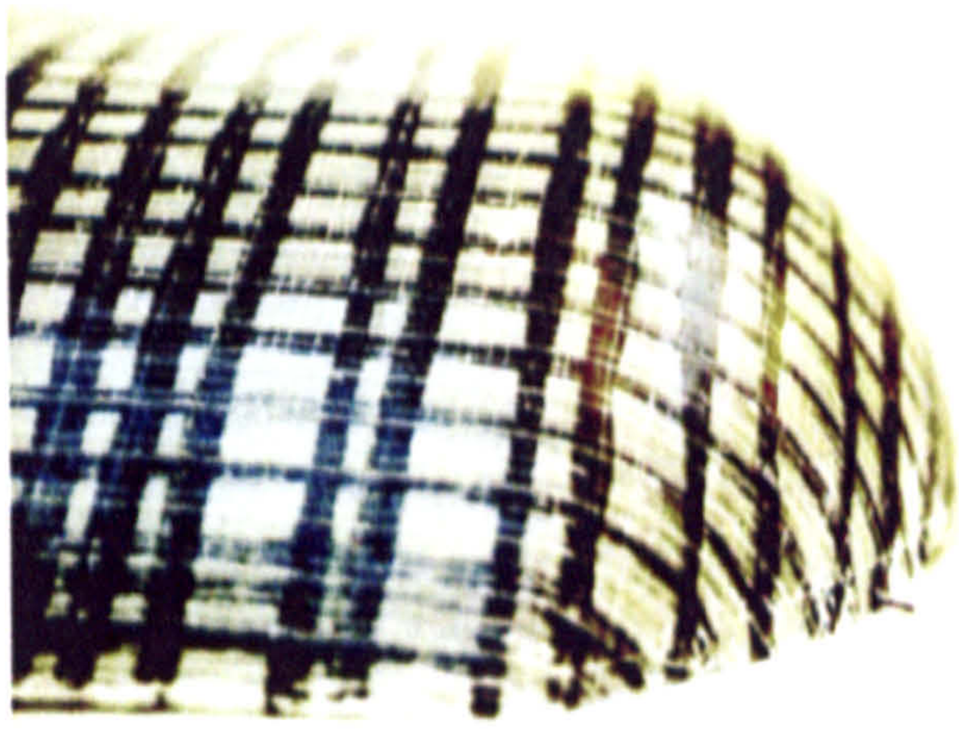

b) Photograph of rear of component

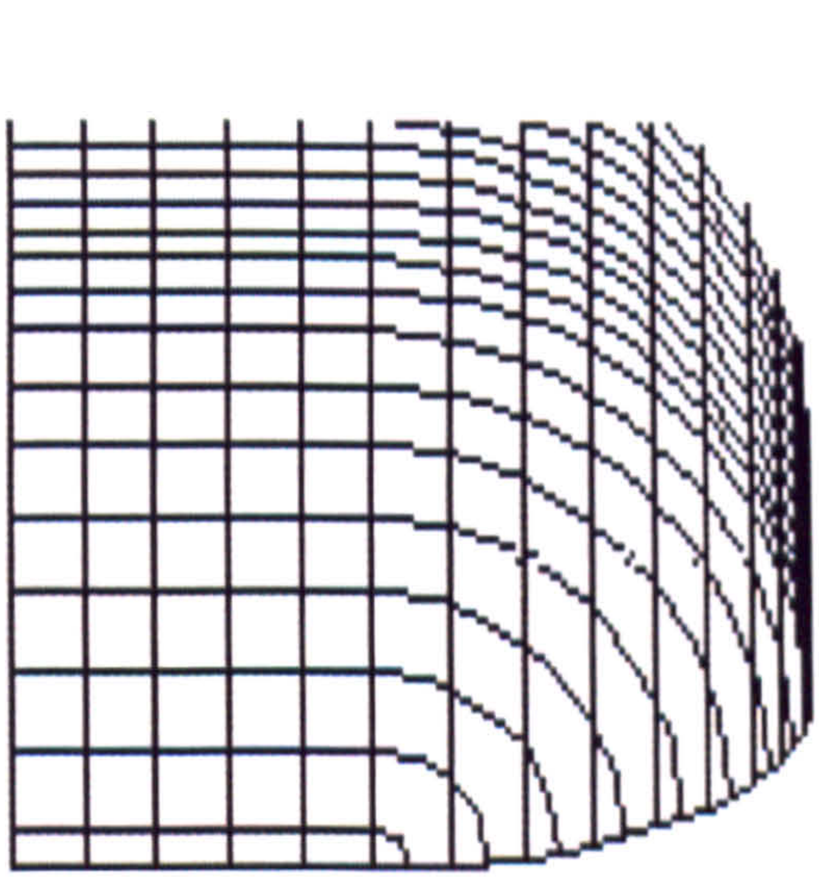

c) As-designed fibre architecture of front of component

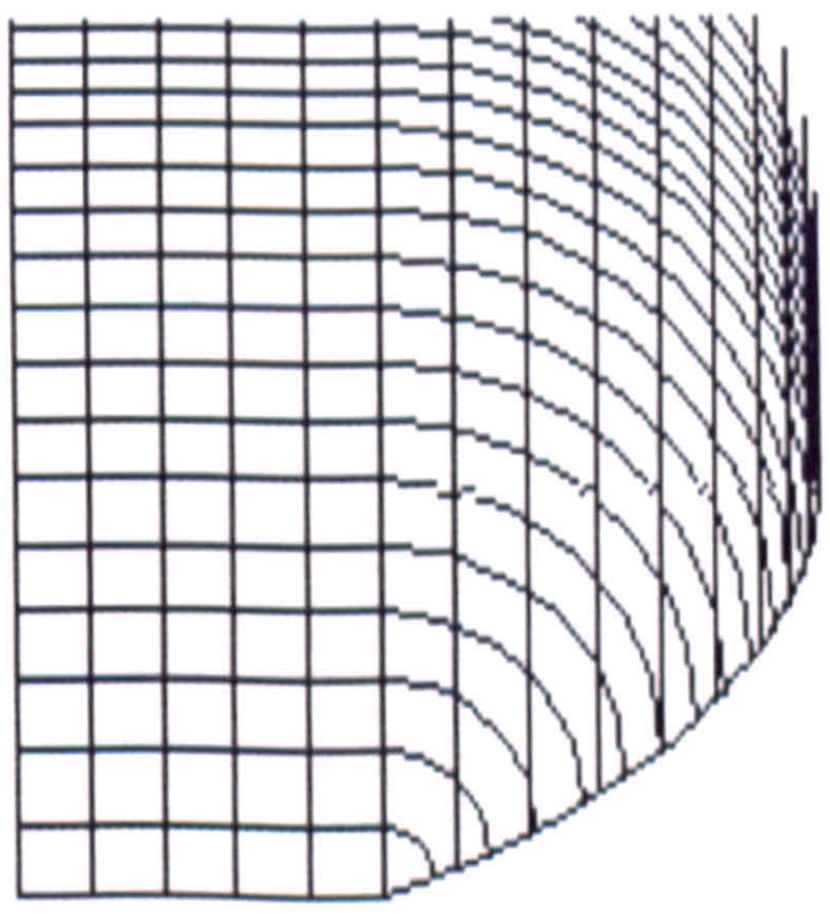

d) As-designed fibre architecture of rear of component

Figure 6.15 Power bulge moulding produced from optimised fibre architecture reinforcement for uniform fibre volume fraction

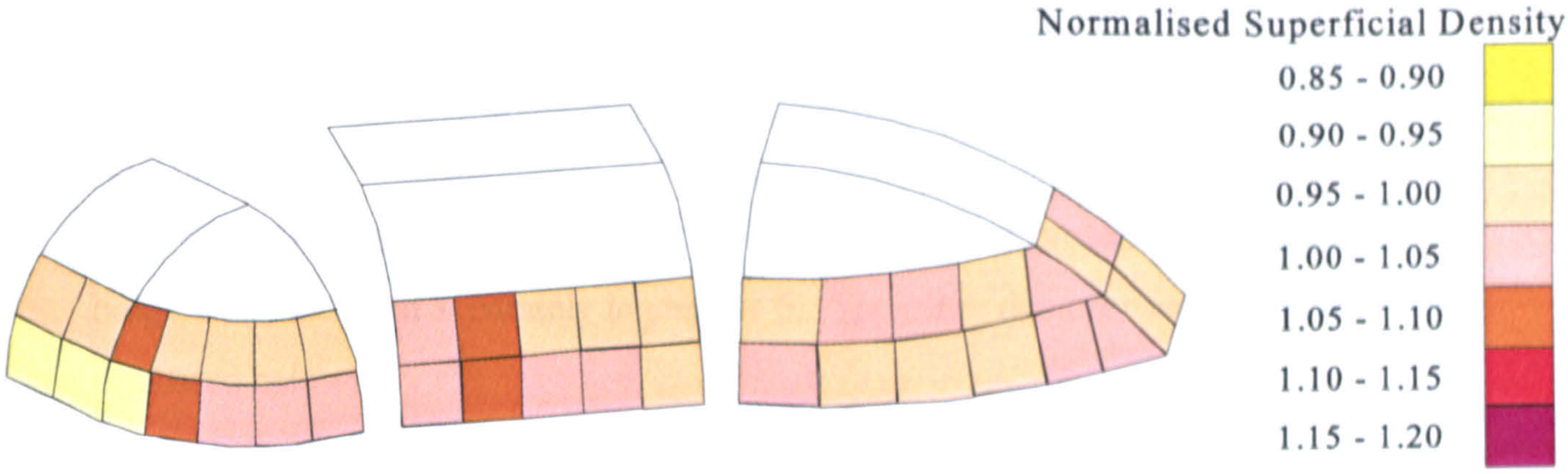

a) Optimised laydowns.

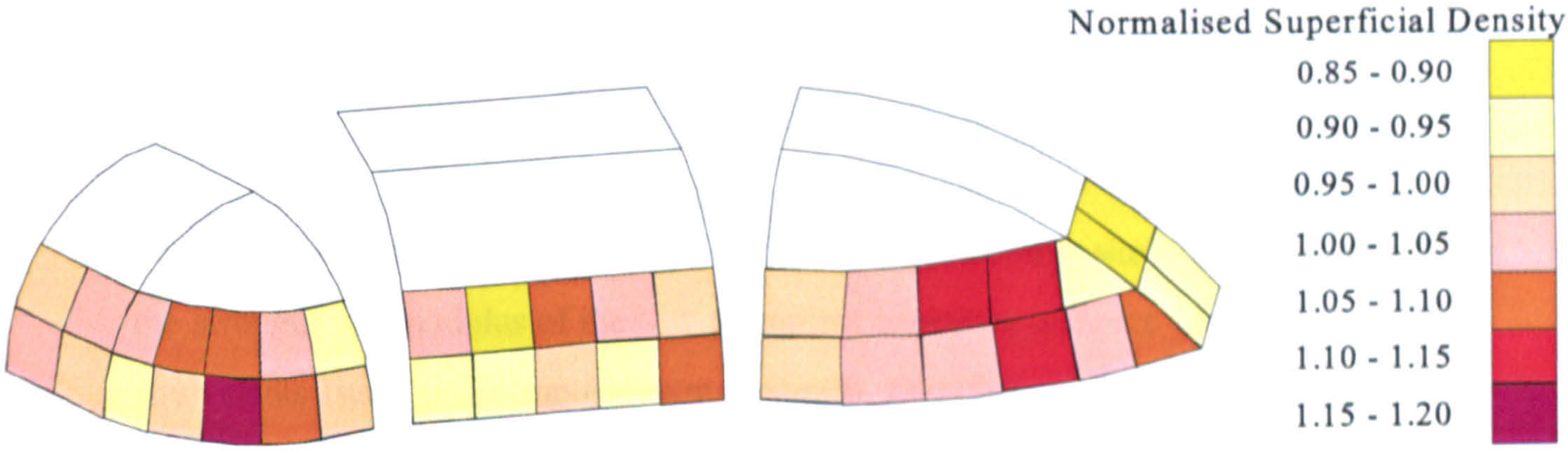

b) Conventional 0°/90° tow placed reinforcement.

Figure 6.16 Normalised superficial density from burn-off specimens in power bulges

Chapter 7
Case Studies

7.1 Introduction

Four technology demonstrators were manufactured in this project. The generic power bulge was discussed separately in chapter 6. The other demonstrator components are discussed below:

7.2 Island Plastics Transom Flange

The Island Plastics transom flange was a load bearing structure used in the manufacture by RTM of rigid inflatable boats (the Avon Rover R2.80 and R3.10). The flange supported an inflatable tube running around the perimeter of the boat (Figure 7.1). The flange preform was produced conventionally from two skins of random reinforcement (Vetrotex Unifilo U816) with a quadri-axial stitch bonded core (Tech Textiles EQX 2336). For comparison purposes, flat plaque mouldings were produced from conventional fabrics and using the airjet tow placement facility before post-curing and mechanical testing.

Table 7.1 shows the results of tensile tests (six for each composite). It can be seen that the strength and modulus of the tow placement laminates compare well with the fabric equivalents (with small improvements overall). One factor here may be the reduced fraction of non-structural stitching yarn which is generally present at up to 5% by mass in fabrics produced by warp-knitting and related techniques. This was not taken into account in the fibre fraction calculation and since the presence of non-structural binder yarns in the tow placed preforms was much lower (c.1%), the effective reinforcement fraction is likely to have been significantly higher.

Table 7.1. Tensile Properties of Marine Transom Flange Flat Plaque Manufactured from Fabric and Tow Placed Reinforcement

Reinforcement	Fibre Volume Fraction (%)	Tensile Modulus [Standard Deviation] (GPa)	UTS [Standard Deviation] (MPa)
Quasi-isotropic fabric + random mat	33.09	11.85 [0.68]	162 [11.4]
Tow placement (airjet)	32.58	13.33 [0.74]	171 [16.9]

7.3 Dowty Aerospace General Aviation Propeller Blade

The blade is constructed conventionally from 90 layers of tailored fabric in orientations of 0°, ±45° with a randomly oriented glass fibre core. The tow placement facility allowed a modified layup plan to be used. 2400 tex glass fibre was used to manufacture a 30 layer preform whilst maintaining the original fibre architecture specifications.

The preform (Figure 7.2) was made using the multi-tow roller placement facility using polyester scrim as a binding agent between each ply. Figure 7.3a shows the time taken to produce each layer of the preform using multi-tow roller placement, whilst figures for a similar preform manufactured using the single tow airjet from a previous study by McGeehin [59] are included in Figure 7.3b. Each ply took longer to lay than those from the previous study due to the cutting operations which must be performed whilst the laydown head is stationary. The possibility of using a sub-routine within the control system, allowing cutting to be performed whilst the machine is moving is under investigation by the developers of the control system for future applications. Although the placement times for each layer were increased, the total preparation time for the preform was reduced by 14% (22 minutes) due to the on-line consolidation associated with roller placement which eliminated the need for separate processing operations. The total preparation time of two hours and thirteen minutes was a 32 minute (20%) reduction over the time taken to produce a preform from tailored fabric. Also material wastage was

reduced from 15% to less than 2%.

7.4 Rolls Royce Outlet Guide Vane

The conventional composite outlet guide vane (OGV) was produced by compression moulding 21 laminates, each comprising five sub-laminates of 6k carbon fibre in the stack $[0_2, 90_1, 0_2]$. The tow placement facility reduced the number of plies required from 105 to 63 by using 12k carbon tow in the stack $[0_1, 90_1, 0_1]$ and adjusting tow spacing (3mm longitudinal and 6mm transverse) to provide the correct proportion of longitudinal and transverse reinforcement.

Plies (Figure 7.4) were manufactured by multi-tow placement for two complete carbon fibre OGV preforms. One of the preforms has been moulded (Figure 7.5) in a matched, oil heated steel tool under the conditions described in 3.4.4 and has been vibration tested by Rolls Royce for comparison to a carbon / epoxy OGV manufactured by RTM from conventional stitch bonded carbon fabric and to an OGV produced by compression moulding from carbon / epoxy pre-preg. Rolls Royce reported that the RTM components had some advantages over the compression moulded vanes, in particular microscopical analysis revealed that fibre waviness and porosity normally associated with compression moulded vanes was no longer evident.

Two of the main design criteria for engine fan OGVs are the first bow and torsion vibration modes. To determine the frequencies of the three moulded vanes, a series of free-free tests were completed at the Rolls Royce Vibration Laboratory. The results for the three mouldings are shown in Table 7.2. It can be seen that there is a reduction in the first bow mode (1B) frequencies of 10% and 18% for the tow placed and stitched core RTM vanes compared to the compression moulded datum vane. Reasons for the large difference in frequencies between the RTM and compression moulded vanes are not easily identifiable. The compression moulded vane was up to 0.38mm thicker and weighed 12% more than the RTM vanes. Both thickness and weight would alter the natural frequencies in opposing directions, although the degree of change could not be determined without some detailed study. Possible differences in volume fraction would alter the stiffness of

the components and thus change their modes although no tests have been performed to determine volume fraction due to a lack of time. Other reductions in bow mode frequencies for the RTM vanes include the lack of leading edge protection which Rolls Royce predicts to be accountable for an extra 1% frequency and the effect of fibre waviness in the tow-placed vane which Rolls Royce predict could account for up to a 3% decrease in first Bow frequency (the second preform produced for Rolls Royce was produced on the latest development of the tow placement facility and is manufactured with a lower degree of inherent fibre waviness (as described in 4.6) but has not been moulded due to time restraints). Values for torsional frequencies were very similar for all three mouldings.

Table 7.2. Trent 700 Composite Fan OGV Vibration Results

Shape	Frequency (Hz)		
	Datum Compression Moulded Vane	Tow-Placed RTM Vane	Conventional Stitched RTM Vane
1B	382	344	315
2B	956	897	827
3B	1470	1460	1390
1T	300	306	294
2T	703	730	694
3T	1160	1180	1120

7.5 Conclusions

The applicability of the tow placement facility has been shown in the successful manufacture of a variety of industrial and generic demonstrator components. The manufacture of the Island Plastics Transom Flange demonstrated that test laminates made using tow placed reinforcement were both stronger (by 5%) and stiffer (by 12%) compared to laminates manufactured from commercial reinforcement. Although only slightly better, the results suggest that the tows remain undamaged during the laydown process and that the facility places the tows accurately.

Cycle times to produce a complete 30 layer propeller blade for Dowty Aerospace were reduced by 32 mins (20%) compared to manual tailoring. This figure would have to be greatly increased, however, if the facility were to be used successfully in the commercial environment. Possible machine downtime and the capital cost of the equipment could reduce any advantages of the system over more traditional processes. Work to speed the facility further by enabling tows to be cut whilst the manipulator is moving would probably reduce cycle times by up to 30% (an extra 35 minute saving for the Dowty propeller blade) and would make the facility much more attractive for commercial exploitation.

The applicability of the facility in manufacturing highly structural components has been demonstrated by the production of two complete carbon fibre outlet guide vane preforms. Tests showed that the major bow and torsion vibration modes of an OGV made using tow placed reinforcement were closer to the modes of a datum compression moulded vane than an OGV made from conventional stitch bonded reinforcement. This suggests that tow placement does not impair the vibrational performance of composites and may even enhance them compared with commercial fabrics.

List of Figures

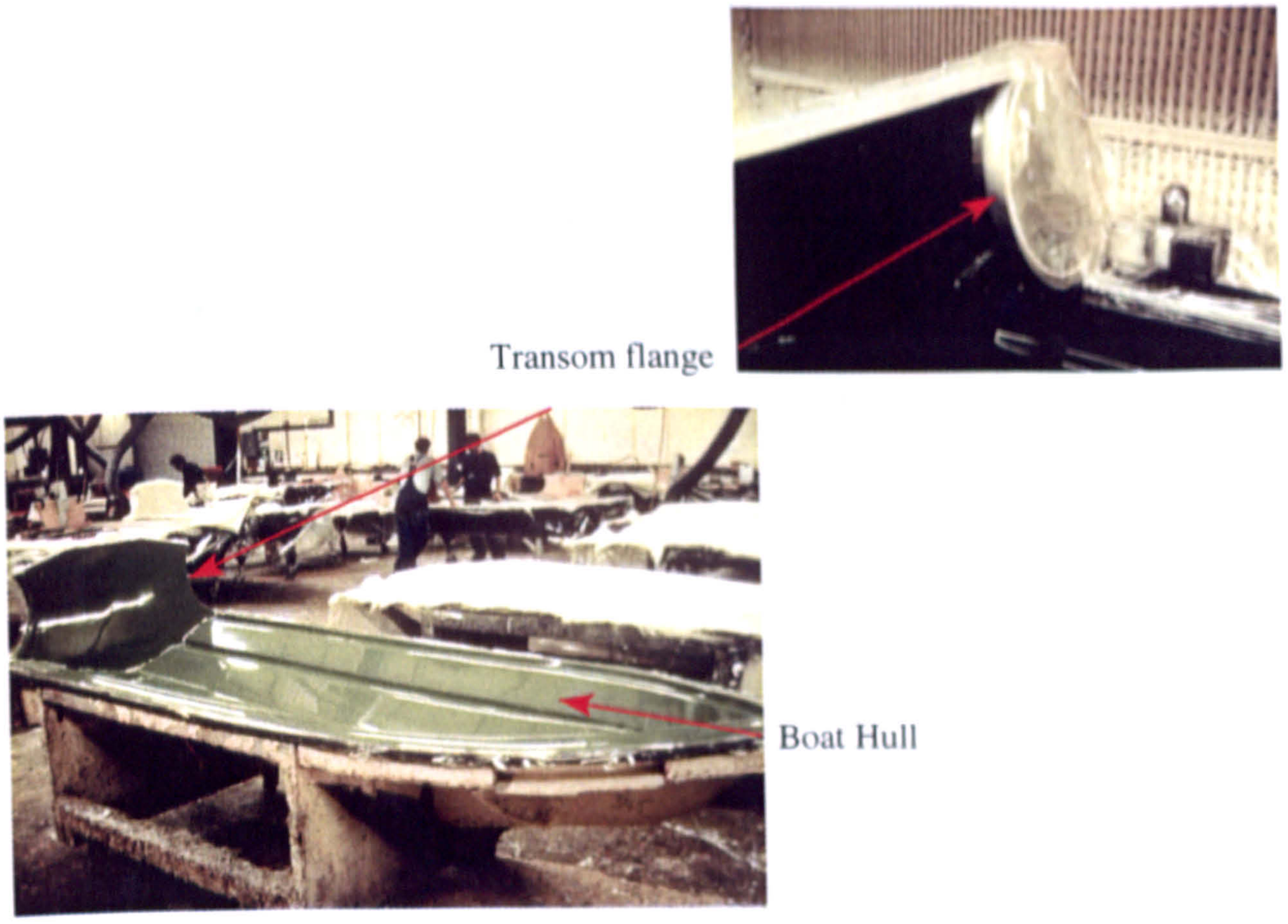

Figure 7.1 Island Plastics Avon rigid inflatable boat hull showing transom flange

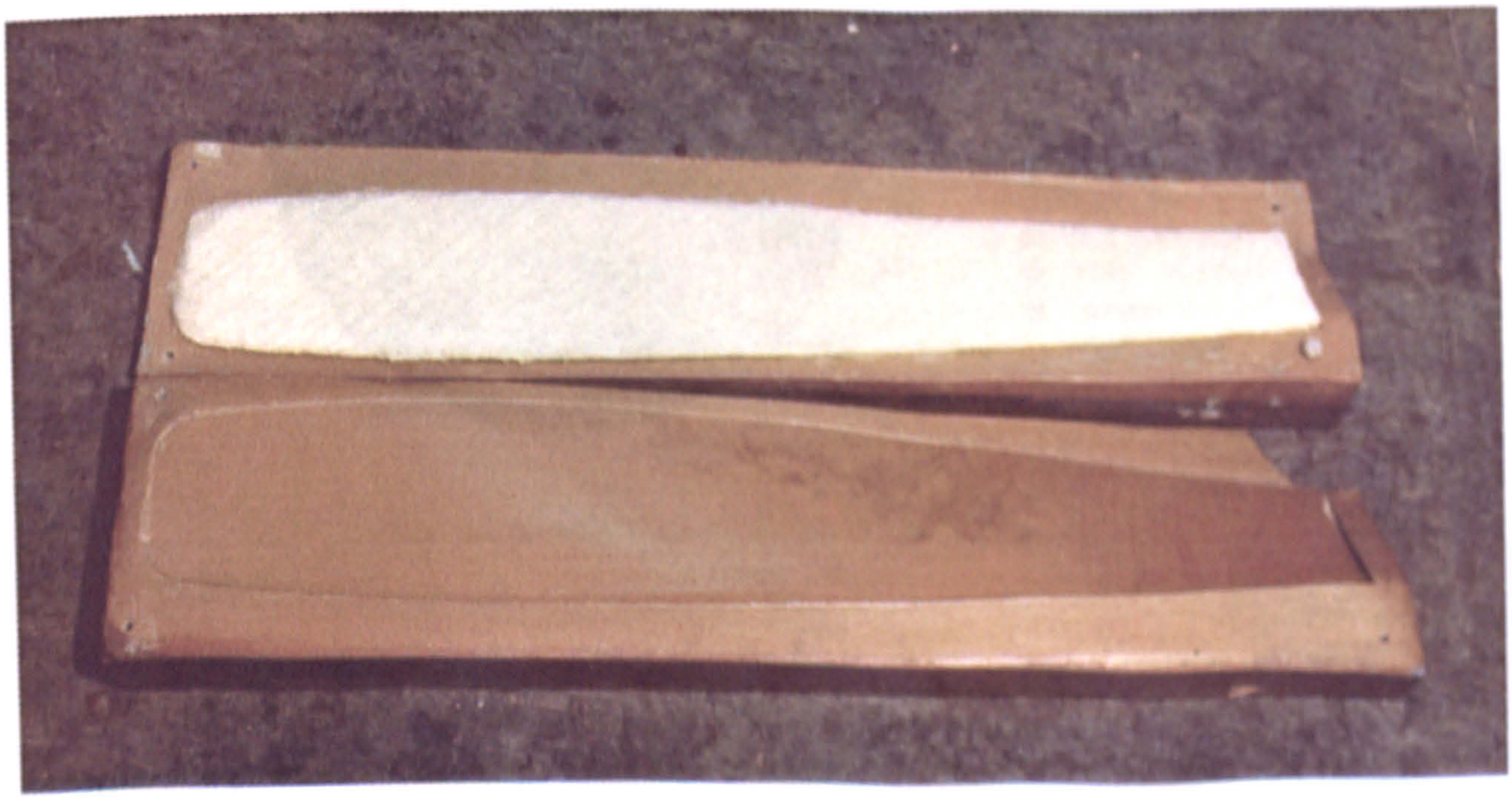

Figure 7.2 Dowty Aerospace General Aviation propeller blade preform and tool

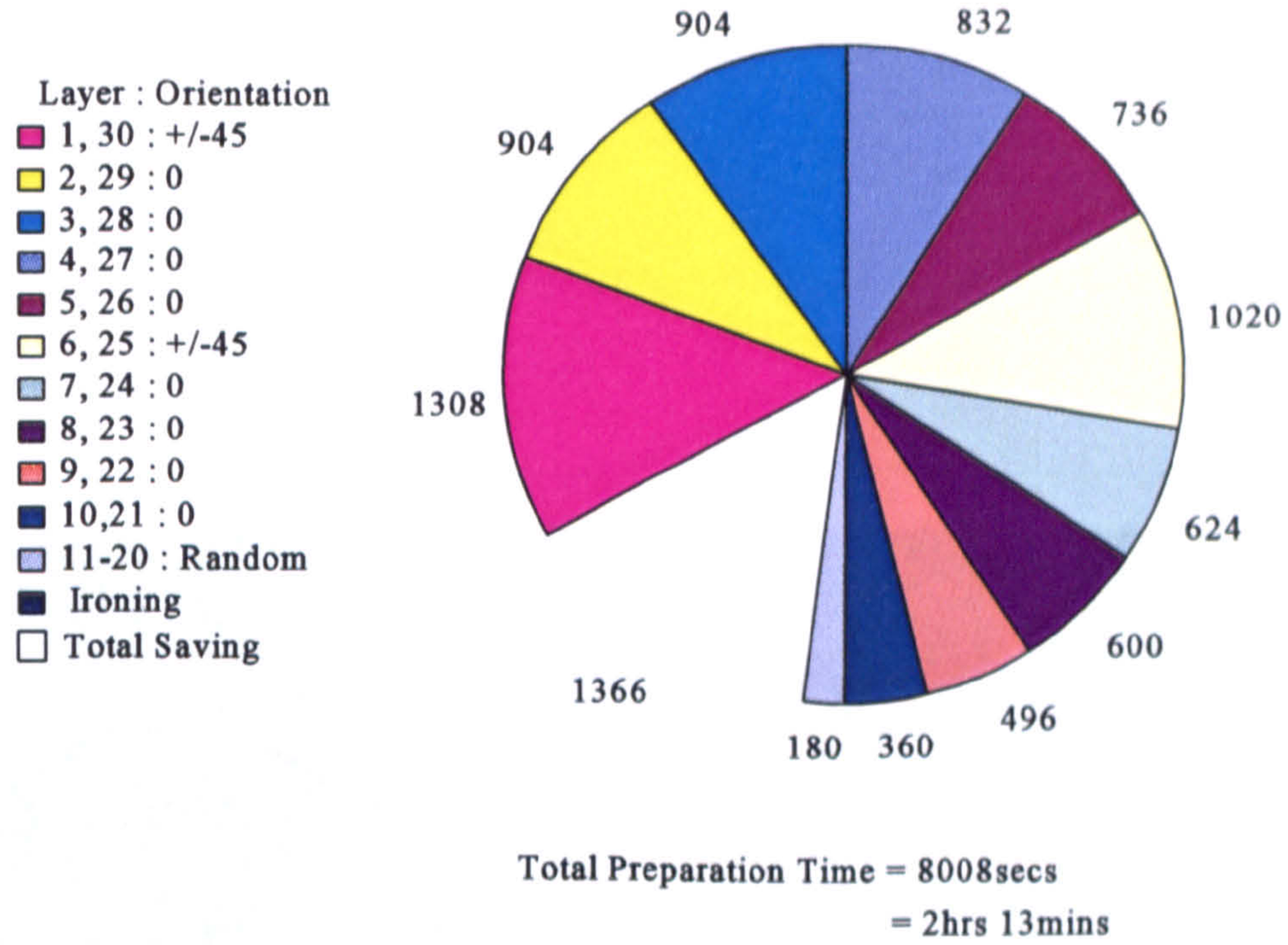

Total Preparation Time = 8008secs
= 2hrs 13mins

a) Current facility times

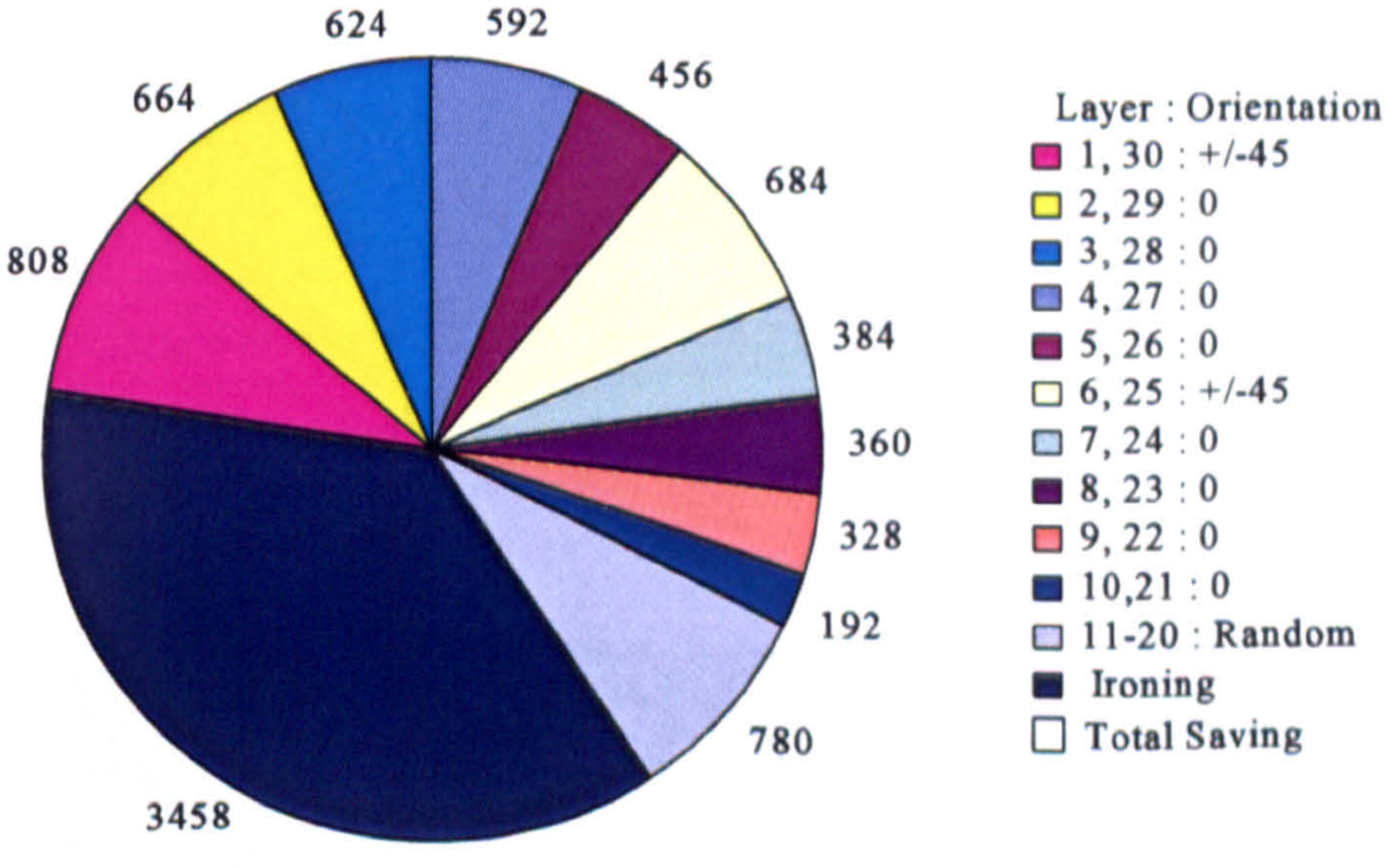

Total Preparation Time = 9330secs
= 2hrs 35mins

b) Figures from a previous study by McGeehin [59] using the single tow airjet

Figure 7.3 Time taken to produce each layer of the Dowty Aerospace General Aviation propeller blade preform

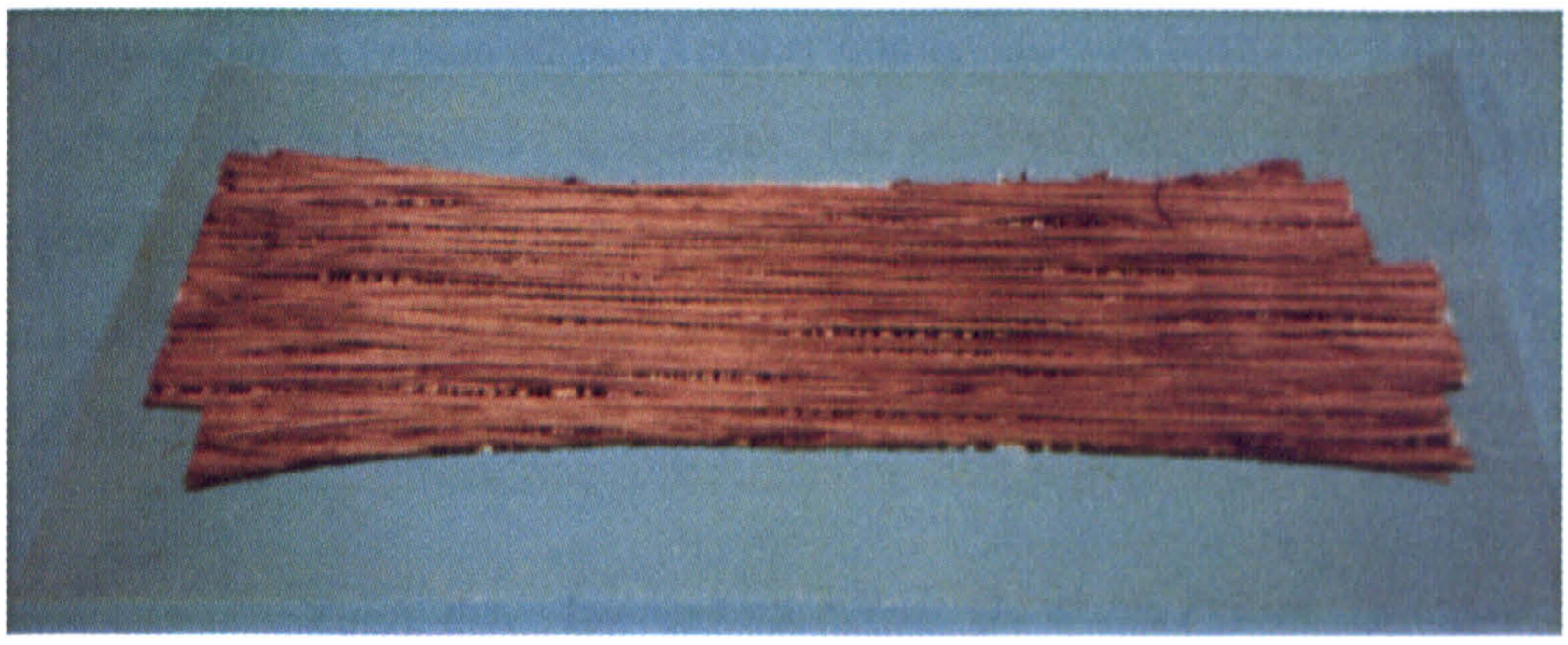

Figure 7.4 Carbon fibre OGV ply manufactured using the tow placement facility

Figure 7.5 Moulded OGV produced using a tow placed preform

Chapter 8
Discussion and Conclusions

8.1 Economic Evaluation

An economic comparison of tow placement with conventional preform manufacture and pre-preg lay-up for a typical carbon / epoxy composite was performed in collaboration with Ciba Polymers and Hexcel Composites. The analysis compares the material costs of carbon / epoxy pre-pregs with similar materials used in RTM including carbon fabric and carbon tow. Table 8.1 compares the cost for individual materials, while Table 8.2 describes the material cost to manufacture a typical composite.

Table 8.1. Approximate Raw Materials Prices

(from materials suppliers)

Description	Cost (GBP)
Tenax Carbon Tow 3k	40/kg
Tenax Carbon Tow 12k	20/kg
Hexcel Composites 5 Harness Carbon Fabric 290g/m^2	25/m^2
Hexcel Composites 5 Harness Carbon Fabric Pre-preg	40/m^2
Fothergills Admesh Polyester Netting	2/m^2
Ciba Geigy LY 5052 resin	15/kg
Hexcel Composites RTM6 resin	45/kg

Table 8.2 shows that the pre-pregging operation invokes a cost penalty of around 20% compared with the equivalent (conventional) RTM materials. A further 20% saving can then be made if tow placement can be substituted for high cost, aerospace fabrics. On this basis then, an RTM composite relying on tow placement can be produced at between 28 and 60% of the cost of a pre-preg, depending upon the specification of the tow and epoxy resin. It should also be pointed out that these costs are based, conservatively, on 100% materials utilisation. Given likely industrial figures of 70%, 80% and 95% for pre-preg, RTM using fabrics and RTM using tow placed preforms respectively [**9**], the economic

case for tow placement would seem to be attractive. However it should be pointed out that this study relates to materials costs only and does not include other costs such as labour, capital expenditure and manufacturing costs which have not been studied but would have an effect on the costs provided.

Table 8.2. Normalised Costs of Pre-preg, Fabric and Tow-placed Composites (assuming 100% materials utilisation)

Description	Cost (GBP/m^2 @50% V_f)	Relative Cost
Carbon/RTM6 pre-preg	200	1
Fabric/RTM6	163	0.82
Fabric/LY5052	138	0.69
3k Tow/RTM6	118	0.59
3k Tow/LY5052	93	0.47
12k Tow/RTM6	81	0.41
12k Tow/LY5052	56	0.28

8.2 General Discussion

The work described in this thesis is concerned with developing techniques for the design and manufacture of preforms for liquid composite moulding. This has included the development of design techniques based on deformation modelling to optimise preform fibre architecture, and the development of a prototype automated CNC tow placement facility. Referring to the project objectives set out in 1.5, this thesis has addressed the deliverables, all of which have been achieved with some amount of success:

To identify techniques for fibre deposition, retention and consolidation

A prototype tow placement facility based on the roller placement of tows onto a flat bed has been developed for the manufacture of preforms for LCM. The facility has the capability of laying up to five tows of carbon or glass fibre independently. Trials have demonstrated that the roller placement facility produced reinforcement with greater positional accuracy compared with airjet deposition. Unidirectional reinforcement

manufactured using the roller placement facility also exhibited less fibre misalignment, higher moulded tensile modulus and a greater degree of anisotropic flow characteristics than similar reinforcement manufactured with a prototype airjet placement technique, further supporting the improved accuracy. Tows were retained using a polyester scrim which although tacky at room temperature, was more effective at elevated temperature, and therefore two heaters were incorporated into the system. Consolidation of these preforms was achieved continuously by the action of a compaction roller, with compliance increased by the local heating.

The techniques for fibre deposition, retention and consolidation were developed over the period of this project and have been found to be effective for the production of preforms for LCM. The following sections detail the advantages and limitations of the facility for preform manufacture as well as describing various tools to help design and manufacture preforms more effectively.

To perform processing and performance studies on preforms produced using the laydown facility.

To determine the performance of materials manufactured using the tow placement facility, a transom flange preform used in the manufacture by RTM of rigid inflatable boats for Island Plastics Ltd was produced. The preform consisted of a quasi-isotropic core sandwiched between randomly oriented skins. Experiments on test laminates made using tow placed reinforcement were both stronger (by 5%) and stiffer (by 12%) compared to laminates manufactured from commercial reinforcement. Although not exhaustively tested for a range of mechanical properties and against a variety of other commercial reinforcement, the results suggest that there is no loss of performance by using tow placed reinforcement which implies that the accuracy of tow placement is good and that the tows remain undamaged during the laydown process.

It had been noted that under certain processing conditions during laydown, the reinforcement may contain some fibre waviness. Two models were developed to determine the effect of fibre waviness on the structural performance of reinforcement

manufactured on the tow placement facility. The models, which predicted the effect of in-plane fibre waviness on tensile modulus, were validated for carbon and E-glass composites by manufacturing reinforcement with induced fibre waviness in the range 0 to 0.4. It was found that for in-plane waviness, the modified rule of mixtures and the classical laminate theory models both predicted reasonable reductions in tensile modulus for a wide range of waviness factors. As the modified rule of mixtures model is the simpler of the two models it would be more suitable to use it rather than the more complex classical laminate model for predicting the effects of waviness on laminates with in-plane waviness.

For laminates containing out-of-plane waviness (e.g. the crimp found in woven fabrics) the classical laminate model outperformed the modified rule of mixtures model probably because it takes account of the material shear modulus and Poissons effects. Out-of-plane waviness was found to be more detrimental than in-plane waviness probably because of a shear coupling adding stiffness to the laminates with in-plane waviness in a similar way to angle ply laminates.

The in-plane permeability of reinforcement containing fibre waviness has been predicted. A model has been developed to determine the effects of waviness on longitudinal and transverse permeability. Although the model failed to predict the exact values, the trend was determined to be very similar to that of experimental results for both longitudinal and transverse permeability. The model is semi-empirical as it is dependent on experimental data for unidirectional reinforcement to predict the effects of waviness with any degree of accuracy. However, in a preform manufactured using the tow placement facility, the likely effect of fibre waviness would be negligible compared to other factors that affect permeability such as positional errors induced by manual handling and ply stacking errors.

Fibre movement can change composite processing and performance properties. A model to predict the deformation of aligned reinforcements during the forming stage has been developed by Long [58]. The model was validated for tow placed reinforcements which were found to deform in a similar way to commercial reinforcements such as woven or

stitch bonded fabrics. This enabled the drape model to be developed as a tool for optimisation of fibre architecture as well as allowing a net-shape to be determined for the production of laydowns which when moulded require minimal trimming and produce minimal waste.

It is more desirable to be able to design and manufacture the preform with an optimised fibre architecture than to predict the deformed architecture of a regular reinforcement. A kinematic undrape algorithm was developed by Long [58] which was successfully validated for an optimised preform with the reduction of superficial density in a hemispherical component from ±9% to ±2% compared to a standard 0°/90° fabric. The optimisation routine was also validated for a generic power bulge, again designed with a constant superficial density, which has shown that the technique can also be used for more complex geometries. The optimised power bulge reduced variations in preform superficial density from 0.85-1.2 to 0.9-1.1 which, although not as successful as the hemisphere, showed that the optimisation technique produces preforms with enhanced qualities compared to conventional reinforcements. Although the design of the fibre architecture for both components illustrated optimisation with regard to uniform superficial density, the process should be applicable for various design scenarios: to optimise architecture for enhanced flow properties (to reduce mould filling times and avoid dry spots); localised tow placement (for extra reinforcement in highly loaded areas); alignment of reinforcement with major load paths (for increased mechanical performance). It could also be possible to incorporate the optimisation routine into other preform manufacturing systems such as knitting and embroidery.

The current method of optimising preform fibre architecture involves creating a model of the nodal (fibre crossover) points manually which is very time consuming. It would be advantageous to automate this part of the process to allow fibres to be positioned on a 3D model of the component, to enable the nodal points to be manipulated and to suggest possible fibre architectures to minimise problems with inter-fibre shear.

To reduce preform cycle time, waste and manual intervention

An analysis of the manufacture of a propeller blade preform produced for Dowty Aerospace revealed the flexibility of the facility in reducing the number of plies to manufacture one preform by 66% compared with commercial reinforcement. Cycle times to produce the complete propeller blade were reduced by 32 mins (20%) compared to manual tailoring. These times would have to be greatly reduced, however, if the facility were to be used successfully in the commercial environment. Possible machine downtime and the capital cost of the equipment could reduce any advantages of the system over more traditional processes. Work to speed the facility further by enabling tows to be cut whilst the manipulator is moving would probably reduce cycle times by up to 30% (an extra 35 minute saving for the Dowty propeller blade) and would make the facility much more attractive for commercial exploitation.

Although material wastage was reduced significantly from 15% (manual tailoring) to 2%, manual intervention is still required to trim small amounts due primarily to a minimum tow length of 110mm which is imposed by the design of the cutting mechanism. This can offset any advantages of producing net-shaped laydowns by forcing an operator to trim excess material and will count against the facility as a commercial viability.

To show the applicability of the design and manufacturing system for industrial components

The manufacture of preforms for the Island Plastics transom flange, the generic power bulge and the Dowty Aerospace propeller blade have been discussed above. The applicability of the manufacturing technique for highly structural components was demonstrated by the manufacture of a carbon fibre outlet guide vane used in the Trent series of jet engines by Rolls Royce. Vibration analysis on the moulded components showed the performance of the vane manufactured with tow placed reinforcement exceeded slightly that of an RTM vane manufactured with commercial fabric, although it failed to perform as well as a compression moulded pre-preg vane. This suggests that tow placement does not impair the vibrational performance of composites and may even enhance them compared with commercial fabrics.

It is probably in areas such as aerospace where the tow placement facility would be of most use. It is unlikely that in its present condition it would be able to perform in a high volume manufacturing environment due to the cycle times involved and its reliance on manual intervention. However, for the aerospace industry where component performance is more of a driver, the advantages of the facility could outweigh its limitations. Of particular benefit in such industries would be the facilities design flexibility for manufacturing low waste preforms with excellent tow positional accuracy providing good mechanical properties in a repeatable process.

8.3 Major Conclusions

This section includes a summary of the major conclusions arising from the work in this thesis.

- A multi-tow placement facility, based on fibre deposition via a roller, has been developed and used to manufacture preforms for LCM. The facility is based around a four axis NC manipulator controlled by a separate hard wired unit and is capable of laying up to five tows of carbon or glass fibre simultaneously or independently.

- Comparison studies revealed that reinforcement manufactured via roller placement was more accurately positioned and had better mechanical properties than similar material produced using airjet placement.

- Reasonably accurate predictions of the effect of fibre waviness can be achieved using a modified rule of mixtures or a classical laminate approach to modelling laminates with in-plane waviness. For out-of-plane waviness, the classical laminate model should be used as it takes account of material shear modulus and Poissons effects. Out-of-plane waviness affects laminate modulus more than in-plane waviness probably because of a shear coupling that adds stiffness to laminates with in-plane waviness.

- It is possible to predict, with reasonable accuracy, the effects of fibre waviness on in-plane permeability using a geometric model. However the model is semi-empirical, requiring experimental data for unidirectional reinforcement. Also the likely levels of fibre waviness found in tow placed reinforcement would have negligible effect on the material permeability.

- It is possible to reduce superficial density variations within a preform by using the tow placement facility to manufacture a preform with modified fibre architecture. Although the fibre architecture optimisation process has only been demonstrated for reducing superficial density variations, the process should be suitable to optimise architecture for other processing or performance gains.

- The tow placement facility can be used to manufacture preforms that offer slight improvements in mechanical performance compared with conventional reinforcement, probably because the tows remain undamaged and are positioned with excellent accuracy in a preform that is robust and handleable.

- A reduction in preform cycle time, material waste and manual intervention compared to conventional fabric based preforming and previous tow placement work was demonstrated for the manufacture of prototype propeller blades. Although the process could be speeded further by development of the NC operating routine to enable on-line cutting, it is uncertain whether the facility would be economical for the manufacture of anything but "hi-tech" components where material performance is more important than cost.

8.4 Recommendations for Further Work

The following recommendations relate to work to improve operating software, models and the utility of the tow placement facility for use in the production environment.

CAE System

- Validation of the drape and undrape models for non-symmetric components.

- Integration of the various software modules under a common operating system.

- Development of optimisation software to enable the automated production of optimised fibre architecture models in a visual model and to enable the user to easily manipulate the nodal points as required.

- Integrate optimisation routine into a complete preforming CAE package to include flow simulation and prediction of structural properties and develop optimisation software to suggest possible optimised fibre architectures to improve preform performance.

Tow Placement Machine

- Automation of the binder application to reduce manual intervention and to reduce cycle times.

- Development of NC operating program to enable on-line cutting within the multi-tow roller head to minimise machine downtime.

- Re-design of the tow cutting assembly to reduce the minimum tow length from the current 110mm.

- Extension of the placement techniques to allow for the placement of tows on generally curved surfaces and to enable direct laydown into forming tools.

References

[1] Lubin, G. "Handbook of Composites" *Van Nostrand Reinhold*, New York, USA, 1982

[2] Jefley, D.C. "McDonnell Douglas all-composite wing stub box successfully tested to failure" *http://larcpubs.larc.nasa.gov/randt/1995/sectionB1.fm59.html*, extract from NASA web pages.

[3] Mossman, S.T.I, Morris, P.J.T. "The Development of Plastics" *The Royal Society of Chemistry*, 1994

[4] Cochran, R, Matson, C, Thoman, S, Wong, D. "Advanced Composite Processes for aerospace applications" *Proceedings from the 42nd International SAMPE Symposium*, Anaheim, CA, USA, May 4-8, 1997, pp 635-640.

[5] McIlroy, D. "Composite rotor blade fabrication, Automated composite fabrication and filament winding" http://www.bmpcoe.org/surveys/BELLHC/BELLHC_info.htm# INFORMATION22, extract from Bell Helicopter Textron web pages.

[6] Benda, B.J., Stump, K.H. "A case study of contoured tape laying" Proceedings of the 52nd Annual Forum of the American Helicopter Society, Washington, DC, USA, June 4-6 1996, pp 603-610.

[7] Holloway, L. "Handbook of polymer composites for engineers" *Woodhead Publishing Ltd.*, 1994

[8] Harrison, A. "A low investment cost composites high roof for the Ford Transit van using electroformed tooling and RTM" *Proceedings of the 4th International Conference on Automated Composites (ICAC 95)*, Nottingham, 6-7 Sept, 1995, Vol 2, pp 511-525.

[9] Rudd, C.D., Long, A.C., Kendall, K.N., Mangin, C.G.E. "Liquid moulding technologies" *Woodhead Publishing Ltd. / SAE*, 1997.

[10] Garg, A., Paton, R., Baddock, K. "Resin transfer moulding for aerospace components" *Proceedings of the 5th Australian Aeronautical Conference*, Sept 13-15, 1993, Crows Nest, NSW, Australia, part 2, pp 363-368.

[11] Kitson, L., Johnson, B. "Fiber placement technology advancements at Boeing

Helicopters" *Proceedings of the 51st Annual Forum of the American Helicopter Society*, May 9-11, 1995, Fort Worth, Texas, USA, part 3, pp 69-79.

[12] Leon, G.F., Hall, J.C., Kelly, J.J., Coffenberry, B.S., Cirino, M. "Affordable thermoplastic processing of marine structures" *Composites Manufacturing*, Vol 6, 1995, pp 193-199.

[13] Anon. "Current composites manufacturing technology" *http://itri.loyola.edu/polymers/c1_s3.htm*, extract from report by International Technology Research institute, Loyola College.

[14] Zhang, Z., Sarhadi, M. "An integrated CAD/CAM system for automated composite manufacture" *Journal of Materials Processing Technology*, Vol 61, No 1-2, Aug 1996, pp 104-109.

[15] Bernardon, E.D. "Fibersim, CAD integrated software tools for composite manufacturing and design" *Proceedings of the 19th International SAMPE European Conference*, Paris, La Defense, France, April 22-24, 1998, pp163-173.

[16] Emerson, R.P., Orlet, M.W., Bakis, C.E. "Fabrication and characterisation of filament wound elastomeric matrix composite materials" *Proceedings of the 42nd international SAMPE symposium*, Anaheim, CA, USA, May 4-8, 1997, pp 342-353.

[17] Shih, P.J., Loos, A.C. "Design of experiments analysis of the on-line consolidation process" *Proceedings of the 11th International Conference on Composite Materials*, Gold Coats, Australia, July 1997, Vol 4, pp 92-102.

[18] Christen, O., Neitzel, M. "Filament winding thermoplastic composite cylinders with on-line impregnation" *Proceedings of the 42nd international SAMPE symposium*, Anaheim, CA, USA, May 4-8, 1997, pp 380-390.

[19] Costen, R.C., Marchello, J.M. "Sensitivity studies for in-situ automated tape placement of thermoplastic composites" *Proceedings of the 42nd international SAMPE symposium*, Anaheim, CA, USA, May 4-8, 1997, pp 33-47.

[20] Steiner, K.V., Faude, E., Don, R.C., Gillespie, J.W. "Cut and re-feed mechanics for thermoplastic tape placement" *Proceedings of the 39th International SAMPE Symposium*, Anaheim, CA, USA, April 11-14, 1994, pp 2627-2636.

[21] Johnston, N.J., Towell, T.W., Marchello, J.M., Grenoble, R.W. "Automated

fabrication of high performance composites: an overview of research at the Langlet Research Center" *Proceedings of the 11th International Conference on Composite Materials*, Gold Coats, Australia, July 1997, Vol 4, pp 85-91.

[22] Pitchumani, R., Gillespie, J.W., Lamontia, M.A. "Design and optimisation of a thermoplastic tow placement process with *in-situ* consolidation" *Journal of Composites Materials*, Vol 31, No 3, 1997, pp 244-275.

[23] Sharp, R., Holmes, S., Woodall, C. "Materials selection/fabrication issues for thermoplastic fiber placement" *Journal of Thermoplastic Composite Materials*, Vol 8, Jan 1995, pp 2-14.

[24] Brailsford, B. "Advanced fiber placement program for aircraft structures" *Proceedings of the 10th ASME/ESD Advanced Composites Conference*, Dearborn, Michigan, USA, 7-10 Nov 1994, pp 299-302.

[25] Measom, R., Sewell, K. "Fiber placement low cost production for complex composite structures" *Proceedings of the 52nd Annual Forum of the American Helicopter Society*, June 4-6 1996, Washington, DC, USA, pp 611-622.

[26] Towell, T.W., Johnston, N.J., Grenoble, R.W., Marchello, J.M. "Thermoplastic fiber placement machine for materials and processing evaluations" *Proceedings of the 41st international SAMPE symposium*, Anaheim, CA, USA, March 24-28, 1996, pp 1701-1711.

[27] Anon "7-Axis fiber placement system" *http://www.milacron.com/MTG/MTG_Viper.htm* extract from Cincinnati Milacron web pages.

[28] Anon "Wolf Track - Premier I features lighter, stronger all-composite fuselage" *http://www.milacron.com/MTG/MTG_*WT7.htm, extract from Cincinnati Milacron web pages.

[29] Martin, J.P, Langone, R.J., Pasenen, M.J., Mondo, J.A "Cost-effective, automated equipment for advanced composite structure development and production" *Proceedings of the 42nd international SAMPE symposium*, Anaheim, CA, USA, May 4-8, 1997, pp 48-57.

[30] Gutowski, T.G. "Advanced Composites Manufacturing" *John Wiley and Sons*, 1997.

[31] Owen, M.J., Rice, E.V., Rudd, C.D., Middleton, V. "Resin transfer moulding for

automobile manufacture: Reality and simulation" *Computer Aided Design in Composite Materials Technology III*, Computational Mechanics, Elsevier Applied Science, 1992, pp 121-142.

[32] Wlosinski, R.K., Kniveton, T.W., "Design and manufacturing pilot of an SRIM composite crossmember", *Proceedings of the 120th Annual ASM/ESD Advanced Composites Conference,* Dearborn, MI, USA, 7-10 Nov 1994, pp 77-82.

[33] Bielefield,M. "Fabrication of Braided RTM Driveshaft Tubes For the RAH-66 Comanche", *Annual Forum Proceedings - American Helicopter Society,* Alexandria, VA, USA, 1994, vol.2, pp1001-1015.

[34] Potter, K.D. "Resin transfer moulding" *Chapman and Hall*, 1997.

[35] McCarthy, R.F.J., Haines, G.H., Newley, R.A. "Polymer composite applications to aerospace equipment" *Composites Manufacturing*, Vol 5, No 2, 1994, pp 83-93.

[36] Bonner, H.M., Teeter, D.B. "Resin transfer molding applications in the kitplane industry" *Proceedings of the 38th international SAMPE symposium and exhibition*, Annaheim, CA, USA, May 10-13, 1993, pp 488-495.

[37] Rudd, C.D., Owen, M.J., Middleton, V. "Effects of process variables on cycle time during resin transfer moulding for high volume manufacture" *Materials Science and Technology*, Vol 6, July 1990, pp 656-665.1

[38] Johnson, M.S. "The application of microwave preheating in resin transfer moulding" P*hD Thesis*, University of Nottingham, UK, 1996.

[39] Blanchard, P.J., Rudd, C.D. "Cycle time reduction in resin transfer moulding by phased catalyst injection" *Composites Science and Technology*, Vol 56, 1996, pp 123-133.

[40] Rudd, C.D., Middleton, V., Owen, M.J., Long, A.C., McGeehin, P., Bulmer, L.J. "Modelling the processing and performance of preforms for liquid moulding processes" *Composites Manufacturing*, Vol 5, No 3, 1994, pp 177-186.

[41] Chavka, N.G., Johnson, C.F. "Critical performance issues for large automotive structures" *Proceedings of the ASM/ESD Advanced Composites Conference*, 1990, pp 413-422.

[42] Gomes, M.P.S.F., Hibberd, R.D., Davies, B.L. "Robotic preforming of dry fibre

reinforcements" Plastics, Rubber and Composites Processing and Applications, Vol 19, 1993, pp 131-136.

[43] Dunbar, S.G. "Preformable continuous strand mat for structural applications" *Proceedings of the 44th Annual Conference of the Composites Institute*, The Society of the Plastics Industry, Cincinnati, OH, USA, 1-5 Feb 1989, Session 10A.

[44] Owen, M.J., Middleton, V., Rudd, C.D. "Fibre reinforcement for high volume resin transfer moulding (RTM)" *Composites Manufacturing*, Vol 1, No 2, June 1990, pp 74-78.

[45] Buckley, D.T. "Manufacturing automation components for net shape, high volume, complex preforms" *Proceedings of the 5th International Conference on Automated Composites (ICAC)*, Institute of Materials, Glasgow, 1997, pp 253-262.

[46] Bannister, M.K., Herszberg, I. "Textile preforming for composite structures" Proceedings of the 5th Australian Aeronautical Conference, Crows Nest, NSW, Australia, Sept 13-15 1993, pt 6, pp 357-362.

[47] Smith, P.S. "Structural preform design for low cost composite processing" *PhD Thesis*, University of Nottingham, UK, 1998.

[48] Pastore, C.M., Frank, K.K. "Near net shape manufacture of composite engine components by 3-D fiber architecture" *Proceedings of the Gas Turbine and Aeroengine Congress and Exposition*, Toronto, Ontario, Canada, June 4-8, 1989, pp 1-7.

[49] Uozomi, T., Hisa, Y. "Braiding pultrusion process" *Proceedings of the 27th International SAMPE Technical Conference*, Albuquerque, NM, USA, Oct 9-12, 1995, Vol 27, pp 371-379.

[50] Xiao, L.H., Jian, Z.X., Yao, Z.M., Xiao, W.M. "Design and manufacturing of new structural 4-step 3-D braided preforms" *Proceedings of the 38th international SAMPE symposium and exhibition*, Annaheim, CA, USA, May 10-13, 1993, pp 1505-1516.

[51] Brown, A.S. "Weaving new strength into composites" *Aerospace America*, Vol 31, No 9, Sept 1993, pp 26-29.

[52] McIllhagger, R., Hill, B.J., Brown, D., Limmer, L. "Construction and analysis of three-dimensional woven composite materials" *Composites Engineering*, Vol 5, No 9, 1995, pp 1187-1197.

[53] Du, G.W., Ko, F. "Analysis of multi-axial warp knit prefroms for composite reinforcement" *Composites Science and Technology*, Vol 56, No 3, 1996, pp 253-260.

[54] Crothers, P.J., Drechsler, K., Feltin, D., Herszberg, I., Bannister, M. "The design and application of tailored fibre placement" *Proceedings of the 11th International Conference on Composite Materials*, Gold Coast, Australia, 14-18 July, 1997, pp 600-610.

[55] Crothers, P.J., Drechsler, K., Feltin, D., Herszberg, I., Kruckenberg, T. "Tailored fibre placement to minimise stress concentrations" *Composites Part A*, Vol 28A, 1997, pp 619-625.

[56] Feltin, D., Gliesche, K. "Preforms for composite parts made by tailored fibre placement" *Proceedings of the 11th International Conference on Composite Materials*, Gold Coast, Australia, 14-18 July, 1997, pt V, pp 17-26.

[57] Warrior, N.A., Rudd, C.D., Ellis, J. "Embroidered reinforcements: A potentially advantageous process for fabricating strong, net shape structural composites" *Materials Technology*, Vol 12, No 1, 1997, pp 6-9.

[58] Long, A.C. "Preform design for liquid moulding processes" *PhD Thesis*, University of Nottingham, UK, 1994.

[59] McGeehin, P. "Preform manufacture for liquid moulding processes" *PhD Thesis*, University of Nottingham, UK, 1994.

[60] Smith, A., Anthony, D. "Robotic placement of complex thermoplastic structures" *Proceedings of the International SAMPE Technical Conference*, 1992, Vol 24, pp 101-115.

[61] Jander, M. "Industrial RTM - new developments in molding and preforming technologies" *Advanced Composites Materials: New Developments and Applications Conference Proceedings*, Sept 1991, pp 29-34.

[62] Bruschke, M.V., Advani, S.G. "A finite element/control volume approach to mold filling in anisotropic porous media" *Polymer Composites*, Vol 11, No 6,

December 1990, pp 398-405.

[63] Advani, S.G. "Flow and rheology in polymer composites manufacturing" *Elsevier Science,* 1994.

[64] Adams, K.L., Rebenfeld, L. "In-plane flow of fluids in fabrics: Structure/flow characterisation" *Textile Research Journal*, Vol 57, 1987, pp 647-654.

[65] Hirt, D.E., Adams, K.L., Prud'homme, R.K., Rebenfeld, L. "In-plane radial fluid flow characterisation of fibrous materials" *Journal of Thermal Insulation*, Vol 10, 1987, pp 153-172.

[66] Chick, J.P., Rudd, C.D., Van Leuwen, P.A., Frenay, T.I. "Material characterisation for flow modelling in structural reaction injection moulding" *Polymer Composites*, Vol 171, 1996, pp 124-135.

[67] Smith, P., Rudd, C.D., Long, A.C. "The effect of shear deformation on the processing and mechanical properties of aligned reinforcements" *Composites Science and Technology*, Vol 57, 1997, pp 327-344.

[68] Cai, Z. "Estimation of the permeability of fibrous preforms for resin transfer moulding processes" *Composites Manufacturing*, Vol 3, No 4, 1992, pp 251-257.

[69] Lam, R.C., Kardos, J.L. "The permeability and compressibility of aligned and cross-plied carbon fibre beds during processing of composites" *Proceedings of the 47th Annual Technical Conference (ANTEC '89)*, New York, USA, 1989, pp 1408-1412.

[70] Gutowski, T.G., Cai, Z., Bauer, S., Boucher, D., Kingey, J., Wineman, S. "Consolidation experiments for laminate composites" *Journal of Composite Materials*, 1987, pp 650-669.

[71] Gebart, B.R. "Permeability of unidirectional reinforcements for RTM" *Journal of Composite Materials*, Vol 26, No 8, 1992, pp 1100-1133.

[72] Krenchel, H. "Fibre reinforcement - theoretical and practical investigations of the elasticity and strength of fibre reinforced materials" *Academisk Forlag*, Copenhagen, 1964.

[73] Tsai, S.W., Hahn, H.T. "Introduction to composite materials" *Technomic Publishing co. Inc*, Lancaster, PA, USA, 1984.

[74] Morley, J.G. "High performance fibre composites" *Academic Press*, 1987.

[75] Jones, R.M. "*Mechanics of composite materials*" *McGraw-Hill*, 1975.

[76] Rudd, C.D., Middleton, V., Owen, M.J., Long, A.C., McGeehin, P. "Design processing and performance of structural preforms" *Proceedings of the 2nd International Conference on Composites (CANCOM 93)*, Ottawa, Canada, Sept 1993, pp 139-152.

[77] Prodromou, A.G., Chen, J. "On the relationship between shear angle and wrinkling of textile composite preforms" *Composites Part A*, Vol 28A, 1997, pp491-503.

[78] Ye, L., Daghyani, H.R., "Characteristics of woven fibre fabric reinforced composites in forming process" *Composites Part A*, Vol 28A, 1997, pp 869-874.

[79] Gelin, J.C., Cherouat, A., Boisse, P., Sabhi, H. "Manufacture of thin composite structures by the RTM process: Numerical simulation of the shaping operation" *Composites Science and Technology*, Vol 56, 1996, pp 711-718.

[80] Van West, B.P., Pipes, R.B., Keefe, M. "A simulation of the draping of bidirectional fabrics over arbitrary surfaces" *Journal of the Textile Institute*, Vol 81, pp 448-460.

[81] Long, A.C., Rudd, C.D. "A simulation of reinforcement deformation during the production of performs for liquid moulding processes" *Proceedings of the IMechE Journal of Engineering Manufacturing*, Vol 208, pp 269-278.

[82] Bergsma, O.K. "Computer simulation of 3D forming processes of fabric reinforced plastics" *Proceedings of the 9th International Conference on Composite Materials*, Madrid, Spain, Vol IV, July 1993, pp 560-567.

[83] Mack, C., Taylor, H.M. "The fitting of woven cloth to surfaces" *Journal of the Textile Institute (transactions)*, Vol 57, 1956, pp 447-488.

[84] Anon "MSC/Patran Operators Manual" *The MacNeal-Schwendler Corporation*, 815 Colorado Boulevard, Los Angeles, California, USA.

[85] Long, A.C., Rudd, C.D., Blagdon, M., Kendall, K.N., Demeri, M.Y. "Simulation and measurement of reinforcement deformation during preform manufacture" *Polymers & Polymer Composites*, Vol 4, No 5, 1996, pp 335-341.

[86] Bakharev, A.S., Tucker, C.L. "Predicting the effect of preforming on RTM mold filling" *Proceedings of the Annual Technical Conference (ANTEC 96)*,

Indianapolis, IN, USA, 1996, Vol 1, pp 797-801.

[87] Long, A.C., Blanchard, P.J., Rudd, C.D., Smith, P. "Combined drape and flow modelling for liquid composite moulding" Proceedings of the 5th International Conference on Automated Composites (ICAC), Glasgow, 1997, pp 51-58.

[88] Bickerton, S., Simacek, P., Guglielmi, S.E., Advani, S.G. "Investigation of draping and its effects on the mold filling process during manufacturing of a compound curved composite part" *Composites Part A*, Vol 28A, 1997, pp 801-816.

[89] Cucinella, F., Long, A.C., Rudd, C.D., Pappalettere, C., "Analysis of an anisotropic prototype composite wheel hub" *Proceedings of the 25th AIAS National Conference*, Gallipoli, Lecce, Italy, 4-7 Sept, 1996, pp 519-528.

[90] Cogswell, F.N. "An obsession with lingerie" *Proceedings of the 4th International Conference on Flow Processes in Composite Materials*, Aberystwyth, 9-11 Sept, 1996, pp 1-3.

[91] Ko, F.K., Ross, E., Lei, C. "Fiber architecture design for CMC engine seal" *Proceedings of the 19th Annual Conference and Exposition on Composites, Advanced Ceramics, Materials and Structures, Part A*, Cocoa Beach, FL, USA, Jan 8-12, 1995, Vol 16, No 4, pp 251-260.

[92] Highsmith, A.L., Davis, J.J., Helms, K.L.E. "The influence of fiber waviness on the compressive behaviour of unidirectional continuous fiber composites" *Proceedings of the 10th Conference on Composite Materials*, ASTM, San Francisco, USA, 24-25 April, 1990, No 1120, pp 20-36.

[93] Piggot, M.R. "The effect of fibre waviness on the mechanical properties of unidirectional fibre composites: A review" *Composites Science and Technology*, Vol 53, 1995, pp 201-205.

[94] Bogetti, T.A., Gillespie, J.W., Lamontia, M.A. "Influence of ply waviness on the stiffness and strength reduction on composite laminates" *Journal of Thermoplastic Composite Materials*, Vol 5, October 1992, pp 344-369.

[95] Bolotin, V.V. "Theory of a reinforced layered medium with random initial irregularities" *Polymer Mechanics*, Vol 2, 1966, pp 7-11.

[96] Ishikawa, T., Chou, T.W. "Stiffness and strength behaviour of woven fabric

composites" *Journal of Materials Science*, Vol 17, 1982, pp 3211-3220.

[97] Chan, W.S., Chou, C.J. "Effects of delamination and ply fiber waviness on effective axial and bending stiffnesses in composite laminates" *Composite Structures*, Vol 30, 1995, pp 299-306.

[98] Rai, H.G., Rogers, C.W., Crane, D.A. "Mechanics of curved fiber composites" *Proceedings of the 47th Annual Forum of the American Helicopter Society*, Phoenix, Arizona, USA, May 6-8, 1991, pp 297-304.

[99] Hsaio, H.M., Daniel, I.M. "Effect of fiber waviness on stiffness and strength reduction of unidirectional composites undre compressive loading" *Composites Science and Technology*, Vol 56, 1996, pp 581-593.

[100] Mrse, A.M., Piggot, M.R. "Compressive properties of unidirectional carbon fibre laminates: II. The effects of unintentional and intentional fibre misalignments" *Composites Science and Technology*, Vol 46, 1993, pp 219-227.

[101] USA Department of Defense "Military handbook - Polymer matrix composites" *Defense Printing Service Detachment Office*, Philadelphia, USA, 1994.

[102] Halpin, J.C. "Primer on composite materials analysis" *Technomic*, 1992, pp 161-176

[103] Alif, N., Carlsson, L.A. "Failure mechanisms of woven carbon and glass composites" *Proceedings of the 6th Symposium on Composites: Fatigue and Fracture (ASTM)*, Denver, CO, USA, May 16-18, 1995, pp 471-493.

[104] Falzon, P.J., Herszberg, I. "Effects of compaction on the stiffness and strength of plain weave fabric RTM composites" *Journal of Composite Materials*, Vol 30, No 11, 1996, pp1210-1247.

[105] Sokolnikoff, I.S. "Mathematical Theory of Elasticity" *McGraw Hill*, New York, 1956.

[106] Wisnom, M.R. "The Effect of Fibre Rotation in ±45° Tension Tests on Measured Shear Properties" *Composites*, 1995, Vol.26, No.1, pp25-32.

Appendix 1.1
Publications

- Turner M.R., Rudd C.D., Long A.C., Middleton V., McGeehin P., "Automated Fibre Lay-Down Techniques for Preform Manufacture", Proceedings of the Fourth International Conference on Automated Composites, 6-7th September 1995, Nottingham, UK, Institute of Materials, pp 431-438.

- Turner M.R., Rudd C.D., Long A.C., Middleton V., McGeehin P., "Net-Shape *Preform Manufacture Using Automated Fibre Placement", Advanced Composites Letters, Vol.4, No.4, 1995, pp121-124.*

- Turner M.R., Rudd C.D., Long A.C., Middleton V., "Computer Integrated Design and Manufacture of Structural Preforms", Proceedings of the fifth International Conference on Automated Composites, 4-5th September 1997, Glasgow, UK, Institute of Materials, pp 245-252.

- Rudd C.D., Turner M.R., Long A.C., Middleton V., "Tow Placement Studies for Liquid Composite Moulding", *submitted to Composites Part A.*

Appendix 3.1
In-mould Measurement of Preform Permeability

This analysis describes the calculation of wetting and wetted permeabilities of reinforcement material in a flat planar mould. The reinforcement is subject to a constant flow rate injection of fluid through a central circular gate of small radius, and air is displaced through vents open to atmospheric pressure, thereby giving no resistance to flow [66].

It is assumed that:

- Darcy's Law is obeyed.
- All pore space, ϕ, is interconnected.
- The resin has constant viscosity.
- The aspect ratio, β, of the ellipse describing the impregnated region of the reinforcement, remains constant.
- The reinforcement does not move or deform.
- Mould cavity gap height, h is very much smaller than the radial position of the flow front, thereby allowing flow to be considered as two-dimensional.
- The principal axes of the ellipse lie on the x and y axes (transducer axes).

Since it is assumed that the principal axes of the ellipse describing the impregnated region of reinforcement lie on the x and y axes, the aspect ratio is defined as:

$$\beta = \frac{r_x}{r_y} = \frac{v_x}{v_y} \qquad (A3.1.1)$$

where v is the macroscopic velocity of the resin, i.e. the velocity of the flow front.

The continuity equation and Darcy's Law state:

$$\Delta.v_0 = 0 \qquad (A3.1.2)$$

$$v_0 = -\frac{\bar{k}}{\mu} \nabla p \qquad \text{(A3.1.3)}$$

where v_0 is the superficial velocity of the fluid, as though no reinforcement material were present, and $\bar{k}$ is the permeability tensor. In this case, the velocity measured, v, is that of the fluid flow front which is related to the superficial velocity thus:

$$v_0 = \phi v \qquad \text{(A3.1.4)}$$

For flow along the principal axes, the macroscopic velocities in the x and y directions are:

$$v_x = -\frac{k_x}{\mu\phi} \frac{\partial p_x}{\partial r_x} \qquad \text{(A3.1.5)}$$

$$v_y = -\frac{k_y}{\mu\phi} \frac{\partial p_y}{\partial r_y} \qquad \text{(A3.1.6)}$$

If the volumetric flow rate, Q, is constant, as in the RTM process, then the rate of increase of area of the ellipse describing the impregnated region of reinforcement is:

$$\frac{Q}{h\phi} = \pi \frac{d}{dt}(r_x r_y) \qquad \text{(A3.1.7)}$$

Using $dr/dt = v$:

$$\frac{Q}{\pi h\phi} = r_x v_y + r_y v_x \qquad \text{(A3.1.8)}$$

Substituting $r_y = \frac{r_x}{\beta}$ and $v_y = \frac{v_x}{\beta}$ from Equation A3.1.1:

$$\frac{Q}{\pi h\phi} = \frac{2 r_x v_x}{\beta} \qquad \text{(A3.1.9)}$$

and:

$$\frac{Q}{\pi h \phi} = 2\beta r_y v_y \qquad \text{(A3.1.10)}$$

Substituting for v_x from Equation A3.1.5 gives:

$$\frac{Q\beta}{2\pi h r_x} = -\frac{k_x}{\mu}\frac{\partial p_x}{\partial r_x} \qquad \text{(A3.1.11)}$$

Substituting for v_y from Equation A3.1.6 gives:

$$\frac{Q}{2\beta\pi h r_y} = -\frac{k_y}{\mu}\frac{\partial p_y}{\partial r_y} \qquad \text{(A3.1.12)}$$

For flow along the *x* axis, Equation A3.1.11 is integrated with respect to r_x to give:

$$\frac{Q\beta}{2\pi h}\ln r_x = -\frac{k_x}{\mu}p_x + const_x \qquad \text{(A3.1.13)}$$

The constant of integration is determined using the known condition that $p_x = p_{0x}$ at a radial position r_{0x}:

$$const_x = \frac{Q\beta}{2\pi h}\ln r_{0x} + \frac{k_x}{\mu}p_{0x} \qquad \text{(A3.1.14)}$$

Substituting into Equation A3.1.13 gives:

$$\frac{Q\beta}{2\pi h}\ln\left(\frac{r_x}{r_{0x}}\right) = -\frac{k_x}{\mu}(p_x - p_{0x}) \qquad \text{(A3.1.15)}$$

Similarly for flow along the *y* axis:

$$\frac{Q}{2\beta\pi h}\ln\left(\frac{r_y}{r_{0y}}\right) = -\frac{k_y}{\mu}(p_y - p_{0y}) \qquad \text{(A3.1.16)}$$

The solutions for the steady state or "wetted" permeability in the principal x and y axes are easily obtained by substituting for a known pressure drop between two fixed points located behind the flow front. To obtain the transient or "wetting" permeability, Equation A3.1.15 is solved using the known condition that the pressure at the flow front is atmospheric. The radial position of the flow front can be calculated using the known condition of constant volumetric flow rate.

The area covered by the ellipse describing the flow of resin at a time t is:

$$\frac{Q}{h\phi}t = \pi r_{xff} r_{yff} \qquad \text{(A3.1.17)}$$

Substituting $r_y = \frac{r_x}{\beta}$ from Equation A3.1.1 gives:

$$r_{xff} = \left(\frac{Qt\beta}{h\phi\pi}\right)^{\frac{1}{2}} \qquad \text{(A3.1.18)}$$

and similarly

$$r_{yff} = \left(\frac{Qt}{h\phi\pi\beta}\right)^{\frac{1}{2}} \qquad \text{(A3.1.19)}$$

Substituting the condition p=0 at $r_x = r_{xff}$ into equation A3.1.15 gives:

$$p_x = -\frac{Q\mu\beta}{2\pi h k_x} \ln\left(\frac{r_x}{\left(\frac{Qt\beta}{h\phi\pi}\right)^{\frac{1}{2}}}\right) \qquad \text{(A3.1.20)}$$

and similarly

$$p_y = -\frac{Q\mu}{2\pi h k_y \beta} \ln\left(\frac{r_y}{\left(\frac{Qt}{h\phi\pi\beta}\right)^{\frac{1}{2}}}\right) \qquad \text{(A3.1.21)}$$

If we introduce the parameter κ such that :

$$\kappa = \frac{Q\mu\beta}{2\pi h k_x} = \frac{Q\mu}{2\pi h \beta k_y} \qquad \text{(A3.1.22)}$$

Then Equations A3.1.20 and 3.1.21 can be written as:

$$p_x = \frac{1}{2}\kappa lnt + \frac{1}{2}\kappa \ln\left(\frac{Q\beta}{h\phi\pi}\right) - \kappa lnr_x \qquad \text{(A3.1.23)}$$

$$p_y = \frac{1}{2}\kappa lnt + \frac{1}{2}\kappa \ln\left(\frac{Q}{h\phi\pi\beta}\right) - \kappa lnr_y \qquad \text{(A3.1.24)}$$

The second and third terms on the right hand side of these expressions are both constant at a given radial location, therefore a plot of p *vs.* $\frac{1}{2}lnt$ will produce a straight line whose slope is equal to κ, from which the values for 'wetting' permeability may be calculated using:

$$k_x = \frac{Q\mu\beta}{2\pi h\kappa} \qquad \text{(A3.1.25)}$$

$$k_y = \frac{Q\mu}{2\pi h\kappa\beta} \qquad \text{(A3.1.26)}$$

Appendix 5.1
Reinforcement Efficiency Factor for Sinusoidal Fibre Distribution

The efficiency factor as developed by Krenchel [72] is:

$$\eta = \sum a_n \cos^4 \theta_n \qquad \text{(A5.1.1)}$$

The model assumes:

- A strong fibre/matrix bond
- Fibres and matrix deform together
- Component only subjected to deformations in loading direction
- Transverse deformations are neglected.

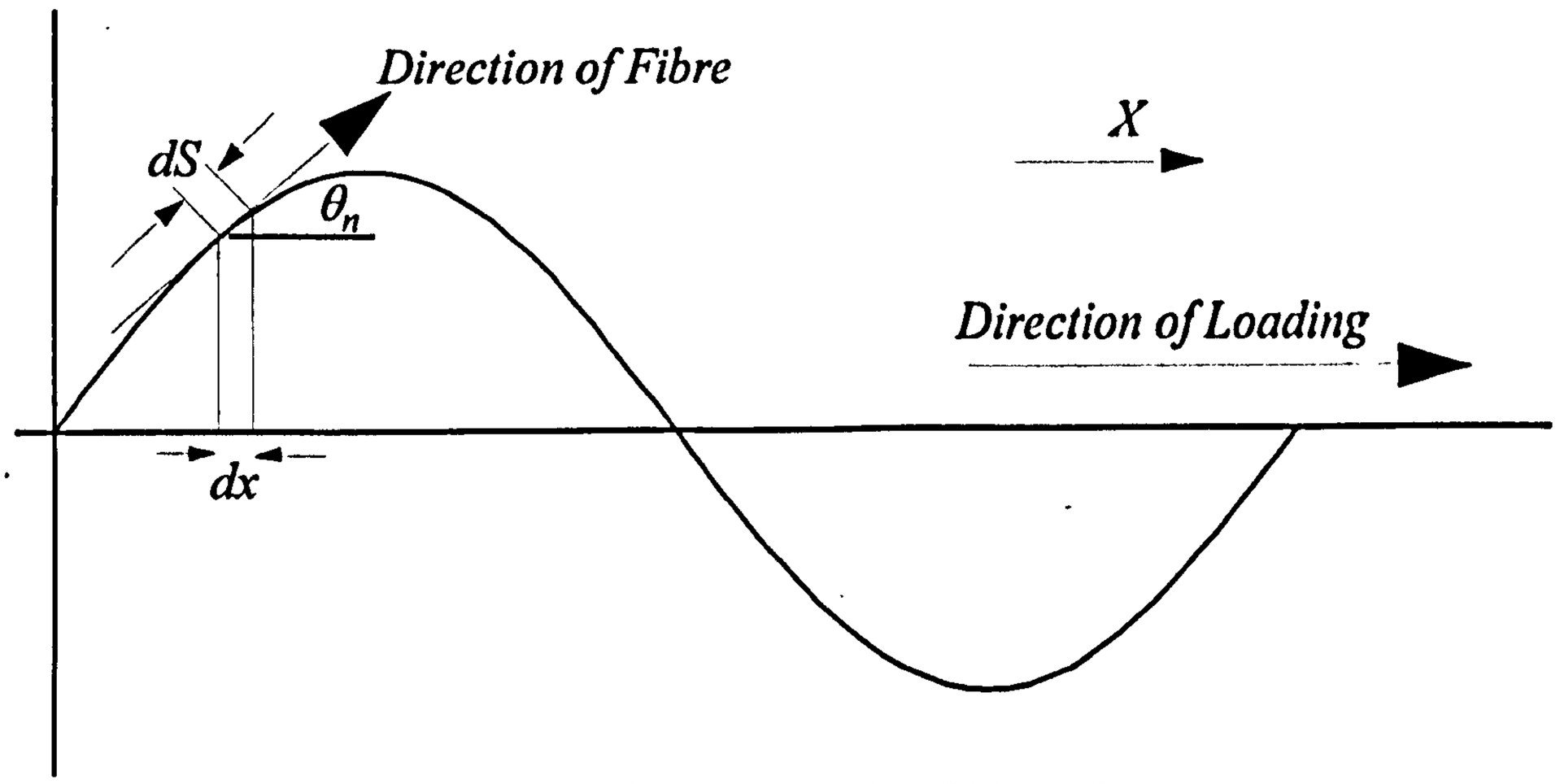

Figure A5.1.1 Schematic of Sine Wave

For any fibre pattern, including a sine wave (Figure A5.1.1), the proportion of fibre in the direction θ_n is:

$$a_n = \frac{dS}{S} \qquad \text{(A5.1.2)}$$

Therefore

$$\eta = \sum \frac{dS}{S} \cos^4 \theta \qquad \text{(A5.1.3)}$$

From trigonometry,

$$\frac{dx}{dS} = \cos\ 0 \qquad \text{(A5.1.4)}$$

i.e.

$$S = \int \frac{1}{\cos\ 0}\ dx \qquad \text{(A5.1.5)}$$

As the step length dS tends to zero, the efficiency becomes:

$$\eta = \frac{1}{S} \int \cos^4\ 0\ dS \qquad \text{(A5.1.6)}$$

And substituting Equation A5.1.4, the efficiency over a full wavelength is:

$$\eta = \frac{1}{S} \int_0^{\lambda} \cos^3\ 0\ dx \qquad \text{(A5.1.7)}$$

The equation of a sine wave of amplitude, a, and wavelength, λ is:

$$f(x) = a\ \sin\ (\frac{2\pi x}{\lambda}) \qquad \text{(A5.1.8)}$$

Given that:

$$\tan\ (\theta) = \frac{df(x)}{dx} = \left(\frac{2\pi}{\lambda}\right) a\ \cos\left(\frac{2\pi x}{\lambda}\right) \qquad \text{(A5.1.9)}$$

then:

$$\theta = \tan^{-1}\left[\left(\frac{2\pi}{\lambda}\right) a\ \cos\left(\frac{2\pi x}{\lambda}\right)\right] \qquad \text{(A5.1.10)}$$

Substituting Equation A5.1.10 into Equation A5.1.7 gives:

$$\eta = \frac{1}{S} \int_0^{\lambda} \cos^3\left(\tan^{-1}\left[\left(\frac{2\pi}{\lambda}\right) a\ \cos\left(\frac{2\pi x}{\lambda}\right)\right]\right) dx \qquad \text{(A5.1.11)}$$

Which can be solved by applying numerical integration techniques such as the trapezium rule within a simple computer program to produce a set of efficiencies for various levels of waviness (a/λ).

Appendix 5.2
Classical Laminate Theory to Predict the Axial Modulus of a Laminate with In-Plane Sinusoidal Fibre Distribution

For a unidirectional laminate loaded in tension (Figure A5.2.1) along the principal material directions and assuming plane stress conditions, the elastic response can be represented as follows:

$$\begin{bmatrix}\varepsilon_1\\ \varepsilon_2\\ \gamma_{12}\end{bmatrix} = [S]\begin{bmatrix}\sigma_1\\ \sigma_2\\ \tau_{12}\end{bmatrix} = \begin{bmatrix}S_{11} & S_{12} & 0\\ S_{12} & S_{22} & 0\\ 0 & 0 & S_{66}\end{bmatrix}\begin{bmatrix}\sigma_1\\ \sigma_2\\ \tau_{12}\end{bmatrix} \qquad (A5.2.1)$$

where

$$S_{11} = \frac{1}{E_1}\ ,\ S_{22} = \frac{1}{E_2}\ ,\ S_{12} = -\frac{\nu_{12}}{E_1}\ ,\ S_{66} = \frac{1}{G_{12}} \qquad (A5.2.2)$$

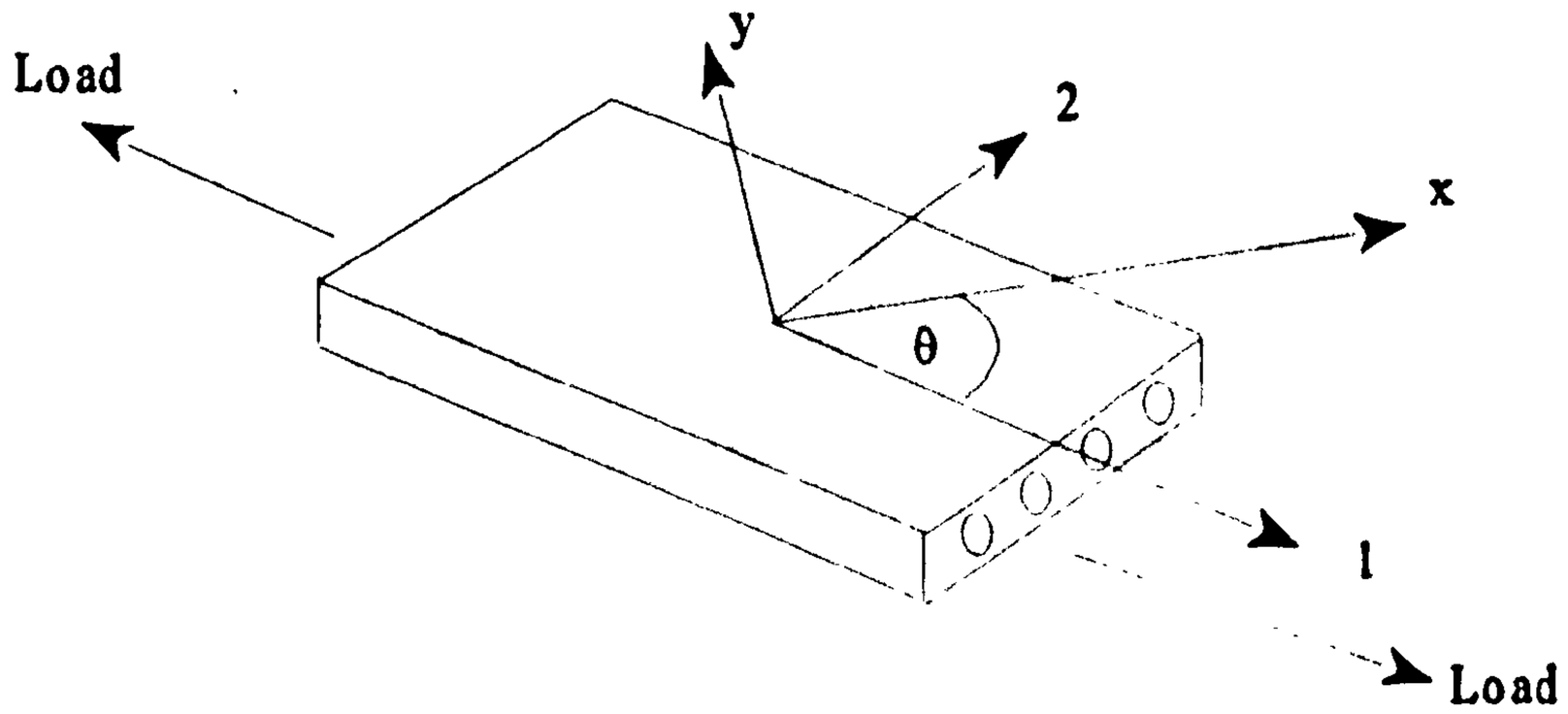

Figure A5.2.1. Rotation of Lamina Coordinate System from 1-2 to x-y Axes

When load is applied to the same laminate at an arbitrary angle, 0, to the principal fibre directions, a coupling occurs between tensile and shear strains [74]. To express stresses in the new coordinate system relative to the old coordinate system, a stress transformation matrix can be used [105]:

$$\begin{bmatrix}\sigma_x\\ \sigma_y\\ \tau_{xy}\end{bmatrix} = [T]\begin{bmatrix}\sigma_1\\ \sigma_2\\ \tau_{12}\end{bmatrix} = \begin{bmatrix}\cos^2\theta & \sin^2\theta & -2\sin\theta\cos\theta\\ \sin^2\theta & \cos^2\theta & 2\sin\theta\cos\theta\\ \sin\theta\cos\theta & -\sin\theta\cos\theta & \cos^2\theta-\sin^2\theta\end{bmatrix}\begin{bmatrix}\sigma_1\\ \sigma_2\\ \tau_{12}\end{bmatrix} \qquad (A5.2.3)$$

To use the strain transformation matrix and engineering terminology, ($\gamma_{xy} = 2\varepsilon_{xy}$ etc.) the transformation matrix [T] must be modified:

$$\begin{bmatrix}\varepsilon_x\\ \varepsilon_y\\ \gamma_{xy}\end{bmatrix} = [T']\begin{bmatrix}\varepsilon_1\\ \varepsilon_2\\ \gamma_{12}\end{bmatrix} = \begin{bmatrix}\cos^2\theta & \sin^2\theta & -\sin\theta\cos\theta\\ \sin^2\theta & \cos^2\theta & \sin\theta\cos\theta\\ 2\sin\theta\cos\theta & -2\sin\theta\cos\theta & \cos^2\theta-\sin^2\theta\end{bmatrix}\begin{bmatrix}\varepsilon_1\\ \varepsilon_2\\ \gamma_{12}\end{bmatrix} \qquad (A5.2.4)$$

To obtain the stress-strain relationship in the new coordinate system:

$$\begin{bmatrix}\varepsilon_x\\ \varepsilon_y\\ \gamma_{xy}\end{bmatrix} = [T']\begin{bmatrix}\varepsilon_1\\ \varepsilon_2\\ \gamma_{12}\end{bmatrix} = [T'][S]\begin{bmatrix}\sigma_1\\ \sigma_2\\ \tau_{12}\end{bmatrix} \qquad (A5.2.5)$$

And

$$\begin{bmatrix}\sigma_1\\ \sigma_2\\ \tau_{12}\end{bmatrix} = [T]^{-1}\begin{bmatrix}\sigma_x\\ \sigma_y\\ \tau_{xy}\end{bmatrix} = \begin{bmatrix}\cos^2\theta & \sin^2\theta & 2\sin\theta\cos\theta\\ \sin^2\theta & \cos^2\theta & -2\sin\theta\cos\theta\\ -\sin\theta\cos\theta & \sin\theta\cos\theta & \cos^2\theta-\sin^2\theta\end{bmatrix}\begin{bmatrix}\sigma_x\\ \sigma_y\\ \tau_{xy}\end{bmatrix} \qquad (A5.2.6)$$

Therefore

$$\begin{bmatrix}\varepsilon_x\\ \varepsilon_y\\ \gamma_{xy}\end{bmatrix} = [T'][S][T]^{-1}\begin{bmatrix}\sigma_x\\ \sigma_y\\ \tau_{xy}\end{bmatrix} \qquad (A5.2.7)$$

Which reduces to

$$\begin{bmatrix} \varepsilon_x \\ \varepsilon_y \\ \gamma_{xy} \end{bmatrix} = [\overline{S}] \begin{bmatrix} \sigma_x \\ \sigma_y \\ \tau_{xy} \end{bmatrix} \qquad (A5.2.8)$$

where

$$\begin{aligned}
\overline{S_{11}} &= S_{11}\cos^4\theta + S_{22}\sin^4\theta + (2S_{12} + S_{66})\sin^2\theta\cos^2\theta \\
\overline{S_{12}} &= S_{12}(\cos^4\theta + \sin^4\theta) + (S_{11} + S_{22} - S_{66})\cos^2\theta\sin^2\theta \\
\overline{S_{16}} &= (2S_{11} - 2S_{12} - S_{66})\sin\theta\cos^3\theta - (2S_{22} - 2S_{12} - S_{66})\sin^3\theta\cos\theta \\
\overline{S_{22}} &= S_{11}\sin^4\theta + S_{22}\cos^4\theta + (2S_{12} + S_{66})\sin^2\theta\cos^2\theta \\
\overline{S_{26}} &= (2S_{11} - 2S_{12} - S_{66})\sin^3\theta\cos\theta - (2S_{22} - 2S_{12} - S_{66})\sin\theta\cos^3\theta \\
\overline{S_{66}} &= 2(2S_{11} + 2S_{22} - 4S_{12} - S_{66})\sin^2\theta\cos^2\theta + S_{66}(\sin^4\theta + \cos^4\theta)
\end{aligned} \qquad (A5.2.9)$$

So it can be seen that by using Eqns A5.2.8 & A5.2.9 the stress-strain relationships for general cases of off-axis loading of unidirectional laminates can be determined. To apply these equations to the loading of a laminate constructed using sinusoidal fibres (Figure A5.2.2) certain boundary conditions must be applied. A laminate constructed using fibres with an in-plane sinusoidal distribution can be thought of as a balanced ±0 laminate because of the symmetry of the fibre distribution.

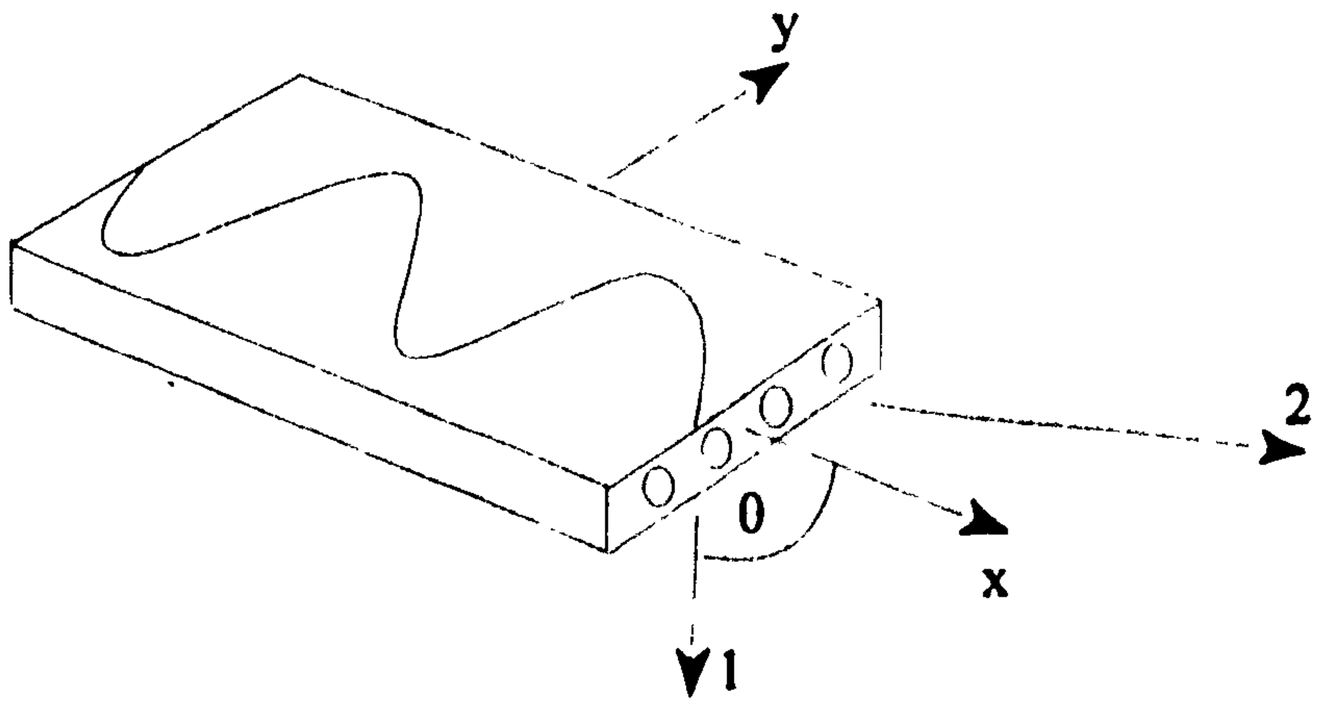

Figure A5.2.2. Coordinate System for Lamina with Sinusoidal Fibres

Because the laminate is balanced, σ_y must be the same in the +θ and -θ plies. Since there is no applied stress in this direction, σ_y must be equal to 0 [106]. Also, because the laminate is balanced, shear strain, γ_{xy}, is equal to 0 and Eqn A.5.2.8 can be re-arranged to show:

$$\begin{bmatrix} \varepsilon_x \\ \varepsilon_y \\ \gamma_{xy} = 0 \end{bmatrix} = \begin{bmatrix} \overline{S_{11}} & \overline{S_{12}} & \overline{S_{16}} \\ \overline{S_{12}} & \overline{S_{22}} & \overline{S_{26}} \\ \overline{S_{16}} & \overline{S_{26}} & \overline{S_{66}} \end{bmatrix} \begin{bmatrix} \sigma_x \\ \sigma_y = 0 \\ \tau_{xy} \end{bmatrix} \qquad \text{(A5.2.10)}$$

So that

$$\varepsilon_x = \overline{S_{11}}\,\sigma_x + \overline{S_{16}}\,\tau_{xy} \qquad \text{(A.5.2.11a)}$$

$$\varepsilon_y = \overline{S_{12}}\,\sigma_x + \overline{S_{26}}\,\tau_{xy} \qquad \text{(A5.2.11b)}$$

$$\gamma_{xy} = \overline{S_{16}}\,\sigma_x + \overline{S_{66}}\,\tau_{xy} = 0 \qquad \text{(A5.2.11c)}$$

And re-arranging Eqn A5.2.11c:

$$\tau_{xy} = \frac{-\,\overline{S_{16}}\,\sigma_x}{\overline{S_{66}}} \qquad \text{(A5.2.12)}$$

Substituting Eqn A5.2.12 into A5.2.11a:

$$\varepsilon_x = \overline{S_{11}}\sigma_x - \frac{\overline{S_{16}^2}\,\sigma_x}{\overline{S_{66}}} \qquad \text{(A5.2.13)}$$

or:

$$\frac{1}{E_x} = \overline{S_{11}} - \frac{\overline{S_{16}^2}}{\overline{S_{66}}} \qquad \text{(A5.2.14)}$$

From Eqns A5.2.2, A5.2.9 & A5.2.14 it can be seen that the modulus is dependent only on the properties of a UD laminate and the off-axis fibre angle, θ. For a laminate containing sinusoidal fibres, θ varies along the wavelength of the fibre. Because sine waves are repeated every wavelength it is possible to determine the laminate modulus by assuming it to contain a single wavelength. Applying numerical integration techniques to Eqn A5.2.14 over the period of a wavelength will produce the effective modulus of the laminate:

$$\frac{1}{E_x} = \int_0^{\lambda} \frac{\left(\overline{S_{11}}\ \overline{S_{66}} - \overline{S_{16}^2}\right)}{\overline{S_{66}}}\, dx \qquad \text{(A5.2.15)}$$

The modified off-axis compliances $\overline{S_{11}}$ etc. depend upon the off-axis angle, 0, which is in turn a function of position, x, (A5.1.10).

Substituting Eqn A5.1.10 into Eqn A5.2.15 and using numerical integration techniques similar to those described in Appendix 5.1 will produce the effective modulus of a laminate with a sinusoidal fibre distribution.

Appendix 5.3
Classical Laminate Theory to Predict the Axial Modulus of a Laminate with Out-of-Plane Sinusoidal Fibre Distribution

As has been described in Appendix 5.2, the stress-strain relationships for general cases of off-axis loading of unidirectional laminates can be determined using the relationships in Equations A5.2.8 and A5.2.9.

Applying these equations to the loading of a laminate constructed using fibres with sinusoidal out-of plane distribution (Figure A5.3.1) certain boundary conditions must be applied. Such a laminate can be thought of as a 0°/90° ply in the x-y plane. Because there are no fibres in directions other than the principal x and y directions, σ_y and τ_{xy} must be equal to 0. Eqn A.5.2.8 can be re-arranged to show:

$$\begin{bmatrix} \varepsilon_x \\ \varepsilon_y \\ \gamma_{xy} \end{bmatrix} = \begin{bmatrix} \overline{S_{11}} & \overline{S_{12}} & \overline{S_{16}} \\ \overline{S_{12}} & \overline{S_{22}} & \overline{S_{26}} \\ \overline{S_{16}} & \overline{S_{26}} & \overline{S_{66}} \end{bmatrix} \begin{bmatrix} \sigma_x \\ \sigma_y = 0 \\ \tau_{xy} = 0 \end{bmatrix} \qquad (A5.3.1)$$

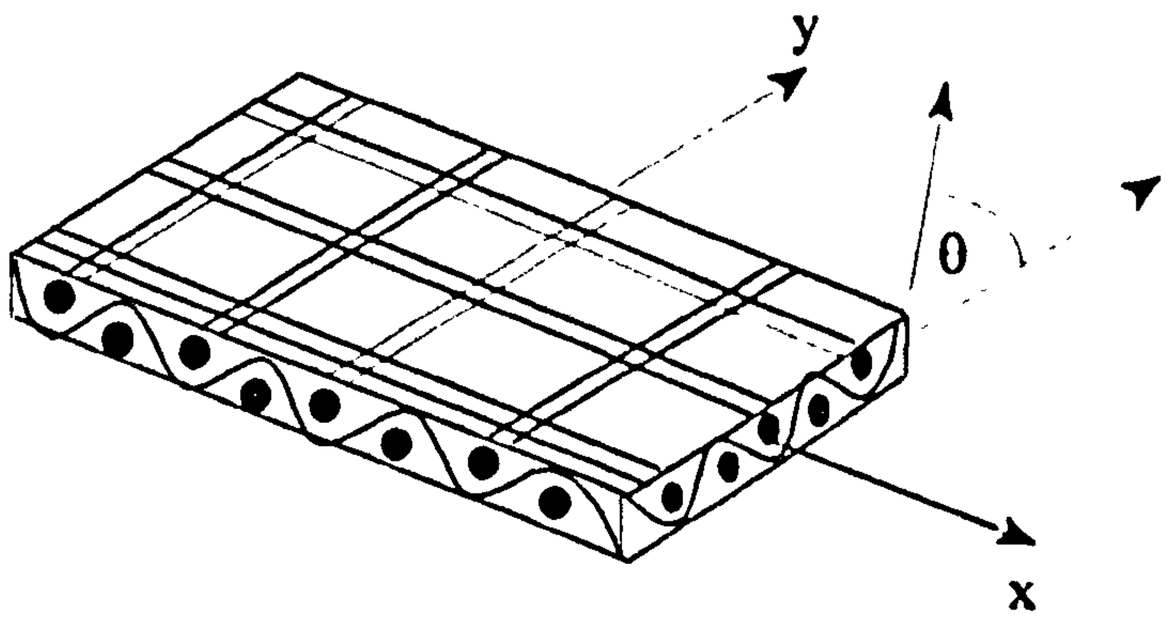

Figure A5.3.1. Schematic of Lamina with Sinusoidal Out-of-Plane Fibre Distribution

So that

$$\varepsilon_x = \overline{S_{11}}\sigma_x \qquad (A5.3.2)$$

or:

$$\frac{1}{E_x} = \overline{S_{11}} \qquad \text{(A5.3.3)}$$

Again modulus is dependent only on the properties of a UD laminate and the off-axis fibre angle, θ and can be determined from Eqns A5.2.9, & A5.3.3 by applying numerical integration techniques similar to those described in Appendix 5.1.

Appendix 5.4
Axial Permeability of a Laminate with Sinusoidal Fibre Distribution

Permeability is defined by Darcy's law for flow through homogeneous porous media:

$$Q = -K \frac{A}{\mu} \frac{\Delta P}{L} \qquad (A5.4.1)$$

For orthotropic flow, the permeability model is based upon the 2D permeability tensor [63]:

$$[K] = \begin{bmatrix} K_1 & 0 \\ 0 & K_2 \end{bmatrix} \qquad (A5.4.2)$$

where K_1 and K_2 are permeabilities in the principal directions (i.e. parallel and transverse to the fibre axis). When flow occurs at an angle 0 to the principal axes, the tensor is transformed to the new coordinate system (x,y) by applying an appropriate transformation [63], giving

$$\begin{bmatrix} K_{xx} & K_{xy} \\ K_{yx} & K_{yy} \end{bmatrix} = \begin{bmatrix} K_1\cos^2\theta + K_2\sin^2\theta & (K_2 - K_1)\sin\theta\cos\theta \\ (K_2 - K_1)\sin\theta\cos\theta & K_1\sin^2\theta + K_2\cos^2\theta \end{bmatrix} \qquad (A5.4.3)$$

The 2D form of Darcy's Law is:

$$\begin{bmatrix} v_x \\ v_y \end{bmatrix} = -\frac{1}{\mu} \begin{bmatrix} K_{xx} & K_{xy} \\ K_{yx} & K_{yy} \end{bmatrix} \begin{bmatrix} \frac{\delta p}{\delta x} \\ \frac{\delta p}{\delta y} \end{bmatrix} \qquad (A5.4.4)$$

Taking v_x

$$v_x = -\frac{1}{\mu} \left[K_{xx} \frac{\delta p}{\delta x} + K_{xy} \frac{\delta p}{\delta y} \right] \qquad (A5.4.5)$$

$$= -\frac{1}{\mu} K_x \frac{\delta p}{\delta x} \qquad \text{(A5.4.6)}$$

where

$$K_x = K_{xx} + K_{xy} \frac{\delta x}{\delta y} \qquad \text{(A5.4.7)}$$

$$= K_{xx} + K_{xy} \frac{\delta p/\delta y}{\delta p/\delta x} \qquad \text{(A5.4.8)}$$

which is the effective permeability.

For flow in the X-direction, transverse flow is assumed to be zero [63], i.e.:

$$v_y = 0 = -\frac{1}{\mu} \left[K_{xy} \frac{\delta p}{\delta x} + K_{yy} \frac{\delta p}{\delta y} \right] \qquad \text{(A5.4.9)}$$

or

$$\frac{\delta p/\delta y}{\delta p/\delta x} = -\frac{K_{xy}^2}{K_{yy}^2} \qquad \text{(A5.4.10)}$$

Substituting Eqn A5.4.10 into A5.4.8 gives:

$$K_x = K_{xx} - \frac{K_{xy}^2}{K_{yy}} \qquad \text{(A5.4.11)}$$

or

$$K_x = K_1 \cos^2\theta + K_2 \sin^2\theta - \frac{(K_2 - K_1)^2 \sin^2\theta \cos^2\theta}{K_1 \sin^2\theta + K_2 \cos^2\theta} \qquad \text{(A5.4.12)}$$

and:

$$K_y = K_1\sin^2\theta + K_2\cos^2\theta - \frac{(K_2-K_1)^2 \sin^2\theta \cos^2\theta}{K_1\cos^2\theta + K_2\sin^2\theta} \qquad \text{(A5.4.13)}$$

where K_1 and K_2 are the principal permeabilities and θ is the angle between the principal axis and the fibre.

When the fibre takes the form of a sine wave of amplitude, a, and wavelength, λ it can be seen that θ varies with x as described in Equation A5.1.10. The permeability through a unit cell of a sine wave from x=0 to x=λ as shown in Figure A5.4.1 can be obtained by considering the unit cell to be composed of a series of short straight fibres.

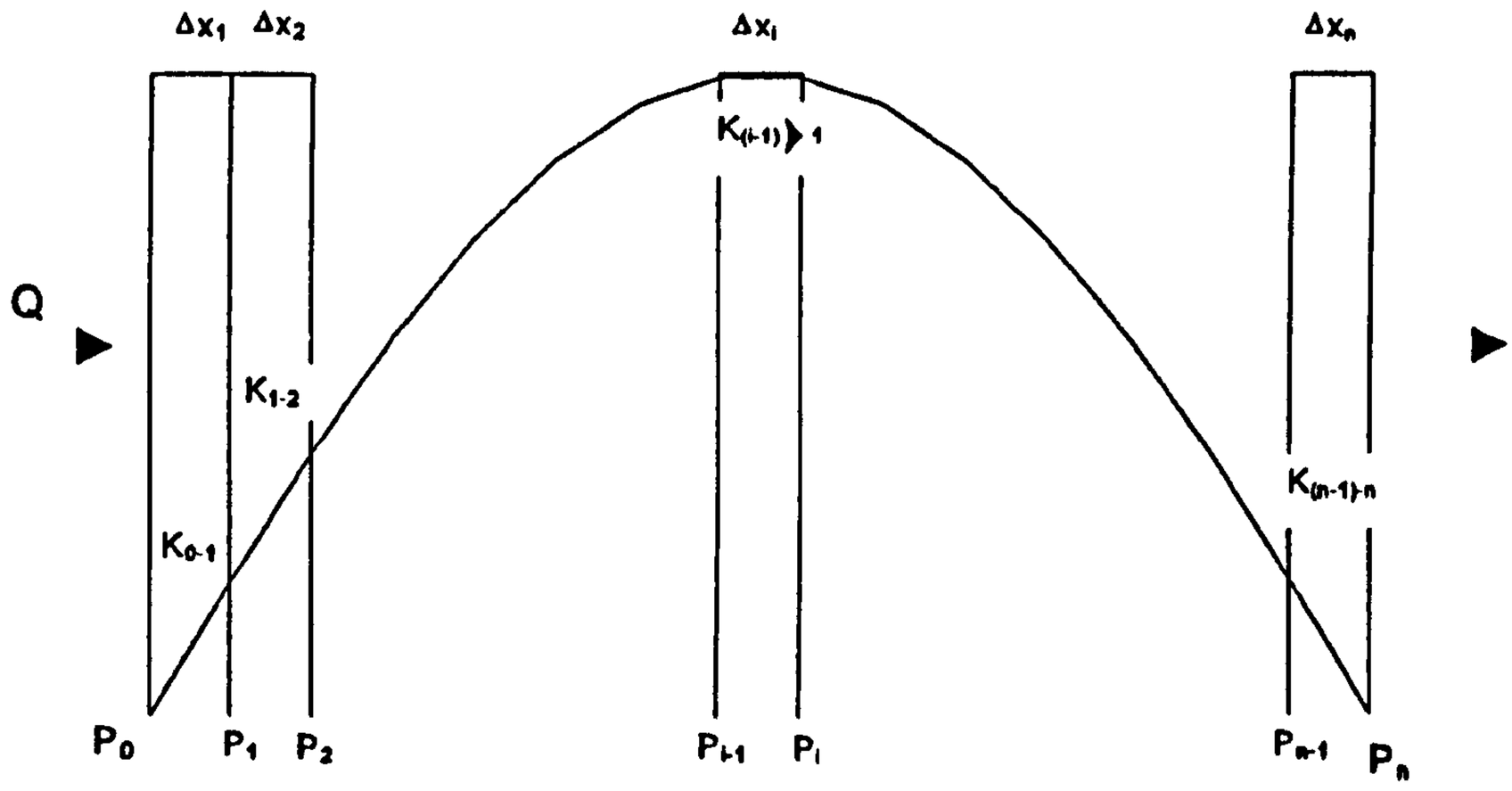

Figure A5.4.1. Unit Cell of an Idealised Fibre Array

where K_{avg} is the overall permeability through the cell and from Darcy's Law [59]:

$$Q = K_{avg}\frac{A}{\mu}\frac{(P_0 - P_n)}{\Delta x} \qquad \text{(A5.4.14)}$$

where A and μ are constant and Δx is the length of the unit cell in the X-direction. At any point the pressure drop is:

$$\frac{Q\mu}{A}\frac{\Delta x_i}{K_i} = P_{i-1} - P_i \qquad \text{(A5.4.15)}$$

Summing across the cell gives:

$$\frac{Q\mu}{A}\sum\frac{\Delta x_i}{K_i} = P_0 - P_n \qquad \text{(A5.4.16)}$$

Comparing to (A5.4.14) gives:

$$\sum\frac{\Delta x_i}{K_i} = \frac{\Delta x}{K_{avg}} \qquad \text{(A5.4.17)}$$

The permeability at any point within the cell, K_i can be obtained by substituting (A5.4.12), the permeability in the direction of the fibre, into the K_i term in (A5.4.17):

$$\frac{\lambda}{K_{avg}} = \int_0^{\lambda}\frac{dx}{K_x(\theta)} \qquad \text{(A5.4.18)}$$

which by substituting Eqn A5.4.12 into A5.4.18 can be easily solved using numerical integration techniques as described in Appendix 5.1.

Appendix 6.1
Drape Algorithm

The kinematic drape algorithm developed by Long [58] is based on the assumptions derived by Mack and Taylor [83]:

a) The fibres are inextensible

b) The method of deformation is by pure in-plane shear only

c) Fibre segments are straight between the joints

d) Uniform surface contact is achieved

These assumptions allow the draped position of each node (fibre crossover point) to be calculated assuming that the position of two intersecting fibre paths are known which determine the initial orientation of the reinforcement. The initial fibre paths are generated by defining geodesic paths over the surface model as described in more detail by Long [58]. Nodes are described by the indices (m,n) which represent their position along the warp and weft axes. The position of each fibre crossover point (node) is found by solving the equations of intersection of the possible end points of each fibre segment and the surface that the reinforcement is being draped onto. Each node is related to its adjacent warp and weft nodes by:

$$\left(X_{m,n} - X_{m-1,n}\right)^2 + \left(Y_{m,n} - Y_{m-1,n}\right)^2 + \left(Z_{m,n} - Z_{m-1,n}\right)^2 = S_m^2 \qquad \text{(A6.1.1)}$$

$$\left(X_{m,n} - X_{m,n-1}\right)^2 + \left(Y_{m,n} - Y_{m,n-1}\right)^2 + \left(Z_{m,n} - Z_{m,n-1}\right)^2 = S_n^2 \qquad \text{(A6.1.2)}$$

And the equation of the surface is given by:

$$aX_{m,n} + bY_{m,n} + cZ_{m,n} = d \qquad \text{(A6.1.3)}$$

These three equations can be solved explicitly to locate the draped node. The drape algorithm is described in further detail by Long [58].

Appendix 6.2
Undrape Algorithm

The three stages to produce an optimised laydown for preforming are:

(a) A 3D computer generated model of the component is produced including the desired fibre paths.

(b) The model is input into the undrape software which maps the fibre paths back to a 2D sheet.

(c) A post processor reads the output from (b) and writes an NC program to produce the laydown using the fibre placement facility.

Within (a), the model (Figure A6.2.1) should be produced from four quadrants and must output the nodal coordinates represented by the fibre cross-over points (Table A6.2.1). Each node is identified by the indices [m,n], with intersections of the four quadrants occurring at m=0, n=0 within each of the four quadrants, Q.

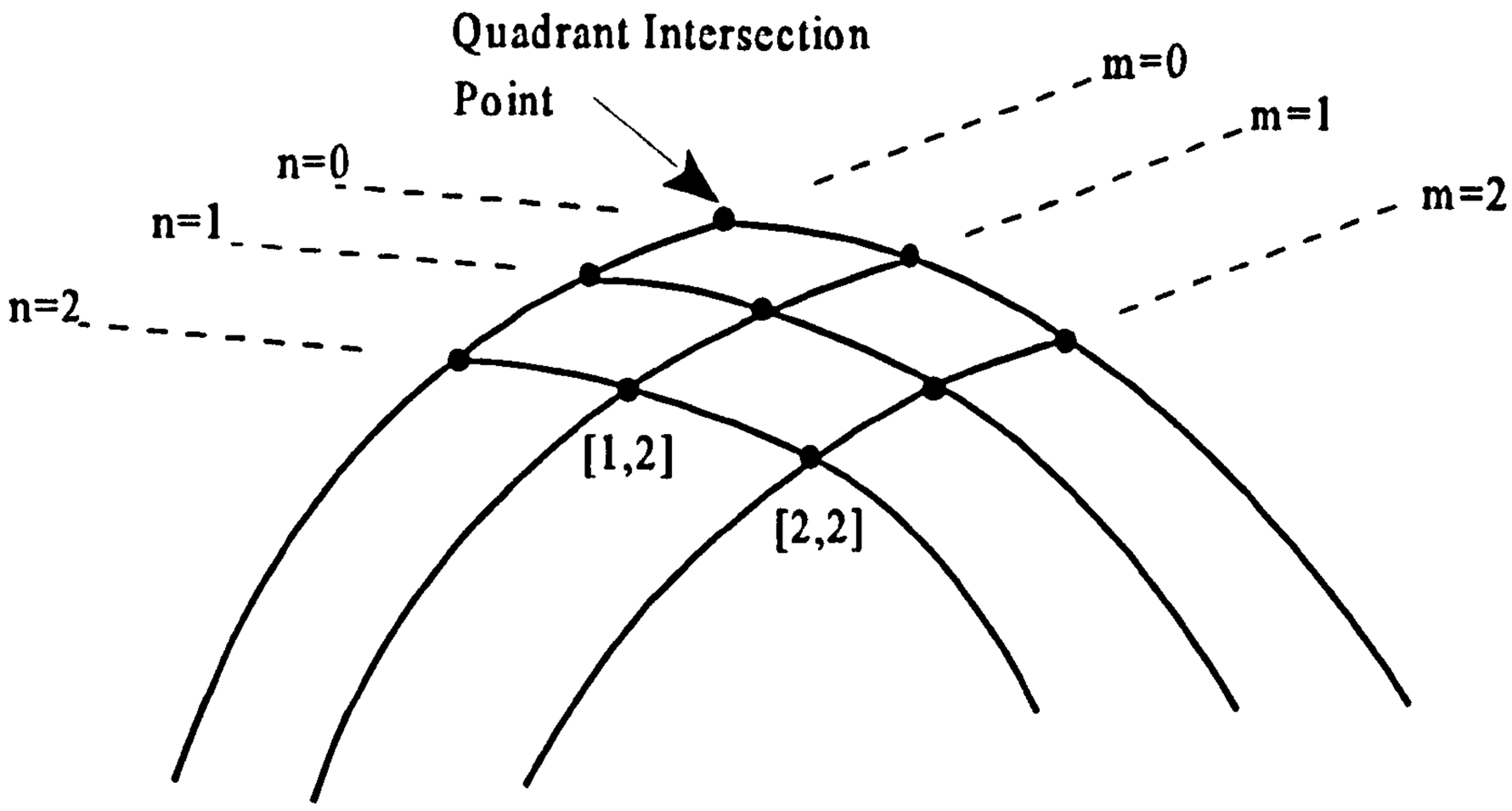

Figure A6.2.1. Schematic of 3D Model of Part Hemisphere Quadrant

Table A6.2.1. Format for Output of 3D Model

Q	m	n	x	y	z
1	0	0	0.00	0	60.49
1	0	1	-5.00	0	60.28
1	0	2	-9.96	0	59.66
1	0	3	-14.85	0	58.64
1	0	4	-19.64	0	57.21
1	0	5	-24.30	0	55.39
.	.	.	.	.	.
.	.	.	.	.	.
1	0	17	-59.66	0	9.96
1	0	18	-60.28	0	5.00
1	0	19	-60.49	0	0.00
1	1	0	0.00	5	60.28
1	1	1	-5.00	5	60.07
1	1	2	-9.96	5	59.45
1	1	3	-14.85	5	58.42
1	1	4	-19.64	5	56.99
.	.	.	.	.	.
.	.	.	.	.	.
1	1	16	-58.64	5	13.98
1	1	17	-59.66	5	8.61
1	1	18	-60.28	5	0.00
.	.	.	.	.	.
.	.	.	.	.	.

The undrape program developed by Long [58] performs several operations on the model output:

1. The draped fibre pattern is loaded into memory (in each quadrant, x,y,z coordinates are stored for each node [m,n]).
2. For each quadrant:
   (i) Map nodes on m=0 to x=0 axis
   n=0 to y=0 axis
   in order to create two intersecting fibre paths which act as the initial constraints for the fabric in the undrape algorithm
   (ii) "Undrape" each node by solving equations of intersections between the possible end-points of fibre segments and the plane z=0 (x-y plane).
3. Save the undraped pattern for all quadrants

The undrape algorithm used to locate each fibre crossover is described in more detail below, including governing equations. Given two adjacent nodes, and the local fibre spacing in two directions (S_m and S_n), the problem is equivalent to finding the two intersections between two circles:

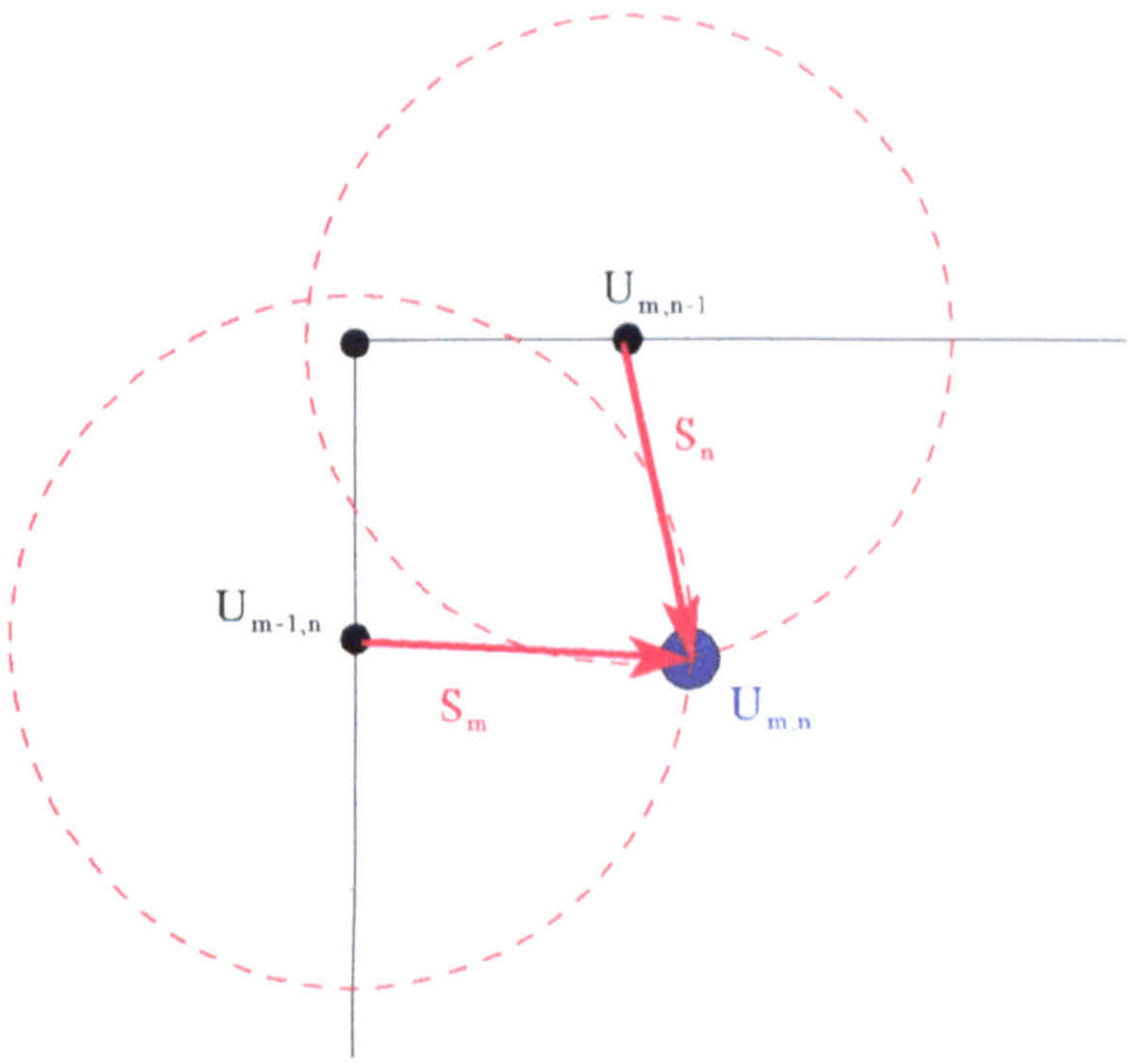

Figure A6.2.2. Schematic of Method to Predict Position of Undraped Node, $U_{m,n}$

Where fibre spacings S_m and S_n are found from the draped fibre pattern (i.e. $S_m = | P_{m,n} - P_{m-1,n} |$ and $S_n = | P_{m,n} - P_{m,n-1} |$ where $P_{m,n}$ is the draped point and $U_{m,n} = [X_{m,n} , Y_{m,n}]$).

i.e.

$$\left(X_{m,n} - X_{m-1,n} \right)^2 + \left(Y_{m,n} - Y_{m-1,n} \right)^2 = S_m^2 \qquad \text{(A6.2.1)}$$

$$\left(X_{m,n} - X_{m,n-1} \right)^2 + \left(Y_{m,n} - Y_{m,n-1} \right)^2 = S_n^2 \qquad \text{(A6.2.2)}$$

These can be expanded to give:

$$X_{m,n}^2 - 2X_{m,n}X_{m-1,n} + X_{m-1,n}^2 + Y_{m,n}^2 - 2Y_{m,n}Y_{m-1,n} + Y_{m-1,n}^2 = S_m^2 \qquad \text{(A6.2.3)}$$

$$X_{m,n}^2 - 2X_{m,n}X_{m,n-1} + X_{m,n-1}^2 + Y_{m,n}^2 - 2Y_{m,n}Y_{m,n-1} + Y_{m,n-1}^2 = S_n^2 \qquad \text{(A6.2.4)}$$

Subtracting Eqn A6.2.3 from Eqn A6.2.4 gives:

$$\alpha X_{m,n} + \beta Y_{m,n} = \gamma \qquad \text{(A6.2.5)}$$

where

$$\alpha = X_{m-1,n} - X_{m,n-1}$$

$$\beta = Y_{m-1,n} - Y_{m,n-1}$$

$$\gamma = \frac{1}{2}\left(S_n^2 - S_m^2 + X_{m-1,n}^2 + Y_{m-1,n}^2 - X_{m,n-1}^2 - Y_{m,n-1}^2 \right)$$

There are two possibilities depending on β:

(i) If $\beta \neq 0$, then Eqn A6.2.5 can be written as:

$$Y_{m,n} = \frac{(\gamma - \alpha X_{m,n})}{\beta}$$

Substituting this into Eqn A6.2.4 gives:

$$aX_{m,n}^2 + bX_{m,n} + c = 0 \qquad \text{(A6.2.6)}$$

where:

$$a = 1 + \left(\frac{\alpha}{\beta}\right)^2$$

$$b = 2\left(\frac{\alpha Y_{m,n-1}}{\beta} - X_{m,n-1} - \frac{\gamma\alpha}{\beta^2}\right)$$

$$c = X_{m,n-1}^2 + Y_{m,n-1}^2 - S_n^2 + \left(\frac{\gamma}{\beta}\right)^2 - \frac{2\gamma Y_{m,n-1}}{\beta}$$

The (two) solutions for $X_{m,n}$ can be substituted into Eqn A6.2.5 to find the corresponding $Y_{m,n}$ values. The correct solution is the one furthest from $X_{m-1,n-1}$, $Y_{m-1,n-1}$ because the other solution represents the projection of the node to a position behind the node $X_{m-1,n-1}$, $Y_{m-1,n-1}$ (see Figure A6.2.2).

When $\beta = 0$, Eqn A6.2.5 becomes:

$$X_{m,n} = \frac{\gamma}{\alpha}$$

Substituting this into Eqn A6.2.2 gives:

$$aY_{m,n}^2 + bY_{m,n} + c = 0 \qquad \text{(A6.2.7)}$$

where

$$a = 1$$

$$b = -2Y_{m,n-1}$$

$$c = \left(X_{m,n} - X_{m,n-1}\right)^2 + Y_{m,n-1}^2 - S_n^2$$

Again, the correct solution will give the furthest distance from $X_{m-1,n-1}$, $Y_{m-1,n-1}$.

The final part of the procedure imports the undrape output into the post processor software. The post processor was written in MS Qbasic and takes each line from the undrape output (m=constant or n=constant representing a single tow) and produces the relevant NC commands to produce a fibre laydown to the same geometry on the fibre placement facility. The program operates in the following way: